frontiers | Research Topics

Rising stars in cancer metabolism 2022

Edited by
Domenica Scumaci and Jose Luis Izquierdo-Garcia

Published in
Frontiers in Oncology

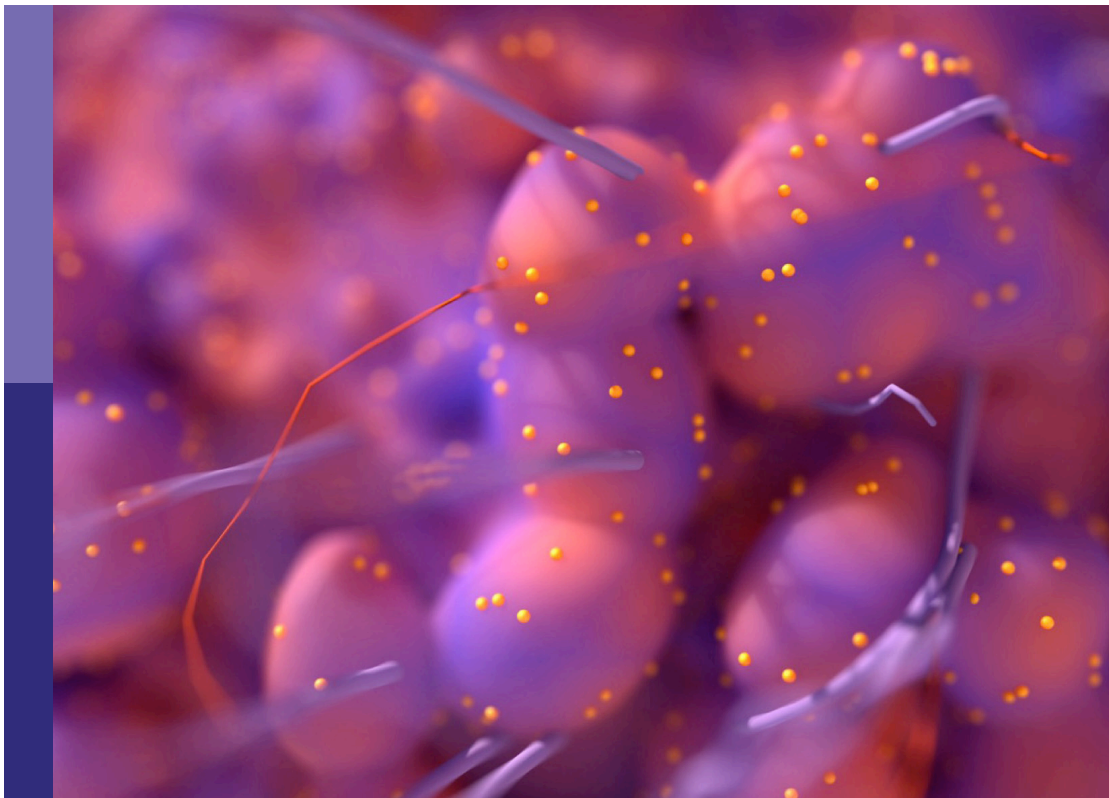

ISSN 1664-8714
ISBN 978-2-8325-2703-0
DOI 10.3389/978-2-8325-2703-0

About Frontiers

Frontiers is more than just an open access publisher of scholarly articles: it is a pioneering approach to the world of academia, radically improving the way scholarly research is managed. The grand vision of Frontiers is a world where all people have an equal opportunity to seek, share and generate knowledge. Frontiers provides immediate and permanent online open access to all its publications, but this alone is not enough to realize our grand goals.

Frontiers journal series

The Frontiers journal series is a multi-tier and interdisciplinary set of open-access, online journals, promising a paradigm shift from the current review, selection and dissemination processes in academic publishing. All Frontiers journals are driven by researchers for researchers; therefore, they constitute a service to the scholarly community. At the same time, the *Frontiers journal series* operates on a revolutionary invention, the tiered publishing system, initially addressing specific communities of scholars, and gradually climbing up to broader public understanding, thus serving the interests of the lay society, too.

Dedication to quality

Each Frontiers article is a landmark of the highest quality, thanks to genuinely collaborative interactions between authors and review editors, who include some of the world's best academicians. Research must be certified by peers before entering a stream of knowledge that may eventually reach the public - and shape society; therefore, Frontiers only applies the most rigorous and unbiased reviews. Frontiers revolutionizes research publishing by freely delivering the most outstanding research, evaluated with no bias from both the academic and social point of view. By applying the most advanced information technologies, Frontiers is catapulting scholarly publishing into a new generation.

What are Frontiers Research Topics?

Frontiers Research Topics are very popular trademarks of the *Frontiers journals series*: they are collections of at least ten articles, all centered on a particular subject. With their unique mix of varied contributions from Original Research to Review Articles, Frontiers Research Topics unify the most influential researchers, the latest key findings and historical advances in a hot research area.

Find out more on how to host your own Frontiers Research Topic or contribute to one as an author by contacting the Frontiers editorial office: frontiersin.org/about/contact

Rising stars in cancer metabolism 2022

Topic editors

Domenica Scumaci — Magna Græcia University of Catanzaro, Italy

Jose Luis Izquierdo-Garcia — Complutense University of Madrid, Spain

Citation

Scumaci, D., Izquierdo-Garcia, J. L., eds. (2023). *Rising stars in cancer metabolism 2022*. Lausanne: Frontiers Media SA. doi: 10.3389/978-2-8325-2703-0

Table of contents

frontiers | Frontiers in Oncology

TYPE Editorial
PUBLISHED 31 May 2023
DOI 10.3389/fonc.2023.1223630

OPEN ACCESS

EDITED AND REVIEWED BY
Ubaldo Emilio Martinez-Outschoorn,
Thomas Jefferson University, United States

*CORRESPONDENCE
Jose Luis Izquierdo-Garcia
jlizquierdo@ucm.es
Domenica Scumaci
scumaci@unicz.it

†These authors have contributed equally to this work

RECEIVED 16 May 2023
ACCEPTED 23 May 2023
PUBLISHED 31 May 2023

CITATION
Izquierdo-Garcia JL and Scumaci D (2023) Editorial: Rising stars in cancer metabolism 2022.
Front. Oncol. 13:1223630.
doi: 10.3389/fonc.2023.1223630

Editorial: Rising stars in cancer metabolism 2022

Jose Luis Izquierdo-Garcia[1,2,3*†] and Domenica Scumaci[4,5*†]

[1]Biomedical Imaging Group, Instituto Pluridisciplinar, Complutense University of Madrid, Madrid, Spain, [2]Department of Chemistry in Pharmaceutical Sciences, Pharmacy School, Complutense University of Madrid, Madrid, Spain, [3]Centro de Investigación Biomédica en Red de Enfermedades Respiratorias (CIBERES), Madrid, Spain, [4]Department of Experimental and Clinical Medicine, Magna Græcia University of Catanzaro, Catanzaro, Italy, [5]Research Center on Advanced Biochemistry and Molecular Biology, Magna Græcia University of Catanzaro, Catanzaro, Italy

KEYWORDS

metabolic reprogramming, metabolic symbiosis, glutamine metabolism, metabolism and redox homeostasis, metabolism and chemoresistance, personalized medicine

Editorial on the Research Topic
Rising stars in cancer metabolism 2022

Recognizing and supporting the next generation of leaders in oncology is crucial for ensuring that we continue to drive innovation and make progress in the fight against cancer. This editorial collection focuses on early-career researchers who have already established themselves as internationally recognized experts in Cancer Metabolism, a rapidly growing area of research that studies metabolic changes in cancer cells (1). By understanding these processes, researchers can develop innovative strategies for diagnosing and treating cancer (2). The collection presents cutting-edge research conducted by future leaders of the discipline, with real-world applications to pressing challenges in cancer research. The study of cancer metabolism has the potential to transform cancer treatment and improve patient outcomes.

During carcinogenesis, cells undergo dramatic metabolic rewiring, acquiring the ability to survive in hard condition. Cancer is a dynamic disease and therefore tumor microenvironment results in heterogeneous cells population characterized by peculiar molecular signatures including those involving metabolism. In this perspective, the article of Amemiya and Yamaguchi aims to address the notion of a metabolic symbiosis between cancer and tumor microenvironment. The authors propose that the co-culture of cancer cells and CAFs might represent a smart model to investigate "real-time" the metabolic oscillations at the single-cell level unveiling the metabolic heterogeneities that surround cell symbiosis. In this scenario, being metabolic cross-talk a driver of invasion, resistance to chemotherapy and malignancies grade, it might represent a strategic target to implement personalized cancer treatments.

On cancer heterogeneity, is also focused the paper of Yi et al. Here the authors integrate omics approaches to profile multiple samples of endometrial tissues disclosing that amino acid and nucleotide metabolism have a crucial role in endometrial cancer (EC). The major strength of this work was the use of multiple samples that allowed the identification of a subset of putative metabolic biomarkers recognizable by using minimally invasive procedures.

Colorectal cancer (CRC) is a prevalent malignancy worldwide and metastasis to the liver and lung is common. Metabolic reprogramming has been implicated in CRC

progression and metastasis. In this Editorial, two recent studies shed light on the metabolic pathways involved in CRC and the potential therapeutic targets that may emerge from this research. Montero-Calle et al. investigated the metabolic and functional differences between two CRC cell lines with different metastatic organotropisms. The study identified several altered lipid metabolism-related targets, including LDLR, CD36, FABP4, SCD, AGPAT1, and FASN, which were associated with the prognosis of CRC patients. The study also found that CD36 was associated with lung metastatic tropism of CRC cells, validating the *in vivo* relevance of the findings. These results suggest specific metabolic adaptations for invasive cancer cells, which could serve as potential therapeutic targets.

In a second study, Hartal-Banishay et al. investigated the role of sterol regulatory element-binding proteins (SREBPs) in CRC proliferation. The study found that membrane-bound transcription factor protease 1 (MBTPS1) is critical for the proliferation of CRC cells. Inhibition of MBTPS1 activity decreased SREBP levels and cell proliferation in CRC-derived cell lines, while CRISPR/Cas9 KO of the MBTPS1 gene resulted in severely attenuated proliferation and downregulation of several energy metabolism pathways. These findings suggest that MBTPS1 plays a critical role in regulating colon cancer proliferation primarily through SREBP-associated lipid metabolism and may serve as a possible therapeutic target in CRC. Taken together, these studies highlight the importance of understanding the metabolic pathways involved in CRC progression and metastasis. The identification of specific metabolic targets, such as CD36 and MBTPS1, may lead to the development of novel therapeutic strategies for CRC.

Recently, several studies pointed out the role of Glutamine metabolism in fueling energy metabolism as well as in maintaining oxidative homeostasis. In this perspective, the review of Gong et al. emphasizes the molecular mechanisms that relate glutamine metabolism and oxidative homeostasis. Here the authors, underling the importance of redox homeostasis relying on glutamine metabolism in cancer cells, endorse the development and improvement of strategies aiming to interfere with this relationship.

A further emergent metabolic pathway that seems to have a key role in redox homeostasis is the glycolytic branch named Hexosamine Biosynthetic Pathway (HBP). That is the main theme of the work of Zerbato et al. that propose a strategy to improve cancer therapy in Pancreatic ductal adenocarcinoma. Authors point out that the use of a novel Phosphoglucomutase 3 (PGM3) enzyme inhibitor, named FR054, sensitizes cancer cells to Erastin treatment by altering the Unfolded Protein Response (UPR).

Wang et al. explored the correlation between ATP-binding cassette (ABC) transporters and immunomodulation in thyroid carcinoma (TC), using data from The Cancer Genome Atlas (TCGA) database. Five hallmark ABC transporters were identified as prognostic factors for TC and were associated with the relapse-free survival rates of patients. These transporters were found to modulate various aspects of immune cell infiltration, and their expression was affected by certain chemicals. Understanding the role of these transporters may lead to potential prognostic and immunotherapeutic strategies for TC.

Understanding metabolic changes during cancer treatments is crucial. Astrocytomas are the most common type of brain tumors, and radiotherapy (RT) is commonly used to treat them. However, monitoring treatment response using magnetic resonance imaging (MRI) only captures structural changes, while molecular changes may occur without visible structural changes. Ruiz-Rodado et al. used liquid chromatography mass spectrometry (LC/MS) and nuclear magnetic resonance (NMR) to identify plasma and tissue metabolic biomarkers of treatment response in a mouse model of astrocytoma undergoing RT. The results showed metabolic changes in mice that underwent RT, and identified fumarate as the best discriminatory feature in plasma. The study suggests these biomarkers could be validated in the clinic to improve the assessment of brain tumor patients throughout radiotherapy.

Lastly, an interesting review of Zhou et al. pointed out the role of human microbiome in maintaining metabolites homeostasis underlying a promising field of investigation. The authors critically discuss recent literature on tumor microbiome metabolism suggesting it as a novel player in the homeostasis of tumor microenvironment metabolites opening an innovative perspective to understand cancer progression and develop novel therapeutic opportunities.

Author contributions

All authors listed have made a substantial, direct, and intellectual contribution to the work, and approved it for publication.

Funding

For this work, DS was supported by the Department of Experimental and Clinical Medicine, Magna Græcia University of Catanzaro. The funders had no role in study design, data collection and analysis, decision to publish, or preparation of the manuscript.

Acknowledgments

We thank the authors and the reviewers of the articles published as a part of this Research Topic for their valuable contributions.

Conflict of interest

The authors declare that the research was conducted in the absence of any commercial or financial relationships that could be construed as a potential conflict of interest.

Publisher's note

References

1. DeBerardinis RJ, Chandel NS. Fundamentals of cancer metabolism. *Sci Adv* (2016) 2:e1600200. doi: 10.1126/sciadv.1600200

2. Stine ZE, Schug ZT, Salvino JM, Dang CV. Targeting cancer metabolism in the era of precision oncology. *Nat Rev Drug Discovery* (2022) 21:141–62. doi: 10.1038/s41573-021-00339-6

frontiers in Oncology

PERSPECTIVE
published: 16 February 2022
doi: 10.3389/fonc.2022.783908

Oscillations and Dynamic Symbiosis in Cellular Metabolism in Cancer

Takashi Amemiya[1*] *and Tomohiko Yamaguchi*[2]

[1] *Graduate School of Environment and Information Sciences, Yokohama National University (YNU), Yokohama, Japan,*
[2] *Meiji Institute for Advanced Study of Mathematical Sciences (MIMS), Nakano, Japan*

The grade of malignancy differs among cancer cell types, yet it remains the burden of genetic studies to understand the reasons behind this observation. Metabolic studies of cancer, based on the Warburg effect or aerobic glycolysis, have also not provided any clarity. Instead, the significance of oxidative phosphorylation (OXPHOS) has been found to play critical roles in aggressive cancer cells. In this perspective, metabolic symbiosis is addressed as one of the ultimate causes of the grade of cancer malignancy. Metabolic symbiosis gives rise to metabolic heterogeneities which enable cancer cells to acquire greater opportunities for proliferation and metastasis in tumor microenvironments. This study introduces a real-time new imaging technique to visualize metabolic symbiosis between cancer-associated fibroblasts (CAFs) and cancer cells based on the metabolic oscillations in these cells. The causality of cellular oscillations in cancer cells and CAFs, connected through lactate transport, is a key point for the development of this novel technique.

Keywords: metabolic oscillations, symbiosis, cancer, malignancy, heterogeneity

OPEN ACCESS

Edited by:
Tuuli Käämbre,
National Institute of Chemical Physics and Biophysics, Estonia

Reviewed by:
Aleksandr Klepinin,
National Institute of Chemical Physics and Biophysics, Estonia
Dongya Jia,
National Cancer Institute, United States

****Correspondence:***
Takashi Amemiya
amemiya-takashi-jk@ynu.ac.jp

Specialty section:
This article was submitted to Cancer Metabolism, a section of the journal Frontiers in Oncology

Received: *29 September 2021*
Accepted: *27 January 2022*
Published: *16 February 2022*

Citation:
Amemiya T and Yamaguchi T (2022) Oscillations and Dynamic Symbiosis in Cellular Metabolism in Cancer. Front. Oncol. 12:783908. doi: 10.3389/fonc.2022.783908

INTRODUCTION

Cancers are classified into more than one hundred types owing to different organs and tissues of origin, cellular shapes, and physiological characteristics (1: https://www.cancer.net/cancer-types). The cancer type determines the grade of malignancy which is diagnosed by parameters such as five-year survival rate, prognosis, and resistance to therapy. The famous statement by Bert Vogelstein, "Cancer is, in essence, a genetic disease" (2) is widely accepted and the grade of cancer malignancy is often discussed in relation to gene expression. However, frontiers of genetic studies have not yet uncovered the causes of variable malignancies in different cancers (3).

Other studies have focused on cancer metabolism (4) and consider cancers to be metabolic diseases (5). Cancer cells are metabolically reprogrammed and enhance glycolysis even under aerobic conditions known as the Warburg effect (6, 7). The Warburg effect indicates that cancer cells produce adenosine triphosphate (ATP) and other biomolecules with high efficiency (8) which is necessary for proliferation and metastasis—one of the hallmarks of cancer (9).

Thus, the grade of cancer malignancy can be explained by the Warburg effect. If we compare cancers in different organs using the five-year survival rates, defined as the percentage of people who live longer than five years following diagnosis (10), pancreatic (8.2%) and liver (17.6%) cancers with low five-year survival rates are reported to enhance glycolysis more than breast (89.7%) and prostate (98.6%) cancers that have high five-year survival rates (11). Even in the case of cancer cells in the

same type, for instance breast cancer, the cell lines with higher glycolysis rates are reported to be more malignant in terms of proliferation and metastasis (12). A review also reports that aerobic glycolysis is a crucial component of the malignant phenotype (13).

However, these studies are contradicted by big data analyses of approximately 10,000 malignant tumors using the Cancer Genome Atlas (14–16). The big data analyses obtained indexes that characterize the enhancement of the glycolytic pathway. The glycolysis score was obtained by using gene set variation analysis (GSVA) (16) and the hypoxia score was obtained by calculating mRNA-based signatures (15), see **Figure 1A** captions in detail. There is a reasonable correlation between these scores (**Figure 1A**).

In the present study, these scores were plotted as a function of the five-year cancer survival rate (10), as shown in **Figure 1B**. Notably, no negative correlation was observed between glycolysis scores and the five-year survival rate. The scores are very low for tumors with low five-year survival rates such as pancreatic (PAAD), liver (LIHC), lung (LUAD), esophagus (ESCA), glioma (LGG), and stomach (STAD) tumors. The above plot does not meet the expectation that the glycolysis scores of high-grade malignant cancers would be relatively high and that there should be a negative correlation between the glycolysis scores and the five-year survival rate. The reasons remain unknown why the pan-cancer analyses (15, 16) disagree with the widely accepted statement that "aerobic glycolysis is a crucial component of the malignant phenotype" (13).

SIGNIFICANCE OF MITOCHONDRIAL BIOGENESIS AND RESPIRATION

In addition to the Warburg effect, the past two decades have witnessed a significant role of OXPHOS and a hybrid of glycolysis and OXPHOS in cancer progression and metastasis (17–21). Emerging evidence shows that mitochondrial energy pathways are reprogrammed to meet the challenges of high energy demand and biomass synthesis (20, 21). For instance, both enhanced glycolytic and increased OXPHOS activities were

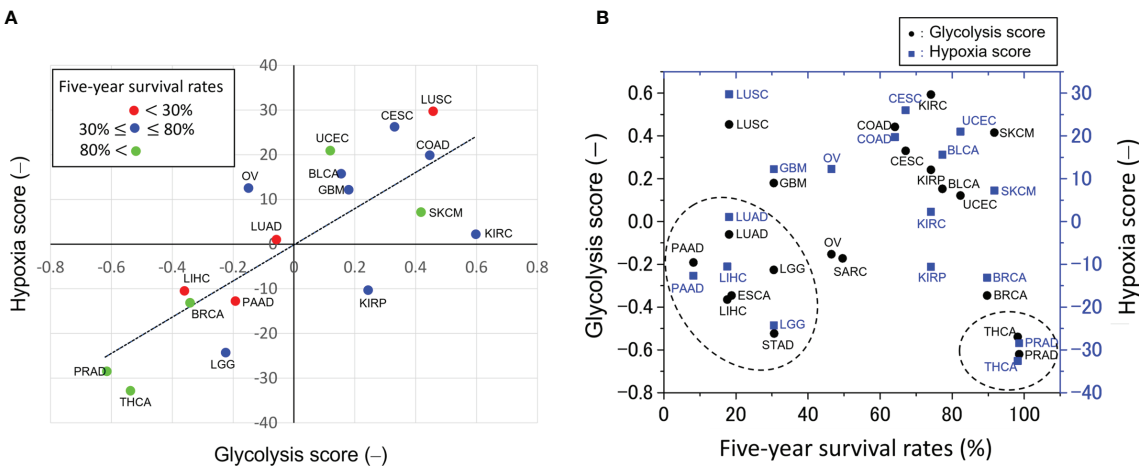

FIGURE 1 | Glycolytic activities across pan-cancers. **(A)** Correlation between glycolysis and hypoxia scores obtained from gene set variation analysis (16) and mRNA-based signatures (15), respectively. This plot was made from the median values of these scores taken from the literature. The straight line is the linear regression line and the decision coefficient is R^2 = 0.601. The glycolysis score in 9,229 tumors across 25 cancer types was calculated as follows (16): first, a 22-gene expression signature (SLC2A1, HK1, HK2, HK3, GPI, PFKL, PFKM, PFKP, ALDOA, ALDOB, ALDOC, TPI1, GAPDH, PGK1, PGAM1, PGAM4, ENO1, ENO2, ENO3, PKLR, PKM and LDHA) that belongs the glycolysis core pathway was selected in each sample; second, in order to classify the glycolytic status, a gene set variation analysis (GSVA) (16) was employed to calculate the GSVA score based on the 22-gene expression signature; third, this score was scaled from -1 to 1 to yield the glycolysis score. On the other hand, the hypoxia score in 8,006 tumors across 19 cancer types was calculated as follows (15): Level 3 mRNA abundance data for all genes in a hypoxia signature developed by Buffa et al. and others (15 and references therein) were extracted from each of the cancer types. Signature-specific mRNA abundance data from all 19 cancer types were joined and scored as one cohort to compare hypoxia across cancer types. Tumors with the top 50% of mRNA abundance values for each gene in a signature were given a score +1, and tumors with the bottom 50% of mRNA abundance values for that gene were given a score -1. This procedure was repeated for every gene in the signature to generate a hypoxia score for each subject by using each signature (15). **(B)** Relation between five-year survival rates, defined as the percentage of people who live longer than five years following diagnosis (10), and the glycolysis scores as shown in **(A)**. These scores of high-grade malignant tumors of low five-year survival rates, indicated by the dotted circle, are unexpectedly very low. The scores of low-grade malignant tumors, indicated by the dotted circle, such as THCA and PRAD are low. A negative correlation between the glycolysis scores and five-year survival rates cannot be seen because the scores of the high-grade malignant tumors are too low. The abbreviations of cancer types are as follows: BLCA, bladder urothelial carcinoma; BRCA, breast invasive carcinoma; CESC, cervical squamous cell carcinoma and endocervical adenocarcinoma; COAD, colon adenocarcinoma; ESCA, esophageal carcinoma; GBM, glioblastoma multiforme; KIRC, kidney renal clear cell carcinoma; KIRP, kidney renal papillary cell carcinoma; LICH, liver hepatocellular carcinoma; LGG, lower grade glioma; LUAD, lung adenocarcinoma; LUSC, lung squamous cell carcinoma; OV, ovarian serous cystadenocarcinoma; PAAD, pancreatic adenocarcinoma; PRAD, prostate adenocarcinoma; SARC, sarcoma; SKCM, skin cutaneous melanoma; STAD, stomach adenocarcinoma; THCA, thyroid carcinoma; UCEC, uterine corpus endometrial carcinoma.

exhibited in highly metastatic mouse breast cancer 4T1 cells as compared with its isogenic non-metastatic 67NR cells (22). Consistently, significantly higher mitochondrial activities were found in circulating tumor cells (CTCs) derived from 4T1 cells (23) with no observable decrease in glycolytic activity. This indicates a hybrid of glycolysis and OXPHOS, which was also found in SiHa human cervix squamous cell carcinoma cells (24). Theoretically, a mathematical model based on the regulatory network of glycolysis and OXPHOS has found three stable metabolic phenotypes, the Warburg state, the OXPHOS state, and the hybrid glycolysis/OXPHOS state (19). All these studies clearly demonstrate the crucial roles of mitochondrial OXPHOS in cancer metastasis, and indicate that cancer cells are able to acquire and switch between different metabolic phenotypes.

METABOLIC SYMBIOSIS IN CANCER AND GRADE OF CANCER MALIGNANCY

Metabolic symbiosis is probably one the leading mechanisms, which can answer the varied malignancy in cancers (25–28). Cancer-associated fibroblasts (CAFs) are one of the candidates for establishing metabolic symbiosis with cancer cells in complex microenvironments (20, 26, 27, 29). Two types of metabolic symbiosis occur: i) cancer cells enhance their glycolytic pathway and produce lactate which is received by CAFs and oxidized in the mitochondria; ii) CAFs enhance their glycolytic pathway and produce lactate which is received by cancer cells and oxidized in the mitochondria. The first type of metabolic symbiosis has been reported in the lung (30) and colorectal (31) cancers, whereas the second type has been reported in pancreatic (32), breast (26), cervical (31) and prostate (33) cancers. In addition, the later metabolic symbiosis is significant because it suggests a modification of the Warburg effect on malignant cancers (13, 34). Metabolic symbiosis has also been proposed to occur in the brain and muscle tissue *via* lactate transport. In the brain, this is referred to as the astrocyte-neuron lactate shuttle (ANLS) (35–37).

The mechanisms of metabolic symbiosis in cancer have been proposed based on the expression levels of enzymes and transporters, such as glucose transporter 1 (GLUT1) and monocarboxylate transporter 1 (MCT1) and 4 (MCT4), in cancer cells and CAFs as determined immunohistochemical analyses (26, 31–33).

In this study, a real-time new imaging technique to visualize metabolic symbiosis between CAFs and cancer cells based on the metabolic oscillations in these cells is demonstrated. The reverse Warburg effect (38) is an essential mechanism for metabolic symbiosis in cancer. The present real-time visualization of the two-compartment tumor metabolism (26) will allow us to measure the effectiveness of anticancer therapies and facilitate more personalized cancer treatments (27).

Furthermore, the present technique has the potential to reveal the spatiotemporal dynamics of metabolic symbiosis in tumor microenvironments where populations of CAFs and cancer cells may form a metabolic network. This method can clarify the time and spatial characteristics of metabolic symbiosis between CAFs and cancer cells in tumor microenvironments. Thus, the mechanism of two-compartment tumor metabolism (26, 27) can be extended to that of multiple-compartment or network-linked tumor metabolism.

Highly malignant cancers have the plasticity to change their metabolism to glycolytic (32, 39), oxidative (27, 40), and their hybrid (20, 21) depending on the experimental conditions or microenvironments. Thus, they can acquire metabolic heterogeneities that are closely connected with proliferation, metastasis, angiogenesis, drug resistance, and other aggressive behaviors of cancer cells (40); resulting in a low five-year survival rate (**Figure 1B**).

METABOLIC OSCILLATIONS IN CANCER AND OTHER CELLS

Metabolic oscillations, including glycolytic oscillations, can provide evidence of metabolic symbiosis between cancer cells and CAFs. The concentrations of all metabolites in the glycolytic pathway, such as glucose-6-phosphate, fructose 1,6-biphosphate, and pyruvate as well as ATP, adenosine diphosphate (ADP), nicotinamide adenine dinucleotide (NAD^+), and its reduced form (NADH) oscillate in the millimolar range with periods of a few tends of seconds, which is called glycolytic oscillation. This has been primarily studied in yeasts (17, 41–44). Yeasts enhance the glycolytic pathway even under aerobic conditions by short-term phenotypic adaptation, known as the Crabtree effect (45, 46). Many types of cancer cells also exhibit Crabtree in addition to the Warburg effect which is caused by genetic mutations that enhance glycolytic activity (47).

We focused on the metabolic similarity between yeast and cancer cells (47) and succeeded in observing glycolytic oscillations in individual HeLa cervical cancer cells in monolayers and in spheroids, and DU145 prostate cancer cells in monolayers (48–51). The median frequencies were 0.0703 Hz, 0.0342 Hz, and 0.0226 Hz for HeLa cells in spheroids, in monolayers, and DU145 cells in monolayers, respectively. On the other hand, their amplitudes of NADH fluorescence were nearly the same among these cells. These oscillations directly reflect enzymatic activities in the glycolytic pathway, thus can be a useful index for evaluating the Warburg effect in cancer cells (49, 50). So far, glycolytic oscillations have not been reported in cancer patients or in healthy people, and thus it is challenging to observe their oscillations *in vivo* and to characterize them across human cancer types.

Glycolytic oscillations in cancer cells were exhibited when glucose, as the only carbon source, was added to glucose-starved cells (48, 50). On the other hand, cancers prefer alternative nutrients, such as acetate and fatty acids, in addition to glucose as the source of ATP production (52–54). However, this is observed under nutrient-rich conditions, such as in conventional tissue culture conditions *in vitro* or *in vivo*. Under the experimental conditions of glycolytic oscillations, glucose is the only source of ATP production and thus we can exclude ATP production from fatty acids, acetate, or glutamine, which are oxidized in the tricarboxylic acid (TCA) cycle.

Mitochondrial membrane potential is also known to oscillate through glucose metabolism (55–57). In pancreatic β-cells, the interaction between glycolysis and mitochondrial oxidative phosphorylation affects metabolic oscillation and plays an important role in pulsatile insulin secretion (57, 58). However, in glucose-fermenting yeasts, glycolytic and mitochondrial interactions are not fully understood. In this context, an experimental study concluded that the mitochondria had little or no regulatory effect on glycolytic oscillations (55). In contrast, other experimental and modeling studies have addressed that glycolytic and mitochondrial processes influence each other through ATP and NADH production in both glycolytic and mitochondrial pathways (59, 60).

Little is known about the glycolytic and mitochondrial interactions in cancer cells when they exhibit glycolytic oscillations (48–50). We assume that extracellular glucose is metabolized to lactate through glycolysis and fermentation without entering the TCA cycle in glucose-starved cancer cells under the experimental conditions of glycolytic oscillations (48). This is due to several different reasons: The activity of the mitochondrial pyruvate carrier (MPC) is reported to be reduced in cancer cells (61), which mainly rely on glycolysis for ATP production when glucose is the only nutrient supply; A study using a genetically encoded biosensor, which enabled monitoring of the MPC activity in living cells, showed that the level of glucose-derived pyruvate that was converted into citrate in the TCA cycle was significantly lower in cancer cells than in normal cells (61); This is further validated by another study using ^{13}C NMR spectroscopy in living cancer cells (62); A review paper by McCommis and Finck (63) also reported evidence of the low activity of MPCs in various cancer cell lines and solid tumors (63); In addition, an LC-MS-based isotope tracer study showed that approximately 90–97% of pyruvate derived from extracellular glucose is metabolized to lactate whilst only 3.1–7.8% enters the TCA cycle in cancer cells (64).

A REAL-TIME NEW IMAGING TECHNIQUE TO VISUALIZE METABOLIC SYMBIOSIS BETWEEN CAFs AND CANCER CELLS BASED ON CAUSALITY BETWEEN GLYCOLYTIC AND MITOCHONDRIAL OSCILLATIONS

If metabolic symbiosis occurs between cancer cells and CAFs, the causality of the donor-acceptor relationship should exist through lactate transport. This metabolic causality is possibly recorded in the propagation of metabolic information from glycolytic oscillations to those in mitochondrial membrane potentials, as shown in **Figure 2A**. For example, in the case of symbiosis in pancreatic cancer, the following processes may occur chronologically: i) CAFs enhance the glycolytic pathway and may exhibit glycolytic oscillations; ii) lactate is produced from

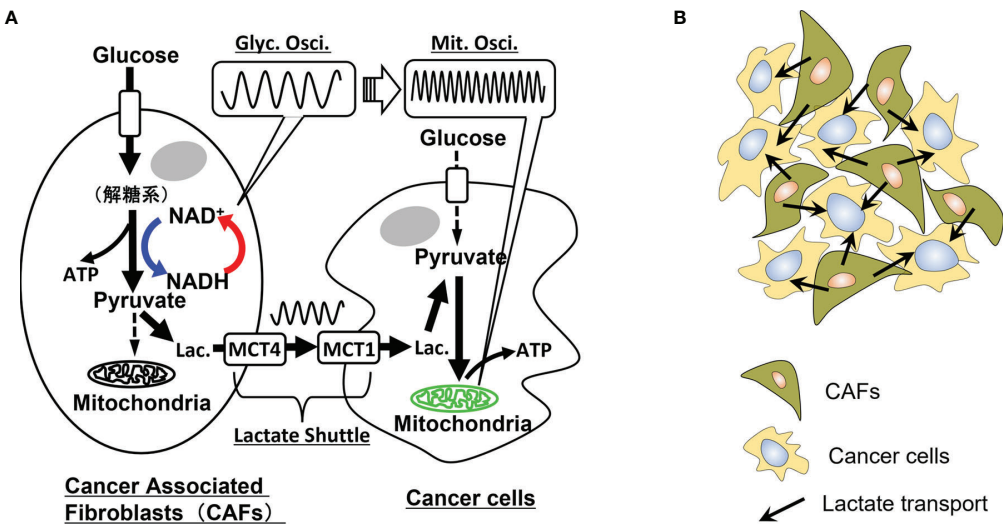

FIGURE 2 | Metabolic oscillations and dynamic symbiosis between cancer cells and cancer-associated fibroblasts (CAFs). **(A)** Oscillatory symbiosis. Glycolytic CAFs enhance the glycolytic pathway and produce lactate from glucose. This lactate is secreted through monocarboxylate transporter 4 (MCT4) of CAFs, received by an oxidative cancer cell through MCT1 and metabolized in mitochondria of the cancer cells (metabolic symbiosis). Oxidative cancers, such as pancreatic and liver cancer cells, may exhibit high-glycolytic activities without the symbiosis, however, parts of the cells may exhibit the reverse Warburg effect in tumor microenvironments. We assume that causality of donor-acceptor relationships should exist between the CAFs and cancer cells metabolically connected through the lactate shuttle. Thus, if these cells exhibit metabolic oscillations, causality analysis of glycolytic oscillations in CAFs and mitochondrial membrane potential oscillations in cancer cells may directly prove the metabolic symbiosis. Glyc. Osci., glycolytic oscillations; Mit. Osci., mitochondrial membrane potential oscillations; Lac., lactate. **(B)** Lactate transport in populations of CAFs and cancer cells. In an experimental system of co-culture of CAFs and cancer cells, a cancer cell is surrounded by some CAFs and receives lactate from them. Causality analysis of their oscillatory data can determine the donor-accepter relationship between the CAFs and the cancer cell, indicating their metabolic symbiosis.

the CAFs and excreted into the extracellular space through MCT4; iii) cancer cells incorporate this lactate through MCT1 and metabolize it in mitochondria; iv) mitochondrial membrane potential may exhibit oscillations accompanied by oxidative phosphorylation.

This series of processes can be monitored by the autofluorescence from NADH and fluorescence from membrane potential sensitive dyes, such as Rhodamine 123 and tetramethylrhodamine methyl ester (TMRM) (65), respectively. A more explicit way to monitor glycolytic and mitochondrial processes independently is to use genetically encoded ATP or NADH fluorescence resonance energy transfer (FRET)-based sensors (66–68). These methods enable us to monitor cytosolic or mitochondrial ATP and/or NADH concentration levels independently.

If the above series of metabolic dynamics is observed by these imaging techniques, and also causality between glycolytic oscillations in CAFs and mitochondrial oscillations in cancer cells is proved by a statistical analysis mentioned below, then it can be the direct evidence of metabolic symbiosis between cancer cells and CAFs. This result will directly prove that highly malignant cancers, such as PAAD, LUAD, LICH, ESCA, LGG, and STAD as shown in **Figure 1B**, are able to acquire and switch between different metabolic phenotypes.

CAUSALITY ANALYSIS

Cancer cells and CAFs are co-cultured in an experimental system for metabolic symbiosis as shown in **Figure 2B**. In this system, it is necessary to determine the donor-acceptor relationship between cancer cells and CAFs. For example, a cancer cell can receive lactate from surrounding CAFs or metabolize glucose by itself without receiving lactate from CAFs. In such circumstances, Granger causality analysis (69), convergent cross-mapping (CCM) (70), and other statistical analyses can be used to investigate the causality between many time series of oscillatory data.

For instance, let $x(t)$ be a time series of glycolytic oscillations in a cell of CAFs:

$$x(t) = \sum_{i=1}^{P} a_i x(t-i) + e_0(t), \tag{1}$$

where a_i is a constant, P is the time required to track back the data and $e_0(t)$ is a noise component. Equation 1 is an autoregressive model of $x(t)$ and represents $x(t)$ based on its past values. In addition, a time-series of mitochondrial membrane potential oscillations in a cancer cell, $y(t)$, can be given by equations (2) and (3):

$$y(t) = \sum_{i=1}^{P} b_i y(t-1) + e_1(t), \tag{2}$$

$$y(t) = \sum_{i=1}^{P} b_i y(t-i) + \sum_{i=1}^{P} a_i x(t-i) + e_2(t), \tag{3}$$

where b_i is a constant and $e_1(t)$ and $e_2(t)$ are noise components. Equation 3 expresses $y(t)$ using its past values, as well as those of $x(t)$. If causality exists from $x(t)$ to $y(t)$, the prediction accuracy of $y(t)$ is higher in Eq. (3) than that in Eq. (2). A multi-variable vector model can be used for a system of time-series data.

SUMMARY

This perspective study attempted to answer the following fundamental and unresolved question: Why does the grade of malignancy differ among cancer cell types? Neither advanced cancer genome studies nor cancer-metabolic studies have completely answered this question. In addition, even the Warburg effect, one of the hallmarks of cancer, cannot answer it consistently. In the present study, the leading role of metabolic symbiosis in cancer in the tumor microenvironment was addressed. Metabolic symbiosis offers metabolic heterogeneities in cancer cells in the tumor microenvironment, resulting in resistance to anti-cancer therapies, thereby increasing the grade of malignancy. We propose that a co-culture system of cancer cells and CAFs is a good *in vitro* model. Moreover, single-cell-level metabolic oscillations and their causality analysis can directly prove metabolic symbiosis in cancer. Real-time visualization of metabolic symbiosis in cancer will allow us to measure the effectiveness of anticancer therapies and facilitate more personalized cancer treatments (27). Our symbiotic model targets metabolic interactions between CAFs and cancer cells for therapeutic strategies, including suppression of oxidative stress from cancer cells to CAFs and inhibition of metabolite transport from CAFs to cancer cells by blocking MCTs (27, 40). Breaking the network of metabolic symbiosis may result in effective anticancer therapeutic outcomes.

DATA AVAILABILITY STATEMENT

Publicly available datasets were analyzed in this study. This data can be found here: https://ourworldindata.org/cancer-death-rates-are-falling-five-year-survival-rates-are-rising.

AUTHOR CONTRIBUTIONS

The idea for this study was conceived by TA and developed by TY. TA wrote the manuscript in consultation with TY and both authors contributed equally to the final manuscript.

FUNDING

This study was supported in part by JSPS KAKENHI Grant Numbers 19H04205 and 20K20631, a grant for a cooperative research project from YNU to TA and MEXT Promotion of Distinctive Joint Research Center Program Grant Number JPMXP0620335886 to TA and TY.

ACKNOWLEDGMENTS

The authors thank Editage (www.editage.com) for English language editing.

REFERENCES

1. National Cancer Institute. Available at: https://www.cancer.net/cancer-types.
2. Vogelstein B, Kinzler KW. Cancer Genes and the Pathways They Control. *Nat Med* (2004) 10:789–99. doi: 10.1038/nm1087
3. The ICGC/TCGA. Pan-Cancer Analysis of Whole Genomes Consortium. Pan-Cancer Analysis of Whole Genomes. *Nature* (2020) 578:82–93. doi: 10.1038/s41586-020-1969-6
4. Reyes MI, Chandel NS. Cancer Metabolism: Looking Forward. *Nat Rev Cancer* (2021) 16:1–12. doi: 10.1038/s41568-021-00378-6
5. Seyfried TN. *Cancer as a Metabolic Disease*. New Jersey: Wiley (2012).
6. Warburg O. Über Den Stoffwechsel Der Carcinomzelle. *Klin Wochenschr* (1925) 4:534–6. doi: 10.1007/BF01726151
7. Warburg O. On the Origin of Cancer Cells. *Science* (1956) 123:309–14. doi: 10.1126/science.123.3191.309
8. Vander Heiden MGV, Cantley LC, Thompson CB. Understanding the Warburg Effect: The Metabolic Requirements of Cell Proliferation. *Science* (2009) 324:1029–33. doi: 10.1126/science.1160809
9. Hanahan D, Weinberg RA. Hallmarks of Cancer: The Next Generation. *Cell* (2011) 144:646–74. doi: 10.1016/j.cell.2011.02.013
10. Ritchie H. *Cancer Death Rates Are Falling; Five-Year Survival Rates Are Rising in Our World Data* (2019). Available at: https://ourworldindata.org/cancer-death-rates-are-falling-five-year-survival-rates-are-rising.
11. Lehuédé C, Dupuy F, Rabinovitch R, Jones RG, Siegel PM. Metabolic Plasticity as a Determinant of Tumor Growth and Metastasis. *Cancer Res* (2016) 76:5201–8. doi: 10.1158/0008-5472.CAN-16-0266
12. Depaoli MR, Karsten F, Madreiter-Sokolowski CT, Klec C, Gottschalk B, Bischof H. Real-Time Imaging of Mitochondrial ATP Dynamics Reveals the Metabolic Setting of Single Cells. *Cell Rep* (2018) 25:501–12. doi: 10.1016/j.celrep.2018.09.027
13. Gatenby RA, Gillies RJ. Why Do Cancers Have High Aerobic Glycolysis? *Nat Rev Cancer* (2004) 4:891–9. doi: 10.1038/nrc1478
14. TCGA. *The Cancer Genome Atlas* (2021). Available at: http://cancergenome.nih.gov/.
15. Bhandari V, Hoey C, Liu LY, Lalonde E, Ray J, Livingstone J, et al. Molecular Landmarks of Tumor Hypoxia Across Cancer Types. *Nat Genet* (2019) 51:308–18. doi: 10.1038/s41588-018-0318-2
16. Wei J, Huang K, Chen Z, Hu M, Bai Y, Lin S, et al. Characterization of Glycolysis-Associated Molecules in the Tumor Microenvironment Revealed by Pan-Cancer Tissues and Lung Cancer Single Cell Data. *Cancers* (2020) 12:1788. doi: 10.3390/cancers12071788
17. WardPS, ThompsonCB. Metabolic Reprogramming: A Cancer Hallmark Even Warburg Did Not Anticipate. *Cancer Cell* (2012) 21:297–308. doi: 10.1016/j.ccr.2012.02.014
18. Pavlova NN, Thompson CB. The Emerging Hallmarks of Cancer Metabolism. *Cell Metab* (2016) 23:27–47. doi: 10.1016/j.cmet.2015.12.006
19. YuL, LuM, JiaD, MaJ, Ben-JacobE, LevineH, et al. Modeling the Genetic Regulation of Cancer Metabolism: Interplay Between Glycolysis and Oxidative Phosphorylation. *Cancer Res* (2017) 77:1564–74. doi: 10.1158/0008-5472.CAN-16-2074
20. Jia D, Park JH, Jung KH, Levine H, Kaipparettu. Elucidating the Metabolic Plasticity of Cancer: Mitochondrial Reprogramming and Hybrid Metabolic States. *Cells* (2018) 7:21. doi: 10.3390/cells7030021
21. Jia D, Lu M, Jung KH, Park JH, Yu L, Onuchic JN, et al. Elucidating Cancer Metabolic Plasticity by Coupling Gene Regulation With Metabolic Pathways. *Proc Natl Acad USA* (2019) 116:3909–18. doi: 10.1073/pnas.1816391116
22. Dupuy F, Tabariès S, Andrzejewski S, Dong Z, Blagih J, Annis MG, et al. PDK1-Dependent Metabolic Reprogramming Dictates Metastatic Potential in Breast Cancer. *Cell Metab* (2015) 22:577–89. doi: 10.1016/j.cmet.2015.08.007
23. LeBleu VS, O'Connell JT, Herrera KNG, Wikman-Kocher H, Pantel K, Haigis MC, et al. PGC-1α Mediates Mitochondrial Biogenesis and Oxidative Phosphorylation to Promote Metastasis. *Nat Cell Biol* (2014) 16:992–1003. doi: 10.1038/ncb3039
24. Porporato PE, Payen VL, Pérez-Escuredo J, De Saedeleer CJ, Danhier P, Copetti T, et al. A Mitochondrial Switch Promotes Tumor Metastasis. *Cell Rep* (2014) 8:754–66. doi: 10.1016/j.celrep.2014.06.043
25. Koukourakis MI, Giatromanolaki A, Harris AL, Sivridis E. Comparison of Metabolic Pathways Between Cancer Cells and Stromal Cells in Colorectal Carcinomas: A Metabolic Survival Role for Tumor-Associated Stroma. *Cancer Res* (2006) 66:632–7. doi: 10.1158/0008-5472.CAN-05-3260
26. SalemAF, Whitaker-MenezesD, LinZ, Martinez-OutschoornUE, TanowitzHB, A.-ZoubiMS, et al. Two-Compartment Tumor Metabolism Autophagy in the Tumor Microenvironment and Oxidative Mitochondrial Metabolism (OXPHOS) in Cancer Cells. *Cell Cycle* (2012) 11(13):2545–56. doi: 10.4161/cc.20920
27. Martinez-Outschoorn UE, Sotgia F, Lisanti MP. Power Surge: Supporting Cells "Fuel" Cancer Cell Mitochondria. *Cell Metab* (2012) 15:4–5. doi: 10.1016/j.cmet.2011.12.011
28. Nakajima EC, Van Houten B. Metabolic Symbiosis in Cancer: Refocusing the Warburg Lens. *Mol Carcinog* (2013) 52:329–37. doi: 10.1002/mc.21863
29. Kim J, DeBerardinis RJ. Mechanisms and Implications of Metabolic Heterogeneity in Cancer. *Cell Metab* (2019) 30:434–46. doi: 10.1016/j.cmet.2019.08.013
30. Koukourakis MI, Giatromanolaki A, Bougioukas G, Sivridis E. Lung Cancer: A Comparative Study of Metabolism Related Protein Expression in Cancer Cells and Tumor Associated Stroma. *Cancer Biol Ther* (2007) 6:1476–9. doi: 10.4161/cbt.6.9.4635
31. Sonveaux P, Végran F, Schroeder T, Wergin MC, Verrax J, Rabbani ZN, et al. Targeting Lactate-Fueled Respiration Selectively Kills Hypoxic Tumor Cells in Mice. *J Clin Invest* (2008) 118:3930–42. doi: 10.1172/JCI36843
32. Cao L, Wu J, Qu X, Sheng J, Cui M, Liu S, et al. Glycometabolic Rearrangements–Aerobic Glycolysis in Pancreatic Cancer: Causes, Characteristics and Clinical Applications. *J Exp Clin Cancer Res* (2020) 39:267. doi: 10.1186/s13046-020-01765-x
33. Pértega-Gomes N, Vizcaíno JR, Attig J, Jurmeister S, Lopes C, Baltazar F. A Lactate Shuttle System Between Tumour and Stromal Cells Is Associated With Poor Prognosis in Prostate Cancer. *BMC Cancer* (2014) 14:352. doi: 10.1186/1471-2407-14-352
34. Cascone T, McKenzie JA, Mbofung RM, Punt S, Wang Z, Xu C, et al. Increased Tumor Glycolysis Characterizes Immune Resistance to Adoptive T Cell Therapy. *Cell Metab* (2018) 27:977–87. doi: 10.1016/j.cmet.2018.02.024
35. Pérez-Escuredo J, Van Hée VF, Sboarina M, Falces J, Payen VL, Pellerin L, et al. Monocarboxylate Transporters in the Brain and in Cancer. *Biochim Biophys Acta* (2016) 1863:2481–97. doi: 10.1016/j.bbamcr.2016.03.013
36. Whitaker-Menezes D, Martinez-Outschoorn UE, Lin Z, Ertel A, Flomenberg N, Witkiewicz AK, et al. Evidence for a Stromal-Epithelial "Lactate Shuttle" in Human Tumors: MCT4 Is a Marker of Oxidative Stress in Cancer-Associated Fibroblasts. *Cell Cycle* (2011) 10:1772–83. doi: 10.4161/cc.10.11.15659
37. Pellerin L, Magistretti PJ. Glutamate Uptake Into Astrocytes Stimulates Aerobic Glycolysis: A Mechanism Coupling Neuronal Activity to Glucose Utilization. *Proc Natl Acad Sci USA* (1994) 91:10625–9. doi: 10.1073/pnas.91.22.10625
38. Pavlides S, Whitaker-Menezes D, Castello-Cros R, Flomenberg N, Witkiewicz AK, Frank PG, et al. The Reverse Warburg Effect: Aerobic Glycolysis in Cancer Associated Fibroblasts and the Tumor Stroma. *Cell Cycle* (2009) 8:3984–4001. doi: 10.4161/cc.8.23.10238
39. Lee NCW, Carella MA, Papa S, Bubici C. High Expression of Glycolytic Genes in Cirrhosis Correlates With the Risk of Developing Liver Cancer. *Front Cell Dev Biol* (2018) 6:138. doi: 10.3389/fcell.2018.00138
40. Fu Y, Liu S, Yin S, Niu W, Xiong W, Tan M, et al. The Reverse Warburg Effect Is Likely to Be an Achilles' Heel of Cancer That Can Be Exploited for Cancer Therapy. *Oncotarget* (2017) 8:57813–25. doi: 10.18632/oncotarget.18175
41. Amemiya T, Obase K, Hiramatsu N, Itoh K, Shibata K, Takinoue M, et al. Collective and Individual Glycolytic Oscillations in Yeast Cells Encapsulated in Alginate Microparticles. *Chaos* (2015) 25:064606. doi: 10.1063/1.4921692
42. Mojica-Benavides M, van Niekerk DD, Mijalkov M, Snoep JL, Mehlig B, Volpe G, et al. Intercellular Communication Induces Glycolytic Synchronization Waves Between Individually Oscillating Cells. *Proc Natl Acad Sci USA* (2021) 118:e2010075118. doi: 10.1073/pnas.2010075118
43. Danø S, Sørensen PG, Hynne F. Sustained Oscillations in Living Cells. *Nature* (1999) 402:320–2. doi: 10.1038/46329
44. Weber A, Zuschratter W, Hauser MJB. Partial Synchronisation of Glycolytic Oscillations in Yeast Cell Populations. *Sci Rep* (2020) 10:19714. doi: 10.1038/s41598-020-76242-8

45. Crabtree HG. Observations on the Carbohydrate Metabolism of Tumours. *Biochem J* (1929) 23:536–45. doi: 10.1042/bj0230536
46. Ibsen KH. The Crabtree Effect: A Review. *Cancer Res* (1961) 21:829–41.
47. Diaz-Ruiz R, Rigoulet M, Devin A. The Warburg and Crabtree Effects: On the Origin of Cancer Cell Energy Metabolism and of Yeast Respiration. *Biochim Biophys Acta* (2011) 1807:568–76. doi: 10.1016/j.bbabio.2010.08.010
48. Amemiya T, Shibata K, Itoh Y, Itoh K, Watanabe M, Yamaguchi T. Primordial Oscillations in Life: Direct Observation of Glycolytic Oscillations in Individual HeLa Cervical Cancer Cells. *Chaos* (2017) 27:104602. doi: 10.1063/1.4986865
49. Amemiya T, Shibata K, Du Y, Nakata S, Yamaguchi T. Modeling Studies of Heterogeneities in Glycolytic Oscillations in HeLa Cervical Cancer Cells. *Chaos* (2019) 29:033132. doi: 10.1063/1.5087216
50. Amemiya T, Shibata K, Watanabe M, Nakata S, Nakamura K, Yamaguchi T. *Glycolytic Oscillations in Cancer Cells in Physics of Biological Oscillators*. In: Stefanovska A, McClintock PVE, editors. Switzerland: Springer (2021). p. 245–59.
51. Amemiya T, Shibata K, Yamaguchi T. Glycolytic Oscillations in Cancer Cells and Their Application to Diagnosis of Grade of Cancer Malignancy. *J Clin Exp Med* (2021) 279:183–7.
52. Koundouros N, Poulogiannis G. Reprogramming of Fatty Acid Metabolism in Cancer. *Br J Cancer* (2020) 122:2–22. doi: 10.1038/s41416-019-0650-z
53. Bose S, Ramesh V, Locasale JW. Acetate Metabolism in Physiology, Cancer, and Beyond. *Trend Cell Biol* (2019) 29:695–703. doi: 10.1016/j.tcb.2019.05.005
54. Mashimo T, Pichumani K, Vemireddy V, Hatanpp KJ, Singh DK, Sirasanagandla S, et al. Acetate Is a Bioenergetic Substrate for Human Glioblastoma and Brain Metastases. *Cell* (2014) 159:1603–14. doi: 10.1016/j.cell.2014.11.025
55. Andersen AZ, Poulsen AK, Brasen JC, Olsen LF. On-Line Measurements of Oscillating Mitochondrial Membrane Potential in Glucose-Fermenting Saccharomyces Cerevisiae. *Yeast* (2007) 24:731–9. doi: 10.1002/yea.1508
56. Aon MA, Cortassa S, Marban E, O'Rourke B. Synchronized Whole Cell Oscillations in Mitochondrial Metabolism Triggered by a Local Release of Reactive Oxygen Species in Cardiac Myocytes. *J Biol Chem* (2003) 278 (45):44735–44. doi: 10.1074/jbc.M302673200
57. Bertram R, Satin LS, Pedersen MG, Luciani DS, Sherman A. Interaction of Glycolysis and Mitochondrial Respiration in Metabolic Oscillations of Pancreatic Islets. *Biophys J* (2007) 92:1544–55. doi: 10.1529/biophysj.106.097154
58. Benninger RKP, Piston DW. Cellular Communication and Heterogeneity in Pancreatic Islet Insulin Secretion Dynamics. *Trends Endocrinol Metab* (2014) 25:399–406. doi: 10.1016/j.tem.2014.02.005
59. Aon MA, Cortassa S, Westerhoff HV, Berden JA, Van Spronsen E, Van Dam K. Dynamic Regulation of Yeast Glycolytic Oscillations by Mitochondrial Functions. *J Cell Sci* (1991) 99:325–34. doi: 10.1242/jcs.99.2.325
60. Lancaster G, Suprunenko YF, Jenkins K, Stefanovska A. Modelling Chronotaxicity of Cellular Energy Metabolism to Facilitate the Identification of Altered Metabolic States. *Sci Rep* (2016) 6:29584. doi: 10.1038/srep29584
61. Compan V, Pierredon S, Vanderperre B, Krznar P, Marchiq I, Zamboni N, et al. Monitoring Mitochondrial Pyruvate Carrier Activity in Real Time Using a BRET-Based Biosensor: Investigation of the Warburg Effect. *Mol Cell* (2015) 59:491–501. doi: 10.1016/j.molcel.2015.06.035
62. Yang C, Harrison C, Jin ES, Chuang DT, Sherry AD, Malloy CR, et al. Simultaneous Steady-State and Dynamic ^{13}C NMR Can Differentiate Alternative Routes of Pyruvate Metabolism in Living Cancer Cells. *J Biol Chem* (2014) 289:6212–24. doi: 10.1074/jbc.M113.543637
63. McCommis KS, Finck BN. Mitochondrial Pyruvate Transport: A Historical Perspective and Future Research Directions. *Biochem J* (2015) 466:443–54. doi: 10.1042/BJ20141171
64. Fan J, Kamphorst JJ, Mathew R, Chung MK, White E, Shlomi T, et al. Glutamine-Driven Oxidative Phosphorylation Is a Major ATP Source in Transformed Mammalian Cells in Both Normoxia and Hypoxia. *Mol Syst Biol* (2013) 9:712. doi: 10.1038/msb.2013.65
65. Lemasters JJ, Ramshesh VK. Imaging of Mitochondrial Polarization and Depolarization With Cationic Fluorophores. *Methods Cell Biol* (2007) 80:283–95. doi: 10.1016/S0091-679X(06)80014-2
66. Imamura H, Nhat KP, Togawa H, Saito K, Iino R, Kato-Yamada Y, et al. Visualization of ATP Levels Inside Single Living Cells With Fluorescence Resonance Energy Transfer-Based Genetically Encoded Indicators. *Proc Natl Acad Sci USA* (2009) 106:15651–6. doi: 10.1073/pnas.0904764106
67. Surin AM, Khiroug S, Gorbacheva LR, Khodorov BI, Pinelis VG, Khiroug L. Comparative Analysis of Cytosolic and Mitochondrial ATP Synthesis in Embryonic and Postnatal Hippocampal Neuronal Cultures. *Front Mol Neurosci* (2012) 5:102. doi: 10.3389/fnmol.2012.00102
68. Díaz-García CM, Mongeon R, Lihmann C, Koveal D, Zucker H, Yellen G. Neuronal Stimulation Triggers Neuronal Glycolysis and Not Lactate Uptake. *Cell Metab* (2017) 26:361–74. doi: 10.1016/j.cmet.2017.06.021
69. Nicolaou N, Constandinou TG. A Nonlinear Causality Estimator Based on Non-Parametric Multiplicative Regression. *Front Neuroinform* (2016) 10:19:19. doi: 10.3389/fninf.2016.00019
70. Ye H, Deyle ER, Gilarranz LJ, Sugihara G. Distinguishing Time-Delayed Causal Interactions Using Convergent Cross Mapping. *Sci Rep* (2015) 5:14750. doi: 10.1038/srep14750

Conflict of Interest: The authors declare that the research was conducted in the absence of any commercial or financial relationships that could be construed as a potential conflict of interest.

Publisher's Note: All claims expressed in this article are solely those of the authors and do not necessarily represent those of their affiliated organizations, or those of the publisher, the editors and the reviewers. Any product that may be evaluated in this article, or claim that may be made by its manufacturer, is not guaranteed or endorsed by the publisher.

frontiers | Frontiers in Oncology

ORIGINAL RESEARCH
published: 29 April 2022
doi: 10.3389/fonc.2022.861142

Multi-Omic Profiling of Multi-Biosamples Reveals the Role of Amino Acid and Nucleotide Metabolism in Endometrial Cancer

Runqiu Yi[1], *Liying Xie*[1], *Xiaoqing Wang*[2], *Chengpin Shen*[2], *Xiaojun Chen*[1]* *and Liang Qiao*[1]*

[1] Department of Chemistry, Shanghai Stomatological Hospital, and Obstetrics and Gynecology Hospital of Fudan University, Fudan University, Shanghai, China, [2] Shanghai Omicsolution Co., Ltd., Shanghai, China

Background: Endometrial cancer (EC) is one of the most common gynecological cancers. The traditional diagnosis of EC relies on histopathology, which, however, is invasive and may arouse tumor spread. There have been many studies aiming to find the metabolomic biomarkers of EC to improve the early diagnosis of cancer in a non-invasive or minimally invasive way, which can also provide valuable information for understanding the disease. However, most of these studies only analyze a single type of sample by metabolomics, and cannot provide a comprehensive view of the altered metabolism in EC patients. Our study tries to gain a pathway-based view of multiple types of samples for understanding metabolomic disorders in EC by combining metabolomics and proteomics.

Methods: Forty-four EC patients and forty-three controls were recruited for the research. We collected endometrial tissue, urine, and intrauterine brushing samples. Untargeted metabolomics and untargeted proteomics were both performed on the endometrial tissue samples, while only untargeted metabolomics was performed on the urine and intrauterine brushing samples.

Results: By integrating the differential metabolites and proteins between EC patients and controls detected in the endometrial tissue samples, we identified several EC-related significant pathways, such as amino acid metabolism and nucleotide metabolism. The significance of these pathways and the potential of metabolite biomarker-based diagnosis were then further verified by using urine and intrauterine brushing samples. It was found that the regulation of metabolites involved in the significant pathways showed similar trends in the intrauterine brushings and the endometrial tissue samples, while opposite trends in the urine and the endometrial tissue samples.

Conclusions: With multi-omics characterization of multi-biosamples, the metabolomic changes related to EC are illustrated in a pathway-based way. The network of altered metabolites and related proteins provides a comprehensive view of altered metabolism in the endometrial tissue samples. The verification of these critical pathways by using urine

OPEN ACCESS

Edited by:
Yongmei Song,
Peking Union Medical College Hospital (CAMS), China

Reviewed by:
Shuhai Lin,
Xiamen University, China
Elavarasan Subramani,
University of Texas MD Anderson Cancer Center, United States

***Correspondence:**
Liang Qiao
liang_qiao@fudan.edu.cn
Xiaojun Chen
cxjlhjj@163.com

Specialty section:
This article was submitted to Cancer Metabolism, a section of the journal Frontiers in Oncology

Received: *24 January 2022*
Accepted: *01 April 2022*
Published: *29 April 2022*

Citation:
Yi R, Xie L, Wang X, Shen C, Chen X and Qiao L (2022) Multi-Omic Profiling of Multi-Biosamples Reveals the Role of Amino Acid and Nucleotide Metabolism in Endometrial Cancer. Front. Oncol. 12:861142. doi: 10.3389/fonc.2022.861142

and intrauterine brushing samples provides evidence for the possible non-invasive or minimally invasive biopsy for EC diagnosis in the future.

Keywords: endometrial cancer, biomarkers, metabolic pathways, metabolomics, proteomics

INTRODUCTION

Endometrial cancer (EC) is one of the most common cancers among women in the world. According to the latest statistics, EC accounted for 417,367 new cases and 97,370 deaths in 2020 worldwide (1). Risk factors like obesity (2), diabetes (3), and hypertension (4) have been found to relate to the occurrence and deterioration of EC, but the pathogenesis of EC is still unclear. Histopathology is the gold standard for tumor diagnosis, but is less efficient in the detection of small lesions (5). Moreover, the traditional histopathology methods require complex operations, which are highly invasive and may arouse tumor spread (6). Finding biomarkers for EC can support early screening, diagnosis, or postoperative follow-up in a non-invasive or minimally invasive way. It has been reported that the increase of serum cancer antigen 125 (CA125) is a sign of several types of cancers including EC (7), but is not specific for any of the cancers. The lack of specific screening methods, the lack of non-invasive diagnostic methods, and the lack of comprehensive understanding of pathogenesis for EC are the major current problems in the study, detection, and treatment of EC.

The quantitative characterization of metabolites involved in various metabolism pathways can reveal the dynamic status of investigated systems, and provide opportunities for finding disease biomarkers and investigating disease mechanisms (8). Previous studies on EC metabolomics mainly measured a single type of biosample, such as tissue (9, 10), plasma (11–16), serum (15, 17–24), urine (25), and cervicovaginal fluids (26), focusing on the up- or down-regulation of specific compounds or the selection of a group of compounds for building diagnostic models. Though many promising results have been achieved in identifying metabolite biomarkers of EC, especially lipids, hormones, and amino acids (27), the inconsistency among various biosamples in the studies was not taken into consideration, and it is still unclear how metabolomic pathways are perturbed in EC (28, 29). Since metabolites are the very downstream compounds in the metabolic process and one metabolite may participate in several reactions, the dysregulation of a specific metabolite may result from various processes, making it difficult to identify the real alteration of metabolic pathways in EC solely by metabolomic analysis. The current limitation of untargeted metabolomics on compound identification (30) requires the utilization of other techniques, e.g., proteomics, to fetch up. As demonstrated in studies on other diseases like COVID-19, multi-omics analyses can facilitate the understanding of metabolic changes related to pathogenesis (31), and multi-organ analyses can provide a comprehensive landscape of the corresponding disease (32).

In this work, we performed multi-omics analysis for characterizing multiple types of clinical samples to study the perturbation of metabolomic pathways in EC. By integrating metabolomics with proteomics, a more credible explanation for the metabolic dysregulation of EC was achieved in a pathway-based way. By combining and comparing the results of multi-biosamples, the selected dysregulated pathways were further verified, and the potential of non-invasive or minimal invasive diagnosis of EC based on metabolite biomarkers was assessed. Forty-four EC patients and forty-three controls were recruited for this research. The endometrial tissue, urine, and intrauterine brushing samples were collected for proteomic and metabolomic analysis. Intrauterine brushings are bioliquid samples collected by aspiration biopsy using special brushes, containing a mixture of endometrial cells, blood cells, and surrounding secretion. Based on the differential metabolites and proteins between EC patients and controls detected in the endometrial tissue samples, EC-related significant pathways, such as amino acid metabolism and nucleotide metabolism, were identified. Then, the significance of the pathways was further evaluated using the urine and intrauterine brushing samples. The up- and down-regulation of the differential metabolites were compared among tissue, urine, and intrauterine brushing samples to illustrate the diversity of metabolism in multi-biosamples. The regulation of metabolites in the intrauterine brushings showed similar trends to that in the endometrial tissue, while the regulation of metabolites in the urine showed opposite trends compared to the tissue. We also demonstrated the potential of non-invasive or minimally invasive biopsy for EC diagnosis using the identified metabolic biomarkers with urine or intrauterine brushing samples.

MATERIALS AND METHODS

Chemicals

Acetonitrile (ACN), formic acid (FA), methanol, and deionized water were all HPLC grade, from Merck (Darmstadt, Germany). Phosphate buffered saline (PBS) and sodium dodecyl sulfate (SDS) were from Solarbio (Beijing, China). Analytical reagent grade acetone was from Sinopharm (Shanghai, China). Iodoacetamide (IAA), trizma base, urea, and C18 ZipTip were from Sigma-Aldrich (Darmstadt, Germany). Proteome grade trypsin was from Promega (Madison, WI, USA). Bond-breaker TCEP solution (0.5 M), triethylammonium bicarbonate (TEAB), protease inhibitor cocktail (EDTA-free, 100X), Pierce enhanced bicinchoninic acid (BCA) protein assay kit, and Pierce quantitative colorimetric peptide assay kit (23275) were from Thermo Fisher Scientific (San Jose, CA, USA).

Clinical Sample Collection and Preparation

The enrolled EC patients were all suffering from type I endometrial carcinoma, or more specifically, grade 1 and grade 2 endometrioid endometrial carcinoma. The enrolled

controlsall had a normal state of endometrium, but suffered from gynecological diseases including hysteromyoma, cyst, endometrial polyps, and cervix diseases.

Endometrial tissues were collected after surgical intervention. Each tissue sample (about 50 mg) was placed in a sterile container, properly labeled, and stored at −80°C immediately after sample collection. Urine specimens were collected in the morning before the day of the surgical operation and after the subjects had fasted for 10–12 h (33). The second micturition was collected for each subject and aliquots (about 5 ml) were stored at −80°C. Intrauterine brushings were collected using a special hollow tube with a brush, as a mixture of endometrial cells, blood cells, and surrounding secretion by aspiration biopsy. The mixture was then added with 1 ml of ice-cold 80% methanol/water immediately and stored at −80°C.

Metabolite Extraction

Ice-cold 80% methanol/water was used as extracting solution to extract metabolites. Concretely, 50 mg of thawed tissue sample was added with 1 ml extracting solution and then ground thoroughly. Thawed urine (200 µl) was added with 800 µl of extracting solution and vortexed for 15 s. The processed tissue and urine samples were stored at −80°C overnight for a thorough extraction of metabolites. Intrauterine brushings had already been added with the extracting solution during collection and stored at −80°C before further steps. All the liquid mixtures of different biosamples were then thawed and centrifuged (12,000 rpm, 5 min, 4°C). The supernatant was lyophilized and stored at −80°C until measurement.

Protein Extraction, Digestion, and Quantification

Tissue samples were rinsed by PBS, ground thoroughly, and resuspended in a lysis solution (8 µl per 1-mg sample) containing 1% SDS, 8 M urea, and 1× protease inhibitor cocktail in deionized water. Samples were then sonicated for 30 min in an ice-water bath using an ultrasonic cell homogenizer (Ningbo Scientz Biotechnology, Ningbo, China) with the working power ≤ 47.5 W to avoid bubble formation. Protein extracts were obtained after centrifugation (15,000 rpm, 15 min, 4°C) and the protein level in the supernatant was determined by the Pierce BCA protein assay kit. One hundred micrograms of protein per sample was transferred into a new centrifuge tube, and the final volume was adjusted to 100 µl with 8 M urea. Two microliters of 0.5 M TCEP was added and the sample was incubated at 37°C for 1 h, and then 4 µl of 1 M IAA was added to the sample and the incubation lasted for 40 min protected from light at room temperature. After that, five volumes of −20°C pre-chilled acetone was added to precipitate the proteins overnight at −20°C. The precipitates were washed twice with 1 ml of pre-chilled 90% acetone aqueous solution and then re-dissolved in 100 µl of 100 mM TEAB. Proteome grade modified trypsin was added at the ratio of 1:50 (enzyme:protein, weight:weight) to digest the proteins at 37°C overnight. The peptide mixture was desalted by C18 ZipTip, quantified by Pierce quantitative colorimetric peptide assay, and then lyophilized.

LC-MS/MS Analysis

For untargeted metabolomic analysis, three replicated injections were performed for each sample. The metabolites were analyzed by an ESI-Q-TOF mass spectrometer (SCIEX TripleTOF 4600, USA) coupled with an LC-20A HPLC system (Shimadzu, Tokyo, Japan). Each lyophilized sample was re-dissolved in 100 µl of 95% solvent A (0.1% FA in water) and centrifuged (8,000 rpm, 20 min, 4°C) to remove the insoluble constituents. Five microliters of the extracted metabolite sample were loaded by an autosampler, and the metabolites were separated by a Waters ACQUITY UPLC HSS T3 C18 column (100 × 2.1 mm, 1.8 µm, Waters, Milford, MA, USA) with the flow rate of 0.2 ml/min. Water (containing 0.1% FA) and ACN were used as solvent A and B, respectively, with the gradient elution program as follows: 0–6–11–13–15–20–30–30–40 min, 5%–25%–35%–40%–55%–95%–95%–5%–5% of solvent B. The ESI-Q-TOF was run in information-dependent acquisition (IDA) mode with parameters optimized as follows: (1) MS: ion spray voltage = +5,500 V; scan range = 50–1,000 m/z; precursor ions = 15; excluding precursor for 3 s; enabling dynamic background subtraction; (2) MS/MS: collision energy = 45 eV.

For untargeted proteomic analysis, the peptides were re-dissolved in solvent A (0.1% FA in water) to reach the concentration of 0.5 µg/µl and analyzed by online nanospray LC-MS/MS with an Orbitrap Fusion™ Lumos™ Tribrid™ mass spectrometer (Thermo Fisher Scientific, MA, USA) coupled to an EASY-nanoLC 1200 system (Thermo Fisher Scientific, MA, USA). The peptide sample (3 µl) was loaded onto an analytical column (Acclaim PepMap C18, 75 µm x 25 cm) and separated with a 120-min gradient. The column flow rate was maintained at 600 nl/min with a column temperature of 40°C. Water and ACN (both containing 0.1% FA) were used as solvent A and B, respectively, with the gradient elution program as follows: 0–4–80–110–112–120 min, 4%–7%–20%–30%–90%–90% of solvent B. The electrospray voltage of 2 kV versus the inlet of the mass spectrometer was used. The mass spectrometer was run under data independent acquisition mode and automatically switched between the MS and MS/MS modes. The parameters were as follows: (1) MS: scan range (m/z) = 350–1500; resolution = 120,000; AGC target = 4e5; maximum injection time = 50 ms; (2) HCD-MS/MS: resolution = 30,000; AGC target = 2e5; collision energy = 32; (3) DIA: variable isolation window; each window overlapping 1 m/z; window number = 60.

Different strategies were utilized for the quality control (QC) of untargeted metabolomic and proteomic analyses. For metabolomic analysis, a mixed QC sample by taking a small volume of each experimental sample served as a technical replicate throughout the data acquisition in three respective batches (tissue, urine, and intrauterine brushings). The EC and control samples were analyzed alternately in a randomized order with 3 replicates of each sample, while QC samples were injected at the beginning of each analytical batch, every 6 samples, and at the end of each analytical batch.

For proteomic analysis, QuiC (Biognosys AG, Switzerland) was used to evaluate MS stability. Full peak width at half maximum (FWHM), retention time (RT), and peak capacity of LC, as well as MS1 area, MS1/MS2 mass accuracy, MS1/MS2 scan intensity, and TIC of MS were calculated to assess the stability of measurement. Coefficient of variation, data

completeness, heatmap of intensity, and consistency of identification were visualized to demonstrate the quality of the data.

Data Analysis

For untargeted metabolomic analysis, raw data were converted to mzXML by MSConvert software (34) and then processed with R package XCMS (35). The retention time range for extraction was set as 0–20 min. The generated matrices of mass spectral features included information on m/z value, retention time, and peak intensity. MS1 signal intensities were then normalized by the summation of all peaks for an individual sample to calculate relative quantity and were performed with log transformation and auto scaling to form the matrices for subsequent statistical analysis. Univariate and multivariate statistical analyses were done by MetaboAnalyst 5.0 (http://www.metaboanalyst.ca) (36). VIP values in PLS-DA models and the *p*-values from *t*-tests on the normalized peak intensities were used to select differential features, the rule of which was VIP > 1 or $p < 0.05$. The structural identification of differential metabolites was performed by MetDNA (http://metdna.zhulab.cn/) (37), including accurate mass, MS/MS spectra, and online databases: METLIN (http://www.metlin.scripps.edu) (38).

For untargeted proteomic analysis, raw data of DIA were processed and analyzed by Spectronaut 14 (Biognosys AG, Switzerland) with default settings, and the retention time prediction type was set to dynamic iRT. Data extraction was determined based on extensive mass calibration. The ideal extraction window was determined dynamically depending on iRT calibration and gradient stability. *Q*-value (FDR) cutoff on precursor and protein level was applied as 1%. Decoy generation was set to mutate. All selected precursors passing the filters were used for quantification. MS2 interference will remove all interfering fragment ions except for the 3 least interfering ones. The average of the top 3 filtered peptides, which passed the 1% *Q*-value (FDR) cutoffs, was used as the major group quantities. The quantitative data were local normalized before statistical analysis. After Welch's ANOVA test, differently expressed proteins were filtered with *p*.adj value < 0.05 and fold change > 1.5.

Multivariant statistical analyses, e.g., principal component analysis (PCA) and partial least squares-discriminant analysis (PLS-DA), of metabolomic and proteomic data were performed using MetaboAnalyst 5.0. Pathway analysis and enrichment analysis of metabolomic data were performed using MetaboAnalyst 5.0. Functional annotation of proteins was carried out based on the euKaryotic orthologous groups of proteins (KOG) database and Gene Ontology (GO) annotations (https://www.ebi.ac.uk/QuickGO/). Network analysis of differential metabolites and differential proteins was performed using MetaboAnalyst 5.0 based on the search tool for interactions of chemicals (STITCH) (39) and the network diagram was generated by Cytoscape 3.9.1 (40).

Metabolomic biomarker analysis was performed using MetaboAnalyst 5.0. Multivariate exploratory analysis was utilized to test the performance of models by ROC curve analyses based on the PLS-DA algorithm. ROC curves were generated by MCCV. In each MCCV, two-thirds of the samples were used to evaluate the feature importance. The top 2, 3, 5, 10…100 (max) important features were then used to build classification models that were validated for 1/3 of the samples that were left out. The procedure was repeated multiple times to calculate the performance and confidence interval of each model.

RESULTS

In this study, 44 patients suffering from EC and 43 controls with a normal state of endometrium were enrolled, and samples of endometrial tissue, urine, and intrauterine brushings were collected for metabolomic and proteomic analysis. The type of EC for all the patients was type I endometrial carcinoma, namely endometrioid endometrial carcinoma grade 1 (G1) and grade 2 (G2), which was estrogen dependent and closely related to metabolic processes (41). The experimental design is illustrated in **Figure 1**. Sampling details and patient information including age, body mass index (BMI), menopausal status, previous pregnancy circumstances, medical history of diabetes and hypertension, smoking history, hormone replacement therapy (HRT) history, and the grade and FIGO stage are described in the "Materials and Methods" section and **Supplementary Table 1**.

Untargeted Metabolomic and Proteomic Profiling of EC Tissue Samples

The significance of tumor tissues in EC pathogenesis research has been demonstrated in previous studies (9, 10), and the histopathological examination of tumor tissues is the "gold standard" of clinical diagnosis of EC (7). Tissue samples were obtained from 24 patients with EC and 18 controls, and measured by both untargeted metabolomics and proteomics for the determination of important pathways. Untargeted metabolomics was performed using an HPLC-QTOF-MS/MS system in the positive ion mode. Total ion-current chromatograms (TICs) of QC samples (**Supplementary Figure 1**) showed a good overlap, demonstrating the stability and repeatability of the measuring system. A total of 4410 features were extracted from the raw data using XCMS (35). After data normalization and transformation, PCA and PLS-DA were performed on the metabolomic data. Results showed that the EC group and control group can hardly be separated by the unsupervised analysis, i.e., PCA (**Supplementary Figure 2**), but can be clustered into two discriminative groups by the supervised analysis, i.e., PLS-DA (**Figure 2A**). Hierarchical clustering heatmap generated using the top 500 features with smallest *p*-values (**Supplementary Figure 3**) also showed that the samples from the EC group and control group bear a trend to be distinguished, but a minority of them were wrongly classified. The results indicated that the metabolomic characteristics between the EC and the control groups were generally similar, but with changes in specific features that might be derived from the metabolomic perturbation in EC. Volcano plot (**Figure 2B**) showed that many features were up- or down-regulated in the EC group compared to the control group.

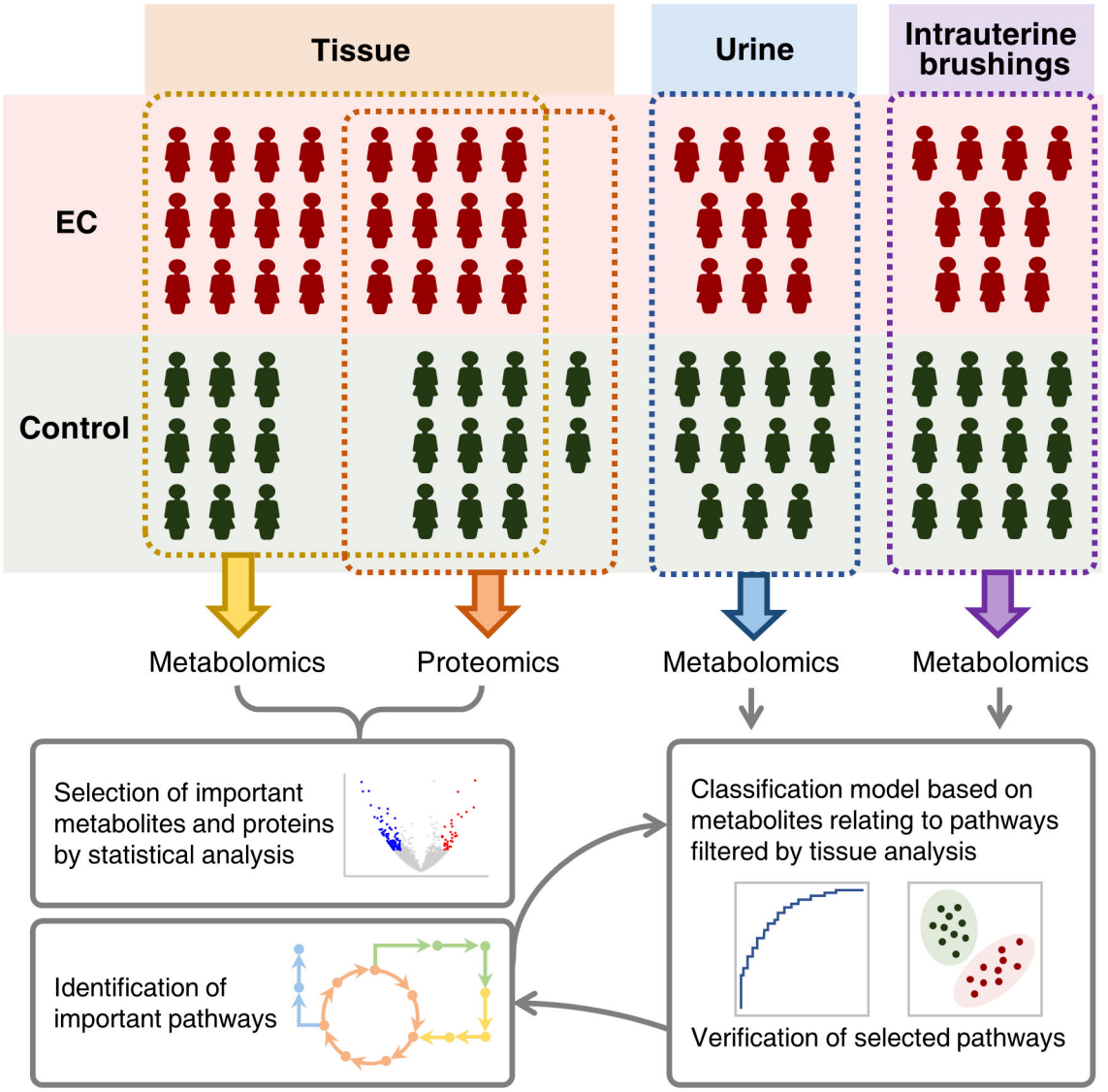

FIGURE 1 | Schematic illustration of integrating metabolomic and proteomic characterization of multi-biosamples from endometrial cancer patients to identify and verify metabolomic pathways significant to the pathogenesis of endometrial cancer.

The differential features were then subjected to structure identification by MetDNA (37). A total of 74 metabolites were identified from the features with *t*-test *p*-values < 0.05 or PLS-DA variable importance in the projection (VIP) values > 1 (**Supplementary Dataset 1**). In order to characterize the roles of the differential metabolites, a Kyoto Encyclopedia of Genes and Genomes (KEGG) pathway analysis was performed using the MetaboAnalyst 5.0 (36). **Figure 2C** shows the top 25 enriched pathways. The highly enriched pathways for the differential metabolites from EC tissue samples include the amino acid metabolism pathways (such as metabolism related with tyrosine, arginine, proline, and alanine), nucleotide metabolism pathways (pyrimidine metabolism and purine metabolism), and metabolism pathways of cofactors and vitamins (such as CoA biosynthesis and biotin synthesis), most of which are associated with energy metabolism (42).

To further explore the metabolomic changes of EC, a subset of the tissue samples with 2 new controls, i.e., 12 EC and 11 controls, were subjected to untargeted proteomic analysis, using a nano-UHPLC-Orbitrap-MS/MS system in the positive ion mode. A total of 9,042 proteins were identified and quantified by combining the EC and control groups. The heatmap containing the intensity information and clustering results of the protein groups (**Supplementary Figure 4**) showed a high consistency among samples as well as a rough division between the EC and control groups, suggesting the stability of the system and the credibility of the data. PCA and PLS-DA were then performed on the proteome data. Results showed that the EC and

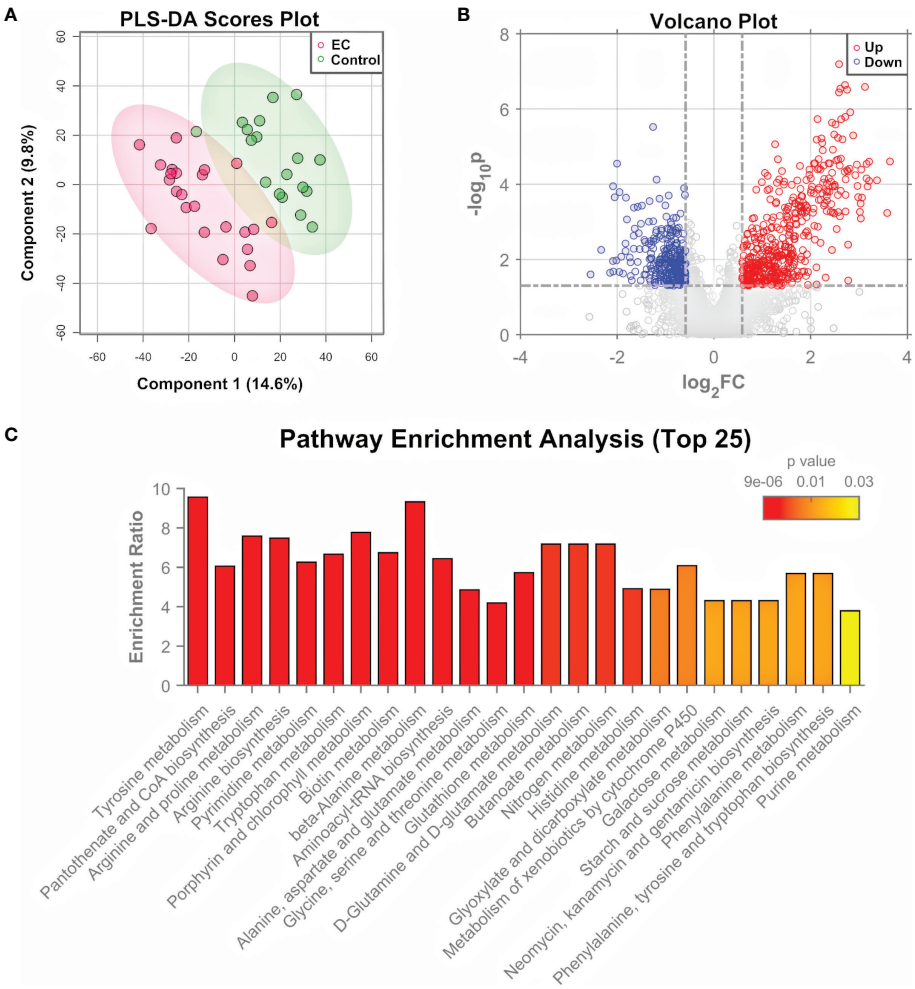

FIGURE 2 | Metabolomic analysis of EC tissue samples. **(A)** PLS-DA score plot for metabolomic data of tissue samples collected from EC and control groups by LC-MS/MS in the positive ion mode. **(B)** Volcano plots of features from the metabolomic data with $\log_2$(FC) as the horizontal axis and $-\log_{10}(p\text{-value})$ as the vertical axis. FC, fold change of EC to control. **(C)** Pathway enrichment analysis of differential metabolites identified from the tissue samples of EC and control groups, showing the results of the top 25 enriched metabolomic pathways.

control groups can be well clustered into two discriminative groups by score plots of both PCA (**Figure 3A**) and PLS-DA (**Figure 3B**), indicating that the proteomic state of EC patient tissue samples was significantly perturbed compared with the control ones. Volcano plot (**Figure 3C**) showed that there were 1,445 proteins (**Supplementary Dataset 2**) significantly up- or downregulated in the EC group compared to the control group (*p*.adj values < 0.05 and FC > 1.5).

To gain a deeper understanding of the significantly changed proteins, the KOG database was applied for functional analysis. According to the annotation results of KOG (**Figure 3D**), the differential proteins were mostly distributed into 4 functional groups: signal transduction mechanisms [T]; posttranslational modification, protein turnover, and chaperones [O]; intracellular trafficking, secretion, and vesicular transport [U]; and transcription [K]. In addition to the 4 most significant functional groups, several functional groups associated with energy metabolism were also found to be prominent here, including the following: lipid transport and metabolism [I], carbohydrate transport and metabolism [G], amino acid transport and metabolism [E], nucleotide transport and metabolism [F], and energy production and conversion [C]. Pathway analysis of the differential metabolites and functional analysis of the differential proteins both emphasized the role of the bioenergetic process, especially those relating to amino acids and nucleotides, showing consistency between the metabolome and proteome data. Other bioinformatics analyses based on the differential proteins, including GO functional analysis and KEGG pathway enrichment analysis, are shown in **Supplementary Figures 5**, **6**. The GO classification indicates that genes relating to the response to hormones were highly annotated, indicating a change in the hormone state of EC (43). KEGG pathway plot showed that half of the top 20 enriched pathways were related to human diseases, which was well correlated with the fact that the samples were cancer-oriented.

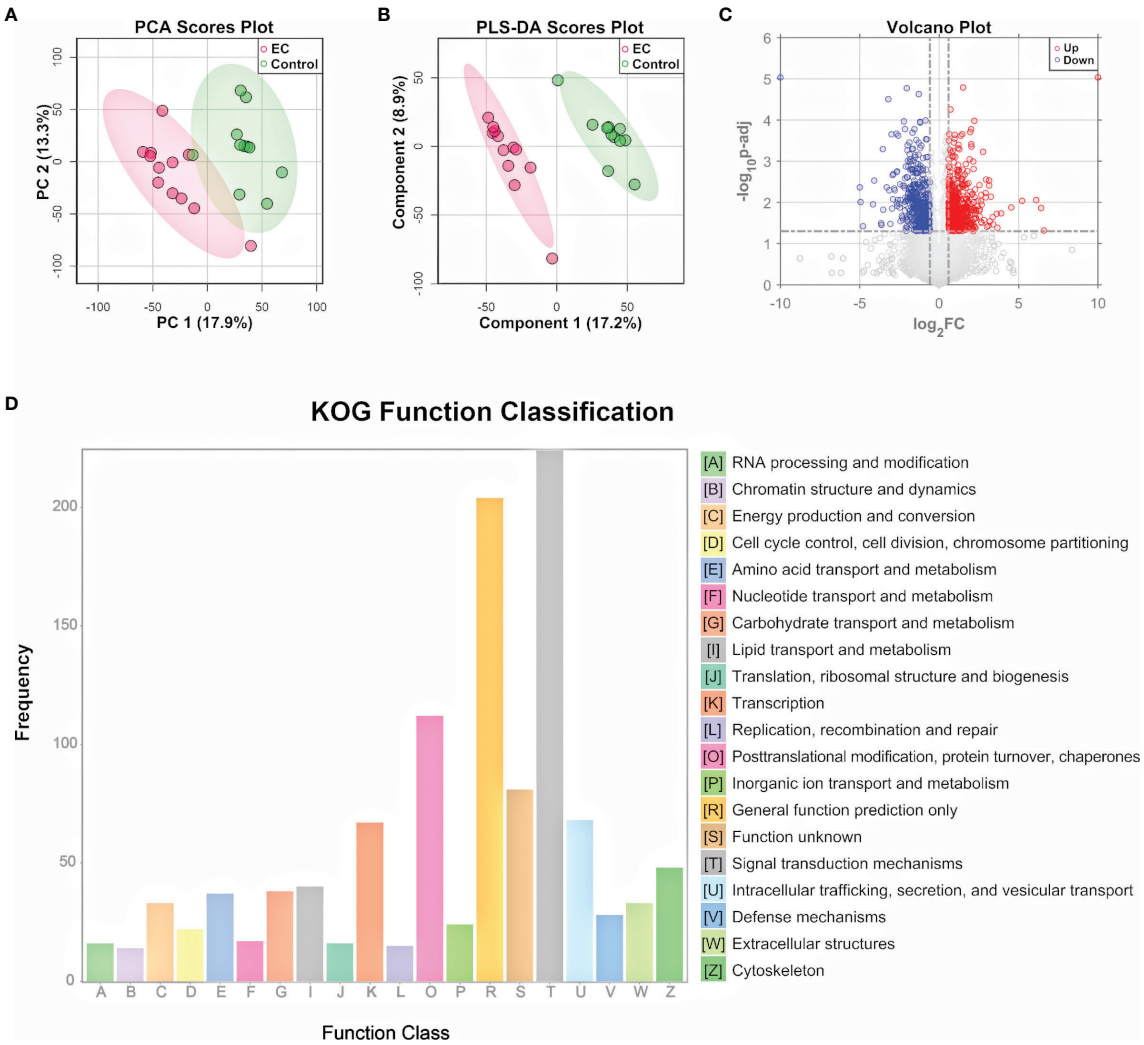

FIGURE 3 | Proteomic analysis of EC tissue samples. **(A)** PCA and **(B)** PLS-DA score plot for proteomic data of tissue samples from EC and control groups by LC-MS/MS in the positive ion mode. **(C)** Volcano plots of proteins with $\log_2$(FC) as the horizontal axis and $-\log_{10}$(*p*-value) as the vertical axis. FC, fold change of EC to control. **(D)** KOG functional annotation of the 1,445 proteins with significant variations in EC tissue samples compared to controls.

Pathway Analysis Integrating Metabolomic and Proteomic Data of Tissue Samples

To find the relation between the metabolomic and proteomic data of tissue samples, network analysis was performed for the differential metabolites and differential proteins according to their chemical structures and molecular activities. The network diagram (**Supplementary Figure 7**) showed a network of 28 metabolites and 135 proteins with 212 connections, from which the nodes highly connected to others can be seen. Among them, glutamate, dopamine, noradrenaline, adenosine 5'-monophosphate (AMP), and guanosine 5'-monophosphate (GMP) were the major centers of sub-networks. Meanwhile, the sub-networks of dopamine and noradrenaline shared overlap of some nodes, and the same occurred for the sub-networks of AMP and GMP. Glutamate, dopamine, and noradrenaline are critical intermediates in amino acid metabolism, while AMP and GMP play critical roles in ribonucleotide biosynthesis of purine metabolism. Incorporating the network analysis results with the pathway enrichment results of differential metabolites and the function classification results of differential proteins, we further focused on the pathways of amino acid metabolism and nucleotide metabolism.

To better understand the metabolomic dysregulation for the pathways of amino acid metabolism and nucleotide metabolism, the interaction among differential metabolites and differential proteins was taken into consideration. Metabolic pathways are composed by reactions of metabolites catalyzed by proteins, so pathways owning direct transformation between differential metabolites or direct interaction between differential metabolites and differential proteins were chosen for further explanation. There were 13 pathways selected, i.e., alanine, aspartate, and glutamate

metabolism; arginine and proline metabolism; arginine biosynthesis; tryptophan metabolism; phenylalanine, tyrosine, and tryptophan biosynthesis; phenylalanine metabolism; cysteine and methionine metabolism; beta-alanine metabolism; lysine degradation; tyrosine metabolism; glutathione metabolism; pyrimidine metabolism; and purine metabolism. To better summarize the metabolomic changes in a pathway-and-compound-based way, 6 out of the 13 selected pathways were illustrated in detail by marking up- and downregulated metabolites and proteins (**Figure 4A**). The change in specific metabolites and proteins is shown in bar plots in **Figure 4B** and **Supplementary Figures 8**, **9**. It should be noted that the six pathways are connected with the metabolites in the TCA cycle, which is an energy-relating anabolic process that can promote cancer growth (42, 44, 45). Though most of the intermediates in the TCA cycle were not detected by the untargeted metabolomic method, the linkage of the TCA cycle with many significant pathways indicated the essential role of the TCA cycle in the growth of a tumor.

In alanine, aspartate, and glutamate metabolism, N-acetylaspartylglutamate (NAAG) and N-acetylaspartylg lutamylglutamate (NAAG2) were upregulated, and the enzyme glutamate carboxypeptidase II (GCPII) catalyzing the reaction from NAAG2 to NAAG as well as NAAG to N-acetylaspartate (NAA) was also upregulated. NAAG and NAAG2 are peptide-based neurotransmitters in the mammalian nervous system and are related to neuro functions (46). Besides the studies of NAAG in brain cancers like glioma (47), it has been reported that NAAG can serve as a reservoir to provide glutamate to tumor cells in cancers expressing GCPII, such as ovarian cancer, where NAAG is more abundant in more malignant tumors and its concentration in plasma is correlated with tumor size (48). Indeed, we have observed the upregulation of glutamate, which further supported that the NAAG here acted as a source of glutamate to promote cancer cell growth (49).

In glutathione metabolism, glutathione disulfide (GSSG) was downregulated, and the enzymes glutathione-disulfide reductase (GSR) and isocitrate dehydrogenase 2 (IDH2), catalyzing, respectively, the process of GSSG to glutathione (GSH) and $NADP^+$ to NADPH, were upregulated. GSH is the most abundant antioxidant in living organisms, and researchers have found that an excess concentration of GSH can promote tumor progression and is correlated with increased metastasis (50). Considering the complex role of GSH in cancer metabolism, its insignificance of change in metabolome was not surprising. The dysregulation of the abovementioned metabolites and proteins indicates an endeavor of maintaining GSH in the reduced state, with the trend of converting $NADP^+$ back to NADPH at the same time.

In tyrosine metabolism, dopamine was downregulated while noradrenaline was upregulated, and the enzyme dopamine β-hydroxylase (DBH) catalyzing the conversion of dopamine to noradrenaline was upregulated. Dopamine is a catecholamine associated with tumorigenesis regulation by affecting angiogenesis and cell proliferation (51), and it can lower the chance of cancer stem cell-induced apoptosis (52). On the other hand, studies have also found that noradrenaline can promote an angiometabolic switch in endothelial cells to activate tumor angiogenesis, resulting in cancer progression (53). Thus, the insufficiency of dopamine and redundancy of noradrenaline emboldened by the activated DBH can both accelerate the growth of a tumor.

In cysteine and methionine metabolism, cystathionine and branched-chain amino acid transaminase 1 (BCAT1) were both upregulated. Cystathionine is a dipeptide generated from serine and homocysteine. A study in breast cancer found that cystathionine accumulates in tissue for cancer cells to gain additional homeostatic stability to their endoplasmic reticulum and mitochondria, elevating the apoptotic threshold (54). BCAT1 catalyzes the catabolism of branched-chain amino acids (BCAAs), and the association of BCAAs with different cancer phenotypes has been demonstrated in a series of studies (55, 56). The overexpression of BCAT1 promotes tumor growth in gynecological cancers, as in ovarian cancer (57) and breast cancer (58). Therefore, the upregulation of both cystathionine and BCAT1 promotes the growth of a tumor.

Nucleotide metabolism includes the generation of purine and pyrimidine molecules for critical procedures like DNA replication, RNA synthesis, and cellular bioenergetics (59). The activation of nucleotide metabolism can promote the uncontrolled growth of a tumor. Genes and proteins relating to the process have already been considered targets of therapy (59). The dysregulation of nucleotide metabolism has been extensively studied for cancers like glioma (60) and breast cancer (61). There are reviews discussing the role of nucleotide metabolism in cancers from both the proliferative (62) and the non-proliferative (59) aspects. In this study, many metabolites and proteins involved in nucleotide metabolism were found to be significantly dysregulated.

In purine metabolism, pyruvate kinase (PK), adenylate kinase 2 (AK2), adenosine monophosphate deaminase 3 (AMPD3), and cytosolic 5'-nucleotidase 3A (NT5C3A) catalyze the 4 reactions from adenosine 5'-triphosphate (ATP) to inosine. They were all upregulated, and AMP, inosine 5'-monophosphate (IMP), and inosine on this reaction chain were upregulated as well, indicating the activation of the whole pathway of purine metabolism. The sequence of conversion further relates to the synthesis of RNA and DNA. It has been reported that purine metabolism could be involved in tumor myometrial invasion of EC (63). PK has two isoforms, PKM1 and PKM2. PKM1 expression following PKM2 loss can cause the proliferation arrest of primary cells and alter nucleotide synthesis, which can influence cell growth (64). AK2 catalyzes the reaction of nucleotide phosphorylation (65). Its localization in mitochondrial intermembrane suggests a unique role of the enzyme in energy metabolism (66). Recent studies provided evidence that AK2 is overexpressed in lung adenocarcinoma, and is associated with tumor progression (67). AK2 has the potential of being a radiosensitive biomarker to predict the toxicity of radiotherapy to normal tissue (68). AMPD3 catalyzes the hydrolytic deamination of AMP to form IMP (69), whose overexpression is associated with the malignant characteristics of gastrointestinal stromal tumors (70). AMPD3 also showed a significantly enhanced level in prostate tumor tissue, indicating high oxidative stress and frequent transformation of nucleotides to nucleosides (71).

In pyrimidine metabolism, despite an absence of significantly differential proteins, the change of metabolism could also be seen

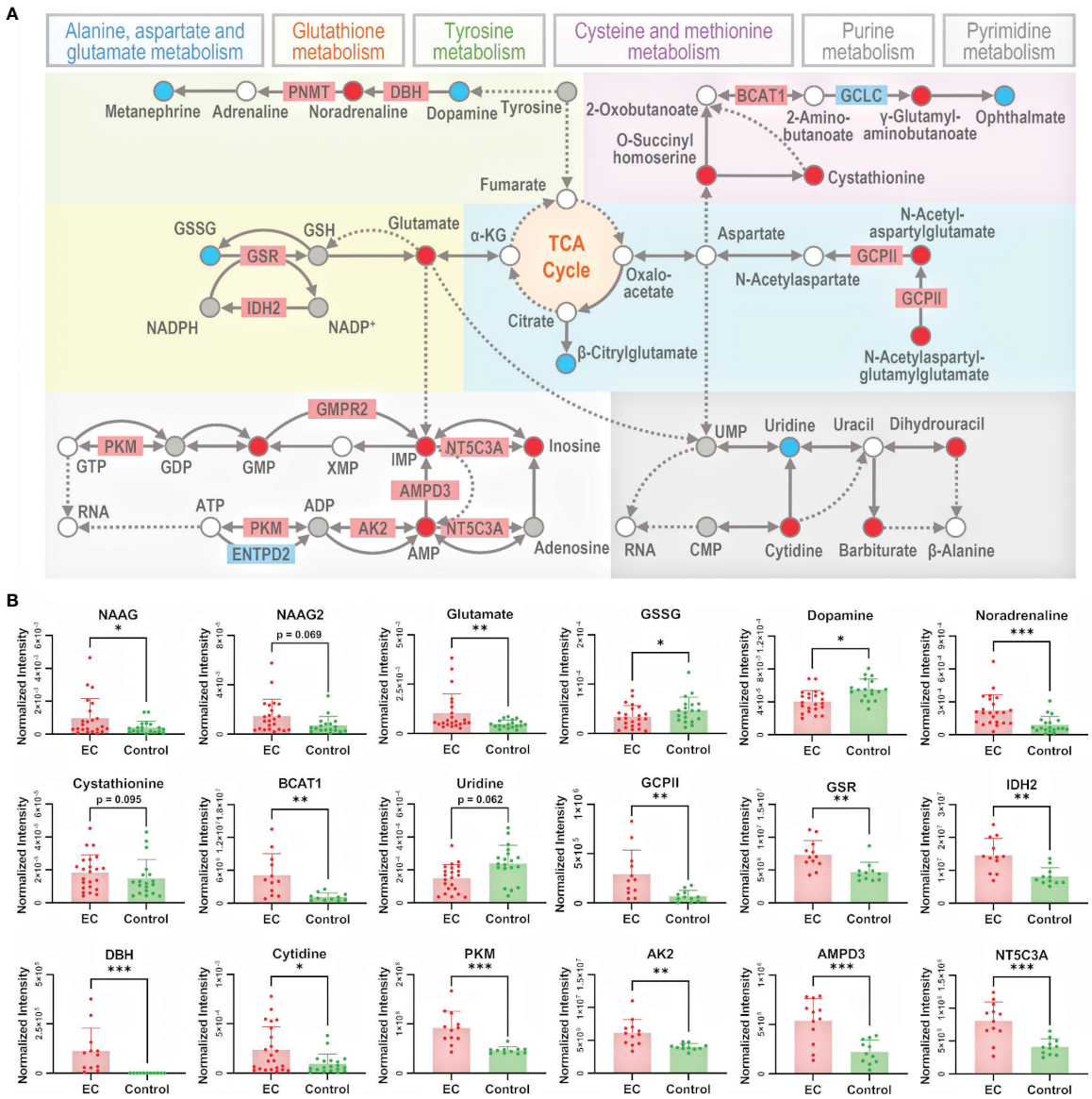

FIGURE 4 | Illustration of the significant pathways and differential metabolites and proteins relating to energy metabolism connected to the TCA cycle. **(A)** Pathway overview of amino acid metabolism and nucleotide metabolism. Circles represent metabolites and rectangles represent proteins. Red-filled circles or rectangles indicate that the metabolites or proteins are upregulated in the EC group compared to the control group, and blue-filled ones indicate downregulation. Gray-filled circles represent the identified but not significantly changed metabolites, and the white-filled ones represent the unidentified metabolites to better connect and explain the pathways. Solid lines indicate direct reactions between metabolites, while dashed lines indicate multi-step reactions. **(B)** Normalized intensity of metabolites and proteins involved in the illustrated pathways. NAAG, NAAG2, GSSG, GCPII, GSR, IDH2, DBH, BCAT1, PKM, AK2, AMPD3, and NT5C3A represent N-acetylaspartylglutamate, N-acetylaspartylglutamylglutamate, glutathione disulfide, glutamate carboxypeptidase II, glutathione-disulfide reductase, isocitrate dehydrogenase 2, dopamine β-hydroxylase, branched chain amino acid transaminase 1, pyruvate kinase M1/2, adenylate kinase 2, adenosine monophosphate deaminase 3, and cytosolic 5'-nucleotidase 3A, respectively. Error bars represent the standard deviation. "*", "**", and "***" indicate *p*-values smaller than 0.05, 0.01, and 0.001, respectively. See also **Supplementary Figures 8**, **9** for other significant metabolites and proteins.

from the dysregulation of metabolites. Cytidine deaminase (CDA) catalyzes the hydrolytic deamination of cytidine to uridine (72), and it has been proven that CDA deficiency leads to DNA damage (73), associating with cancer development (74). The upregulation of cytidine and downregulation of uridine in this study suggests a lack of CDA.

Verification of the Significant Pathways Using Urine and Intrauterine Brushing Samples

Since the collection of tissue samples cannot avoid invasive procedures like biopsy, hysteroscopy, or surgery, there is a high demand for diagnosis methods with non-invasive or

minimally invasive sampling. Urine and intrauterine brushing samples can be collected in a non-invasive or minimally invasive way. The significant pathways identified using tissue samples were then verified by the metabolomic analysis of urine and intrauterine brushing samples, focusing on the metabolites relating to the pathways of amino acid metabolism and nucleotide metabolism. Urine samples were obtained from another 10 patients with EC and another 12 controls. Intrauterine brushing samples were obtained from 10 patients with EC and 11 controls, different from the donors of tissue and urine samples. Untargeted metabolomic analysis, data processing, and structure identification were done in the same way as for the tissue samples. TICs of QC samples (**Supplementary Figures 10A**, **11A**) showed a good overlap, demonstrating the stability and repeatability of the measuring system. A total of 8,066 features were obtained for the urine samples with 349 differential metabolites (p-values < 0.05 or VIP values > 1) being structurally identified. A total of 4,296 features were obtained for the intrauterine brushing samples with 93 differential metabolites (p-values < 0.05 or VIP values > 1) being structurally identified. Statistical analysis based on features, including PCA score plots, PLS-DA score plots, and volcano plots, is shown in **Supplementary Figures 10**, **11**. From the volcano plots, there is a trend of general downregulation of urine metabolites in EC patients.

To verify the 13 selected pathways by the analysis of tissue samples, we focus on the metabolites identified from the urine and intrauterine brushing samples related to the 13 pathways. The lists of 285 urine metabolites and 122 intrauterine brushing metabolites are shown in **Supplementary Dataset 3**. For each pathway of both biosamples, the numbers of metabolites that were detected and significantly regulated between the EC and control groups (p-values < 0.05 or VIP values > 1) are shown in **Figure 5A** and **Supplementary Table 2**. Metabolites of all the 13 pathways were also highly identified and altered for the urine EC samples, and 10 out of 13 for the intrauterine brushing EC samples.

We then assessed whether the 285 urine metabolites and the 122 intrauterine brushing metabolites relating to the 13 pathways could include potential biomarkers for the classification of EC patients and controls. PLS-DA was used as the classification method. Cross-validations (described in the "Materials and Methods" section) were performed to generate the receiver operating characteristic (ROC) curves (**Figures 5B, C**). For the urine samples, the highest area under the curve (AUC) was 0.808 with the top 100 selected metabolites, but the AUC values did not change much when changing the number of selected top metabolites from 5 to 100 (**Figure 5B**). The results indicated that urine metabolites relating to the 13 pathways selected by the analysis of tissue samples can serve as potential biomarkers for the identification of EC, and the models based on top several significant metabolites showed good classification performance. Some of the significant urine metabolites, which were selected most frequently (among the top 15, frequency ≥ 0.94) during the 100-feature-model based cross-validation, are shown in the bar charts (**Figure 5D**). Most of the significant metabolites were downregulated in the urine samples of EC patients compared to the controls.

For the intrauterine brushing samples, the AUC values increased with the number of selected metabolites and reached the highest AUC value of 0.847 with 100 selected metabolites (**Figure 5C**). The result indicated that for intrauterine brushing samples, limited metabolites (5–25) were not sufficient for building classification models because of the fluctuation of different metabolites. Some of the significant intrauterine brushing metabolites, which were selected most frequently (among top 25, frequency = 1.0) during the 100-feature-model-based cross-validation, are shown in the bar charts (**Figure 5E**).

To compare the metabolomic changes in tissue, urine, and intrauterine brushings, the 74 significant metabolites identified from tissue samples were chosen, and the regulations of the metabolites were compared among the three types of samples. The $\log_2$(FC) values between the EC patients and controls are shown as a heatmap in **Figure 6**. Among the 74 metabolites, 47 were upregulated and 27 were downregulated in the tissue samples. Forty-nine of them were also detected and identified in urine samples, with 6 upregulated and 43 downregulated, showing, in general, an opposite trend compared to the tissue metabolites. Twenty-one of the 74 metabolites were detected in the intrauterine brushing samples, with 9 upregulated and 12 downregulated, which showed a generally consistent trend compared to the tissue metabolites.

DISCUSSION

Metabolomic analysis is an increasingly attractive approach to researching EC (27–29). Researchers have focussed on the diagnosis of EC (9–14, 16, 18–26), the differentiation of EC stages (10, 18, 20, 22), the influence of risk factors (13, 15–17), and the possible pathogenesis of tumor development (9–14, 17–22, 24–26) using metabolomic methods. These studies have provided massive information for EC, like the alteration of metabolomics, the establishment of possible diagnosis models, and the enrichment of critical metabolism pathways. Every single study can provide pieces of enlightening results. However, limited correlation among the different studies can be identified, and sometimes contradiction may even be found. This is mainly due to the diversified sample collection and measurement strategies used in different studies. Thus, there are results like alanine, leucine, tyrosine, and valine upregulated in tissue (9) but downregulated in serum (22), and serine upregulated according to GC-MS-based analysis (22) but downregulated according to NMR-based analysis (18) in the metabolomics study of EC. In addition, as one metabolite can be involved in multiple reactions, the dysregulation of a specific metabolite can be a result of several different processes. Therefore, it is difficult to identify the real altered metabolic pathways in EC solely by metabolomic analysis.

In this work, we applied multi-omics analyses to multiple types of biosamples, aiming at exploring the metabolomic change of EC in a pathway-based instead of metabolite-based way. To gain a more reasonable illustration of this view, the patients selected for the EC group were all women suffering from type I endometrial carcinoma, including endometrial carcinoma G1 and G2. Since type I EC is correlated with prolonged estrogen

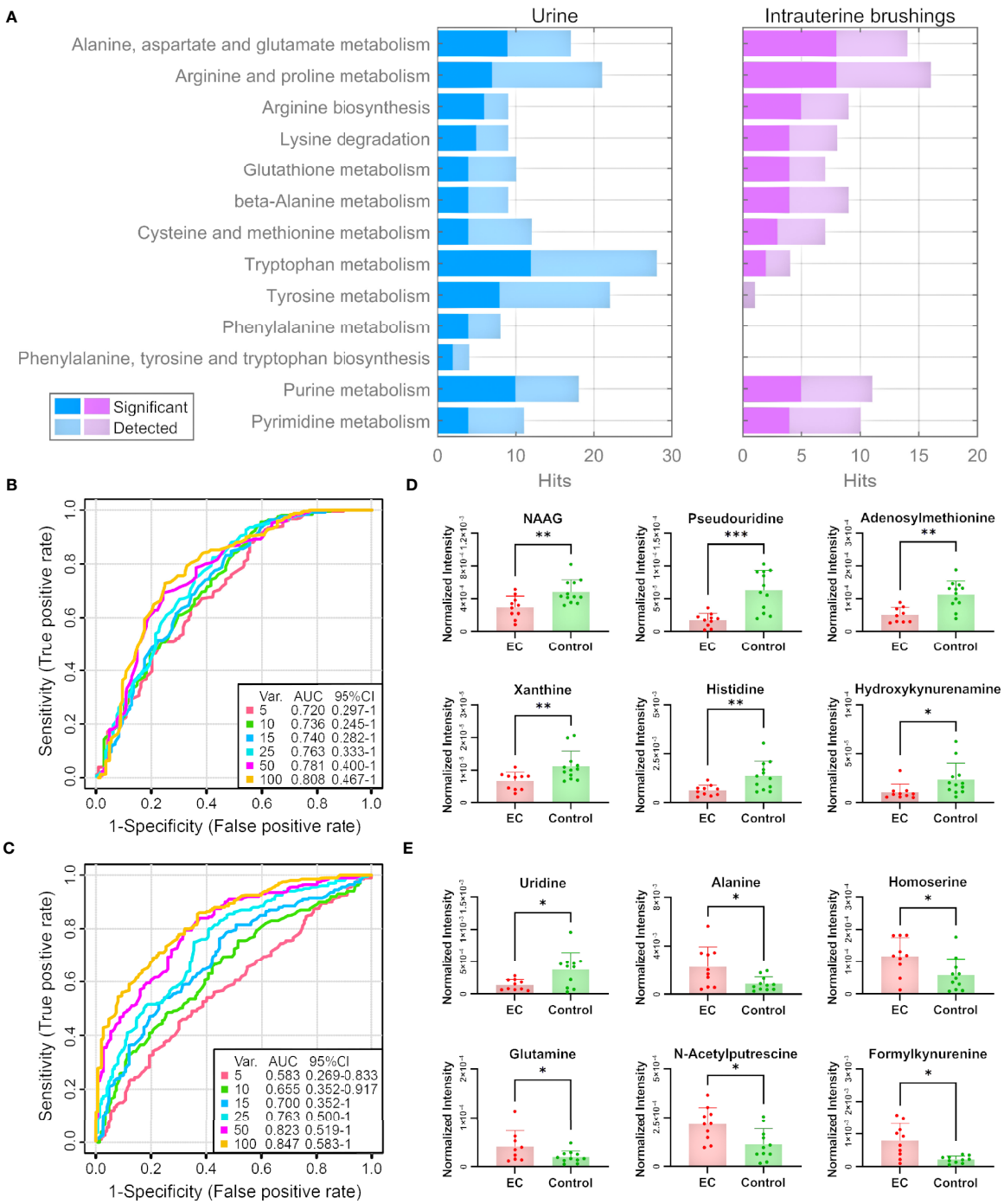

FIGURE 5 | Pathway and biomarker analyses with EC urine and intrauterine brushing samples based on the 13 selected pathways by the analysis of EC tissue samples. **(A)** Numbers of detected and significant metabolites (*p*-values < 0.05 or VIP values > 1) from the urine and intrauterine brushing samples relating to the 13 selected pathways. **(B, C)** ROC curves for the classification of EC patients and controls using the metabolites detected in **(B)** urine and **(C)** intrauterine brushing samples relating to the 13 selected pathways. PLS-DA was used as the classification method, and 100 rounds of Monte Carlo cross-validation were performed to generate the ROC curve. Details are described in the "Materials and Methods" section. **(D, E)** The normalized intensity of representative metabolites detected in **(D)** urine and **(E)** intrauterine brushing samples relating to the 13 selected pathways. NAAG represents N-acetylaspartylglutamate. "*", "**", and "***" indicate *p*-values smaller than 0.05, 0.01, and 0.001, respectively. See also **Supplementary Figures 12**, **13** for other significant metabolites.

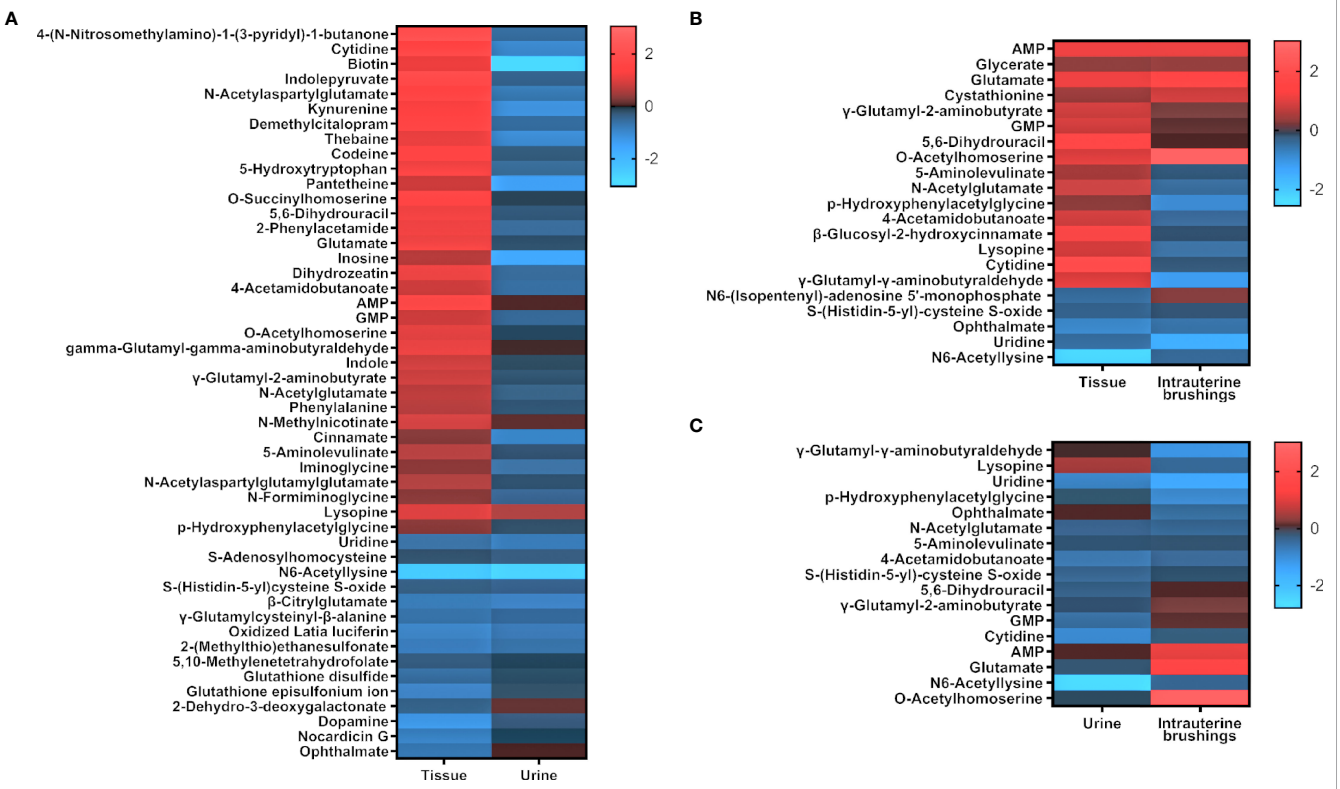

FIGURE 6 | The regulation of significant metabolites identified from tissue samples compared to those in urine and intrauterine brushing samples. Heatmaps show the comparison of log_2(FC) values (EC patients to controls) between **(A)** tissue and urine, **(B)** tissue and intrauterine brushings, and **(C)** urine and intrauterine brushings. Red indicates upregulation; blue indicates downregulation; dark indicates no change.

exposure and does not have progesterone protection, it has been proved to be sensitive to the change in metabolism (75).

Starting with the integration of metabolomic and proteomic analysis of tissue samples, we take advantage of the fact that proteins catalyze chemical reactions among metabolites and embody information of genes. While metabolites function as the substrates or products of metabolomic reactions, the regulation of proteins can provide clear information on the activation or inactivation of metabolomic reactions. Blending the alteration of proteins into the network of metabolites, a more evident map of changes in metabolomic pathways can be obtained. Herein, by integrating the proteomic and metabolomic analysis, significant pathways of amino acid metabolism and nucleotide metabolism were revealed. Meanwhile, the network illustration connecting pathways of amino acid metabolism and nucleotide metabolism not only provides a possible explanation for energy metabolism in EC but also offsets some shortcomings of metabolomic measurement. A previous review has pointed out that the downregulation of amino acids can be a signal of EC, but the changes in amino acids are not significant (28). Although no significantly changed amino acids were identified in the tissue samples in this work, the network illustration shows that the amino acid metabolism pathways are significantly changed and can be alternatives to the amino acid themselves as biomarkers of EC.

Based on the proteomic and metabolomic analysis results of tissue samples, we moved forward to the metabolomics of urine and intrauterine brushings. Non-invasive diagnosis by urine and vaginal samples has been reported (76). Urine collection is non-invasive but research on EC urine metabolomics is still limited (25). Using special brushes to collect intrauterine fluids is a minimally invasive method now widely used in clinical diagnosis (77, 78), but to date, there is no metabolomics study on intrauterine brushings for EC. Non-invasive or minimally invasive sample collection strategies for disease diagnosis are an undeniable future trend, but the theoretical and experimental foundation is indispensable. In contrast to diagnosis by videography or pathology, the "invisibility" of metabolomics prompts the method to require more evidence and verification before clinical usage. Compared with tissues and intrauterine brushings, which can be regarded as "*in situ*" collected tumor-related samples, urine contains additional metabolomic information of other organs, such as the metabolic process in the kidney and bladder, wherein the possibility of EC affecting the functions of the organs cannot be excluded in the urine-based metabolomics study of EC (79).

The metabolomic analysis of urine and intrauterine brushings are not only a verification of the results obtained with the tissue samples, they also preliminarily demonstrate the feasibility of EC

diagnosis using urine or intrauterine brushing metabolites. Monte Carlo cross-validation (MCCV) was performed for the identification of EC using the models built with urine or intrauterine brushing metabolites, while the metabolites were selected based on the 13 significant pathways, relating to the amino acid metabolism and nucleotide metabolism, suggested by the analysis of tissue samples. The results again proved the significance of the 13 pathways in urine and intrauterine brushing samples. It should be noted that since the metabolites for building the classification models were not directly chosen by machine learning from the metabolomic data of urine and intrauterine brushings, the models were not optimized in distinguishing EC patients and controls. For minimal and non-invasive diagnosis of EC, future work is needed for the metabolomic study of large cohorts of intrauterine brushings and urine samples to find biomarkers and build reliable classification models.

The comparison of the FC values (EC/control) of significant metabolites among the samples of tissue, urine, and intrauterine brushings showed that many metabolites were regulated in opposite ways in tissue and urine, while most of the metabolites kept a consistent regulation trend in tissue and intrauterine brushings. Intrauterine brushings are more closely related to tissue, while urine is a biofluid reflecting very downstream metabolism after the treatment of several organs (80, 81). The opposite trend could also be related to a hypothesis that the abnormal metabolism in a tumor may result in the accumulation of metabolites in lesions, thus decreasing their concentrations in urine. In this study, results were limited because different cohorts were involved in the metabolomic analysis of tissue, urine, and intrauterine brushing samples, making it difficult to compare in a paired way. Nevertheless, all the analyses demonstrated the significance of amino acid metabolism and nucleotide metabolism in EC, which again strengthen the conclusion.

In summary, this study demonstrated the important roles of amino acid metabolism and nucleotide metabolism in EC using multi-biosamples, illustrating the network interaction between metabolites and proteins, as well as among pathways. We also provided supporting evidence for the non-invasive or minimally invasive diagnosis of EC using urine and intrauterine brushing samples with metabolomic analysis. We expect that more comprehensive multi-omics analyses will be applied to the study of EC to further explore the mechanism and that simpler but effective diagnostic methods can be developed based on further research on multi-biosamples.

DATA AVAILABILITY STATEMENT

Proteomics data have been deposited to ProteomeXchange *via* the iProX (82) partner repository with the dataset identifiers PXD030222 and IPX0003827000. Metabolomics data have been deposited to the EMBL-EBI MetaboLights database (83) with the identifier MTBLS3935. The complete dataset can be accessed here: https://www.ebi.ac.uk/metabolights/MTBLS3935.

ETHICS STATEMENT

The studies involving human participants were reviewed and approved by The Ethics Committee of Obstetrics and Gynecology Hospital of Fudan University. The patients/participants provided their written informed consent to participate in this study.

AUTHOR CONTRIBUTIONS

RY did the majority of the experiment and wrote the first draft of the manuscript. LX collected all the clinical samples. XW and CS performed the proteomic analysis and the proteome data analysis. XC and LQ designed the work and acquired the funding for the project. LQ supervised all aspects of the work and prepared the final manuscript. All authors contributed to the article and approved the submitted version.

FUNDING

This research was funded by the National Natural Science Foundation of China (NSFC, 22022401, 22074022, and 21934001), the Ministry of Science and Technology of China (2020YFF0304502 and 2020YFF0426500), and the National Key Research and Development Program of China (2019YFC1005200 and 2019YFC1005201).

SUPPLEMENTARY MATERIAL

The Supplementary Material for this article can be found online at: https://www.frontiersin.org/articles/10.3389/fonc.2022.861142/full#supplementary-material

REFERENCES

1. Sung H, Ferlay J, Siegel RL, Laversanne M, Soerjomataram I, Jemal A, et al. Global Cancer Statistics 2020: GLOBOCAN Estimates of Incidence and Mortality Worldwide for 36 Cancers in 185 Countries. *CA Cancer J Clin* (2021) 71(3):209–49. doi: 10.3322/caac.21660
2. Zhang Y, Liu H, Yang S, Zhang J, Qian L, Chen X. Overweight, Obesity and Endometrial Cancer Risk: Results From a Systematic Review and Meta-Analysis. *Int J Biol Markers* (2014) 29(1):e21-9. doi: 10.5301/jbm.5000047
3. Friberg E, Mantzoros CS, Wolk A. Diabetes and Risk of Endometrial Cancer: A Population-Based Prospective Cohort Study. *Cancer Epidemiol Biomarkers Prev* (2007) 16(2):276–80. doi: 10.1158/1055-9965.EPI-06-0751
4. Aune D, Sen A, Vatten LJ. Hypertension and the Risk of Endometrial Cancer: A Systematic Review and Meta-Analysis of Case-Control and Cohort Studies. *Sci Rep* (2017) 7:44808. doi: 10.1038/srep44808
5. Feng J, Li B, Ying J, Pan W, Liu C, Luo T, et al. Liquid Biopsy: Application in Early Diagnosis and Monitoring of Cancer. *Small Struct* (2020) 1(3):2000063. doi: 10.1002/sstr.202000063

6. Shyamala K, Girish HC, Murgod S. Risk of Tumor Cell Seeding Through Biopsy and Aspiration Cytology. *J Int Soc Prev Community Dent* (2014) 4 (1):5–11. doi: 10.4103/2231-0762.129446
7. Amant F, Mirza MR, Koskas M, Creutzberg CL. Cancer of the Corpus Uteri. *Int J Gynaecol Obstet* (2018) 143 Suppl 2:37–50. doi: 10.1002/ijgo.12612
8. Liu X, Locasale JW. Metabolomics: A Primer. *Trends Biochem Sci* (2017) 42 (4):274–84. doi: 10.1016/j.tibs.2017.01.004
9. Trousil S, Lee P, Pinato DJ, Ellis JK, Dina R, Aboagye EO, et al. Alterations of Choline Phospholipid Metabolism in Endometrial Cancer Are Caused by Choline Kinase Alpha Overexpression and a Hyperactivated Deacylation Pathway. *Cancer Res* (2014) 74(23):6867–77. doi: 10.1158/0008-5472.CAN-13-2409
10. Altadill T, Dowdy TM, Gill K, Reques A, Menon SS, Moiola CP, et al. Metabolomic and Lipidomic Profiling Identifies the Role of the RNA Editing Pathway in Endometrial Carcinogenesis. *Sci Rep* (2017) 7(1):8803. doi: 10.1038/s41598-017-09169-2
11. Ihata Y, Miyagi E, Numazaki R, Muramatsu T, Imaizumi A, Yamamoto H, et al. Amino Acid Profile Index for Early Detection of Endometrial Cancer: Verification as a Novel Diagnostic Marker. *Int J Clin Oncol* (2014) 19(2):364–72. doi: 10.1007/s10147-013-0565-2
12. Knific T, Vouk K, Smrkolj S, Prehn C, Adamski J, Rizner TL. Models Including Plasma Levels of Sphingomyelins and Phosphatidylcholines as Diagnostic and Prognostic Biomarkers of Endometrial Cancer. *J Steroid Biochem Mol Biol* (2018) 178:312–21. doi: 10.1016/j.jsbmb.2018.01.012
13. Strand E, Tangen IL, Fasmer KE, Jacob H, Halle MK, Hoivik EA, et al. Blood Metabolites Associate With Prognosis in Endometrial Cancer. *Metabolites* (2019) 9(12):302. doi: 10.3390/metabo9120302
14. Dossus L, Kouloura E, Biessy C, Viallon V, Siskos AP, Dimou N, et al. Prospective Analysis of Circulating Metabolites and Endometrial Cancer Risk. *Gynecol Oncol* (2021) 162(2):475–81. doi: 10.1016/j.ygyno.2021.06.001
15. Kliemann N, Viallon V, Murphy N, Beeken RJ, Rothwell JA, Rinaldi S, et al. Metabolic Signatures of Greater Body Size and Their Associations With Risk of Colorectal and Endometrial Cancers in the European Prospective Investigation Into Cancer and Nutrition. *BMC Med* (2021) 19(1):101. doi: 10.1186/s12916-021-01970-1
16. Njoku K, Campbell AE, Geary B, MacKintosh ML, Derbyshire AE, Kitson SJ, et al. Metabolomic Biomarkers for the Detection of Obesity-Driven Endometrial Cancer. *Cancers (Basel)* (2021) 13(4):718. doi: 10.3390/cancers13040718
17. Gaudet MM, Falk RT, Stevens RD, Gunter MJ, Bain JR, Pfeiffer RM, et al. Analysis of Serum Metabolic Profiles in Women With Endometrial Cancer and Controls in a Population-Based Case-Control Study. *J Clin Endocrinol Metab* (2012) 97(9):3216–23. doi: 10.1210/jc.2012-1490
18. Bahado-Singh RO, Lugade A, Field J, Al-Wahab Z, Han B, Mandal R, et al. Metabolomic Prediction of Endometrial Cancer. *Metabolomics* (2017) 14(1):6. doi: 10.1007/s11306-017-1290-z
19. Audet-Delage Y, Gregoire J, Caron P, Turcotte V, Plante M, Ayotte P, et al. Estradiol Metabolites as Biomarkers of Endometrial Cancer Prognosis After Surgery. *J Steroid Biochem Mol Biol* (2018) 178:45–54. doi: 10.1016/j.jsbmb.2017.10.021
20. Audet-Delage Y, Villeneuve L, Gregoire J, Plante M, Guillemette C. Identification of Metabolomic Biomarkers for Endometrial Cancer and Its Recurrence After Surgery in Postmenopausal Women. *Front Endocrinol* (2018) 9:87. doi: 10.3389/fendo.2018.00087
21. Shi K, Wang Q, Su Y, Xuan X, Liu Y, Chen W, et al. Identification and Functional Analyses of Differentially Expressed Metabolites in Early Stage Endometrial Carcinoma. *Cancer Sci* (2018) 109(4):1032–43. doi: 10.1111/cas.13532
22. Troisi J, Sarno L, Landolfi A, Scala G, Martinelli P, Venturella R, et al. Metabolomic Signature of Endometrial Cancer. *J Proteome Res* (2018) 17 (2):804–12. doi: 10.1021/acs.jproteome.7b00503
23. Troisi J, Raffone A, Travaglino A, Belli G, Belli C, Anand S, et al. Development and Validation of a Serum Metabolomic Signature for Endometrial Cancer Screening in Postmenopausal Women. *JAMA Netw Open* (2020) 3(9): e2018327. doi: 10.1001/jamanetworkopen.2020.18327
24. Kozar N, Kruusmaa K, Dovnik A, Bitenc M, Argamasilla R, Adsuar A, et al. Identification of Novel Diagnostic Biomarkers in Endometrial Cancer Using Targeted Metabolomic Profiling. *Adv Med Sci* (2021) 66(1):46–51. doi: 10.1016/j.advms.2020.12.001
25. Shao X, Wang K, Liu X, Gu C, Zhang P, Xie J, et al. Screening and Verifying Endometrial Carcinoma Diagnostic Biomarkers Based on a Urine Metabolomic Profiling Study Using UPLC-Q-TOF/Ms. *Clin Chim Acta* (2016) 463:200–6. doi: 10.1016/j.cca.2016.10.027
26. Cheng SC, Chen K, Chiu CY, Lu KY, Lu HY, Chiang MH, et al. Metabolomic Biomarkers in Cervicovaginal Fluid for Detecting Endometrial Cancer Through Nuclear Magnetic Resonance Spectroscopy. *Metabolomics* (2019) 15(11):146. doi: 10.1007/s11306-019-1609-z
27. Njoku K, Sutton CJ, Whetton AD, Crosbie EJ. Metabolomic Biomarkers for Detection, Prognosis and Identifying Recurrence in Endometrial Cancer. *Metabolites* (2020) 10(8):314. doi: 10.3390/metabo10080314
28. Raffone A, Troisi J, Boccia D, Travaglino A, Capuano G, Insabato L, et al. Metabolomics in Endometrial Cancer Diagnosis: A Systematic Review. *Acta Obstet Gynecol Scand* (2020) 99(9):1135–46. doi: 10.1111/aogs.13847
29. Tokarz J, Adamski J, Rizner TL. Metabolomics for Diagnosis and Prognosis of Uterine Diseases? A Systematic Review. *J Pers Med* (2020) 10(4):294. doi: 10.3390/jpm10040294
30. Dias DA, Jones OA, Beale DJ, Boughton BA, Benheim D, Kouremenos KA, et al. Current and Future Perspectives on the Structural Identification of Small Molecules in Biological Systems. *Metabolites* (2016) 6(4):46. doi: 10.3390/metabo6040046
31. Shen B, Yi X, Sun Y, Bi X, Du J, Zhang C, et al. Proteomic and Metabolomic Characterization of COVID-19 Patient Sera. *Cell* (2020) 182(1):59–72.e15. doi: 10.1016/j.cell.2020.05.032
32. Nie X, Qian L, Sun R, Huang B, Dong X, Xiao Q, et al. Multi-Organ Proteomic Landscape of COVID-19 Autopsies. *Cell* (2021) 184(3):775–91.e14. doi: 10.1016/j.cell.2021.01.004
33. Gouda M, Moustafa A, Hussein L, Hamza M. Three Week Dietary Intervention Using Apricots, Pomegranate Juice or/and Fermented Sour Sobya and Impact on Biomarkers of Antioxidative Activity, Oxidative Stress and Erythrocytic Glutathione Transferase Activity Among Adults. *Nutr J* (2016) 15(1):52. doi: 10.1186/s12937-016-0173-x
34. Chambers MC, Maclean B, Burke R, Amodei D, Ruderman DL, Neumann S, et al. A Cross-Platform Toolkit for Mass Spectrometry and Proteomics. *Nat Biotechnol* (2012) 30(10):918–20. doi: 10.1038/nbt.2377
35. Smith CA, Want EJ, O'Maille G, Abagyan R, Siuzdak G. XCMS: Processing Mass Spectrometry Data for Metabolite Profiling Using Nonlinear Peak Alignment, Matching, and Identification. *Anal Chem* (2006) 78(3):779–87. doi: 10.1021/ac051437y
36. Pang Z, Chong J, Zhou G, de Lima Morais DA, Chang L, Barrette M, et al. MetaboAnalyst 5.0: Narrowing the Gap Between Raw Spectra and Functional Insights. *Nucleic Acids Res* (2021) 49(W1):W388–W96. doi: 10.1093/nar/gkab382
37. Shen X, Wang R, Xiong X, Yin Y, Cai Y, Ma Z, et al. Metabolic Reaction Network-Based Recursive Metabolite Annotation for Untargeted Metabolomics. *Nat Commun* (2019) 10(1):1516. doi: 10.1038/s41467-019-09550-x
38. Smith CA, O'Maille G, Want EJ, Qin C, Trauger SA, Brandon TR, et al. METLIN: A Metabolite Mass Spectral Database. *Ther Drug Monit* (2005) 27 (6):747–51. doi: 10.1097/01.ftd.0000179845.53213.39
39. Kuhn M, Szklarczyk D, Franceschini A, Campillos M, von Mering C, Jensen LJ, et al. STITCH 2: An Interaction Network Database for Small Molecules and Proteins. *Nucleic Acids Res* (2010) 38(Database issue):D552–6. doi: 10.1093/nar/gkp937
40. Shannon P, Markiel A, Ozier O, Baliga NS, Wang JT, Ramage D, et al. Cytoscape: A Software Environment for Integrated Models of Biomolecular Interaction Networks. *Genome Res* (2003) 13(11):2498–504. doi: 10.1101/gr.1239303
41. Bokhman JV. Two Pathogenetic Types of Endometrial Carcinoma. *Gynecol Oncol* (1983) 15(1):10–7. doi: 10.1016/0090-8258(83)90111-7
42. DeBerardinis RJ, Chandel NS. Fundamentals of Cancer Metabolism. *Sci Adv* (2016) 2(5):e1600200. doi: 10.1126/sciadv.1600200
43. van Weelden WJ, Massuger L, Enitec, Pijnenborg JMA, Romano A. Anti-Estrogen Treatment in Endometrial Cancer: A Systematic Review. *Front Oncol* (2019) 9:359. doi: 10.3389/fonc.2019.00359
44. Cardaci S, Ciriolo MR. TCA Cycle Defects and Cancer: When Metabolism Tunes Redox State. *Int J Cell Biol* (2012) 2012:161837. doi: 10.1155/2012/161837
45. Martinez-Reyes I, Chandel NS. Mitochondrial TCA Cycle Metabolites Control Physiology and Disease. *Nat Commun* (2020) 11(1):102. doi: 10.1038/s41467-019-13668-3

46. Neale JH, Olszewski RT, Zuo D, Janczura KJ, Profaci CP, Lavin KM, et al. Advances in Understanding the Peptide Neurotransmitter NAAG and Appearance of a New Member of the NAAG Neuropeptide Family. *J Neurochem* (2011) 118(4):490–8. doi: 10.1111/j.1471-4159.2011.07338.x
47. Long PM, Moffett JR, Namboodiri AMA, Viapiano MS, Lawler SE, Jaworski DM. N-Acetylaspartate (NAA) and N-Acetylaspartylglutamate (NAAG) Promote Growth and Inhibit Differentiation of Glioma Stem-Like Cells. *J Biol Chem* (2013) 288(36):26188–200. doi: 10.1074/jbc.M113.487553
48. Nguyen T, Kirsch BJ, Asaka R, Nabi K, Quinones A, Tan J, et al. Uncovering the Role of N-Acetyl-Aspartyl-Glutamate as a Glutamate Reservoir in Cancer. *Cell Rep* (2019) 27(2):491–501.e6. doi: 10.1016/j.celrep.2019.03.036
49. Yi H, Talmon G, Wang J. Glutamate in Cancers: From Metabolism to Signaling. *J BioMed Res* (2019) 34(4):260–70. doi: 10.7555/JBR.34.20190037
50. Bansal A, Simon MC. Glutathione Metabolism in Cancer Progression and Treatment Resistance. *J Cell Biol* (2018) 217(7):2291–8. doi: 10.1083/jcb.201804161
51. Chakroborty D, Sarkar C, Basu B, Dasgupta PS, Basu S. Catecholamines Regulate Tumor Angiogenesis. *Cancer Res* (2009) 69(9):3727–30. doi: 10.1158/0008-5472.CAN-08-4289
52. Wang S, Mou Z, Ma Y, Li J, Li J, Ji X, et al. Dopamine Enhances the Response of Sunitinib in the Treatment of Drug-Resistant Breast Cancer: Involvement of Eradicating Cancer Stem-Like Cells. *Biochem Pharmacol* (2015) 95(2):98–109. doi: 10.1016/j.bcp.2015.03.013
53. Zahalka AH, Arnal-Estape A, Maryanovich M, Nakahara F, Cruz CD, Finley LWS, et al. Adrenergic Nerves Activate an Angio-Metabolic Switch in Prostate Cancer. *Science* (2017) 358(6361):321–6. doi: 10.1126/science.aah5072
54. Sen S, Kawahara B, Mahata SK, Tsai R, Yoon A, Hwang L, et al. Cystathionine: A Novel Oncometabolite in Human Breast Cancer. *Arch Biochem Biophys* (2016) 604:95–102. doi: 10.1016/j.abb.2016.06.010
55. Ananieva EA, Wilkinson AC. Branched-Chain Amino Acid Metabolism in Cancer. *Curr Opin Clin Nutr Metab Care* (2018) 21(1):64–70. doi: 10.1097/MCO.0000000000000430
56. Sivanand S, Vander Heiden MG. Emerging Roles for Branched-Chain Amino Acid Metabolism in Cancer. *Cancer Cell* (2020) 37(2):147–56. doi: 10.1016/j.ccell.2019.12.011
57. Wang ZQ, Faddaoui A, Bachvarova M, Plante M, Gregoire J, Renaud MC, et al. BCAT1 Expression Associates With Ovarian Cancer Progression: Possible Implications in Altered Disease Metabolism. *Oncotarget* (2015) 6 (31):31522–43. doi: 10.18632/oncotarget.5159
58. Zhang L, Han J. Branched-Chain Amino Acid Transaminase 1 (BCAT1) Promotes the Growth of Breast Cancer Cells Through Improving mTOR-Mediated Mitochondrial Biogenesis and Function. *Biochem Biophys Res Commun* (2017) 486(2):224–31. doi: 10.1016/j.bbrc.2017.02.101
59. Siddiqui A, Ceppi P. A Non-Proliferative Role of Pyrimidine Metabolism in Cancer. *Mol Metab* (2020) 35:100962. doi: 10.1016/j.molmet.2020.02.005
60. Wang X, Yang K, Xie Q, Wu Q, Mack SC, Shi Y, et al. Purine Synthesis Promotes Maintenance of Brain Tumor Initiating Cells in Glioma. *Nat Neurosci* (2017) 20(5):661–73. doi: 10.1038/nn.4537
61. Lv Y, Wang X, Li X, Xu G, Bai Y, Wu J, et al. Nucleotide *De Novo* Synthesis Increases Breast Cancer Stemness and Metastasis *via* cGMP-PKG-MAPK Signaling Pathway. *PloS Biol* (2020) 18(11):e3000872. doi: 10.1371/journal.pbio.3000872
62. Yin J, Ren W, Huang X, Deng J, Li T, Yin Y. Potential Mechanisms Connecting Purine Metabolism and Cancer Therapy. *Front Immunol* (2018) 9:1697. doi: 10.3389/fimmu.2018.01697
63. Jove M, Gatius S, Yeramian A, Portero-Otin M, Eritja N, Santacana M, et al. Metabotyping Human Endometrioid Endometrial Adenocarcinoma Reveals an Implication of Endocannabinoid Metabolism. *Oncotarget* (2016) 7 (32):52364–74. doi: 10.18632/oncotarget.10564
64. Lunt SY, Muralidhar V, Hosios AM, Israelsen WJ, Gui DY, Newhouse L, et al. Pyruvate Kinase Isoform Expression Alters Nucleotide Synthesis to Impact Cell Proliferation. *Mol Cell* (2015) 57(1):95–107. doi: 10.1016/j.molcel.2014.10.027
65. Dzeja PP, Zeleznikar RJ, Goldberg ND. Adenylate Kinase: Kinetic Behavior in Intact Cells Indicates It Is Integral to Multiple Cellular Processes. *Mol Cell Biochem* (1998) 184(1/2):169–82. doi: 10.1023/a:1006859632730
66. Gellerich FN. The Role of Adenylate Kinase in Dynamic Compartmentation of Adenine Nucleotides in the Mitochondrial Intermembrane Space. *FEBS Lett* (1992) 297(1-2):55–8. doi: 10.1016/0014-5793(92)80326-c
67. Liu H, Pu Y, Amina Q, Wang Q, Zhang M, Song J, et al. Prognostic and Therapeutic Potential of Adenylate Kinase 2 in Lung Adenocarcinoma. *Sci Rep* (2019) 9(1):17757. doi: 10.1038/s41598-019-53594-4
68. Lacombe J, Brengues M, Mange A, Bourgier C, Gourgou S, Pelegrin A, et al. Quantitative Proteomic Analysis Reveals AK2 as Potential Biomarker for Late Normal Tissue Radiotoxicity. *Radiat Oncol* (2019) 14(1):142. doi: 10.1186/s13014-019-1351-8
69. Morisaki T, Sabina RL, Holmes EW. Adenylate Deaminase. A Multigene Family in Humans and Rats. *J Biol Chem* (1990) 265(20):11482–6. doi: 10.1016/s0021-9258(19)38422-4
70. Wong M, Funasaka K, Obayashi T, Miyahara R, Hirooka Y, Hamaguchi M, et al. AMPD3 Is Associated With the Malignant Characteristics of Gastrointestinal Stromal Tumors. *Oncol Lett* (2017) 13(3):1281–7. doi: 10.3892/ol.2016.5532
71. Dudka I, Thysell E, Lundquist K, Antti H, Iglesias-Gato D, Flores-Morales A, et al. Comprehensive Metabolomics Analysis of Prostate Cancer Tissue in Relation to Tumor Aggressiveness and TMPRSS2-ERG Fusion Status. *BMC Cancer* (2020) 20(1):437. doi: 10.1186/s12885-020-06908-z
72. Demontis S, Terao M, Brivio M, Zanotta S, Bruschi M, Garattini E. Isolation and Characterization of the Gene Coding for Human Cytidine Deaminase. *Biochim Biophys Acta (BBA)* (1998) 1443(3):323–33. doi: 10.1016/s0167-4781(98)00235-8
73. Chabosseau P, Buhagiar-Labarchede G, Onclercq-Delic R, Lambert S, Debatisse M, Brison O, et al. Pyrimidine Pool Imbalance Induced by BLM Helicase Deficiency Contributes to Genetic Instability in Bloom Syndrome. *Nat Commun* (2011) 2:368. doi: 10.1038/ncomms1363
74. Mameri H, Bieche I, Meseure D, Marangoni E, Buhagiar-Labarchede G, Nicolas A, et al. Cytidine Deaminase Deficiency Reveals New Therapeutic Opportunities Against Cancer. *Clin Cancer Res* (2017) 23(8):2116–26. doi: 10.1158/1078-0432.CCR-16-0626
75. Sherman ME. Theories of Endometrial Carcinogenesis: A Multidisciplinary Approach. *Mod Pathol* (2000) 13(3):295–308. doi: 10.1038/modpathol.3880051
76. O'Flynn H, Ryan NAJ, Narine N, Shelton D, Rana D, Crosbie EJ. Diagnostic Accuracy of Cytology for the Detection of Endometrial Cancer in Urine and Vaginal Samples. *Nat Commun* (2021) 12(1):952. doi: 10.1038/s41467-021-21257-6
77. Wang Y, Li L, Douville C, Cohen JD, Yen TT, Kinde I, et al. Evaluation of Liquid From the Papanicolaou Test and Other Liquid Biopsies for the Detection of Endometrial and Ovarian Cancers. *Sci Transl Med* (2018) 10 (433):eaap8793. doi: 10.1126/scitranslmed.aap8793
78. Williams AR, Brechin S, Porter AJ, Warner P, Critchley HO. Factors Affecting Adequacy of Pipelle and Tao Brush Endometrial Sampling. *BJOG* (2008) 115 (8):1028–36. doi: 10.1111/j.1471-0528.2008.01773.x
79. Torres da Costa ESV, Costalonga EC, Coelho FO, Caires RA, Burdmann EA. Assessment of Kidney Function in Patients With Cancer. *Adv Chronic Kidney Dis* (2018) 25(1):49–56. doi: 10.1053/j.ackd.2017.10.010
80. Zhang A, Sun H, Wu X, Wang X. Urine Metabolomics. *Clin Chim Acta* (2012) 414:65–9. doi: 10.1016/j.cca.2012.08.016
81. Bouatra S, Aziat F, Mandal R, Guo AC, Wilson MR, Knox C, et al. The Human Urine Metabolome. *PloS One* (2013) 8(9):e73076. doi: 10.1371/journal.pone.0073076
82. Ma J, Chen T, Wu S, Yang C, Bai M, Shu K, et al. Iprox: An Integrated Proteome Resource. *Nucleic Acids Res* (2019) 47(D1):D1211–D7. doi: 10.1093/nar/gky869
83. Haug K, Cochrane K, Nainala VC, Williams M, Chang J, Jayaseelan KV, et al. MetaboLights: A Resource Evolving in Response to the Needs of Its Scientific Community. *Nucleic Acids Res* (2020) 48(D1):D440–D4. doi: 10.1093/nar/gkz1019

Conflict of Interest: Authors XW and CS were employed by Shanghai Omicsolution Co., Ltd.

The remaining authors declare that the research was conducted in the absence of any commercial or financial relationships that could be construed as a potential conflict of interest.

this article, or claim that may be made by its manufacturer, is not guaranteed or endorsed by the publisher.

frontiers | Frontiers in Oncology

ORIGINAL RESEARCH
published: 28 June 2022
doi: 10.3389/fonc.2022.781686

Identification and Validation of Prognostic Related Hallmark ATP-Binding Cassette Transporters Associated With Immune Cell Infiltration Patterns in Thyroid Carcinoma

Lidong Wang[1], *Xiaodan Sun*[2,3], *Jingni He*[1] *and Zhen Liu*[1]*

[1] Department of General Surgery, Shengjing Hospital of China Medical University, Shenyang, China, [2] Postdoctoral Research Workstation, Jilin Cancer Hospital, Changchun, China, [3] Department of 1st Gynecologic Oncology Surgery, Jilin Cancer Hospital, Changchun, China

OPEN ACCESS

Edited by:
Nadia Judith Jacobo-Herrera, Instituto Nacional de Ciencias Médicas y Nutrición Salvador Zubirán (INCMNSZ), Mexico

Reviewed by:
Gabriela Figueroa González, Universidad Nacional Autónoma de México, Mexico
Jossimar Coronel Hernández, National Autonomous University of Mexico, Mexico

***Correspondence:**
Zhen Liu
liuzhen1973@aliyun.com

Specialty section:
This article was submitted to Cancer Metabolism, a section of the journal Frontiers in Oncology

Received: 04 October 2021
Accepted: 01 June 2022
Published: 28 June 2022

Citation:
Wang L, Sun X, He J and Liu Z (2022) Identification and Validation of Prognostic Related Hallmark ATP-Binding Cassette Transporters Associated With Immune Cell Infiltration Patterns in Thyroid Carcinoma. Front. Oncol. 12:781686. doi: 10.3389/fonc.2022.781686

ATP-binding cassette (ABC) transporters are a large superfamily of membrane proteins that facilitate the translocation of heterogeneous substrates. Studies indicate that ABC transporters may play important roles in various carcinomas. However, the correlation between ABC transporters and immunomodulation in thyroid carcinoma (TC), as well as the prognoses for this disease, is poorly understood.TC data from The Cancer Genome Atlas (TCGA) database were used to identify prognostic hallmark ABC transporters associated with immune cell infiltration patterns *via* multiple bioinformatic analyses. Thereafter, quantitative real-time polymerase chain reaction (qRT-PCR) was performed to validate the expression of these selected hallmark ABC transporters in both TC and para-cancerous thyroid tissues. Of a total of 49 ABC transporters, five (*ABCA8*, *ABCA12*, *ABCB6*, *ABCB8*, and *ABCC10*) were identified as hallmark ABC transporters. All five were differentially expressed in TC and associated with the relapse-free survival rates of patients with TC. Immunoregulation by these five hallmark ABC transporters involved the modulation of various aspects of immune cell infiltration, such as hot or cold tumor subsets and the abundances of infiltrating immune cells, as well as specific immunomodulators and chemokines. Besides the diverse significantly correlated factors, the five hallmark ABC transporters and correlated genes were most highly enriched in plasma membrane, transporter activity, and transmembrane transport of small molecules. In addition, many chemicals, namely bisphenol A and vincristine, affected the expression of these five transporters. The qRT-PCR results of collected TC and para-cancerous thyroid tissues were consistent with those of TCGA. The findings in this study may reveal the role played by these five hallmark ABC transporters in regulating immune cell infiltration patterns in TC as well as the molecular mechanisms underlying their

functions, leading to a better understanding of their potential prognostic and immunotherapeutic values.

Keywords: thyroid carcinoma, ATP-binding cassette transporters, prognosis, immune cell infiltration, immunomodulation

INTRODUCTION

Thyroid carcinoma (TC) is the most common endocrine malignancy worldwide, and its global incidence rate has been growing over the last three decades. Before the 1990s, the incidence of TC in the United States was relatively stable at approximately 5/100,000. However, its incidence had tripled (15/100,000) by 2014 (1). The incidence of TC in Canada from 2012–2016 was reportedly 17.4/100,000, a figure closely similar to that of the United States (2). Such dramatic increases in the incidence of TC have also been observed in many other countries, including 29 European countries and China (3, 4). According to Global Cancer Statistics, 586,202 new TC cases were reported worldwide in 2020, amounting to an incidence of 13.2/100,000 (5). However, the mortality rate of TC has remained relatively low and stable (<1/100,000); (1–4, 6). The etiology of TC remains unclear. Exposure to ionizing radiation during childhood is considered to be risk factor that is most and closely associated with TC (7). Moreover, other factors, such as chromosomal (genetic) alterations and obesity, are reportedly associated with the occurrence and development of TC (8, 9).

Based on histological features, TC is mainly divided into the following four types: papillary thyroid carcinoma (PTC); follicular thyroid carcinoma (FTC); anaplastic thyroid carcinoma (ATC); and medullary thyroid carcinoma (MTC); (10). PTC represents the most common differentiated subtype of TC, and its incidence has reportedly increased over the past decade (11). Most PTC patients receive favorable prognoses involving 10-year survival rates ranging from 93–97% (12, 13). The 10-year survival rates for FTC and MTC are 85% and 75%, respectively, and thus worse than that for PTC (12). ATC begets the worst prognosis, with a 10-year survival rate of 14% and a median survival of six months (12, 14). Although the majority of TCs, which remain indolent, are associated with an innocuous clinical course, some cases manifest aggressive behavioral patterns, such as metastasis and recurrence, resulting in poorer prognoses. The recurrence rate of PTC following conventional treatment is reportedly as high as 28% (15). Metastasis in TC, which mostly involves the cervical lymph system, acts as an unfavorable factor which leads to poor prognoses (16). The 8th edition of the American Joint Committee on Cancer (AJCC) tumor-node-metastasis (TNM) staging system identifies sex, age, N classification, pathological subtype, and radioactive iodine avidity as some of the major factors affecting the prognosis of PTC (17). In addition, the 10-year cancer-specific survival rate for IVb stage PTC patients over 55 years old presenting with extensive extrathyroidal extension is reportedly 33.3% (18). The limited number of alternative therapeutic strategies that have been used against surgically inoperable and radioiodine-refractory TC have not been successful at improving the survival of TC patients. Therefore, development of new intervention strategies against TC are felt to be warranted.

The tumor microenvironment (TME), which is composed of the extracellular matrix, stromal cells, immune cells, and some secreted factors, plays an important role in TC (19). Of these, tumor immune cell infiltration has been demonstrated to be closely associated with TC progression and prognosis (20, 21). Tumors may be categorized as immunologically hot or cold types, which definitions are based on the degree of immune infiltration in the TME (22). The hot type is characterized by high tumor immunity, indicating association with a stronger immune response and a better survival outcome. By contrast, the TME of a cold tumor is much more immunosuppressive, responding poorly to treatment (23). Various immune cells that infiltrate tumors may either accelerate or decelerate tumor progression, depending on population and activation status (24). Tumor-promoting immune cells, including dendritic cells (DCs), macrophages, and monocytes, may promote tumor growth, metastasis, and drug resistance in the TME, whereas antitumor immune cells, namely B cells, natural killer (NK) cells, and $CD8^+$ T cells, suppress tumor cell proliferation, invasion, adhesion, and metastasis. DCs, which play a key role in antigen presentation and cytokine secretion, are increased in TC (25). In TC, infiltrating DCs activate T cells and NK cells *via* tumor antigen presentation. Moreover, these infiltrating DCs are known to produce some immunosuppressive cytokines that inhibit immune responses (26). Tumor-associated macrophages (TAMs), which originate from monocytic precursors, infiltrate into the tumor stroma, and facilitate macrophage polarization from the antitumor M1 phenotype to the tumor-promoting M2 phenotype, thereby aggravating TC growth and metastasis (27–29). Monocytes that differentiate in the bone marrow are mainly responsible for inflammation. Increased monocyte infiltration in a mouse TC model promotes tumor progression by elevating immune-related gene and cytokine expression (30). These results show that immunosuppressive cells in the TME of TC can strengthen the ability of tumor cells to fight immune response, thereby enhancing immune escape. Therefore, investigating immune cell infiltration in relation to regulatory mechanisms of TC may be vital for developing new immunotherapeutic strategies that improve TC patient outcomes.

ATP-binding cassette (ABC) transporters are a large superfamily of membrane proteins that acquire energy from ATP hydrolysis to facilitate the translocation of heterogeneous substrates (31). A total of 49 human ABC transporters are grouped into seven distinct subfamilies as follows: ABCA; ABCB; ABCC; ABCD; ABCE; ABCF; and ABCG (32). All ABC transporters are composed of transmembrane domains (TMDs) and nucleotide-binding domains (NBDs); (33). ATP hydrolysis which occurs at the NBDs, induces conformational changes in

TMDs, which, in turn, facilitate inward or outward transportation of specific substrates across the membrane (34). ABC transporters, which are ubiquitous, have been found to be associated with diverse biochemical and physiological processes, such as maintenance of cellular environments, protection from harmful materials, and modulation of drug kinetics (35–37). ABC transporters reportedly play vital roles in numerous carcinomas (38). For example, *ABCG1*, which is overexpressed in clear cell renal cell carcinoma, has been found to be associated with overall patient survival, indicating its potential as a diagnostic and prognostic biomarker in clear cell renal cell carcinoma (39). *ABCB1* and *ABCG2* reportedly play a critical role in the prevention of chemo-resistant liver cancer stem cell death in hepatocellular carcinoma (40). Differentially expressed *ABCC2* and *ABCC5* are considered as diagnostic biomarkers of lung adenocarcinoma, while *ABCC2*, *ABCC6*, and *ABCC8* are reportedly associated with its prognosis (40). Many ABC transporters which are differentially expressed between colorectal cancer (CRC) and non-neoplastic control tissues, may be linked to both the onset and treatment outcomes of CRC (41). The functions of ABC transporters known to be involved in immunity against infection and cancer have been summarized and reviewed, providing a broader understanding of the effects of ABC transporters on immunity to viruses and tumors (42). However, the prognostic roles and immune-related mechanisms of ABC transporters in TC remain unclear.

In this study, we aim to predict the prognostic implications and immune cell infiltration related features of ABC transporters by performing comprehensive analyses followed by validation *via* RT-PCR. Here, we attempt to provide a deeper insight into the immune cell infiltration patterns seen in TC as well as to identify some potential prognostic and immunotherapeutic targets in TC.

MATERIALS AND METHODS

Pre-Processing of Public Data Sources

High-throughput RNA sequencing (RNA-seq) data of 502 TC and 58 normal thyroid tissues obtained from The Cancer Genome Atlas (TCGA) database were considered as the public data source for the purposes of this study. The RNA-seq data in a fragments per kilobase per million format were converted into a transcript per million (TPM) reads format and log2 transformed. The clinical features of TC patients obtained from TCGA dataset are summarized (**Table 1**).

Patients and Specimens

A total of 45 TC patients who received surgical therapy at the Shengjing Hospital of China Medical University were selected for the study. The exclusion and inclusion criteria were similar to those of a previously reported study of ours (43). Both TC and para-cancerous thyroid tissues were collected. A para-cancerous thyroid tissue is defined as a tissue situated at least 2 cm far away from the TC area, as confirmed without TC cells by pathologists. Based on postoperative pathological diagnoses, all included TC tissue specimens were the PTC histological type. Informed consent was obtained from all patients. This study was approved by the Ethics Committee of Shengjing Hospital of China Medical University. The clinical features of all collected patients were summarized (**Table 1**). All specimens were immediately stored until needed for total RNA extraction, qRT-PCR and hematoxylin-eosin staining.

Identification of Hallmark ABC Transporters in TC

We compared the expression levels of all ABC transporters known to be active in TC as well as in normal thyroid tissues, that were available in the public TCGA database. R software, version 3.6.3, with the ggplot2 package (version 3.3.3), was used for this comparison. Correlation between the expression levels of individual genes and prognoses was analyzed *via* the online database Kaplan–Meier plotter (44). To analyze the relapse-free survival (RFS), TC patient samples from TCGA were split into two groups by the relative expression levels of individual genes and assessed by a Kaplan-Meier survival plot. The best performing threshold was considered as the best cutoff value. The hazard ratio (HR) with 95% confidence intervals (CIs) and log rank *P*-value of individual genes were performed. Differentially expressed, prognostic ABC transporters were selected as hallmark transporters for further analysis.

TABLE 1 | Clinical features of TC patients included in the study.

Characteristic	Number (%)	
	TCGA	Collected
Total	502 (100)	45 (100)
Gender		
Female	367 (73.1)	35 (77.8)
Male	135 (26.9)	10 (22.2)
Age		
< 55	335 (66.7)	32 (71.1)
≥ 55	167 (33.3)	13 (28.9)
Histological type		
Classical	356 (70.9)	45 (100)
Follicular	101 (20.1)	0 (0.0)
Other	9 (1.8)	0 (0.0)
Tall cell	36 (7.2)	0 (0.0)
T stage		
T1	143 (28.5)	34 (75.5)
T2	164 (32.7)	8 (17.8)
T3	170 (33.9)	3 (6.7)
T4	23 (4.6)	0 (0.0)
Tx	2 (0.3)	0 (0.0)
N stage		
N0	229 (45.6)	27 (60.0)
N1	223 (44.4)	18 (40.0)
Nx	50 (10.0)	0 (0.0)
M stage		
M0	282 (56.2)	45 (100)
M1	9 (1.8)	0 (0.0)
Mx	211 (42.0)	0 (0.0)
Pathologic stage		
I	281 (56.0)	38 (84.4)
II	52 (10.4)	7 (15.6)
III	112 (22.3)	0 (0.0)
IV	55 (10.9)	0 (0.0)
NR	2 (0.4)	0 (0.0)

NR, Not reported.

Immune-Associated Analysis

Immune and stromal scores *via* ESTIMATE (Estimation of STromal and Immune cells in MAlignant Tumor tissues using Expression data) were used to calculate the levels of infiltrating immune and stromal cells (45). The ESTIMATE score is equal to the sum of immune and stromal scores. The abundance of 24 immune cell type in different kinds of tumors can be estimated using gene expression levels obtained from datasets, such as RNA-seq and microarray data, which are calculated *via* the Immune Cell Abundance Identifier (ImmuCellAI); (46). Therefore, the abundance of tumor-infiltrating immune cells in TC and normal thyroid tissues was determined and compared using ImmuCellAI. The correlation between the expression levels of hallmark ABC transporters and the abundance of gene markers of immune cells infiltrating TC tissues were adjusted for corresponding tumor purity and assessed using Tumor IMmune Estimation Resource 2.0 (TIMER 2.0); (47–49). In addition, immunomodulators and chemokines were compared against the expression of each hallmark ABC transporter using an integrated repository portal for tumor–immune system interactions (TISIDB), in order to analyze the correlation between them (50).

Significant Correlation Analysis and Interaction Network Construction

LinkedOmics is a publicly available platform that includes multi-omics data of 32 TCGA cancer types, and supports multi-omics analysis in a cancer type or pan-cancer analysis. (51). In the LinkFinder modules of LinkedOmics, genes and microRNAs (miRNAs), that were significantly associated with each hallmark ABC transporter, were analyzed statistically using Pearson's correlation coefficient and presented in both volcano plots and heat maps. In the LinkInterpreter modules of LinkedOmics, transcription factor (TF) targets, that were significantly associated with each hallmark ABC transporter, were enriched through Gene Set Enrichment Analysis. The rank criterion was P-value < 0.05, the minimum number of genes (Size) was 3, and the simulations was 500. The GeneMANIA prediction algorithm is an interface and a large database that can be utilized to analyze gene functions and build an interaction network (52). We predicted the functions of hallmark ABC transporters and 100 resultant closely associated genes. Thereafter, a regulation network was constructed for visualization.

Enrichment Analysis

We chose FunRich software (version 3.1.3) to perform enrichment analysis of these five hallmark ABC transporters with the top 100 genes that were closely related to them. Prediction of the functional enrichment of these genes was based on four aspects: cellular component; molecular function; biological process; and biological pathway (53). Gene set analysis of these five hallmark ABC transporters involved in cancer-related pathway activities was performed in GSCALite (54). The following cancer-related pathways were included: TSC/mTOR; RTK; RAS/MAPK; PI3K/AKT; hormone ER; hormone AR; epithelial–mesenchymal transition (EMT); DNA damage response; cell cycle; and apoptosis pathways.

Chemical–Gene–Disease Correlation Analysis

The Comparative Toxicogenomics Database (CTD, version 16548) provides manually curated information regarding chemical–gene, chemical–disease, and gene–disease relationships. This information helps understand the effects exerted by environmental factors on human health (55). The interaction between these five hallmark ABC transporters and chemicals in TC was inferred *via* curated chemical–gene and chemical–disease associations.

Prognostic Value Analysis

The prognostic value of these five hallmark ABC transporters in TC patients was determined *via* receiver operating characteristic (ROC) curve analysis. ROC analysis was performed using R software (version 3.6.3) with the pROC (version 1.17.0.1) and ggplot2 (version 3.3.3) packages. The area under the curve (AUC) ranges between 0.5 and 1, with an AUC value closer to 1 indicating a better prognostic effect, particularly a longer RFS (AUCs of 0.5–0.7; 0.7–0.9; and AUC > 0.9 indicate low accuracy; moderate accuracy; and high accuracy, respectively).

Total RNA Extraction and qRT-PCR

Total RNA was extracted from tissues using Trizol (Takara, Dalian, China), and cDNA was synthesized *via* reverse transcription using a PrimeScript™ RT reagent Kit with gDNA Eraser (Takara, Dalian, China). Thereafter, qRT-PCR analysis was performed on a Roche LightCycler 480 II system using a TB Green®Premix Ex Taq™II kit (Takara, Dalian, China), according to the manufacturers' protocols. Primer sequences are listed (**Table 2**). The housekeeping gene *glyceraldehyde-3-phosphate dehydrogenase* (*GAPDH*) was used as an internal control. The relative expression of target genes was determined using the $2^{-\Delta\Delta}$ CT method, which was similar to that of a previously reported study of ours (43).

Hematoxylin-Eosin Staining

Paraffin-fixed sample sections with 3 μm thick were prepared. Briefly, slides were dewaxed and rehydrated, then nuclei were stained with hematoxylin and cytoplasm was stained with eosin. After dehydrating, slides were mounted with neutral balsam. The images were photographed by a microscope.

Statistical Analysis

Student's *t*-tests or Wilcoxon rank-sum tests were used to compare between the levels of gene expression in TC and normal tissues. Log-rank test and the Kaplan–Meier method were used to depict survival curves. Pearson's correlation coefficient was selected to analyze significantly correlated genes. Spearman's rank correlation coefficient was used to analyze the results of immune-associated analyses. Statistical significance was set at $P < 0.05$.

TABLE 2 | Primers used in this study.

Gene	Primer sequence	Product size (bp)
ABCA8	Forward:5'-TCCTTGCTCCTGGACAACAACC-3' Reverse: 5'-GCTATGTTCTGGTGCTCCACAG-3'	112
ABCA12	Forward:5'-CGGCATTTCAGATACCACCGTG-3' Reverse: 5'-CAGGAGTTGAGATGCCATTGGC-3'	137
ABCB6	Forward:5'-GTTCTTCAACGCCTGGTTTGGC-3' Reverse: 5'-AGCACGACGAAACTTGGTTCTCC-3'	103
ABCB8	Forward:5'-CCTGCTTATCCTCTATGGTGTCC-3' Reverse: 5'-GCCCTGTCTTATTGGCGTCAAAG-3'	158
ABCC10	Forward:5'-TCCAGTTTGCCACCATCCGAGA-3' Reverse: 5'-ACCTCTGTCTGGTCTCCAGCAG-3'	133
GAPDH	Forward: 5'-GCACCGTCAAGGCTGAGAAC-3' Reverse: 5'-TGGTGAAGACGCCAGTGGA-3'	138

RESULTS

Selected Hallmark ABC Transporters Were Differentially Expressed and Correlated With TC Progression

To determine the expression and significance of ABC transporters in TC, we compared the transcription levels of all ABC transporters in TC and normal thyroid tissues obtained from the TCGA database. We also analyzed the correlation between the expression levels of all ABC transporters and TC prognoses using the Kaplan–Meier plotter. An integrated comparison indicated that five ABC transporters, namely *ABCA8*, *ABCA12*, *ABCB6*, *ABCB8*, and *ABCC10*, were differentially expressed. In addition, these five were also significantly associated with the RFS of TC. As such, these five were considered as hallmark ABC transporters ($P < 0.05$; **Figure 1**). Among these hallmark genes, *ABCA12* and *ABCC10* showed significantly higher expression in TC and were associated with a worse RFS as well, indicating that these played a prominent role in promoting TC progression. Moreover, *ABCA8*, *ABCB6*, and *ABCB8* showed significantly lower expression levels in TC, in addition to being associated with a worse RFS, demonstrating that these three mainly functioned as inhibitors of TC progression. Therefore, we subsequently analyzed these five hallmark ABC transporters in order to elucidate the molecular mechanisms underlying the role played by them in TC progression.

Immune-Associated Analysis of Hallmark ABC Transporters in TC

Since immunomodulation plays a vital role in TC progression, we investigated the correlation between immune cell infiltration and the expression levels of the five selected hallmark ABC transporters in TC. Firstly, we evaluated enrichment differences between immune, stromal, and ESTIMATE scores based on the expression of the five hallmark ABC transporters, respectively. The results revealed that the expression levels of all five hallmark ABC transporters were associated with at least one of the immune, stromal, and ESTIMATE scores of TC obtained from TCGA database (**Figures 2A-E**). Especially, both *ABCB6* and *ABCB8* were related to all three types of scores. Thereafter, we investigated the differences between the infiltration of 24 immune cell types in TC and normal thyroid tissues using ImmuCellAI. Among them, a total of 16 types of immune cells were discovered to be differentially infiltrated between TC and normal thyroid tissues, indicating that they may be performing immunoregulatory functions in the progression of TC. These results showed that the abundances of cytotoxic T cells (Tc), type 1 T regulatory cells (Tr1), regulatory T cells (Treg), mucosal-associated invariant T cells, DCs, macrophages, and monocytes in TC tissues were higher than those in normal thyroid tissues. Meanwhile, the abundances of T helper 1 cells (Th1), Th2, follicular helper T cells (Tfh), central memory T cells (Tcm), B cells, NK cells, gamma delta (γδ) T cells (Tgd), $CD4^+$ T cells, and $CD8^+$ T cells in TC tissues were decreased (**Figure 2F**). Thereafter, we used TIMER 2.0 to explore the correlation between the expression levels of hallmark ABC transporters and the abundances of gene markers of differentially infiltrated immune cells in TC. All five hallmark ABC transporters were associated with Th2 cells, Tcm cells, Treg cells, monocytes, and DCs. Of all the expression levels of these transporters, the expression level that was most significantly negatively correlated with the abundance of Tregs (rho = −0.305, $P < 0.001$) was that of *ABCA8*. In addition, the results showed that *ABCA8* expression was associated with most gene markers of infiltrated immune cells, except those of Th1 cells and monocytes. In addition to being the expression level that was most positively correlated with DCs (rho = 0.654, $P < 0.001$), the expression of *ABCA12* was correlated with nearly all infiltrated immune cells, except M1 macrophages. *ABCB6* expression, which showed the most positive correlation with $CD8^+$ T cells (rho = 0.493, $P < 0.001$), appeared to be negatively correlated with most gene markers, except with NK. *ABCB8* expression, which showed the most negative correlation with DCs (rho = −0.364, $P < 0.001$), showed no correlation with Th2 cells, Tfh cells, or NK cells. *ABCC10* expression showed the highest positive correlation with the abundance of M2 macrophages and most gene markers, except with that of NK cells and DCs (rho = 0.284, $P < 0.001$); (**Table 3**; **Figure 2G**).

Moreover, we analyzed the relationship between immunomodulators and the expression levels of hallmark ABC

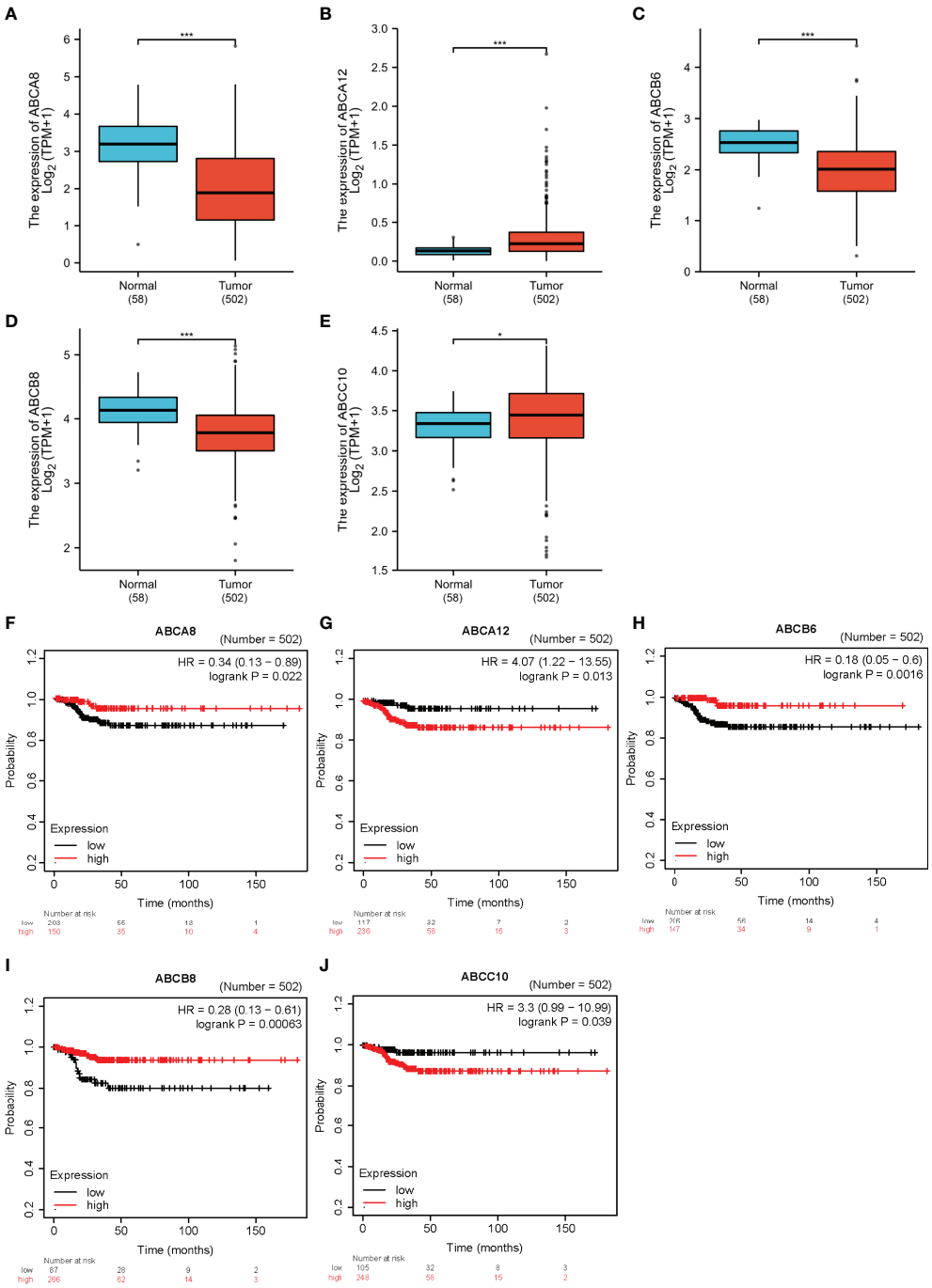

FIGURE 1 | The expression levels and prognostic values of five hallmark ABC transporters in TC. **(A–E)** *ABCA8*, *ABCB6*, and *ABCB8* mRNA expression was downregulated in TC compared with that in normal tissues, while that of *ABCA12* and *ABCC10* was upregulated. **(F–J)** Correlation between expression of the five hallmark ABC transporters and prognoses for TC. *$P < 0.05$, ***$P < 0.001$.

transporters using TISIDB (**Figures 3A-C**). Of all five expression levels, that of *ABCA8* showed the most negative correlation with *VTCN1* (rho = −0.369, $P < 0.001$) as well as the most positive correlation with *KDR* (rho = 0.467, $P < 0.001$). *ABCA12* expression had the most positive correlation with *VTCN1* (rho = 0.755, $P < 0.001$) and the most negative correlation with *KDR* (rho = −0.540, $P < 0.001$). *ABCB6* expression showed a weak to moderate negative correlation with most immunomodulators, particularly *CD274* (rho = −0.550, $P < 0.001$), *TGFBR1* (rho = −0.546, $P < 0.001$), and TNFSF18 (rho = −0.545, $P < 0.001$).

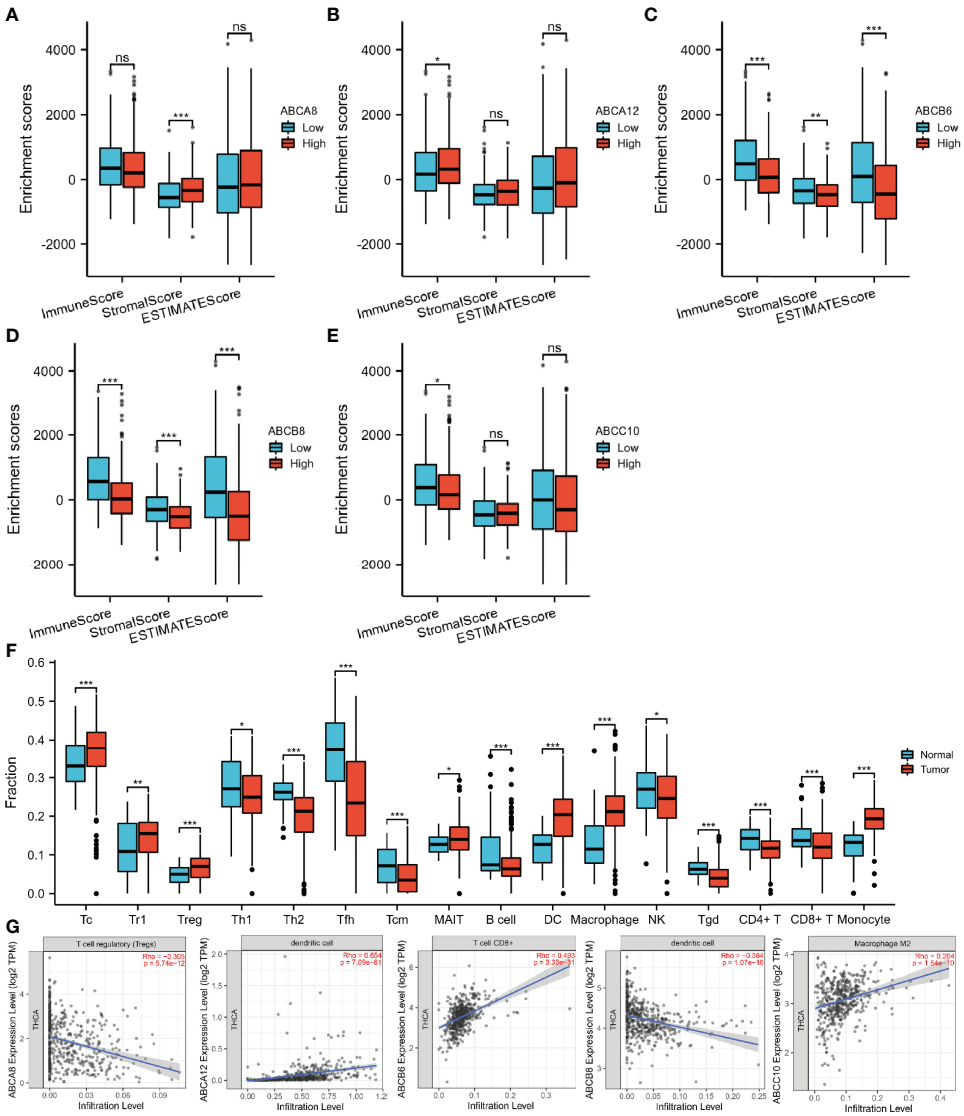

FIGURE 2 | Immune-associated analysis of the hallmark ABC transporters in TC. **(A–E)** Correlation between the expression levels of hallmark ABC transporters and immune, stromal, and ESTIMATE scores. **(F)** Differential abundances of tumor-infiltrating immune cells between TC and normal thyroid tissues. **(G)** Correlation between the expression levels of hallmark ABC transporters and the abundances of tumor-infiltrating immune cells, which were most associated with each hallmark ABC transporters. *$P < 0.05$, **$P < 0.01$, ***$P < 0.001$. ns, not significant..

Similarly, the expression levels of *ABCB6*, and *ABCB8* showed a weak to moderate negative correlation with most immunomodulators, particularly *TGFBR1* (rho = −0.559, $P < 0.001$) and *TNFSF15* (rho = −0.518, $P < 0.001$). Moreover, the highest positive correlation with *TNFRSF25* (rho = 0.499, $P < 0.001$) was shown by *ABCC10* expression. Finally, we analyzed the association between the five hallmark ABC transporters and 41 types of chemokine ligands and 18 types of receptors (**Figures 3D, E**). The results showed that *ABCA8* expression had the most positive correlation with *CCL14* (rho = 0.359, $P < 0.001$) and the most negative correlation with *CXCL17* (rho = −0.406, $P < 0.001$). *ABCA12* expression showed a moderate to strong positive correlation with most ligands and receptors, particularly *CCL20* (rho = 0.684, $P < 0.001$), *CXCL5* (rho = 0.670, $P < 0.001$), *CXCL16* (rho = 0.638, $P < 0.001$), and *CCR9* (rho = 0.431, $P < 0.001$). *ABCB6* expression showed a weak to moderate negative correlation with most ligands and receptors, including *CXCL17* (rho = −0.546, $P < 0.001$), *CXCL5* (rho = −0.496, $P < 0.001$), *CCL20* (rho = −0.496, $P < 0.001$), and *CCR8* (rho = −0.446, $P < 0.001$). The expression level which was most positively correlated with *CCL14* (rho = 0.273, $P < 0.001$) and most negatively correlated with *CXCL5* (rho = −0.387, $P < 0.001$) was that of *ABCB8*. *ABCC10* showed the most positive correlation with *CXCL14* (rho = 0.345, $P < 0.001$). Considered together, these results

TABLE 3 | Transcription factor targets of the five hallmark ABC transporters in TC.

ABC family	Transcription factor target	Enrichment ratio	FDR
ABCA8	V$LXR_DR4_Q3	1.3328	0.0042905
	V$MZF1_01	1.2438	0.0016919
	V$FOX_Q2	1.2433	0.0016919
	V$AHRARNT_01	1.2431	0.011955
	V$CMYB_01	1.2150	0.0028618
ABCA12	V$NFKB_C	1.1400	0.044392
	RGAGGAARY_V$PU1_Q6	1.1116	0.018903
	RYTTCCTG_V$ETS2_B	1.0815	0.010427
	TGANTCA_V$AP1_C	1.0725	0.018903
ABCB6	V$ELK1_02	1.1574	0.019029
	V$E2F_Q4_01	1.1382	0.047158
	GTGACGY_V$E4F1_Q6	1.0871	0.045609
	SCGGAAGY_V$ELK1_02	1.0822	0.0021504
ABCB8	V$ELK1_02	1.1567	0.0035876
	V$YY1_02	1.1456	0.0073703
	V$NRF1_Q6	1.1425	0.0092683
	V$NRF2_01	1.1373	0.0083046
	SCGGAAGY_V$ELK1_02	1.1214	6.2184e-10
ABCC10	V$PAX8_01	1.4316	0.011985
	V$SP1_Q6	1.2090	0.0016837
	V$MYCMAX_B	1.1981	0.0022301
	V$NFKAPPAB65_01	1.1864	0.0061827
	V$NFKB_C	1.1806	0.0051293

FDR, false discovery rate.

revealed that the expression of these five hallmark ABC transporters was closely correlated with immune cell infiltration patterns and immunoregulation in TC.

Analysis of the Significant Correlations of Hallmark ABC Transporters in TC

To explore the molecular mechanisms underlying the regulation of immune cell infiltration in TC by the five hallmark ABC transporters, we identified significantly correlated genes, using the LinkFinder module of LinkedOmics and visualized them in the form of heatmaps and volcano plots. The results showed that the genes which were most significantly positively correlated with the regulation of immune cell infiltration by *ABCA8*, *ABCA12*, *ABCB6*, *ABCB8*, and *ABCC10* were *platelet endothelial aggregation receptor 1 (PEAR1*; rho = 0.604, $P < 0.001$), *V-set domain-containing T cell activation inhibitor 1* (*VTCN1*; rho = 0.754, $P < 0.001$), *microtubule associated protein 1 light chain 3 alpha* (*MAP1LC3A*; rho = 0.694, $P < 0.001$), *chromosome 2 open reading frame 7* (*C2orf7*; rho = 0.782, $P < 0.001$), and *zinc finger protein 513* (*ZNF513*; rho = 0.682, $P < 0.001$), respectively (**Figure 4**). In addition, the genes that were most significantly negatively correlated with the regulation of immune cell infiltration by *ABCA8*, *ABCA12*, *ABCB6*, *ABCB8*, and *ABCC10* were *abhydrolase domain-containing protein 12* (*ABHD12*; rho = −0.523, $P < 0.001$), *BTB domain containing 11* (*BTBD11*; rho = −0.687, $P < 0.001$), *calpastatin* (*CAST*; rho = −0.687, $P < 0.001$), *lysine demethylase 5B* (*KDM5B*; rho = −0.727, $P < 0.001$), and *mitochondrial ribosomal protein S35* (*MRPS35*; rho = −0.589, $P < 0.001$), respectively (**Figure 4**).

It is widely accepted that miRNAs and TFs are key regulators of gene expression. Therefore, we also identified the miRNAs and TF targets that were significantly correlated with the five hallmark ABC transporters, using the LinkFinder and LinkInterpreter modules of LinkedOmics. The results of correlated miRNAs were also present in the form of heatmaps and volcano plots. The miRNAs most significantly positively correlated with *ABCA8*, *ABCA12*, *ABCB6*, *ABCB8*, and *ABCC10* were hsa-mir-145 (rho = 0.454, $P < 0.001$), hsa-mir-934 (rho = 0.677, $P < 0.001$), hsa-mir-204 (rho = 0.517, $P < 0.001$), hsa-mir-22 (rho = 0.538, $P < 0.001$), and hsa-mir-187 (rho = 0.391, $P < 0.001$), respectively (**Figure 5**). Moreover, the miRNAs that were most significantly negatively correlated with *ABCA8*, *ABCA12*, *ABCB6*, *ABCB8*, and *ABCC10* were hsa-mir-203 (rho = −0.432, $P < 0.001$), hsa-mir-1179 (rho = −0.573, $P < 0.001$), hsa-mir-21 (rho = −0.445, $P < 0.001$), hsa-mir-146b (rho = −0.493, $P < 0.001$), and hsa-mir-874 (rho = −0.355, $P < 0.001$), respectively (**Figure 5**). In addition, the TF targets that were most correlated with *ABCA8*, *ABCA12*, *ABCB6*, *ABCB8*, and *ABCC10* were VLXR_DR4_Q3, VNFKB_C, V$ELK1_02, V$ELK1_02, and V$PAX8_01, respectively (**Table 4**).

Regulation Network Construction and Functional Enrichment Analysis of Hallmark ABC Transporters and Their Correlated Genes in TC

To identify the molecular mechanisms underlying the regulation of immune cell infiltration by hallmark ABC transporters more precisely, we constructed a gene regulation network and conducted functional enrichment analysis of the five hallmark ABC transporters and a 100 of the genes that were most correlated with them, using GeneMANIA and Funrich. The network revealed that these genes were closely associated with transmembrane transporter activity and regulation of lipid transport (**Figure 6**). The enrichment analyses indicated that the most highly enriched cellular components were the plasma

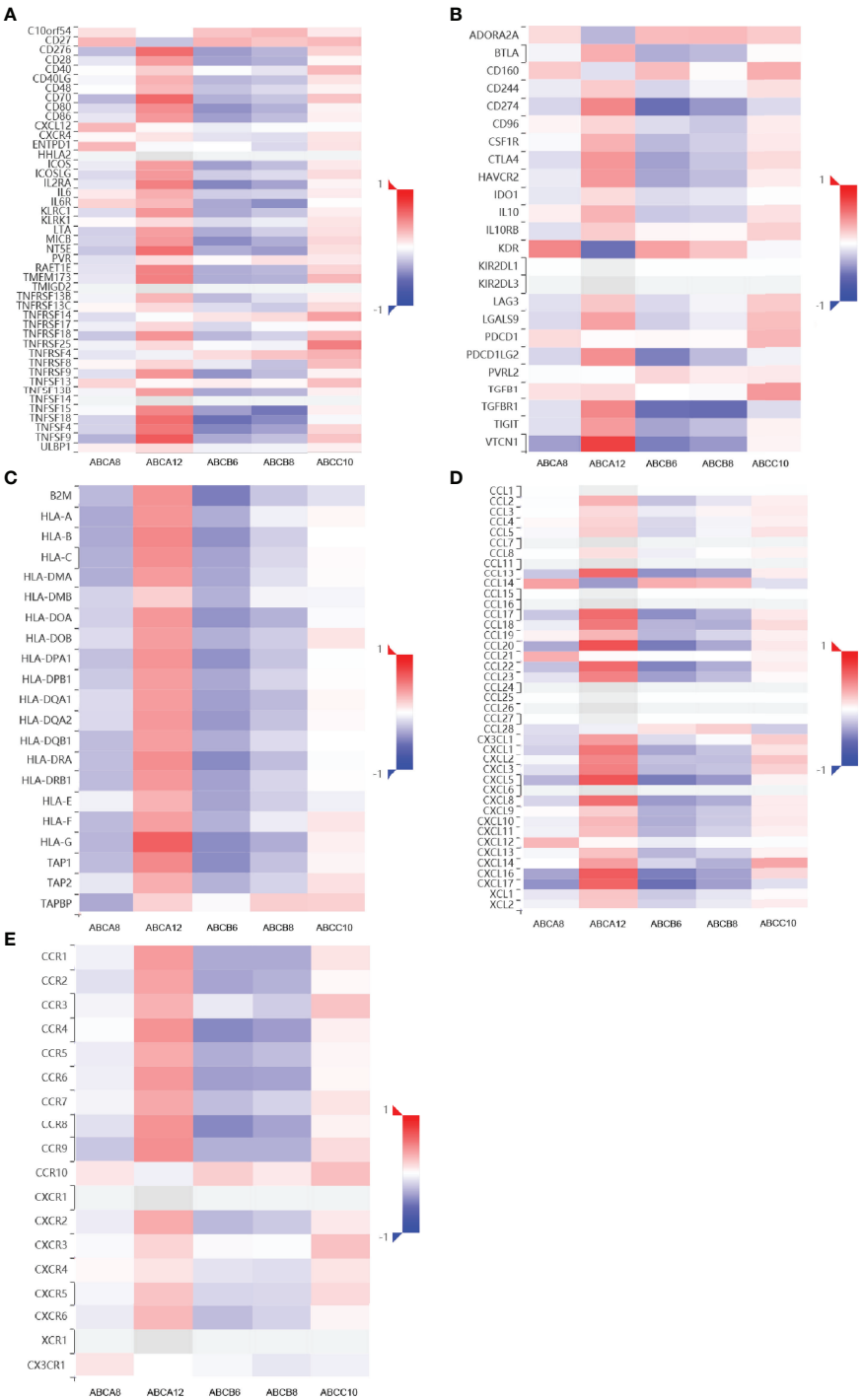

FIGURE 3 | Immunomodulators and chemokines-associated analysis of the hallmark ABC transporters in TC. **(A–C)** Correlation between the expression levels of hallmark ABC transporters and immunomodulators in TC. **(D, E)** Correlation between the expression levels of hallmark ABC transporters and chemokine ligands and receptors in TC.

membrane (53.7%) and lysosomes (26.3%); (**Figure 7A**). Transporter activity (37.6%) and auxiliary transport protein activity (10.9%) were the most highly enriched molecular functions (**Figure 7B**). The biological processes of genes were most highly enriched in transport (49.5%); (**Figure 7C**). Some biological pathways, including transmembrane transport of small molecules (46.3%) and ABC family protein-mediated transport (40.7%), were also most highly enriched (**Figure 7D**). In addition, cancer process and cancer-related pathway enrichment analyses of these hallmark ABC transporters were performed and visualized

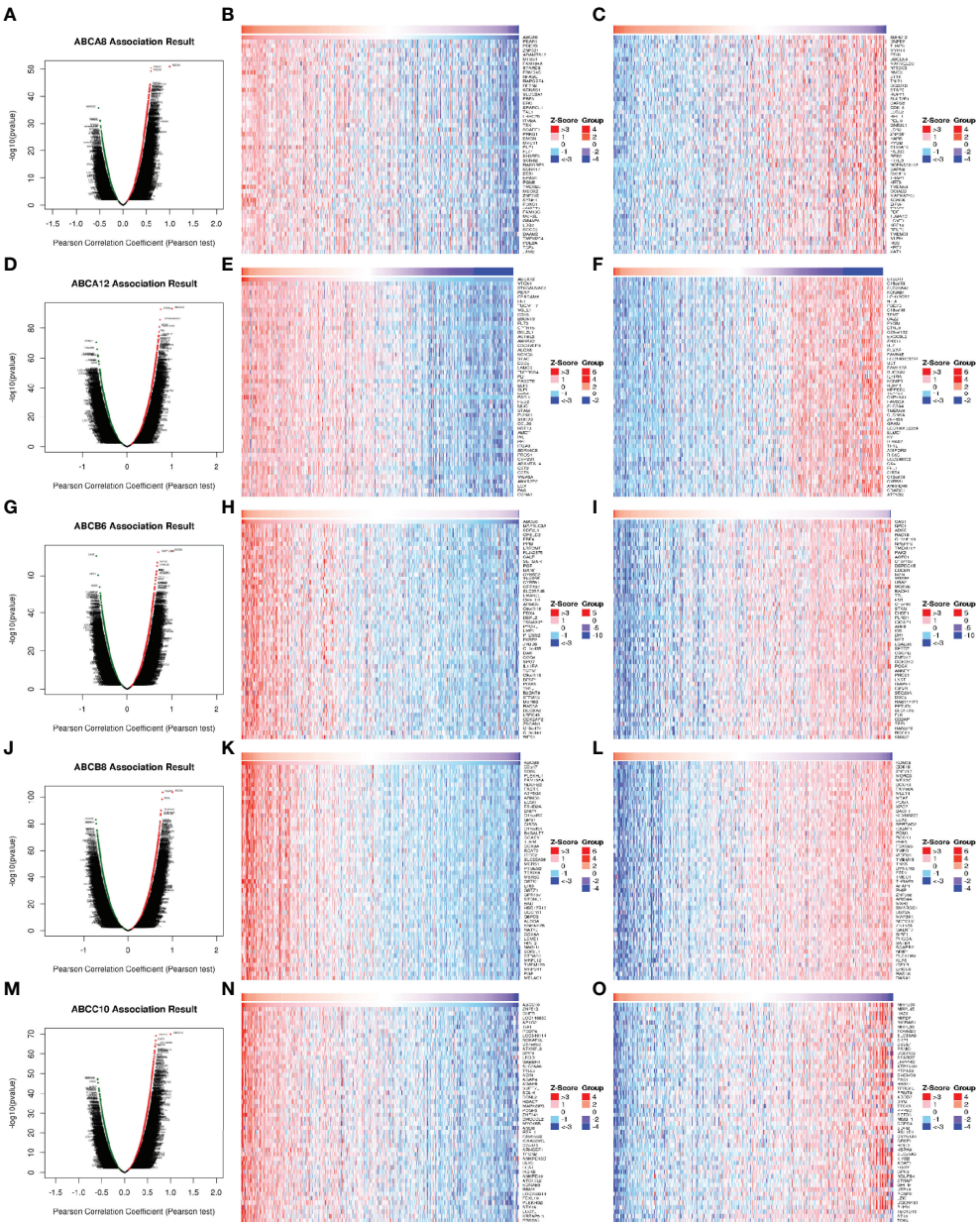

FIGURE 4 | Correlation of differentially expressed genes with five hallmark ABC transporters in TC. **(A, D, G, J, M)** Differentially expressed genes, which were correlated with five hallmark ABC transporters, were analyzed by Pearson test, and visualized in form of volcano plots. **(B, E, H, K, N)** The top 50 genes, which were positively correlated with five hallmark ABC transporters, were visualized in form of heatmaps. **(C, F, I, L, O)** The top 50 genes, which were negatively correlated with five hallmark ABC transporters, were also visualized in form of heatmaps.

using GSCALite. The results showed that all five hallmark ABC transporters were involved in regulating these cancer-related pathways (**Figure 7E**).

Chemical–Gene Correlation Analysis of Hallmark ABC Transporters in TC

Since hallmark ABC transporters were closely associated with the transmembrane transport of small molecules, we screened out TC-associated chemicals and inferred their association with these five hallmark ABC transporters, using the CTD database. The results showed that multiple types of chemicals, including bisphenol A and vincristine, affected the expression or mutagenesis of these hallmark ABC transporters (**Table 5**). These findings provided important information regarding the nature of interaction between chemicals and hallmark ABC transporters and their effects on the progression of TC.

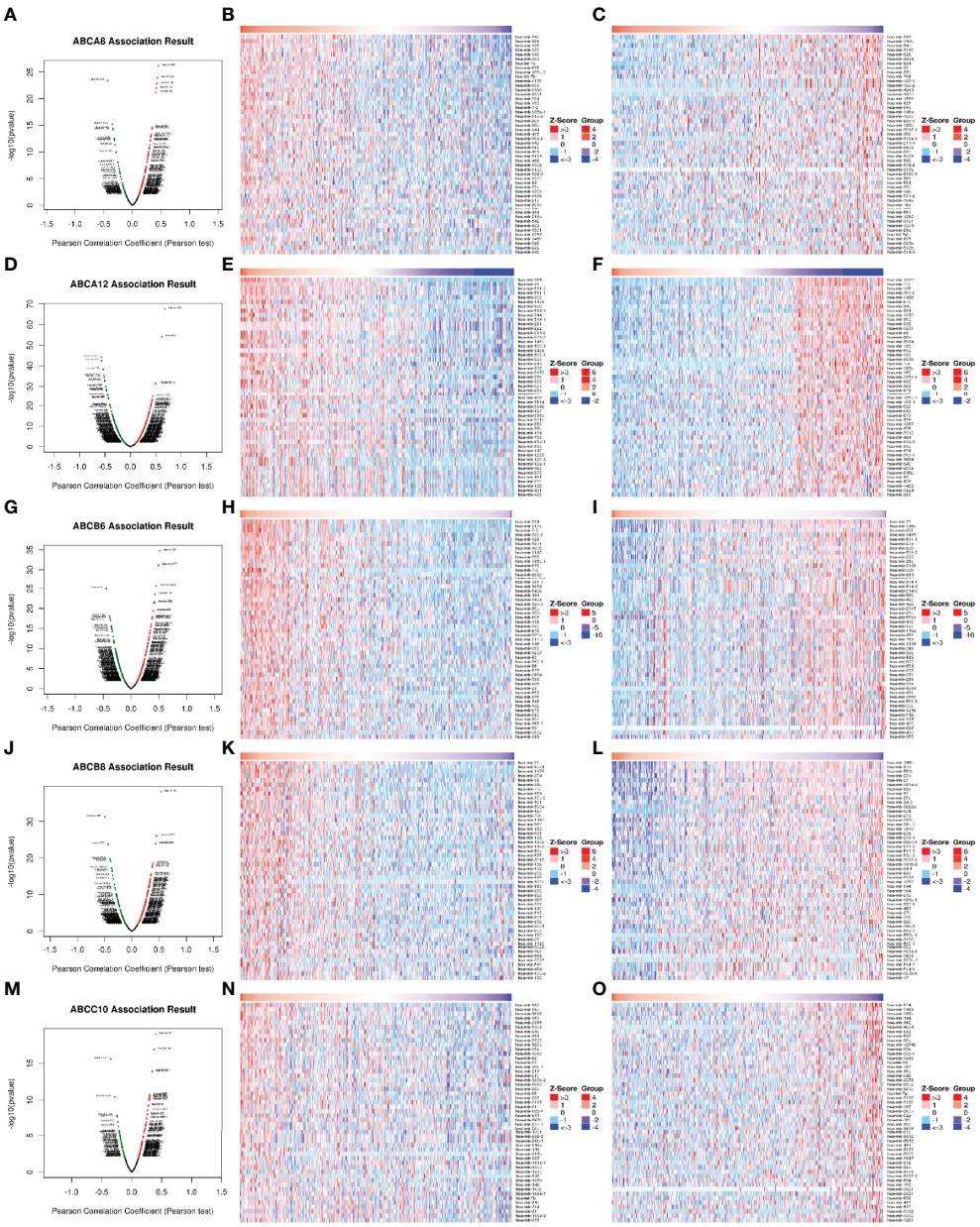

FIGURE 5 | Correlation of differentially expressed miRNAs with five hallmark ABC transporters in TC. **(A, D, G, J, M)** Differentially expressed miRNAs, which were correlated with five hallmark ABC transporters, were analyzed by Pearson test, and visualized in form of volcano plots. **(B, E, H, K, N)** The top 50 miRNAs, which were positively correlated with five hallmark ABC transporters, were visualized in form of heatmaps. **(C, F, I, L, O)** The top 50 miRNAs, which were negatively correlated with five hallmark ABC transporters, were also visualized in form of heatmaps.

Prognostic Value of Hallmark ABC Transporters in TC

To evaluate the prognostic value of these five hallmark ABC transporters, ROC curves were generated using the expression data of TC and normal thyroid tissues obtained from TCGA (**Figure 8A**). The AUCs and 95% CI values of these five hallmark ABC transporters were calculated (**Table 6**). Among the five hallmark ABC transporters, *ABCA8* showed the highest relative accuracy while that of *ABCC10* appeared to be the lowest. These results indicated the considerable potential shown by these five hallmark ABC transporters for predicting the RFS of TC.

Validation of Hallmark ABC Transporters in TC

Representative hematoxylin and eosin staining images of both collected TC and para-cancerous thyroid tissues were performed (**Supplemental Figure 1**). To validate the bioinformatic analyses of these five hallmark ABC transporters in TC, we performed qRT-

TABLE 4 | Correlations of the expression of the five hallmark ABC transporters with the abundance of gene markers of immune cell infiltration in TC.

Cell type	Gene markers	*ABCA12*		*ABCA8*		*ABCB6*		*ABCB8*		*ABCC10*	
		r	*P*	r	*P*	r	*P*	r	*P*	r	*P*
B cell		-0.216	*	0.157	*	0.073	ns	0.08	ns	-0.142	*
	CD19	0.176	*	0.055	ns	-0.148	*	-0.184	*	0.031	*
	CD79A	0.224	*	-0.047	ns	-0.256	*	-0.208	*	-0.012	ns
Th1		-0.147	*	-0.358	*	-0.097	ns	-0.079	ns	-0.288	*
	IFNG	0.159	*	0.027	ns	-0.187	*	-0.175	*	0.063	ns
	STAT1	0.481	*	-0.032	ns	-0.288	*	-0.174	*	0.169	*
	STAT4	0.383	*	-0.035	ns	-0.219	*	-0.270	*	0.189	*
	TNF	0.179	*	0.087	ns	-0.112	*	-0.133	*	0.162	*
	TBX21	0.052	ns	0.105	*	-0.012	ns	-0.064	ns	0.171	*
Th2		0.223	*	-0.198	*	-0.249	*	-0.102	*	-0.12	*
	GATA3	0.316	*	-0.011	ns	-0.073	ns	-0.104	*	0.157	*
	IL13	0.106	*	0.003	ns	-0.085	ns	-0.071	ns	0.124	*
	STAT5A	0.319	*	0.108	*	-0.165	*	-0.088	ns	0.192	*
	STAT6	0.242	*	0.258	*	-0.019	ns	0.016	ns	0.425	*
Tfh		-0.107	*	0.163	*	0.119	*	0.072	ns	-0.06	ns
	BCL6	0.276	*	0.148	*	0.023	ns	-0.039	ns	0.234	*
	IL21	0.070	ns	-0.006	ns	-0.077	ns	-0.079	ns	0.054	ns
Tcm		-0.315	*	0.272	*	0.355	*	0.129	*	0.211	*
Treg		0.403	*	-0.305	*	-0.358	*	-0.275	*	0.106	*
	CCR8	0.417	*	-0.022	ns	-0.274	*	-0.121	*	0.152	*
	FOXP3	0.443	*	-0.101	*	-0.302	*	-0.257	*	0.134	*
	TGFB1	0.129	*	0.342	*	0.184	*	0.105	*	0.519	*
$CD8^+$ T		-0.299	*	0.291	*	0.493	*	0.224	*	-0.078	ns
	CD8A	0.074	ns	0.117	*	-0.048	ns	-0.077	ns	0.115	*
	CD8B	0.288	*	0.018	ns	-0.086	ns	-0.224	*	0.212	*
NK		-0.128	*	0.279	*	0.246	*	0.064	ns	-0.129	*
	KIR2DL1	-0.102	*	0.090	ns	0.051	ns	-0.016	ns	-0.013	ns
	KIR2DL3	-0.020	ns	0.069	ns	0.012	ns	-0.042	ns	0.081	ns
	KIR2DS4	-0.100	ns	0.112	*	-0.005	ns	-0.035	ns	0.062	ns
	KIR3DL1	-0.141	*	0.152	*	0.073	ns	0.048	ns	0.102	*
	KIR3DL2	-0.002	ns	0.109	*	0.006	ns	-0.059	ns	0.163	*
	KIR3DL3	-0.067	ns	0.021	ns	-0.062	ns	-0.073	ns	0.017	ns
M1		0.098	ns	0.141	*	-0.137	*	-0.068	ns	-0.111	ns
	IRF5	0.480	*	-0.057	ns	-0.301	*	-0.197	*	0.255	*
	NOS2	0.020	ns	0.191	*	0.106	*	0.179	*	0.219	*
	PTGS2	0.561	*	0.009	ns	-0.277	*	-0.235	*	0.188	*
M2		0.401	*	-0.069	ns	-0.154	*	-0.138	*	0.284	*
	CD163	0.344	*	0.168	*	-0.183	*	-0.061	ns	0.160	*
	MS4A4A	0.352	*	0.090	ns	-0.219	*	-0.163	*	0.126	*
	VSIG4	0.336	*	0.072	ns	-0.276	*	-0.149	*	0.079	ns
Monocyte		0.33	*	-0.166	*	-0.364	*	-0.286	*	0.281	*
	CD86	0.374	*	-0.001	ns	-0.306	*	-0.252	*	0.062	ns
	CSF1R	0.286	*	0.096	ns	-0.173	*	-0.145	*	0.149	*
DC		0.654	*	-0.166	*	-0.432	*	-0.364	*	0.129	*
	CD1C	0.463	*	-0.058	ns	-0.328	*	-0.280	*	0.030	ns
	HLA-DPA1	0.386	*	-0.178	*	-0.406	*	-0.309	*	-0.073	ns
	HLA-DPB1	0.350	*	-0.134	*	-0.344	*	-0.276	*	-0.060	ns
	HLA-DQB1	0.342	*	-0.212	*	-0.377	*	-0.322	*	-0.120	*
	HLA-DRA	0.408	*	-0.166	*	-0.404	*	-0.280	*	-0.061	ns
	ITGAX	0.392	*	-0.030	ns	-0.271	*	-0.252	*	0.206	*
	NRP1	-0.049	ns	0.407	*	0.331	*	0.284	*	0.453	*

*Correlations were analyzed using Spearman's test and adjusted for tumor purity. Th, helper T cell; Tfh, follicular helper T cell; Treg, regulatory T cell; NK, natural killer cell; DC, dendritic cell; r, the purity-adjusted partial Spearman's rho value. *P < 0.05, ns, not significant.*

PCR tests to examine their transcriptional expression in both TC and para-cancerous thyroid tissues. The results indicated that the expression levels of *ABCA12* and *ABCC10* in TC were higher compared to those in para-cancerous thyroid tissue, while the expression levels of *ABCA8*, *ABCB6*, and *ABCB8* in TC were significantly lower (P <0.05; **Figure 8B**). These results were consistent with those obtained from the public *via* TCGA database.

DISCUSSION

It has become increasingly evident that ABC transporters play important roles in the immunomodulation of tumors. For example, multidrug resistance protein 1 (MDR1), encoded by *ABCB1*, is expressed in cytotoxic T lymphocytes and NK cells, and mediates immune responses (56). A high level of the $MDR1^+$

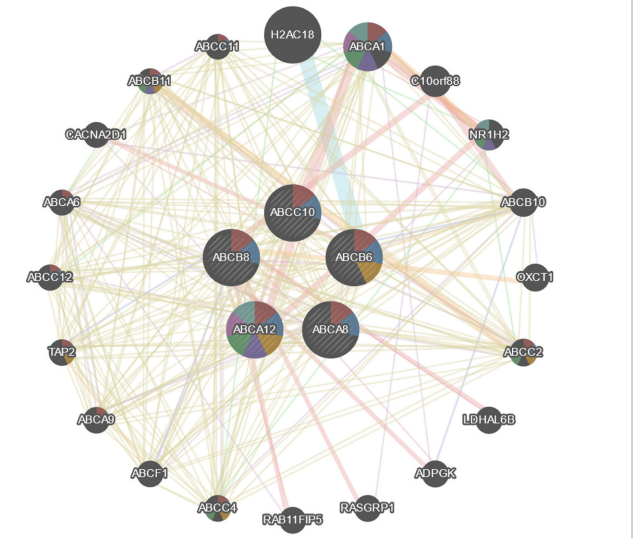

FIGURE 6 | The constructed gene regulation network of five hallmark ABC transporters and 100 genes, which were most highly correlated with five hallmark ABC transporters.

immune cell infiltrate, mostly comprising M2 macrophages, was confirmed as an independent prognostic factor associated with poor prognoses for epithelial ovarian cancer (57). *ABCA1* regulates the immune sensitivity of osteosarcoma cells. Moreover, the *ABCB1*: *ABCA1* ratio was reportedly upregulated in osteosarcoma cells and positively correlated with a higher probability of relapse (58). *ABCA8* expression was downregulated in stomach adenocarcinoma and was positively associated with six types of infiltrated immune cells, particularly M2 macrophages (59). Major histocompatibility complex class I (MHC-I) molecules play a vital role in immune surveillance as well as in the presentation of antigen peptides on the cell surface (60). The heterodimer of transporter associated with antigen processing (TAP) transports antigenic peptides and provides peptides to MHC-I molecules (61, 62). TAP blockade in DCs reportedly impaired classic MHC-I presentation for $CD8^+$ T cell priming (63). Moreover, low TAP1/TAP2 expression led to the overexpression and efficient presentation of the antigen preprocalcitonin in lung carcinoma, as recognized *via* tumor-specific cytotoxic T lymphocytes (64). *ABCC8* is considered a prognostic risk factor which is closely related to the LUAD microenvironment (65). Single-nucleotide polymorphisms (SNPs) in *TAP1* and *TAP2* affected their expression and were associated with cervical cancer in the Chinese Han population (66). *ABCD3* expression, which is considered as an independent prognostic factor of CRC, was decreased in CRC tissues and associated with the overall survival of CRC patients (67).

Previous studies have demonstrated that altered expression levels of some ABC transporters were associated with their molecular roles in TC. *ABCA9* expression was upregulated by hsa_circ_0039411 sponging miR-1179, leading to enhanced oncogenic properties in PTC (68). *ABCB5* expression was reported to be associated with larger tumor size in PTC (69). Moreover, in the solid variant of PTC, high *ABCC1* expression was associated with larger tumor size, while high *ABCG2* expression was correlated with lymphovascular invasion (70). *ABCG2* expression was also found to be closely related to the induction of EMT in PTC (71). High *ABCC2* expression was observed in advanced stage MTC (72). In ATC, high expression levels of *ABCB1*, *ABCC1* and *ABCG2* observed in several cell lines and tissues, were associated with cancer drug resistance (73). However, the prognostic and immunotherapeutic value of ABC transporters in TC has not been well characterized. Therefore, the current study aimed to explore the prognostic and immune related value of ABC transporters in TC, leading to the provision of new directions and targets for its treatment.

In this study, data of TC and normal thyroid tissues from TCGA were analyzed to screen out hallmark ABC transporters, which are differentially expressed and associated with the prognosis for TC. Based on the results, *ABCA8*, *ABCA12*, *ABCB6*, *ABCB8*, and *ABCC10* were selected as hallmark ABC transporters in TC. Of these, the expression of *ABCA8*, *ABCB6*, and *ABCB8* was down-regulated in TC, compared with those in normal thyroid tissues, while that of *ABCA12* and *ABCC10* was up-regulated. Usually, up-regulation of oncogenes and down-regulation of anti-oncogenes affect many behavior patterns of malignant tumor cells, including metastasis and immune resistance. Our results revealed that *ABCA8*, *ABCB6*, and *ABCB8* may inhibit the malignant progression of TC. Conversely, *ABCA12* and *ABCC10* may promote the occurrence and growth of TC. Since these are differentially expressed in TC and closely associated with the prognoses for TC, we selected these five as hallmark ABC transporters in TC for subsequent analyses.

It is increasingly becoming evident that immunotherapies play a vital role in tumor treatment, wherein the efficacy of immunomodulation depends mainly on immune cell infiltration. Based on our results, the five hallmark ABC transporters exert a variety of effects on immune cell infiltration in TC. Firstly, the expression of five hallmark ABC transporters was associated with two different TC subsets (hot or cold), indicating that the five hallmark ABC transporters may be useful for converting immunosuppressive (cold) TCs into immunosensitive (hot) ones. Moreover, our results showed that all five hallmark ABC transporters were associated with Th2 cells, Tcm cells, Treg cells, monocytes, and DCs, which revealed that their roles in immune cell infiltration-related immunoregulation were similar. In addition, the specificity of the transporters in regulating Th1 cells, Tfh cells, $CD8^+$ T cells, NK cells, M1 macrophages, and B cells demonstrated the diversity of their roles. Our results also indicated that multiple immunomodulators, such as KDR, MHC

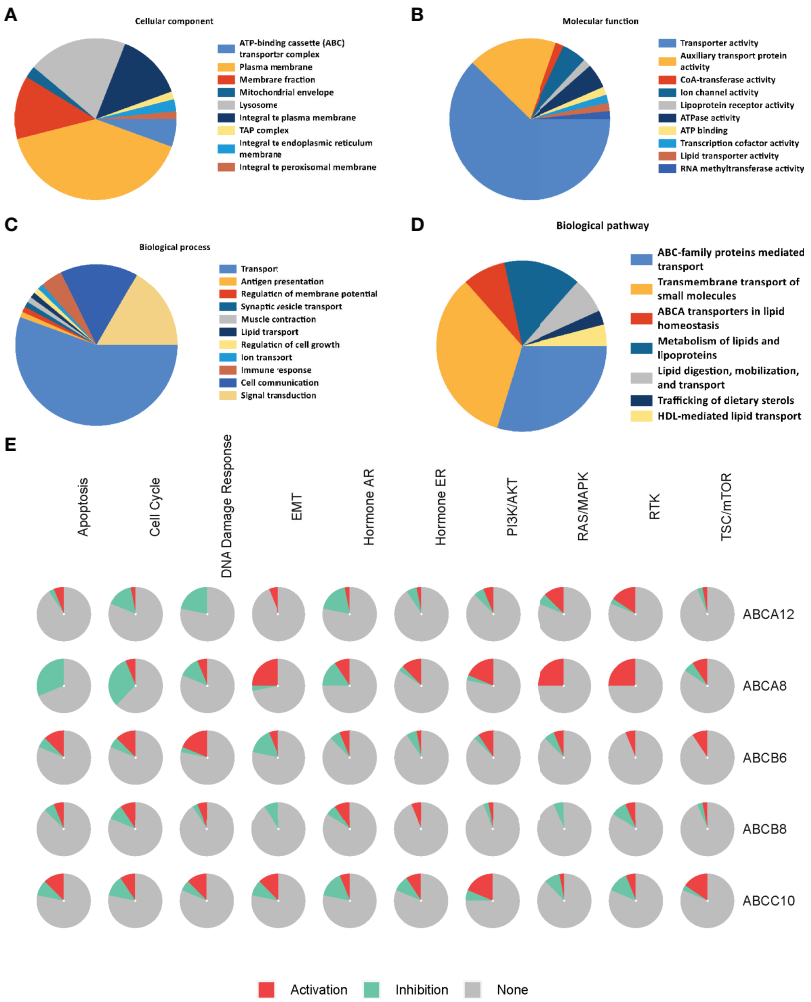

FIGURE 7 | Functional and pathway enrichment analysis of the five hallmark ABC transporters in TC. **(A)** The most enriched cellular components of correlated genes of the five hallmark ABC transporters. **(B)** The most enriched molecular functions of correlated genes of the five hallmark ABC transporters. **(C)** The most enriched biological processes of correlated genes of the five hallmark ABC transporters. **(D)** The most enriched biological pathways of correlated genes of the five hallmark ABC transporters. **(E)** The cancer related pathway enrichment of the five hallmark ABC transporters.

molecules, VTCN1, CD274, TGFBR1, TNFSF18, and TNFSF15, were closely associated with these five hallmark ABC transporters. KDR, also known as vascular endothelial growth factor receptor 2 (VEGFR2), is the main receptor of VEGF signaling (74). Activation of KDR, which promotes endothelial cell mitogenesis and vascular permeability, plays a vital role in the induction of tumor angiogenesis (75). The VEGF-KDR signaling pathway was found to play an immunosuppressive role in TME and immune effector cell activity (76). MHC molecule expression is known to mediate immune escape mechanisms in tumors (77). VTCN1, also termed B7-H4, reportedly inhibits T cell proliferation and cytokine secretion, thereby negatively regulating T cell immune response, and positively regulating immune escape (78). CD274, also commonly referred to as programmed cell death 1 ligand 1 (PD-L1), is a ligand of PD-1, which is expressed on many immune cells. The PD-1/PD-L1 axis, which is exploited by tumor cells, may inhibit immune response and block immune cell activation (78). Cancer cells generate multiple factors, including TGF-β1, to create an immune inhibitory environment and evade T cell surveillance (79, 80). As the irreplaceable receptor of TGF-β1, TGFBR1, which is observed in different tumor types, participates in tumor immunological reactions (81). Tumor necrosis factor (TNF) superfamily ligands, such as TNFSF15 and TNFSF18, exert diverse modulatory effects by influencing immune responses and impacting immune cells (82–84). Moreover, chemokine–chemokine receptor interactions regulate immune cell recruitment into tumors and the stimulation of immune response (85). Our results demonstrated that the immune regulation by hallmark ABC transporters was partly mediated *via* chemokine ligands and receptors.

The presence of complex regulatory networks that affect almost all molecular processes at both intracellular as well as

TABLE 5 | Inferred correlation between hallmark ABC transporters and chemicals in TC.

Gene Name	Chemical name	Interaction	References (PubMed ID)
ABCA8	Bisphenol A	Bisphenol A results in decreased *ABCA8* expression	29050248; 25181051
ABCA8	Doxorubicin	Doxorubicin results in decreased *ABCA8* expression	32173973; 17909728; 16010429; 29803840
ABCA8	Indomethacin	Indomethacin results in increased *ABCA8* expression	18791128; 24737281
ABCA8	Perfluorooctane sulfonic acid	Perfluorooctane sulfonic acid results in decreased *ABCA8* expression	24420840; 27153767
ABCA8	Rosiglitazone	Rosiglitazone results in decreased *ABCA8* expression	17188145; 14736730; 11352223; 25572481
ABCA8	Vincristine	Vincristine results in decreased susceptibility to vincristine, which affects *ABCA8* expression	9571977; 19944135
ABCA12	1,2-Dimethylhydrazine	1,2-Dimethylhydrazine results in decreased *ABCA12* expression	21864636; 22206623
ABCA12	Bisphenol A	Bisphenol A results in both increased *ABCA12* gene methylation and decreased *ABCA12* expression	29050248; 22576693
ABCA12	Tretinoin	Tretinoin results in decreased *ABCA12* expression	17045167; 16026305; 23724009
ABCA12	Vincristine	Vincristine results in increased *ABCA12* expression	9571977; 23649840; 19944135
ABCB6	1,2-Dimethylhydrazine	1,2-Dimethylhydrazine results in decreased *ABCB6* expression	21864636; 22206623
ABCB6	4,4'-diaminodiphenylmethane	4,4'-diaminodiphenylmethane results in increased *ABCB6* expression	7505956; 3712494; 6582329; 6587162; 18648102
ABCB6	Acrylamide	Acrylamide results in decreased *ABCB6* expression	28606764; 32763439
ABCB6	Bisphenol A	Bisphenol A affects *ABCB6* expression	29050248; 29275510
ABCB6	Chloroprene	Chloroprene results in increased *ABCB6* expression	23125180; 12562636
ABCB6	Copper	Copper results in increased *ABCB6* expression	19497425; 30556269
ABCB6	Paclitaxel	Paclitaxel results in decreased *ABCB6* expression	20025538; 20737486
ABCB6	Phenobarbital	*ABCB6* gene mutant form results in increased susceptibility to phenobarbital; Phenobarbital results in increased *ABCB6* expression	28245158; 3356011; 3133336; 3137195; 3865012; 3856057; 6850638; 2910521; 19159669
ABCB6	Troglitazone	Troglitazone results in increased *ABCB6* expression	15785241; 25596134
ABCB6	Vincristine	Vincristine results in decreased susceptibility to vincristine, which affects *ABCB6* expression	9571977; 19944135
ABCB8	1,2-Dimethylhydrazine	1,2-Dimethylhydrazine results in increased *ABCB8* expression	21864636; 22206623
ABCB8	Bisphenol A	Bisphenol A results in decreased *ABCB8* expression	29050248; 30816183; 25181051
ABCC10	2-Acetylaminofluorene	2-Acetylaminofluorene results in increased *ABCC10* expression	28245158; 12566991
ABCC10	4,4'-diaminodiphenylmethane	4,4'-diaminodiphenylmethane results in increased *ABCC10* expression	7505956; 1399818; 3712494; 6582329; 6587162; 18648102
ABCC10	Acrylamide	Acrylamide results in decreased *ABCC10* expression	28606764; 32763439
ABCC10	Bisphenol A	Bisphenol A results in both increased *ABCC10* intron methylation and decreased *ABCC10* expression	29050248; 25181051; 30906313
ABCC10	Doxorubicin	Doxorubicin results in decreased *ABCC10* expression	32173973; 17909728; 16010429; 29803840
ABCC10	Imatinib mesylate	Imatinib mesylate inhibits the reaction [ABCC10 protein results in decreased susceptibility to paclitaxel and vincristine]	16940797; 19841739
ABCC10	Paclitaxel	Paclitaxel results in increased *ABCC10* expression	20025538; 20737486
ABCC10	Vincristine	ABCC10 protein results in decreased susceptibility to vincristine	9571977; 19841739

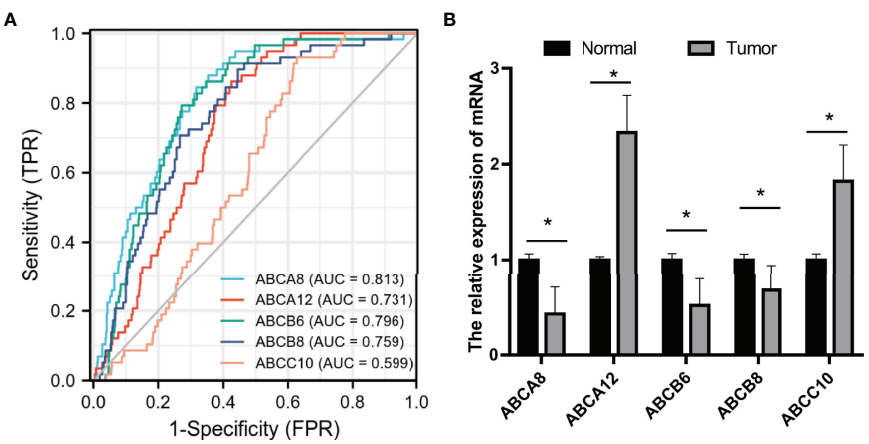

FIGURE 8 | Prognostic prediction value and validation of the five hallmark ABC transporters in TC. **(A)** The ROC curves of the five hallmark ABC transporters in TC. **(B)** Relative mRNA expression of the five hallmark ABC transporters in TC and normal thyroid tissues. FPR, false positive rate; TPR, true positive rate. *$P < 0.05$.

TABLE 6 | Prognostic value prediction of five hallmark ABC transporters in TC.

Variables	AUC	CI	Sensitivity	Specificity
ABCA8	0.813	0.763–0.863	84.5%	68.2%
ABCA12	0.731	0.681–0.781	86.2%	57.5%
ABCB6	0.796	0.747–0.845	79.3%	72.7%
ABCB8	0.759	0.703–0.816	89.7%	55.5%
ABCC10	0.599	0.540–0.657	93.1%	37.3%

AUC, area under the curve; CI, confidence interval.

TME levels, is well known. The results of the analysis conducted on correlated genes, miRNAs, and TF targets showed that each hallmark ABC transporters possessed a unique feature and a distinctive regulatory pattern. The constructed regulation network and enrichment of these five transporters showed that the genes, which were most correlated with the five hallmark ABC transporters, were closely associated with transmembrane transporter activity and ABC family protein-mediated transport. In addition, multiple cancer processes and cancer-related pathways, including RTK, RAS/MAPK, PI3K/AKT, and EMT, were partly activated or suppressed by these five hallmark ABC transporters. These findings indicated that these five hallmark ABC transporters may modulate immune cell infiltration patterns by altering the expression levels of correlated genes, regulating transmembrane transporter activity, and influencing cancer-related pathways. However, the exact regulatory mechanisms have not yet been fully elucidated and further discovery and validation are felt to be required.

The known risk factors for TC include female sex, obesity, smoking status, radioactive iodine exposure history, and family genetic history (86–88). However, these recognized causative factors do not fully explain the increasing incidence of TC. Recent studies have demonstrated the influence of anthropogenic environmental chemical factors on TC (89). For example, individuals with higher cadmium exposure were observed to be more susceptible to TC (90). Environmental radiation exposure, such as that due to the Chernobyl accident, led to radiation dose-associated DNA double-strand breaks, subsequently resulting in PTC growth (91). Artificial light at night has also been found to be positively associated with TC incidence (92). Exposure to multiple essential microelements, including manganese and strontium, were positively associated with capsular invasion, multifocality, and tumor stage of PTC (93). Bisphenol A altered endocrine function and partly facilitated EMT in PTC (94). In this study, we focused on elucidating the associations between TC-associated chemicals and the five hallmark ABC transporters. We indicated that these chemicals exerted significant effects on the expression of these five hallmark ABC transporters in TC. The methylation and mRNA expression levels of these five hallmark ABC transporters were mostly affected by bisphenol A and vincristine. The findings of the present study are consistent with those of previous studies. Therefore, more attention should be paid to regulating the impact of chemical factors on TC.

Moreover, to verify the results of bioinformatic analyses, we performed qRT-PCR to detect the mRNA expression of these five hallmark ABC transporters in collected TC and para-cancerous thyroid tissues. The qRT-PCR results were entirely consistent with our TCGA analysis. In the future, we expect to directly confirm probable mechanisms underlying the regulation of immune cell infiltration patterns in TC by these five hallmark ABC transporters, *via in vitro* and *in vivo* experiments.

Our study was affected by several limitations. Firstly, in our effort to elucidate the specific roles of hallmark ABC transporters in modulating TC prognosis and progression, we analyzed the data of all TCs obtained from the TCGA database, without differentiating between its pathological subtypes. Secondly, compared with PTC, the incidence rates of MTC and ATC are very low. As such, it is relatively difficult to collect ATC and MTC case data for qRT-PCR analysis. Therefore, only PTC and para-cancerous thyroid tissues could be collected and used for experimental validation.

CONCLUSIONS

The findings of this study indicate that five hallmark ABC transporters (*ABCA8*, *ABCA12*, *ABCB6*, *ABCB8*, and *ABCC10*) are strongly associated with immunomodulation in TC, as well as with the prognoses for TC. In addition, factors, as well as chemicals and regulatory networks, that are significantly correlated with these five hallmark ABC transporters in TC, are elucidated. These findings may help better understand the molecular mechanisms underlying the role played by these hallmark ABC transporters in TC. The findings of this study also indicate that these hallmark ABC transporters may help enhance prognostic prediction and enable the development of effective immunotherapies against TC.

DATA AVAILABILITY STATEMENT

The original contributions presented in the study are included in the article/**Supplementary Material**. Further inquiries can be directed to the corresponding author.

ETHICS STATEMENT

The studies involving human participants were reviewed and approved by the Ethics Committee of Shengjing Hospital of China Medical University. The patients/participants provided their written informed consent to participate in this study.

AUTHOR CONTRIBUTIONS

Conceptualization, LW and ZL; Methodology, LW, XS and JH; Investigation, LW and XS; Resources, LW, XS and JH; Writing – Original Draft Preparation, LW; Writing – Review & Editing, XS, JH and ZL; Supervision, ZL. All authors read and approved the final manuscript.

FUNDING

This work was supported by the National Natural Science Foundation of China (Grant number: 81672644), the Young Scholar Support Program 2018 of China Medical University (Grant number: QGZD2018061), and the 345 Talent Project of Shengjing Hospital of China Medical University (50A; 30).

ACKNOWLEDGMENTS

We would like to thank Dr. Yang Fan (Shengjing Hospital of China Medical University) for her critical reading of the manuscript.

SUPPLEMENTARY MATERIAL

The Supplementary Material for this article can be found online at: https://www.frontiersin.org/articles/10.3389/fonc.2022.781686/full#supplementary-material

Supplementary Figure 1 | Representative hematoxylin and eosin staining images of both collected TC and para-cancerous thyroid tissues. **(A)** Representative hematoxylin and eosin staining image of para-cancerous thyroid tissues. **(B)** Representative hematoxylin and eosin staining image of PTC tissues. Magnification 200×.

REFERENCES

1. Roman BR, Morris LG, Davies L. The Thyroid Cancer Epidemic 2017 Perspective. *Curr Opin Endocrinol Diabetes Obes* (2017) 24(5):332–6. doi: 10.1097/MED.0000000000000359
2. Ellison LF, Bushnik T. Changing Trends in Thyroid Cancer Incidence in Canada: A Histologic Examination 1992 to 2016. *Health Rep* (2020) 31(1):15–25. doi: 10.25318/82-003-x202000100002-eng
3. Dal Maso L, Tavilla A, Pacini F, Serraino D, van Dijk BAC, Chirlaque MD, et al. Survival of 86,690 Patients With Thyroid Cancer: A Population-Based Study in 29 European Countries From EUROCARE-5. *Eur J Cancer* (2017) 77:140–52. doi: 10.1016/j.ejca.2017.02.023
4. Dal Maso L, Panato C, Franceschi S, Serraino D, Buzzoni C, Busco S, et al. The Impact of Overdiagnosis on Thyroid Cancer Epidemic in Italy,1998-2012. *Eur J Cancer* (2018) 94:6–15. doi: 10.1016/j.ejca.2018.01.083
5. Sung H, Ferlay J, Siegel RL, Laversanne M, Soerjomataram I, Jemal A, et al. Global Cancer Statistics 2020: GLOBOCAN Estimates of Incidence and Mortality Worldwide for 36 Cancers in 185 Countries. *CA Cancer J Clin* (2021) 71(3):209–49. doi: 10.3322/caac.21660
6. Vaccarella S, Franceschi S, Bray F, Wild CP, Plummer M, Dal Maso L. Worldwide Thyroid-Cancer Epidemic? The Increasing Impact of Overdiagnosis. *N Engl J Med* (2016) 375(7):614–7. doi: 10.1056/NEJMp1604412
7. Bogovic Crncic T, Ilic Tomas M, Girotto N, Grbac Ivankovic S. Risk Factors for Thyroid Cancer: What Do We Know So Far? *Acta Clin Croat* (2020) 59 (Suppl 1):66–72. doi: 10.20471/acc.2020.59.s1.08
8. Asa SL, Mete O. Oncocytic Change in Thyroid Pathology. *Front Endocrinol (Lausanne)* (2021) 12:678119. doi: 10.3389/fendo.2021.678119
9. Franchini F, Palatucci G, Colao A, Ungaro P, Macchia PE, Nettore IC. Obesity and Thyroid Cancer Risk: An Update. *Int J Environ Res Public Health* (2022) 19(3):1116. doi: 10.3390/ijerph19031116
10. Fagin JA, Wells SAJr. Biologic and Clinical Perspectives on Thyroid Cancer. *N Engl J Med* (2016) 375(11):1054–67. doi: 10.1056/NEJMra1501993
11. Carling T, Udelsman R. Thyroid Cancer. *Annu Rev Med* (2014) 65:125–37. doi: 10.1146/annurev-med-061512-105739
12. Hundahl SA, Fleming ID, Fremgen AM, Menck HR. A National Cancer Data Base Report on 53,856 Cases of Thyroid Carcinoma Treated in the U.S. 1985-1995 [See Commetns]. *Cancer* (1998) 83(12):2638–48. doi: 10.1002/(sici)1097-0142(19981215)83:12<2638::aid-cncr31>3.0.co;2-1
13. Ito Y, Miyauchi A, Kihara M, Fukushima M, Higashiyama T, Miya A. Overall Survival of Papillary Thyroid Carcinoma Patients: A Single-Institution Long-Term Follow-Up of 5897 Patients. *World J Surg* (2018) 42(3):615–22. doi: 10.1007/s00268-018-4479-z
14. Nachalon Y, Stern-Shavit S, Bachar G, Shvero J, Limon D, Popovtzer A. Aggressive Palliation and Survival in Anaplastic Thyroid Carcinoma. *JAMA Otolaryngol Head Neck Surg* (2015) 141(12):1128–32. doi: 10.1001/jamaoto.2015.2332
15. Grogan RH, Kaplan SP, Cao H, Weiss RE, Degroot LJ, Simon CA, et al. A Study of Recurrence and Death From Papillary Thyroid Cancer With 27 Years of Median Follow-Up. *Surgery* (2013) 154(6):1436–46. doi: 10.1016/j.surg.2013.07.008
16. Maksimovic S, Jakovljevic B, Gojkovic Z. Lymph Node Metastases Papillary Thyroid Carcinoma and Their Importance in Recurrence of Disease. *Med Arch* (2018) 72(2):108–11. doi: 10.5455/medarh.2018.72.108-111
17. Perrier ND, Brierley JD, Tuttle RM. Differentiated and Anaplastic Thyroid Carcinoma: Major Changes in the American Joint Committee on Cancer Eighth Edition Cancer Staging Manual. *CA Cancer J Clin* (2018) 68(1):55–63. doi: 10.3322/caac.21439
18. Lee YK, Kim D, Shin DY, Lee CR, Lee EJ, Kang SW, et al. The Prognosis of Papillary Thyroid Cancer With Initial Distant Metastasis is Strongly Associated With Extensive Extrathyroidal Extension: A Retrospective Cohort Study. *Ann Surg Oncol* (2019) 26(7):2200–9. doi: 10.1245/s10434-019-07314-x
19. Ferrari SM, Fallahi P, Galdiero MR, Ruffilli I, Elia G, Ragusa F, et al. Immune and Inflammatory Cells in Thyroid Cancer Microenvironment. *Int J Mol Sci* (2019) 20(18):4413. doi: 10.3390/ijms20184413
20. Ahn J, Jin M, Song E, Ryu YM, Song DE, Kim SY, et al. Immune Profiling of Advanced Thyroid Cancers Using Fluorescent Multiplex Immunohistochemistry. *Thyroid* (2021) 31(1):61–7. doi: 10.1089/thy.2020.0312
21. Cameselle-Garcia S, Abdulkader-Sande S, Sanchez-Ares M, Rodriguez-Carnero G, Garcia-Gomez J, Gude-Sampedro F, et al. PD-L1 Expression and Immune Cells in Anaplastic Carcinoma and Poorly Differentiated Carcinoma of the Human Thyroid Gland: A Retrospective Study. *Oncol Lett* (2021) 22(1):553. doi: 10.3892/ol.2021.12814
22. Too NSH, Ho NCW, Adine C, Iyer NG, Fong ELS. Hot or Cold: Bioengineering Immune Contextures Into *In Vitro* Patient-Derived Tumor Models. *Adv Drug Deliv Rev* (2021) 175:113791. doi: 10.1016/j.addr.2021.05.001
23. Galon J, Bruni D. Approaches to Treat Immune Hot, Altered and Cold Tumours With Combination Immunotherapies. *Nat Rev Drug Discov* (2019) 18(3):197–218. doi: 10.1038/s41573-018-0007-y
24. Wu T, Dai Y. Tumor Microenvironment and Therapeutic Response. *Cancer Lett* (2017) 387:61–8. doi: 10.1016/j.canlet.2016.01.043
25. Hilly O, Koren R, Raz R, Rath-Wolfson L, Mizrachi A, Hamzany Y, et al. The Role of S100-Positive Dendritic Cells in the Prognosis of Papillary Thyroid Carcinoma. *Am J Clin Pathol* (2013) 139(1):87–92. doi: 10.1309/AJCPAKYDO56NKMYZ
26. Scouten WT, Francis GL. Thyroid Cancer and the Immune System: A Model for Effective Immune Surveillance. *Expert Rev Endocrinol Metab* (2006) 1 (3):353–66. doi: 10.1586/17446651.1.3.353
27. Ryder M, Ghossein RA, Ricarte-Filho JC, Knauf JA, Fagin JA. Increased Density of Tumor-Associated Macrophages is Associated With Decreased Survival in Advanced Thyroid Cancer. *Endocr Relat Cancer* (2008) 15 (4):1069–74. doi: 10.1677/ERC-08-0036

28. Kim S, Cho SW, Min HS, Kim KM, Yeom GJ, Kim EY, et al. The Expression of Tumor-Associated Macrophages in Papillary Thyroid Carcinoma. *Endocrinol Metab (Seoul)* (2013) 28(3):192–8. doi: 10.3803/EnM.2013.28.3.192
29. Fang W, Ye L, Shen L, Cai J, Huang F, Wei Q, et al. Tumor-Associated Macrophages Promote the Metastatic Potential of Thyroid Papillary Cancer by Releasing CXCL8. *Carcinogenesis* (2014) 35(8):1780–7. doi: 10.1093/carcin/bgu060
30. Park S, Zhu J, Altan-Bonnet G, Cheng SY. Monocyte Recruitment and Activated Inflammation are Associated With Thyroid Carcinogenesis in a Mouse Model. *Am J Cancer Res* (2019) 9(7):1439–53.
31. Locher KP. Mechanistic Diversity in ATP-Binding Cassette (ABC) Transporters. *Nat Struct Mol Biol* (2016) 23(6):487–93. doi: 10.1038/nsmb.3216
32. Dean M, Hamon Y, Chimini G. The Human ATP-Binding Cassette (ABC) Transporter Superfamily. *J Lipid Res* (2001) 42(7):1007–17.
33. Thomas C, Tampe R. Structural and Mechanistic Principles of ABC Transporters. *Annu Rev Biochem* (2020) 89:605–36. doi: 10.1146/annurev-biochem-011520-105201
34. Theodoulou FL, Kerr ID. ABC Transporter Research: Going Strong 40 Years on. *Biochem Soc Trans* (2015) 43(5):1033–40. doi: 10.1042/BST20150139
35. Sarkadi B, Homolya L, Szakacs G, Varadi A. Human Multidrug Resistance ABCB and ABCG Transporters: Participation in a Chemoimmunity Defense System. *Physiol Rev* (2006) 86(4):1179–236. doi: 10.1152/physrev.00037.2005
36. Chai AB, Ammit AJ, Gelissen IC. Examining the Role of ABC Lipid Transporters in Pulmonary Lipid Homeostasis and Inflammation. *Respir Res* (2017) 18(1):41. doi: 10.1186/s12931-017-0526-9
37. Amawi H, Sim HM, Tiwari AK, Ambudkar SV, Shukla S. ABC Transporter-Mediated Multidrug-Resistant Cancer. *Adv Exp Med Biol* (2019) 1141:549–80. doi: 10.1007/978-981-13-7647-4_12
38. Theile D, Wizgall P. Acquired ABC-Transporter Overexpression in Cancer Cells: Transcriptional Induction or Darwinian Selection? *Naunyn Schmiedebergs Arch Pharmacol* (2021) 394(8):1621–32. doi: 10.1007/s00210-021-02112-3
39. Meng F, Xiao Y, Xie L, Liu Q, Qian K. Diagnostic and Prognostic Value of ABC Transporter Family Member ABCG1 Gene in Clear Cell Renal Cell Carcinoma. *Channels (Austin)* (2021) 15(1):375–85. doi: 10.1080/19336950.2021.1909301
40. Yin W, Xiang D, Wang T, Zhang Y, Pham CV, Zhou S, et al. The Inhibition of ABCB1/MDR1 or ABCG2/BCRP Enables Doxorubicin to Eliminate Liver Cancer Stem Cells. *Sci Rep* (2021) 11(1):10791. doi: 10.1038/s41598-021-89931-9
41. Hlavata I, Mohelnikova-Duchonova B, Vaclavikova R, Liska V, Pitule P, Novak P, et al. The Role of ABC Transporters in Progression and Clinical Outcome of Colorectal Cancer. *Mutagenesis* (2012) 27(2):187–96. doi: 10.1093/mutage/ger075
42. Thurm C, Schraven B, Kahlfuss S. ABC Transporters in T Cell-Mediated Physiological and Pathological Immune Responses. *Int J Mol Sci* (2021) 22(17):9186. doi: 10.3390/ijms22179186
43. Wang L, Huang Y, Liu C, Guo M, Ma Z, He J, et al. Deltex3 Inhibits Epithelial Mesenchymal Transition in Papillary Thyroid Carcinoma *via* Promoting Ubiquitination of XRCC5 to Regulate the AKT Signal Pathway. *J Cancer* (2021) 12(3):860–73. doi: 10.7150/jca.48141
44. Nagy A, Munkacsy G, Gyorffy B. Pancancer Survival Analysis of Cancer Hallmark Genes. *Sci Rep* (2021) 11(1):6047. doi: 10.1038/s41598-021-84787-5
45. Yoshihara K, Shahmoradgoli M, Martinez E, Vegesna R, Kim H, Torres-Garcia W, et al. Inferring Tumour Purity and Stromal and Immune Cell Admixture From Expression Data. *Nat Commun* (2013) 4:2612. doi: 10.1038/ncomms3612
46. Miao YR, Zhang Q, Lei Q, Luo M, Xie GY, Wang H, et al. ImmuCellAI: A Unique Method for Comprehensive T-Cell Subsets Abundance Prediction and its Application in Cancer Immunotherapy. *Adv Sci (Weinh)* (2020) 7(7):1902880. doi: 10.1002/advs.201902880
47. Danaher P, Warren S, Dennis L, D'Amico L, White A, Disis ML, et al. Gene Expression Markers of Tumor Infiltrating Leukocytes. *J Immunother Cancer* (2017) 5:18. doi: 10.1186/s40425-017-0215-8
48. Li T, Fu J, Zeng Z, Cohen D, Li J, Chen Q, et al. TIMER2.0 for Analysis of Tumor-Infiltrating Immune Cells. *Nucleic Acids Res* (2020) 48(W1):W509–14. doi: 10.1093/nar/gkaa407
49. Lin T, Zhang E, Mai PP, Zhang YZ, Chen X, Peng LS. CXCL2/10/12/14 are Prognostic Biomarkers and Correlated With Immune Infiltration in Hepatocellular Carcinoma. *Biosci Rep* (2021) 41(6):BSR20204312. doi: 10.1042/BSR20204312
50. Ru B, Wong CN, Tong Y, Zhong JY, Zhong SSW, Wu WC, et al. TISIDB: An Integrated Repository Portal for Tumor-Immune System Interactions. *Bioinformatics* (2019) 35(20):4200–2. doi: 10.1093/bioinformatics/btz210
51. Vasaikar SV, Straub P, Wang J, Zhang B. LinkedOmics: Analyzing Multi-Omics Data Within and Across 32 Cancer Types. *Nucleic Acids Res* (2018) 46(D1):D956–63. doi: 10.1093/nar/gkx1090
52. Warde-Farley D, Donaldson SL, Comes O, Zuberi K, Badrawi R, Chao P, et al. The GeneMANIA Prediction Server: Biological Network Integration for Gene Prioritization and Predicting Gene Function. *Nucleic Acids Res* (2010) 38(Web Server issue):W214–220. doi: 10.1093/nar/gkq537
53. Pathan M, Keerthikumar S, Ang CS, Gangoda L, Quek CY, Williamson NA, et al. FunRich: An Open Access Standalone Functional Enrichment and Interaction Network Analysis Tool. *Proteomics* (2015) 15(15):2597–601. doi: 10.1002/pmic.201400515
54. Liu CJ, Hu FF, Xia MX, Han L, Zhang Q, Guo AY. GSCALite: A Web Server for Gene Set Cancer Analysis. *Bioinformatics* (2018) 34(21):3771–2. doi: 10.1093/bioinformatics/bty411
55. Davis AP, Grondin CJ, Johnson RJ, Sciaky D, Wiegers J, Wiegers TC, et al. Comparative Toxicogenomics Database (CTD): Update 2021. *Nucleic Acids Res* (2021) 49(D1):D1138–43. doi: 10.1093/nar/gkaa891
56. Chen ML, Sun A, Cao W, Eliason A, Mendez KM, Getzler AJ, et al. Physiological Expression and Function of the MDR1 Transporter in Cytotoxic T Lymphocytes. *J Exp Med* (2020) 217(5):e20191388. doi: 10.1084/jem.20191388
57. Badmann S, Heublein S, Mayr D, Reischer A, Liao Y, Kolben T, et al. M2 Macrophages Infiltrating Epithelial Ovarian Cancer Express MDR1: A Feature That May Account for the Poor Prognosis. *Cells* (2020) 9(5):1224. doi: 10.3390/cells9051224
58. Belisario DC, Akman M, Godel M, Campani V, Patrizio MP, Scotti L, et al. ABCA1/ABCB1 Ratio Determines Chemo- and Immune-Sensitivity in Human Osteosarcoma. *Cells* (2020) 9(3):647. doi: 10.3390/cells9030647
59. Guo Y, Wang ZW, Su WH, Chen J, Wang YL. Prognostic Value and Immune Infiltrates of ABCA8 and FABP4 in Stomach Adenocarcinoma. *BioMed Res Int* (2020) 2020:4145164. doi: 10.1155/2020/4145164
60. Van Kaer L. Major Histocompatibility Complex Class I-Restricted Antigen Processing and Presentation. *Tissue Antigens* (2002) 60(1):1–9. doi: 10.1034/j.1399-0039.2002.600101.x
61. Ritz U, Seliger B. The Transporter Associated With Antigen Processing (TAP): Structural Integrity, Expression, Function, and its Clinical Relevance. *Mol Med* (2001) 7(3):149–58.
62. Parcej D, Tampe R. ABC Proteins in Antigen Translocation and Viral Inhibition. *Nat Chem Biol* (2010) 6(8):572–80. doi: 10.1038/nchembio.410
63. Barbet G, Nair-Gupta P, Schotsaert M, Yeung ST, Moretti J, Seyffer F, et al. TAP Dysfunction in Dendritic Cells Enables Noncanonical Cross-Presentation for T Cell Priming. *Nat Immunol* (2021) 22(4):497–509. doi: 10.1038/s41590-021-00903-7
64. El Hage F, Durgeau A, Mami-Chouaib F. TAP Expression Level in Tumor Cells Defines the Nature and Processing of MHC Class I Peptides for Recognition by Tumor-Specific Cytotoxic T Lymphocytes. *Ann N Y Acad Sci* (2013) 1283:75–80. doi: 10.1111/j.1749-6632.2012.06777.x
65. Wang Z, Xu H, Zhu L, He T, Lv W, Wu Z. Establishment and Evaluation of a 6-Gene Survival Risk Assessment Model Related to Lung Adenocarcinoma Microenvironment. *BioMed Res Int* (2020) 2020:6472153. doi: 10.1155/2020/6472153
66. Yang J, Liu W, Yan Z, Li C, Liu S, Yang X, et al. Polymorphisms in Transporter Associated With Antigen Presenting are Associated With Cervical Intraepithelial Neoplasia and Cervical Cancer in a Chinese Han Population. *HLA* (2021) 98(1):23–36. doi: 10.1111/tan.14333
67. Zhang Y, Zhang Y, Wang J, Yang J, Yang G. Abnormal Expression of ABCD3 is an Independent Prognostic Factor for Colorectal Cancer. *Oncol Lett* (2020) 19(5):3567–77. doi: 10.3892/ol.2020.11463
68. Yang Y, Ding L, Li Y, Xuan C. Hsa_circ_0039411 Promotes Tumorigenesis and Progression of Papillary Thyroid Cancer by miR-1179/ABCA9 and miR-1205/MTA1 Signaling Pathways. *J Cell Physiol* (2020) 235(2):1321–9. doi: 10.1002/jcp.29048

69. Karas Zella MA, Sebastiao APM, Collaco LM, Ogata DC, Cecchetti G, Bartolomei IJP, et al. Prognostic Significance of CD133 and ABCB5 Expression in Papillary Thyroid Carcinoma. *Eur J Histochem* (2020) 64 (4):3143. doi: 10.4081/ejh.2020.3143
70. Ohashi R, Kawahara K, Namimatsu S, Okamura R, Igarashi T, Sugitani I, et al. Expression of MRP1 and ABCG2 is Associated With Adverse Clinical Outcomes of Papillary Thyroid Carcinoma With a Solid Component. *Hum Pathol* (2017) 67:11–7. doi: 10.1016/j.humpath.2017.03.012
71. Mato E, Gonzalez C, Moral A, Perez JI, Bell O, Lerma E, et al. ABCG2/BCRP Gene Expression is Related to Epithelial-Mesenchymal Transition Inducer Genes in a Papillary Thyroid Carcinoma Cell Line (TPC-1). *J Mol Endocrinol* (2014) 52(3):289–300. doi: 10.1530/JME-14-0051
72. Ruggeri RM, Sciacchitano S, Vitarelli E, Trimarchi F, Barresi G, Trovato M. Immunoexpression of Multidrug-Resistance Protein 2 and Cyclooxygenase 2 in Medullary Thyroid Carcinomas. *Arch Pathol Lab Med* (2006) 130(7):1014–9. doi: 10.5858/2006-130-1014-IOMPAC
73. Abbasifarid E, Sajjadi-Jazi SM, Beheshtian M, Samimi H, Larijani B, Haghpanah V. The Role of ATP-Binding Cassette Transporters in the Chemoresistance of Anaplastic Thyroid Cancer: A Systematic Review. *Endocrinology* (2019) 160(8):2015–23. doi: 10.1210/en.2019-00241
74. Shibuya M. Vascular Endothelial Growth Factor Receptor-2: Its Unique Signaling and Specific Ligand, VEGF-E. *Cancer Sci* (2003) 94(9):751–6. doi: 10.1111/j.1349-7006.2003.tb01514.x
75. Apte RS, Chen DS, Ferrara N. VEGF in Signaling and Disease: Beyond Discovery and Development. *Cell* (2019) 176(6):1248–64. doi: 10.1016/j.cell.2019.01.021
76. Fukumura D, Kloepper J, Amoozgar Z, Duda DG, Jain RK. Enhancing Cancer Immunotherapy Using Antiangiogenics: Opportunities and Challenges. *Nat Rev Clin Oncol* (2018) 15(5):325–40. doi: 10.1038/nrclinonc.2018.29
77. Shklovskaya E, Rizos H. MHC Class I Deficiency in Solid Tumors and Therapeutic Strategies to Overcome it. *Int J Mol Sci* (2021) 22(13):6741. doi: 10.3390/ijms22136741
78. Wang JY, Wang WP. B7-H4, a Promising Target for Immunotherapy. *Cell Immunol* (2020) 347:104008. doi: 10.1016/j.cellimm.2019.104008
79. Andersson J, Tran DQ, Pesu M, Davidson TS, Ramsey H, O'Shea JJ, et al. CD4 + FoxP3+ Regulatory T Cells Confer Infectious Tolerance in a TGF-Beta-Dependent Manner. *J Exp Med* (2008) 205(9):1975–81. doi: 10.1084/jem.20080308
80. Peng L, Yuan XQ, Zhang CY, Ye F, Zhou HF, Li WL, et al. High TGF-Beta1 Expression Predicts Poor Disease Prognosis in Hepatocellular Carcinoma Patients. *Oncotarget* (2017) 8(21):34387–97. doi: 10.18632/oncotarget.16166
81. Wang J, Xiang H, Lu Y, Wu T. Role and Clinical Significance of TGFbeta1 and TGFbetaR1 in Malignant Tumors (Review). *Int J Mol Med* (2021) 47(4):55. doi: 10.3892/ijmm.2021.4888
82. Sag D, Ayyildiz ZO, Gunalp S, Wingender G. The Role of TRAIL/DRs in the Modulation of Immune Cells and Responses. *Cancers (Basel)* (2019) 11 (10):1469. doi: 10.3390/cancers11101469
83. Valatas V, Kolios G, Bamias G. TL1A (TNFSF15) and DR3 (TNFRSF25): A Co-Stimulatory System of Cytokines With Diverse Functions in Gut Mucosal Immunity. *Front Immunol* (2019) 10:583. doi: 10.3389/fimmu.2019.00583
84. Vanamee ES, Faustman DL. On the TRAIL of Better Therapies: Understanding TNFRSF Structure-Function. *Cells* (2020) 9(3):764. doi: 10.3390/cells9030764
85. Vilgelm AE, Richmond A. Chemokines Modulate Immune Surveillance in Tumorigenesis, Metastasis, and Response to Immunotherapy. *Front Immunol* (2019) 10:333. doi: 10.3389/fimmu.2019.00333
86. Kitahara CM, Preston DL, Neta G, Little MP, Doody MM, Simon SL, et al. Occupational Radiation Exposure and Thyroid Cancer Incidence in a Cohort of U.S. Radiologic Technologists 1983-2013. *Int J Cancer* (2018) 143(9):2145–9. doi: 10.1002/ijc.31270
87. An SY, Kim SY, Oh DJ, Min C, Sim S, Choi HG. Obesity is Positively Related and Tobacco Smoking and Alcohol Consumption are Negatively Related to an Increased Risk of Thyroid Cancer. *Sci Rep* (2020) 10(1):19279. doi: 10.1038/s41598-020-76357-y
88. Lee JH, Youn S, Jung S, Kim K, Chai YJ, Chung YS, et al. A National Database Analysis for Factors Associated With Thyroid Cancer Occurrence. *Sci Rep* (2020) 10(1):17791. doi: 10.1038/s41598-020-74546-3
89. Marotta V, Malandrino P, Russo M, Panariello I, Ionna F, Chiofalo MG, et al. Fathoming the Link Between Anthropogenic Chemical Contamination and Thyroid Cancer. *Crit Rev Oncol Hematol* (2020) 150:102950. doi: 10.1016/j.critrevonc.2020.102950
90. Zhang Q, Jiang C, Li H, Zhang C, Wu H, Huang F. Effect of the Interaction Between Cadmium Exposure and CLOCK Gene Polymorphisms on Thyroid Cancer: A Case-Control Study in China. *Biol Trace Elem Res* (2020) 196 (1):86–95. doi: 10.1007/s12011-019-01904-2
91. Morton LM, Karyadi DM, Stewart C, Bogdanova TI, Dawson ET, Steinberg MK, et al. Radiation-Related Genomic Profile of Papillary Thyroid Carcinoma After the Chernobyl Accident. *Science* (2021) 372(6543):eabg2538. doi: 10.1126/science.abg2538
92. Zhang D, Jones RR, James P, Kitahara CM, Xiao Q. Associations Between Artificial Light at Night and Risk for Thyroid Cancer: A Large US Cohort Study. *Cancer* (2021) 127(9):1448–58. doi: 10.1002/cncr.33392
93. Hu MJ, He JL, Tong XR, Yang WJ, Zhao HH, Li GA, et al. Associations Between Essential Microelements Exposure and the Aggressive Clinicopathologic Characteristics of Papillary Thyroid Cancer. *Biometals* (2021) 34(4):909–21. doi: 10.1007/s10534-021-00317-w
94. Li L, Li H, Zhang J, Gao X, Jin H, Liu R, et al. Bisphenol A at a Human Exposed Level can Promote Epithelial-Mesenchymal Transition in Papillary Thyroid Carcinoma Harbouring BRAF(V600E) Mutation. *J Cell Mol Med* (2021) 25(3):1739–49. doi: 10.1111/jcmm.16279

Conflict of Interest: The authors declare that the research was conducted in the absence of any commercial or financial relationships that could be construed as a potential conflict of interest.

Publisher's Note: All claims expressed in this article are solely those of the authors and do not necessarily represent those of their affiliated organizations, or those of the publisher, the editors and the reviewers. Any product that may be evaluated in this article, or claim that may be made by its manufacturer, is not guaranteed or endorsed by the publisher.

frontiers | Frontiers in Oncology

TYPE Review
PUBLISHED 25 July 2022
DOI 10.3389/fonc.2022.933407

OPEN ACCESS

EDITED BY
Domenica Scumaci,
Magna Græcia University of Catanzaro, Italy

REVIEWED BY
Liza Makowski,
University of Tennessee Health Science Center (UTHSC), United States
Lan Zhao,
Stanford University, United States

*CORRESPONDENCE
Qingfei Zheng
Qingfei.Zheng@osumc.edu

SPECIALTY SECTION
This article was submitted to Cancer Metabolism, a section of the journal Frontiers in Oncology

RECEIVED 30 April 2022
ACCEPTED 28 June 2022
PUBLISHED 25 July 2022

CITATION
Zhou X, Kandalai S, Hossain F and Zheng Q (2022) Tumor microbiome metabolism: A game changer in cancer development and therapy. *Front. Oncol.* 12:933407. doi: 10.3389/fonc.2022.933407

Tumor microbiome metabolism: A game changer in cancer development and therapy

Xiaozhuang Zhou[1,2], Shruthi Kandalai[1,2], Farzana Hossain[1,2] and Qingfei Zheng[1,2]*

[1]Department of Radiation Oncology, College of Medicine, The Ohio State University, Columbus, OH, United States, [2]Center for Cancer Metabolism, James Comprehensive Cancer Center, The Ohio State University, Columbus, OH, United States

Accumulating recent evidence indicates that the human microbiome plays essential roles in pathophysiological states, including cancer. The tumor microbiome, an emerging concept that has not yet been clearly defined, has been proven to influence both cancer development and therapy through complex mechanisms. Small molecule metabolites produced by the tumor microbiome through unique biosynthetic pathways can easily diffuse into tissues and penetrate cell membranes through transporters or free diffusion, thus remodeling the signaling pathways of cancer and immune cells by interacting with biomacromolecules. Targeting tumor microbiome metabolism could offer a novel perspective for not only understanding cancer progression but also developing new strategies for the treatment of multiple cancer types. Here, we summarize recent advances regarding the role the tumor microbiome plays as a game changer in cancer biology. Specifically, the metabolites produced by the tumor microbiome and their potential effects on the cancer development therapy are discussed to understand the importance of the microbial metabolism in the tumor microenvironment. Finally, new anticancer therapeutic strategies that target tumor microbiome metabolism are reviewed and proposed to provide new insights in clinical applications.

KEYWORDS

tumor microbiome, metabolism, cancer therapy, cancer development, immune response

Introduction

The human microbiota is a broad category consisting of diverse bacteria, fungi, protists, archaea, and viruses that occur in and on the human body (1). The total number of these microbes is believed to be more than 100 trillion, which amounts to 2 kg in mass (2). Due to its important pathophysiological role in human health and disease, the microbiome has also been referred to as "the last human organ under active research" (3)

and "the second brain" (4). Moreover, the number of unique genes from the microbiome is estimated to be 100-fold higher than that from human cells, as noted by the NIH Human Microbiome Project (5, 6). The proteins encoded by these genes and the metabolites biosynthesized by these microbes are able to influence not only their own microbial communities, but also the biological functions of host cells (7, 8). Notably, small molecule metabolites secreted by the human microbiome affect local and systemic bodily functions, including energy generation, metabolism of dietary components, biosynthesis of vitamins, immune responses, behavior, and even mood (9–11).

While microbes were implicated in diseases long ago, the contributions of the tumor microbiome to carcinogenesis, cancer progression, metastasis, and treatment have been poorly understood until recently (12–14). Previous studies have shown that microbes belonging to the genera *Salmonella* and *Helicobacter* affect cellular dysplasia and carcinogenesis (15, 16). Microbiota homeostasis can also play a role in cancer development (17). For instance, dysbiosis is associated with the carcinogenesis of gastrointestinal (GI) and non-GI tumors while also acting as an oncogenic driver of colorectal cancer (CRC) (18). Current research indicates that human-associated microbes interact with host cells and affect disease states, especially cancer, *via* diverse mechanisms (19, 20). One key mechanism is microbial metabolites serving as small molecule messengers to mediate crosstalk between microbes and host cells (21). Specifically, microbial metabolites can alter the tumor microenvironment (TME) (22), which includes inflammatory mediators, recruited immune cells, fibroblasts, adipocytes, endothelial cells, and pericytes (22, 23), thereby directly influencing cancer progression (23, 24) and the efficacy of immunotherapy (1, 23). One well-studied example of this is the genotoxic metabolite colibactin, produced by pathogenic *Escherichia coli*, that can directly induce DNA double-strand breaks (DSBs) (25), thus motivating CRC development (26).

As the tumor microbiome metabolism exhibits direct and indirect impacts on cancer development, novel therapy strategies may be developed by targeting these unique metabolic pathways (27, 28). Chemical biology, synthetic biology, and biomedical engineering approaches facilitate the remodeling of the microbiome-containing TME and will provide new opportunities for the future development of bacterial, viral, chemical, and immunological therapies.

In this review, we intend to highlight the tumor microbiome and how it affects cancer development and therapy as a new game changer. Among the multiple crosstalk mechanisms between microbes and cancer cells, we specifically focus on the unique metabolites produced by the tumor microbiome. The chemical structures and biochemical mechanisms through which tumor microbiome metabolism affects cancer biology are addressed. Finally, yet importantly, the potential clinical applications of targeting tumor microbiome metabolism through multidisciplinary methods for future cancer therapy have been proposed and discussed.

What is tumor microbiome?

The tumor microbiome is an emerging concept that has yet to be clearly defined. It broadly refers to all microorganisms located within the TME (Figure 1) and encompasses bacteria, fungi, archaea, viruses, and other microbes (29) that contribute to the reshaping of the microenvironment. These microbes are widespread in the TME and inhabit inside or outside the tumor cells and immune cells. It has long been in debate whether these microbes constitute a predetermined niche or rather represent a transient stochastic colonization (29).

Within cancer biology, intratumoral bacteria and their effects are a newly raised concept (30). While bacteria were observed in tumor isolates previously, it was assumed that these were contaminants and were not associated with cancer cells

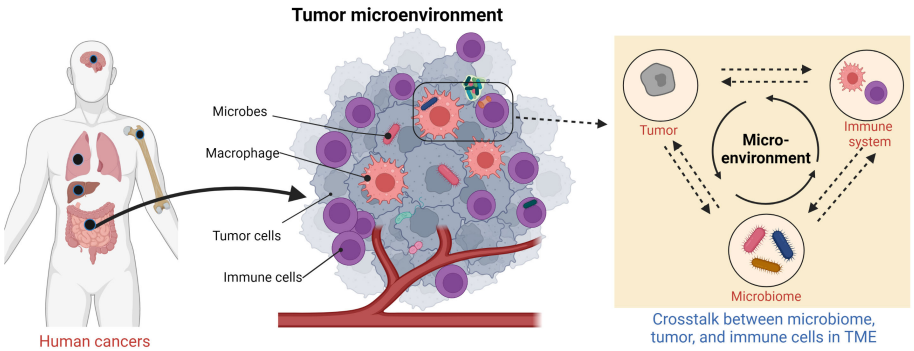

FIGURE 1
Schematic of human tumor microenvironment that contains tumor microbiome.

(31). Recently, a large-scale analysis of over 1,500 clinical samples indicated that the majority of the tumor microbiome is intracellular bacteria that exhibit tumor-site-specific properties (32). Intratumoral bacteria and host cancer cells mutually influence each other through the transcriptome and metabolome (33). Since these intracellular bacteria inhabit cancer cells, direct crosstalk between host and microbes is easily mediated by biomacromolecules and small molecule metabolites. However, this still leads to a chicken-and-egg situation—is the accumulation of intratumoral bacteria a cause or effect of cancer? Further investigations are required to address this question. Intracellular microbes hiding inside other type of cells, such as macrophages and fibroblasts, have also been shown to remodel the TME (34, 35) and thus affect cancer development and treatment (36, 37).

On the other hand, viruses that directly cause cancer (also known as oncoviruses) have been thoroughly studied. These viruses currently include hepatitis B virus (HBV), hepatitis C virus (HCV), human papillomaviruses (HPVs), Kaposi's sarcoma-associated herpesvirus (KSHV/HHV-8), human T-lymphotropic virus (HTLV), Merkel cell polyomavirus (MCV), and Epstein–Barr virus (EBV) (38). They induce cancer through diverse mechanisms, such as the integration of viral DNA into the host genome (39) and the inactivation of tumor suppressor genes like p53 and Rb (40). Globally, these oncoviruses are associated with approximately 10%–16% of cancer cases (41, 42). It has also been suggested that other viruses, similar to the bacteria mentioned previously, may play a role in carcinogenesis, without directly causing cancer (37). Other microbes, such as fungi, have also been implicated in cancer (43, 44), although this is less studied.

Extracellular microorganisms in the TME, such as those in the gut microbiota, oral microbiota, vaginal flora, and skin flora, also play essential roles in cancer development (45–47) and have significant impacts on curative outcomes (48). For instance, it has long been known that the colonization by *Helicobacter pylori* in stomach can directly cause gastric cancer (49), as well as gastric mucosa–associated lymphoid tissue (MALT) lymphoma (50). As a result, *H. pylori* is associated with approximately 5% of cancers worldwide (42). Multiple studies have shown that the gut microbiota interacts with the host by producing of a diverse set of metabolites and toxins from exogenous dietary substrates and endogenous host cellular compounds (51). Host metabolic disorders are systematically associated with alterations in the composition and function of the gut microbiota (52). Specific classes of microbiota-derived metabolites, notably bile acids (BAs), short-chain fatty acids (SCFAs), branched-chain amino acids, trimethylamine N-oxide, and tryptophan and indole derivatives, have been implicated in the pathogenesis of host cell metabolic disorders, some of which directly relate to carcinogenesis (53). In addition, the gut microbiome is essential in shaping the development of innate and adaptive immunity (54) and plays an essential role in the clinical efficiency of cancer immunotherapy (55).

Crosstalk between tumor microbiome and cancer cells

The crosstalk between the tumor microbiome and cancer cells is diverse and complex, involving cell–cell direct interactions and messenger molecule-mediated effects (Figure 2). With respect to host cell–microbe direct interactions, intracellular microbe–induced autophagy and extracellular microbe–caused inflammation are two well-studied examples. For instance, it has been shown that *Fusobacterium nucleatum* modulates the autophagy pathways of CRC cells by targeting TLR4 and MYD88 innate immune signaling and specific microRNAs, thereby promoting CRC chemoresistance and migration (56). Moreover, it has been accepted for decades that inflammation is a critical component of tumor progression (57). Inflammatory cells significantly influence the TME, thereby affecting neoplastic processes and fostering the proliferation, survival, and migration of cancer cells (58). Chronic, dysregulated, persistent, and unresolved inflammation is associated with an increased risk of malignancies, as well as the malignant progression of most types of cancer (58). As microorganisms are one of the major causes of inflammation, the tumor microbiome can manipulate cancer development by remodeling the TME through the recruitment of inflammatory cells. In fact, it has been pointed out that bacterial infections can trigger chronic inflammation that leads to host cell proliferation and tumor development (59).

Messenger molecule–mediated interactions between host cells and microbes are another key machinery linking the tumor microbiome to cancer progression. These messenger molecules involve secreted proteins, peptide toxins, and small-molecule metabolites. For example, the virulence factor cytolethal-distending toxin produced by *Campylobacter jejuni* is one of the major causes for infectious diarrhea worldwide and has been shown to induce carcinogenesis *in vivo* (60, 61). Moreover, tumor microbiome–derived small molecule metabolites can reach remote tumor entities through systemic circulation, free diffusion, and active transport (such as the transport of lactate and pyruvate by proton-coupled monocarboxylate transporters) (62). These metabolites are able to stimulate antitumoral or carcinogenic innate immune responses (22) *via* non-covalent interactions. For instance, evolutionary conserved pathogen-associated molecular patterns (PAMPs) from commensal microbes or pathogens can be systematically sensed by the innate immune system *via* pattern recognition receptors, such as Toll-like receptors and NOD-like receptors, leading to the host's innate immune responses (63). There is evidence showing that bacterial PAMPs can boost

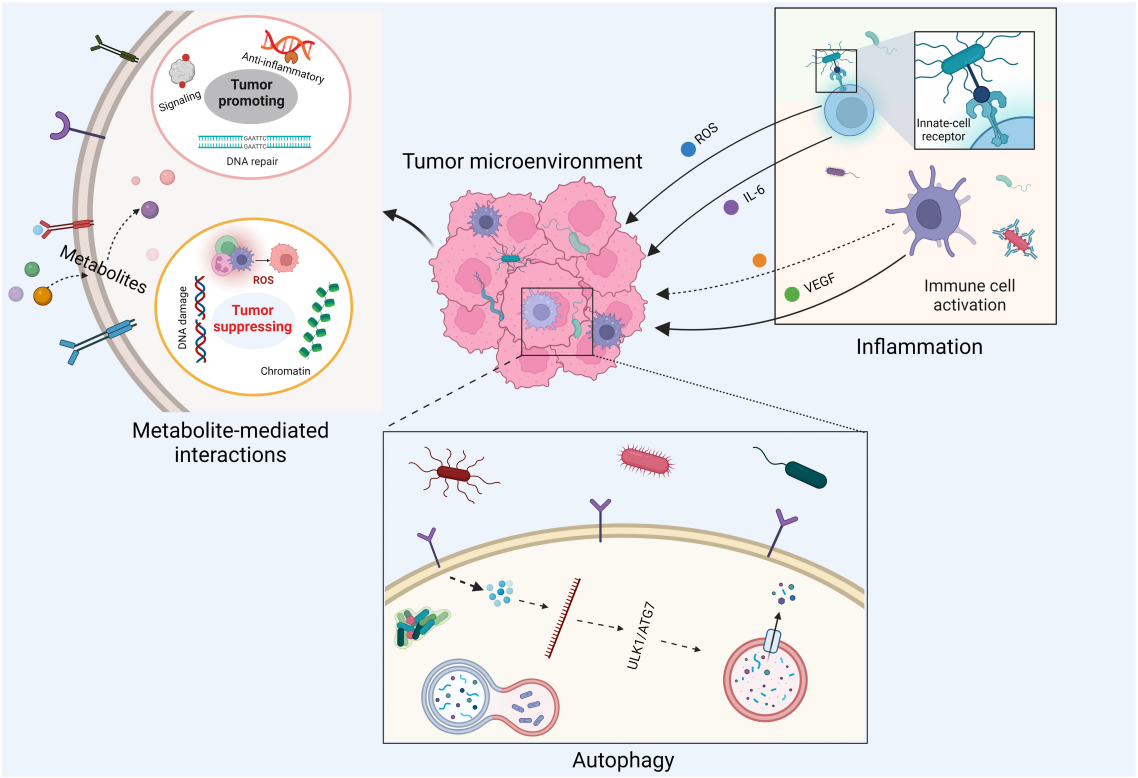

FIGURE 2
Impacts of tumor microbiome on cancer development.

antitumor immunity by augmenting Toll-like receptor signaling and serving as cancer vaccine adjuvants (64–66). Additionally, commensal gut bacteria can recruit natural killer T immune cells to control the growth of liver tumors *via* their unique microbial metabolism of BAs (67). Moreover, chemically reactive metabolites from the tumor microbiome can promote or inhibit tumor growth through the covalent modifications of DNA, RNA, histones, and other essential enzymes involved in host signaling transduction pathways (68). These modifications can be enzymatic or non-enzymatic and are capable of inducing cancer-causing and cancer-promoting epigenetic changes of host cells (69). As a result of this complex crosstalk between the host and tumor microbiome, both cancer and immune cells change their own metabolic status to adapt to the reshaped TME (70).

Furthermore, due to its novel metabolic and catabolic pathways, the gut microbiome is capable of converting human-ingested nutrients into functional microbial metabolites that closely link diet, cancer, and other metabolic diseases (19, 71, 72). These microbial metabolites produced by microbes from diet, such as BAs and SCFAs, have significant impacts on cancer and immune cells (73–78), thereby affecting cancer development and immunotherapies through complex mechanisms (79–81). Based on the important role of the microbiome in connecting diet and different types of cancer, recent research advances have suggested that gut microbiota modulation would become a novel strategy for prevention and treatment of CRC (82). As diet and microbial communities affect one another, dietary interventions have proven to be an efficient approach to modulate the intestinal microbiota, which is in line with the growing recognition of significant impacts of diet and lifestyle on human health through microbiome regulation (83).

Metabolites produced by tumor microbiome

The consequence of metabolism is the production of small molecule metabolites, which are typically classified into two categories: primary metabolites and secondary metabolites. Primary metabolites are compounds that are directly involved in an organism's growth and development, while secondary metabolites are not directly involved in these processes and tend to vary more by species (84). There are a number of primary metabolites produced by microbes that contribute to cancer development or suppression, such as methylglyoxal (MGO), SCFAs, BAs, reactive oxygen species (ROS), amines, and methane (CH_4) (85–87). These molecules are biosynthesized

by diverse human-associated microorganisms, including archaea (88), bacteria (89, 90), fungi (90) protists (91) and parasites (91, 92).

There are several examples of secondary metabolites with well-established functions, such as colibactin, peptide aldehyde, and thiopeptide, that have been known to affect cancer development, and these metabolites have diverse chemical structures (Figure 3). As a well-studied secondary metabolite molecule, colibactin is a cytotoxin mainly produced by pathogenic *Escherichia coli*, as well as other members of the family *Enterobacteriaceae*. The production of colibactin was shown to have a direct and significant association with CRC *via* the induction of DNA DSBs (25, 26). Peptide aldehydes were discovered as metabolites from a variety of microbes (including *E. coli*, *Bacillus subtilis*, and *Streptomyces* species) and are known to inhibit protease functions (93, 94), which may increase carcinogenicity. Thiopeptides have complex structures and strong antibacterial activities (95, 96), which can affect the distribution of human flora (97). In addition to being isolated from multiple environmental microbes, thiopeptides have been discovered from many microbial species in various parts of the body, including *Lactobacillus gasseri* in the urogenital tract, *Propionibacterium acnes* on the skin, *Streptococcus downei* in the oral cavity, and *Enterococcus faecalis* in the gut (98). Moreover, emerging studies have suggested that thiopeptides may also serve as anticancer agents by targeting proteasomes and transcription factor FOXM1 (99).

Impacts of tumor microbiome metabolites on cancer development

Since small molecule metabolites from tumor microbiome play essential roles in cancer development, we would like to summarize some examples in this section to emphasize the neglected but significant impacts of tumor microbiome

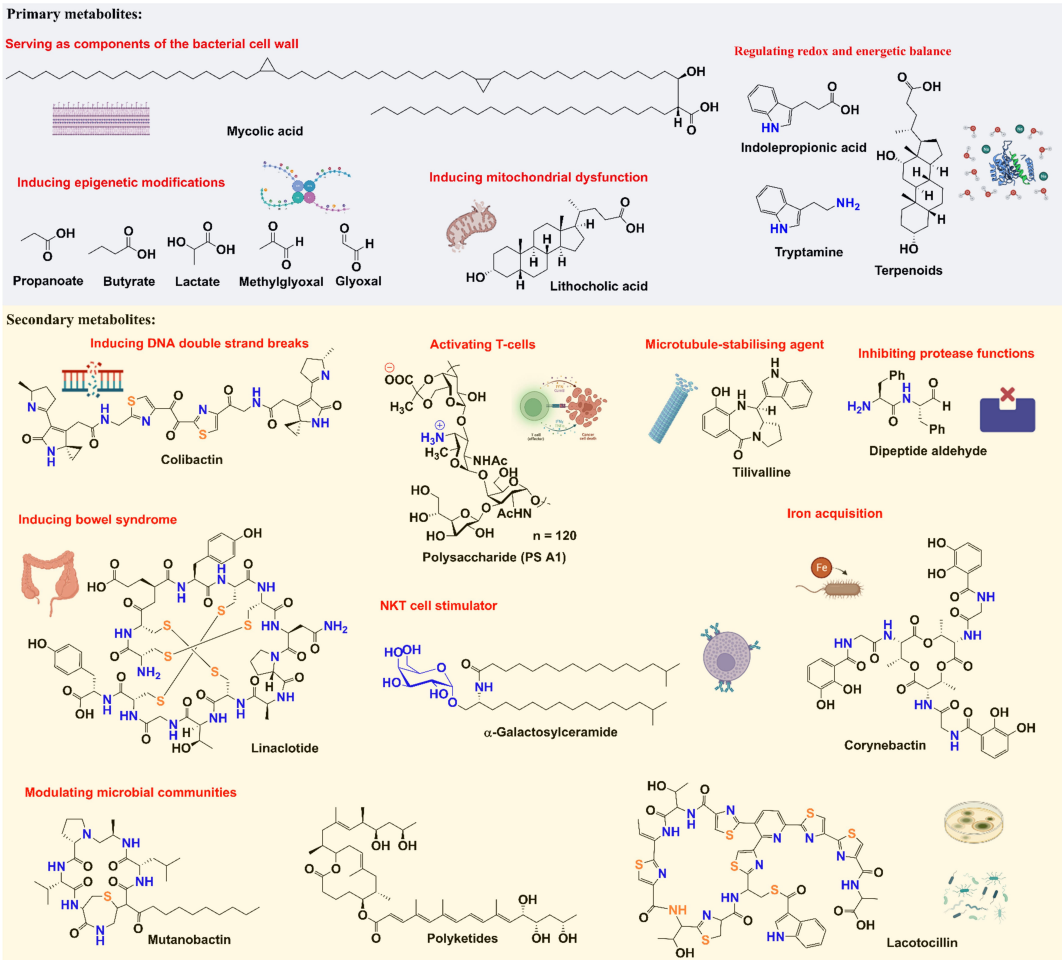

FIGURE 3
Chemical structures and functions of representative metabolites from tumor microbiome.

metabolism on the TME (Figure 3). As stated above, colibactin's ability to cause DNA DSBs allows it to promote tumorigenesis (100). Recently, it has been shown that colibactin also targets bacteria by triggering prophage induction (101), which may explain how this metabolite further affects the communities in the tumor microbiome.

SCFAs are mainly bacterial fermentation products from starch and other polysaccharides (102) and include a wide range of molecules including acetate, propionate, butyrate, and lactate (89). Among these, butyrate has been shown to potently inhibit the activity of histone deacetylases (103–105), whereas propionate does so moderately and acetate has no effect (106, 107). Lactate is known to play significant roles in the Warburg effect and reverse Warburg effect (108–110), as well as affect chromatin biology through histone modification (111, 112). It has also been shown that SCFAs can: 1) modulate macrophage functions by promoting the production of nitric oxide, IL-6, IL-12 (113), and IL-22 (114); 2) induce the differentiation of T_{reg} cells (115–117); and 3) regulate the migration of neutrophils (118). There are many connections between SCFAs and cancer, where SCFAs function as a double-edged sword in tumorigenesis. SCFAs have been implicated to have cancer-promoting or cancer-suppressing effects that vary under different conditions and with different types of cancer. Previous research has shown that SCFAs are able to: inhibit human colon cancer invasion (119, 120), inhibit the migration and invasion of fibrosarcoma cells (121), increase IGF1 levels to promote the proliferation of prostate cancer cells (122), upregulate proapoptotic protein BAK (123), downregulate adhesion protein $\alpha_2\beta_1$ integrin (124), induce cell stress responses and apoptosis in colorectal cells (125), inhibit proliferation and increase differentiation and apoptosis of adenocarcinoma cells (126), impair hypoxia-induced angiogenesis (127), and regulate p53 expression (128, 129).

BAs are steroid derivatives that play essential regulatory roles in the GI system and cancer development. While primary BAs are produced by the liver, secondary BAs, mainly deoxycholic acid and lithocholic acid, occur when primary BAs are further metabolized by gut bacteria. Secondary BAs have long been proposed to promote tumors (130). In addition, further derivatives of secondary bile salts can cause apoptosis, increase ROS production, and lessen pro-apoptotic effects (131). Deoxycholic acid is believed to be associated with oncogenic mutations of proto-oncogene *KRAS* (132) and can lead to DNA DSBs and apoptosis (133). Lithocholic acid has been shown to modulate T_h17 and T_{reg} cells (73), inhibit HLA class I genes (134), and induce endoplasmic reticulum stress and mitochondrial dysfunction in human prostate cancer cells (135). Moreover, CRC cells can obtain resistance to apoptosis after being exposed to specific bile salts (136, 137).

Polyamines are small molecule metabolites with two or more amino groups, which exhibit a variety of functions. The most common polyamines, putrescine, cadaverine, spermidine, and spermine, are metabolized from arginine (138) but can also be produced by gut bacteria (139, 140). Polyamines are known to protect cells from ROS (141) due to their reducing activities and have been significantly correlated with CRC (142, 143). Polyamines have been shown to be associated with inhibiting the growth of prostate cancer cells (144–146), downregulating estrogen receptor α in breast cancer cells (147), serving as a downstream effector from *H. pylori*, leading to DNA damage and immune cell apoptosis in stomach cancer (148–151), and increasing the risk for development of skin cancer in mouse models (152, 153). Moreover, microbial polyamines exhibit unique activities in the regulation of macrophage polarization and function, thereby affecting host immune responses (154).

MGO is a chemically reactive dicarbonyl metabolite of glucose metabolism (155, 156). In mammalian cells, MGO is mainly generated as a byproduct through a non-enzymatic dephosphorylation process during glycolysis, although it can also be produced by tumor microbes that contain microorganism-specific methylglyoxal synthases (88, 157). MGO can react with nucleophilic groups of biomacromolecules, such as lysine and arginine residues in proteins (158), as well as guanine residues in DNA and RNA (159). This MGO-induced non-enzymatic covalent modification (glycation) can result in the formation of advanced glycation end products (AGEs) (160–162) and changes in the three-dimensional chromatin architecture (163–165). It has been shown that elevated levels of MGO in the TME lead to the overexpression of an MGO detoxifier, glyoxalase I (Glo1), in cancer cells (166, 167). There is evidence showing that low concentrations of MGO are beneficial for cancer cell growth, while high levels of MGO contribute negatively to cell survival by disrupting multiple signaling pathways (168, 169). The biphasic model proposed recently is a convincing explanation for the function of MGO-induced glycation in manipulating chromatin damage and cancer cell survival (166). Moreover, the recently identified histone MGO-glycation eraser and rewriter enzymes, DJ-1 and PAD4, have been recognized to possess cancer-promoting effects as oncoproteins (163, 164). Thus, developing deglycase activity–oriented high-throughput screening assays for identifying DJ-1 and PAD4 inhibitors will provide new insights for the mechanistic studies of host deglycation pathways, as well as clinical applications (170).

Targeting tumor microbiome for cancer therapy

As noted above, due to the inseparable connections between microbes, host immune cells, and cancer cells, targeting the tumor microbiome seems to be a practical tactic for cancer therapy (Figure 4). Specifically, strategies include the development of wild-type and/or engineered microbes for bacterial and viral therapies and the application of chemical biology, synthetic biology, and biomedical engineering to target

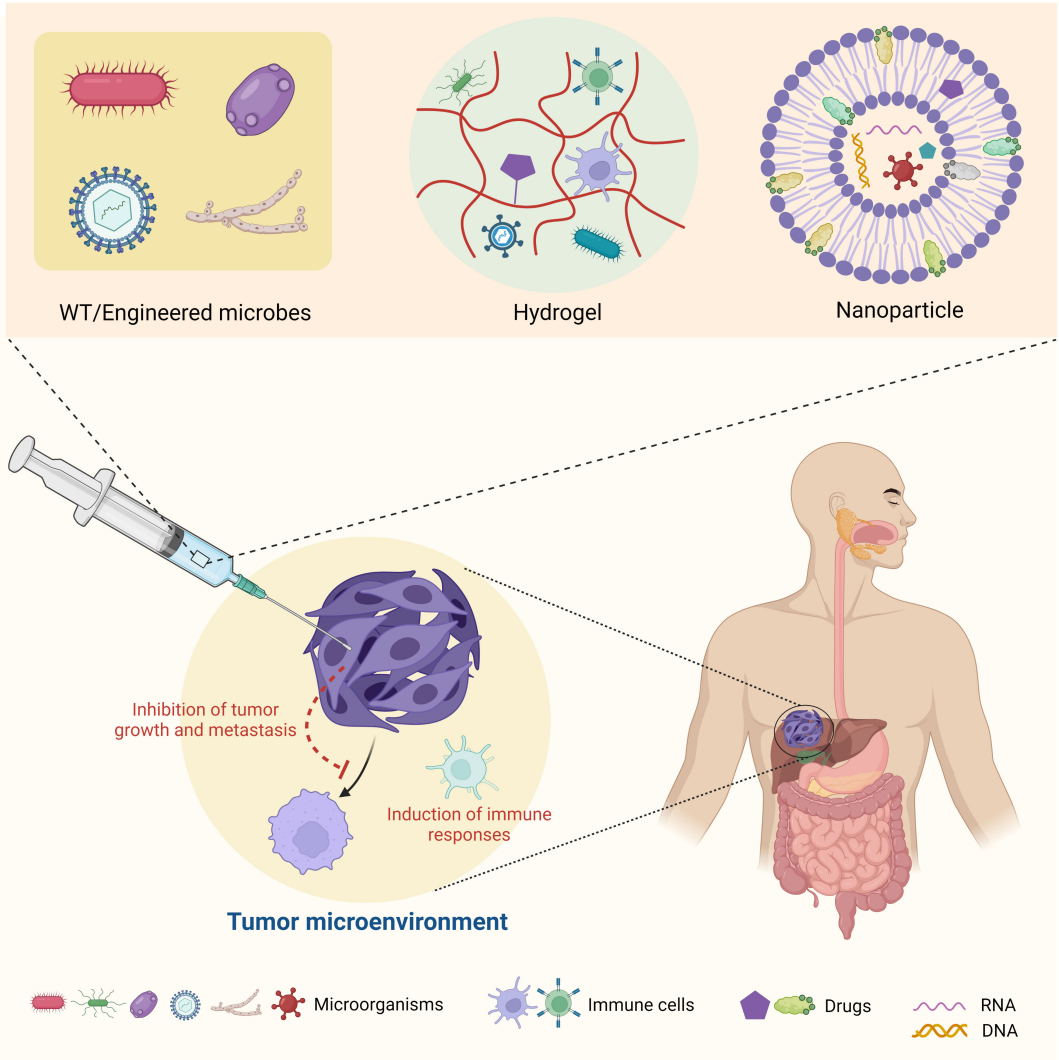

FIGURE 4
Summary of therapeutic strategies targeting tumor microbiome metabolism.

the tumor microbiome metabolism for reshaping TME. Ideally, with a deeper understanding of the tumor microbiome's function in the TME and cancer development, we could build up an artificial ecosystem of microorganisms in the TME to prevent cancer cells from spreading and enhance the efficiency of immunotherapy.

Based on their functions in suppressing or promoting cancer progression, microbes within the TME can be classified to "good bugs" or "bad bugs" for cancer therapies (171). A straightforward treatment strategy is to take advantage of "good bugs" and get rid of "bad bugs" in the TME. For example, *Enterococcus* species have been noted to promote responses to immune checkpoint immunotherapy (ICI) (172). *Bifidobacterium pseudolongum* and *Akkermansia muciniphila* were observed to produce the metabolite inosine, which enhances ICI through T_h1 activation (173). Following biomaterial modulation, mice with increased levels of *Peptostreptococcus anaerobius* and reduced levels of other bacterial species responded better to oral squamous cell carcinoma ICI (174). Bacteria belonging to the *Gammaproteobacteria* family have been found to inactivate the chemotherapy drug gemcitabine, which is often used for the treatment of pancreatic ductal adenocarcinoma (175). Overall, modulating the microbial communities in the TME can provide new opportunities for cancer therapies (176). Accordingly, synthetic biology approaches have been applied to engineer specific tumor microbiome species to develop enhanced bacteria-based cancer therapies. For instance, as low concentrations of L-arginine can cause poor responses to PD-L1 ICI, probiotic strain *E. coli* Nissle 1917 was engineered to

convert ammonia to L-arginine, thereby increasing T-cell infiltration and enhancing ICI (177). Additionally, Nissle 1917 and other *E. coli* strains were engineered to release nanobodies with diverse functions to motivate T-cell infiltration and tumor shrinkage (178, 179). There are also a number of clinical trials in various phases regarding the applications of engineered bacteria for cancer therapies, some of which have shown promising results (180) (Table 1).

Similarly, oncolytic virotherapy has also been applied as an immunotherapy for cancer treatment (181–183). For example, alphavirus M1 was identified for such use, as it specifically targets cancer cells deficient in zinc-finger antiviral protein (184). Engineered oncolytic viruses expressing PD-L1 inhibitors have clinical potentials for curing cancers resistant to PD-1/PD-L1 ICI, as they are able to activate tumor neoantigen–specific T-cell responses (185). Notably, virotherapy has been approved in some countries for use against cancer. Imlygic, which is engineered from herpes simplex virus I (HSV1) and contains granulocyte-macrophage colony-stimulating factor, was approved in 2015 by the US Food and Drug Administration and European Medical Agency for the treatment of melanoma (186). G47Δ, which is engineered from HSV1, was approved in 2021 by Japan Ministry of Health, Labor and Welfare for the treatment of malignant glioma and other brain cancers (187). Oncorine, which is engineered from adenovirus, was approved in 2005 by the China Food and Drug Administration Department in combination with chemotherapy for the treatment of nasopharyngeal carcinoma (186). Moreover, there are other oncolytic virotherapies engineered from HSV1, adenovirus, and measles virus currently in various phases of clinical trials (186) (Table 1).

The toxins and chemicals extracted from microbes can also be used for cancer treatment. This strategy dates back to the late 19th century when Coley's toxins (a mixture of toxins filtered from killed *Streptococcus pyogenes* and *Serratia marcescens*) were utilized to cure cancer (188). Although this was an unstable approach with poor repeatability, the application of Coley's toxins led to milestone breakthroughs in immuno-oncology, such as the discovery of tumor necrosis factor α (TNF-α) (189). TNF-α has since been identified to suppress tumor growth and improve the efficacy of immunotherapy by activating cell death pathways (190, 191). Commensal bacteria have been found to play significant roles in CpG-oligodeoxynucleotide immunotherapy, which depend on the increased production of TNF-α (192). Microbial SCFAs have also been shown to improve CAR-T cell therapy by enhancing the levels of TNF-α in different cancer models (193).

Last but not least, recent advances in biomedical engineering have provided new opportunities for cancer treatment by targeting the tumor microbiome. For example, the utilization of biomaterials, such as nanoparticles (194, 195) and hydrogels (174), to modulate and deliver microbial communities to specific sites of the TME opens a new door for future cancer therapies (Figure 4). These novel materials can be designed to be stimuli responsive (196) and utilized for the controlled and targeted release of toxic chemotherapy drugs (197), therapeutic antibodies (198, 199), CAR-T cells (200, 201), or live microbes to reshape the TME (202–204). These applications of new biomaterials will offer a promising platform for basic and translational research and will accelerate clinical outcomes of drugs that may have poor solubility and high toxicity.

Outlook and perspectives

In this review, we have summarized the research process of the tumor microbiome, mainly focusing on the impacts of its unique microbial metabolism on cancer development and therapy. Over the past few decades, microorganisms have been regarded only as a cause of infectious disease. The pathophysiological functions of human-associated microbes have long been neglected until recently when the microbiome was identified to manipulate and affect diverse disease states, as well as therapeutic efficacy. The impacts of the human microbiome are so broad that research papers on the topic have exploded in the past few years. Accordingly, a number of new concepts have been raised to describe the omnipotent human microbiota, including the "brain-gut axis" and "second brain." Despite these, the tumor microbiome still lacks a precise definition. Nevertheless, the tumor microbiome plays constructive roles in cancer biology, some of which are still elusive. Among these macro- and micropathophysiological effects induced by the tumor microbiome, small molecule metabolite–mediated crosstalk appears to be particularly important due to the free diffusion of metabolites that can easily impact local and distant tumor tissues *via* covalent modifications and/or non-covalent interactions. Here, we have provided representative examples to emphasize the role of tumor microbiome metabolism as a game changer in cancer biology and clinical treatment, as well as its broad biomedical effects that were once disregarded.

Targeting the pathways of microbial metabolism and crosstalk between host and microbes will provide future avenues for cancer diagnosis, treatment, and recovery. Accordingly, therapy strategies have been developed at distinct levels to target tumor microbiome metabolism: 1) directly applying wild-type or engineered live microbes in immuno-oncology; 2) utilizing the microbial-extracted fractions or synthetic chemicals that interfere with corresponding metabolic pathways for cancer treatment; and 3) utilizing rationally designed biomaterials to rebuild a benign TME by modulating the microbial ecosystem. All in all, after having a deeper understanding of the close correlation between the tumor microbiome and human cancer, we would change our perception of these microorganisms' identities in tumor tissues from "short-term tenants" to "permanent residents."

TABLE 1 Representative microorganisms applied for cancer therapy.

Microorganism	Clinical Phase	Cancer Type	Status (Trial Identifier)
***Salmonella* Typhimurium VNP20009**	I	Metastatic melanoma or renal cell carcinoma	Results published (N/A)
***Salmonella* Typhimurium TAPET-CD (VNP20009 expressing cytosine deaminase)**	I	Head and neck solid cell carcinoma or esophageal adenocarcinoma	Results published (N/A)
***Salmonella* Typhimurium (χ4550 expressing human IL-2)**	I	Liver metastases of solid tumors	Results published (NCT01099631)
***Salmonella* Typhimurium VXM01 (Ty21a expressing VEGFR2)**	I	Pancreatic cancer	Completed (NCT01486329)
***Clostridium novyi*-NT**	I	Solid tumor malignancies	Results published (NCT01924689)
***Clostridium novyi*-NT**	Ib	Treatment-refractory advanced solid tumors	Recruiting (NCT03435952)
CRS-100 (live-attenuated *Listeria monocytogenes*)	I	Liver metastases of solid tumors	Completed (NCT00327652)
Listeria monocytogenes	II	Metastatic pancreatic tumors	Results published (NCT01417000)
Listeria monocytogenes	II	Cervical cancer	Results published (NCT01266460)
VE800 (11 commensal bacteria strains)	I/II	Metastatic cancer, melanoma, gastric cancer, or colorectal cancer	Active (NCT04208958)
***MET-4* bacterial strains**	N/A	Locoregionally-advanced oropharyngeal squamous cell carcinoma	Recruiting (NCT03838601)
***Enterococcus* strain MNC-168**	I	Advanced malignant solid tumors	Not yet recruiting (NCT05383703)
***Lactobacillus johnsonii* LA1 and *Bifidobacterium longum* BB536**	II	Colorectal cancer	Completed (NCT00936572)
Plasmodium vivax	I/II	Non-small cell lung cancer	Unknown (NCT02786589)
Plasmodium vivax	I/II	Advanced breast cancer or advanced liver cancer	Unknown (NCT03474822)
***Agaricus bisporus* extract**	I	Breast cancer recurrence	Completed (NCT00709020)
***Agaricus bisporus* extract**	I	Prostate cancer recurrence	Completed (NCT00779168)
***Trametes versicolor* extract**	I	Breast cancer	Completed (NCT00680667)
***Ganoderma lucidum* spore**	II	Non-small cell lung cancer	Unknown (NCT02844114)
Ganoderma lucidum	III	Pediatric cancers	Completed (NCT00575926)
Modified measles virus	I	Mesothelioma	Completed (NCT01503177)
Modified measles virus	I	Ovarian cancer and peritoneal cavity cancer	Results published (NCT00408590)
GL-ONC1 (modified vaccinia virus)	I	Solid tumors	Completed (NCT00794131)
M032 (modified herpes simplex virus)	I	Glioblastoma, astrocytoma, or gliosarcoma	Active (NCT02062827)
G207 (modified herpes simplex virus)	I/II	Glioblastoma, astrocytoma, or gliosarcoma	Completed (NCT00028158)
H101 (modified adenovirus)	N/A	Gynecological cancer	Recruiting (NCT05051696)
Modified fowlpox virus and modified vaccina virus	II	Prostate cancer	Completed (NCT00003871)
Talimogene laherparepvec (modified herpes simplex virus)	III	Melanoma	Results published (NCT00769704)
Pexastimogene Devacirepvec (modified vaccinia virus)	III	Hepatocellular carcinoma	Results published (NCT02562755)

Microorganisms including bacteria (in blue), protists (in orange), fungi (in green), and viruses (in gray) have been utilized in clinical trials for cancer treatment. All information is from ClinicalTrials.gov.

Author contributions

QZ proposed the conception, wrote, and edited the manuscript. XZ drafted the manuscript and figures. SK participated drafting and editing the manuscript as well as references. FH drafted and edited the chemical structures. All authors listed in the paper have made a substantial, direct, and intellectual contribution to the work and approved it for publication.

Funding

This study is supported by OSUCCC startup funds for QZ.

Conflict of interest

The authors declare that the research was conducted in the absence of any commercial or financial relationships that could be construed as a potential conflict of interest.

Publisher's note

All claims expressed in this article are solely those of the authors and do not necessarily represent those of their affiliated organizations, or those of the publisher, the editors and the reviewers. Any product that may be evaluated in this article, or claim that may be made by its manufacturer, is not guaranteed or endorsed by the publisher.

References

1. Berg G, Rybakova D, Fischer D, Cernava T, Vergès MC, Charles T, et al. Microbiome definition re-visited: old concepts and new challenges. *Microbiome* (2020) 8(1):103. doi: 10.1186/s40168-020-00875-0

2. Flint HJ. The impact of nutrition on the human microbiome. *Nutr Rev* (2012) 70 Suppl 1:S10–3. doi: 10.1111/j.1753-4887.2012.00499.x

3. Baquero F, Nombela C. The microbiome as a human organ. *Clin Microbiol Infect* (2012) 18 Suppl 4:2–4. doi: 10.1111/j.1469-0691.2012.03916.x

4. Ochoa-Repáraz J, Kasper LH. The second brain: Is the gut microbiota a link between obesity and central nervous system disorders? *Curr Obes Rep* (2016) 5 (1):51–64. doi: 10.1007/s13679-016-0191-1

5. Qin J, Li R, Raes J, Arumugam M, Burgdorf KS, Manichanh C, et al. A human gut microbial gene catalogue established by metagenomic sequencing. *Nature* (2010) 464(7285):59–65. doi: 10.1038/nature08821

6. Turnbaugh PJ, Ley RE, Hamady M, Fraser-Liggett CM, Knight R, Gordon JI. The human microbiome project. *Nature* (2007) 449(7164):804–10. doi: 10.1038/nature06244

7. Koren O. Moody microbes: Do microbes influence our behavior? *Eur Neuropsychopharmacol* (2017) 27:S478. doi: 10.1016/j.euroneuro.2016.09.561

8. Martin AM, Sun EW, Rogers GB, Keating DJ. The influence of the gut microbiome on host metabolism through the regulation of gut hormone release. *Front Physiol* (2019) 10:428. doi: 10.3389/fphys.2019.00428

9. Van Treuren W, Dodd D. Microbial contribution to the human metabolome: Implications for health and disease. *Annu Rev Pathol* (2020) 15:345–69. doi: 10.1146/annurev-pathol-020117-043559

10. Huang TT, Lai JB, Du YL, Xu Y, Ruan LM, Hu SH. Current understanding of gut microbiota in mood disorders: An update of human studies. *Front Genet* (2019) 10:98. doi: 10.3389/fgene.2019.00098

11. Merchak A, Gaultier A. Microbial metabolites and immune regulation: New targets for major depressive disorder. *Brain Behav Immun Health* (2020) 9:100169. doi: 10.1016/j.bbih.2020.100169

12. Bultman SJ. Emerging roles of the microbiome in cancer. *Carcinogenesis* (2014) 35(2):249–55. doi: 10.1093/carcin/bgt392

13. von Frieling J, Fink C, Hamm J, Klischies K, Forster M, Bosch TCG, et al. Grow with the challenge - microbial effects on epithelial proliferation, carcinogenesis, and cancer therapy. *Front Microbiol* (2018) 9:2020. doi: 10.3389/fmicb.2018.02020

14. Al-Hilu SA, Al-Shujairi WH. Dual role of bacteria in carcinoma: Stimulation and inhibition. *Int J Microbiol* (2020) 2020:4639761. doi: 10.1155/2020/4639761

15. Mager DL. Bacteria and cancer: cause, coincidence or cure? a review. *J Transl Med* (2006) 4:14. doi: 10.1186/1479-5876-4-14

16. Díaz P, Valenzuela Valderrama M, Bravo J, Quest AFG. And gastric cancer: Adaptive cellular mechanisms involved in disease progression. *Front Microbiol* (2018) 9:5. doi: 10.3389/fmicb.2018.00005

17. Li Y, Ye Z, Zhu J, Fang S, Meng L, Zhou C. Effects of gut microbiota on host adaptive immunity under immune homeostasis and tumor pathology state. *Front Immunol* (2022) 13:844335. doi: 10.3389/fimmu.2022.844335

18. Sheflin AM, Whitney AK, Weir TL. Cancer-promoting effects of microbial dysbiosis. *Curr Oncol Rep* (2014) 16(10):406. doi: 10.1007/s11912-014-0406-0

19. Thomas S, Izard J, Walsh E, Batich K, Chongsathidkiet P, Clarke G, et al. The host microbiome regulates and maintains human health: A primer and perspective for non-microbiologists. *Cancer Res* (2017) 77(8):1783–812. doi: 10.1158/0008-5472.CAN-16-2929

20. Gilbert JA, Blaser MJ, Caporaso JG, Jansson JK, Lynch SV, Knight R. Current understanding of the human microbiome. *Nat Med* (2018) 24(4):392–400. doi: 10.1038/nm.4517

21. Levy M, Thaiss CA, Elinav E. Metabolites: messengers between the microbiota and the immune system. *Genes Dev* (2016) 30(14):1589–97. doi: 10.1101/gad.284091.116

22. Hanus M, Parada-Venegas D, Landskron G, Wielandt AM, Hurtado C, Alvarez K, et al. Immune system, microbiota, and microbial metabolites: The unresolved triad in colorectal cancer microenvironment. *Front Immunol* (2021) 12:612826. doi: 10.3389/fimmu.2021.612826

23. Rossi T, Vergara D, Fanini F, Maffia M, Bravaccini S, Pirini F. Microbiota-derived metabolites in tumor progression and metastasis. *Int J Mol Sci* (2020) 21 (16):5786. doi: 10.3390/ijms21165786

24. Krautkramer KA, Fan J, Bäckhed F. Gut microbial metabolites as multi-kingdom intermediates. *Nat Rev Microbiol* (2021) 19(2):77–94. doi: 10.1038/s41579-020-0438-4

25. Nougayrède JP, Homburg S, Taieb F, Boury M, Brzuszkiewicz E, Gottschalk G, et al. Escherichia coli induces DNA double-strand breaks in eukaryotic cells. *Science* (2006) 313(5788):848–51. doi: 10.1126/science.1127059

26. Cuevas-Ramos G, Petit CR, Marcq I, Boury M, Oswald E, Nougayrède JP. Escherichia coli induces DNA damage *in vivo* and triggers genomic instability in mammalian cells. *Proc Natl Acad Sci U S A* (2010) 107(25):11537–42. doi: 10.1073/pnas.1001261107

27. Mikó E, Kovács T, Sebő É, Tóth J, Csonka T, Ujlaki G, et al. Microbiome-microbial metabolome-cancer cell interactions in breast cancer-familiar, but unexplored. *Cells* (2019) 8(4):293. doi: 10.3390/cells8040293

28. Ting NL, Lau HC, Yu J. Cancer pharmacomicrobiomics: targeting microbiota to optimise cancer therapy outcomes. *Gut* (2022) 71:1412–25. doi: 10.1136/gutjnl-2021-326264

29. Oliva M, Mulet-Margalef N, Ochoa-De-Olza M, Napoli S, Mas J, Laquente B, et al. Tumor-associated microbiome: Where do we stand? *Int J Mol Sci* (2021) 22 (3):1446. doi: 10.3390/ijms22031446

30. Poore GD, Kopylova E, Zhu Q, Carpenter C, Fraraccio S, Wandro S, et al. Microbiome analyses of blood and tissues suggest cancer diagnostic approach. *Nature* (2020) 579(7800):567–74. doi: 10.1038/s41586-020-2095-1

31. Robinson KM, Crabtree J, Mattick JS, Anderson KE, Dunning Hotopp JC. Distinguishing potential bacteria-tumor associations from contamination in a secondary data analysis of public cancer genome sequence data. *Microbiome* (2017) 5(1):9. doi: 10.1186/s40168-016-0224-8

32. Nejman D, Livyatan I, Fuks G, Gavert N, Zwang Y, Geller LT, et al. The human tumor microbiome is composed of tumor type-specific intracellular bacteria. *Science* (2020) 368(6494):973–80. doi: 10.1126/science.aay9189

33. Qiu Q, Lin Y, Ma Y, Li X, Liang J, Chen Z, et al. Exploring the emerging role of the gut microbiota and tumor microenvironment in cancer immunotherapy. *Front Immunol* (2020) 11:612202. doi: 10.3389/fimmu.2020.612202

34. Ma J, Huang L, Hu D, Zeng S, Han Y, Shen H. The role of the tumor microbe microenvironment in the tumor immune microenvironment: bystander, activator, or inhibitor? *J Exp Clin Cancer Res* (2021) 40(1):327. doi: 10.1186/s13046-021-02128-w

35. Mola S, Pandolfo C, Sica A, Porta C. The macrophages-microbiota interplay in colorectal cancer (CRC)-related inflammation: Prognostic and therapeutic significance. *Int J Mol Sci* (2020) 21(18):6886. doi: 10.3390/ijms21186866

36. Livyatan I, Nejman D, Shental N, Straussman R. Characterization of the human tumor microbiome reveals tumor-type specific intra-cellular bacteria. *Oncoimmunology* (2020) 9(1):1800957. doi: 10.1080/2162402X.2020.1800957

37. Jain T, Sharma P, Are AC, Vickers SM, Dudeja V. New insights into the cancer-Microbiome-Immune axis: Decrypting a decade of discoveries. *Front Immunol* (2021) 12:622064. doi: 10.3389/fimmu.2021.622064

38. American Cancer Society. *Infections that can lead to cancer n.d* . Available at: https://www.cancer.org/cancer/cancer-causes/infectious-agents/infections-that-can-lead-to-cancer.html.

39. Fujii YR. Oncoviruses and pathogenic MicroRNAs in humans. *Open Virol J* (2009) 3:37–51. doi: 10.2174/1874357900903010037

40. Tornesello ML, Annunziata C, Tornesello AL, Buonaguro L, Buonaguro FM. Human oncoviruses and p53 tumor suppressor pathway deregulation at the origin of human cancers. *Cancers (Basel)* (2018) 10(7):213. doi: 10.3390/cancers10070213

41. Zapatka M, Borozan I, Brewer DS, Iskar M, Grundhoff A, Alawi M, et al. The landscape of viral associations in human cancers. *Nat Genet* (2020) 52(3):320–30. doi: 10.1038/s41588-019-0558-9

42. de Martel C, Georges D, Bray F, Ferlay J, Clifford GM. Global burden of cancer attributable to infections in 2018: a worldwide incidence analysis. *Lancet Glob Health* (2020) 8(2):e180–e90. doi: 10.1016/S2214-109X(19)30488-7

43. Aykut B, Pushalkar S, Chen R, Li Q, Abengozar R, Kim JI, et al. The fungal mycobiome promotes pancreatic oncogenesis *via* activation of MBL. *Nature* (2019) 574(7777):264–7. doi: 10.1038/s41586-019-1608-2

44. Vallianou N, Kounatidis D, Christodoulatos GS, Panagopoulos F, Karampela I, Dalamaga M. Mycobiome and cancer: What is the evidence? *Cancers (Basel)* (2021) 13(13):3149. doi: 10.3390/cancers13133149

45. Zitvogel L, Galluzzi L, Viaud S, Vétizou M, Daillère R, Merad M, et al. Cancer and the gut microbiota: an unexpected link. *Sci Transl Med* (2015) 7 (271):271ps1. doi: 10.1126/scitranslmed.3010473

46. Gaonkar PP, Patankar SR, Tripathi N, Sridharan G. Oral bacterial flora and oral cancer: The possible link? *J Oral Maxillofac Pathol* (2018) 22(2):234–8. doi: 10.4103/jomfp.JOMFP_89_16

47. Kyrgiou M, Mitra A, Moscicki AB. Does the vaginal microbiota play a role in the development of cervical cancer? *Transl Res* (2017) 179:168–82. doi: 10.1016/j.trsl.2016.07.004

48. Cheng WY, Wu CY, Yu J. The role of gut microbiota in cancer treatment: friend or foe? *Gut* (2020) 69(10):1867–76. doi: 10.1136/gutjnl-2020-321153

49. McNamara D, O'Morain C. Helicobacter pylori and gastric cancer. *Ital J Gastroenterol Hepatol* (1998) 30 Suppl 3:S294–8.

50. Wotherspoon AC, Ortiz-Hidalgo C, Falzon MR, Isaacson PG. Helicobacter pylori-associated gastritis and primary b-cell gastric lymphoma. *Lancet* (1991) 338 (8776):1175–6. doi: 10.1016/0140-6736(91)92035-Z

51. Rooks MG, Garrett WS. Gut microbiota, metabolites and host immunity. *Nat Rev Immunol* (2016) 16(6):341–52. doi: 10.1038/nri.2016.42

52. Festi D, Schiumerini R, Eusebi LH, Marasco G, Taddia M, Colecchia A. Gut microbiota and metabolic syndrome. *World J Gastroenterol* (2014) 20(43):16079–94. doi: 10.3748/wjg.v20.i43.16079

53. Fang Y, Yan C, Zhao Q, Xu J, Liu Z, Gao J, et al. The roles of microbial products in the development of colorectal cancer: a review. *Bioengineered* (2021) 12 (1):720–35. doi: 10.1080/21655979.2021.1889109

54. Wu HJ, Wu E. The role of gut microbiota in immune homeostasis and autoimmunity. *Gut Microbes* (2012) 3(1):4–14. doi: 10.4161/gmic.19320

55. Gopalakrishnan V, Helmink BA, Spencer CN, Reuben A, Wargo JA. The influence of the gut microbiome on cancer, immunity, and cancer immunotherapy. *Cancer Cell* (2018) 33(4):570–80. doi: 10.1016/j.ccell.2018.03.015

56. Yu T, Guo F, Yu Y, Sun T, Ma D, Han J, et al. Fusobacterium nucleatum promotes chemoresistance to colorectal cancer by modulating autophagy. *Cell* (2017) 170(3):548–63.e16. doi: 10.1016/j.cell.2017.07.008

57. Coussens LM, Werb Z. Inflammation and cancer. *Nature* (2002) 420 (6917):860–7. doi: 10.1038/nature01322

58. Mantovani A, Allavena P, Sica A, Balkwill F. Cancer-related inflammation. *Nature* (2008) 454(7203):436–44. doi: 10.1038/nature07205

59. Khatun S, Appidi T, Rengan AK. The role played by bacterial infections in the onset and metastasis of cancer. *Curr Res Microb Sci* (2021) 2:100078. doi: 10.1016/j.crmicr.2021.100078

60. Lai CK, Chen YA, Lin CJ, Lin HJ, Kao MC, Huang MZ, et al. Molecular mechanisms and potential clinical applications of campylobacter jejuni cytolethal distending toxin. *Front Cell Infect Microbiol* (2016) 6:9. doi: 10.3389/fcimb.2016.00009

61. Graillot V, Dormoy I, Dupuy J, Shay JW, Huc L, Mirey G, et al. Genotoxicity of cytolethal distending toxin (CDT) on isogenic human colorectal cell lines: Potential promoting effects for colorectal carcinogenesis. *Front Cell Infect Microbiol* (2016) 6:34. doi: 10.3389/fcimb.2016.00034

62. Sun X, Wang M, Yao L, Li X, Dong H, Li M, et al. Role of proton-coupled monocarboxylate transporters in cancer: From metabolic crosstalk to therapeutic potential. *Front Cell Dev Biol* (2020) 8:651. doi: 10.3389/fcell.2020.00651

63. Akira S, Takeda K, Kaisho T. Toll-like receptors: critical proteins linking innate and acquired immunity. *Nat Immunol* (2001) 2(8):675–80. doi: 10.1038/90609

64. Heeg K, Dalpke A, Peter M, Zimmermann S. Structural requirements for uptake and recognition of CpG oligonucleotides. *Int J Med Microbiol* (2008) 298(1-2):33–8. doi: 10.1016/j.ijmm.2007.07.007

65. Tosch C, Geist M, Ledoux C, Ziller-Remi C, Paul S, Erbs P, et al. Adenovirus-mediated gene transfer of pathogen-associated molecular patterns for cancer immunotherapy. *Cancer Gene Ther* (2009) 16(4):310–9. doi: 10.1038/cgt.2008.85

66. Wolska A, Lech-Marańda E, Robak T. Toll-like receptors and their role in carcinogenesis and anti-tumor treatment. *Cell Mol Biol Lett* (2009) 14(2):248–72. doi: 10.2478/s11658-008-0048-z

67. Ma C, Han M, Heinrich B, Fu Q, Zhang Q, Sandhu M, et al. Gut microbiome-mediated bile acid metabolism regulates liver cancer *via* NKT cells. *Science* (2018) 360(6391):5931. doi: 10.1126/science.aan5931

68. Sun L, Zhang H, Gao P. Metabolic reprogramming and epigenetic modifications on the path to cancer. *Protein Cell* (2022) 13(12):877–919. doi: 10.1007/s13238-021-00846-7

69. Park JW, Han JW. Targeting epigenetics for cancer therapy. *Arch Pharm Res* (2019) 42(2):159–70. doi: 10.1007/s12272-019-01126-z

70. Hinshaw DC, Shevde LA. The tumor microenvironment innately modulates cancer progression. *Cancer Res* (2019) 79(18):4557–66. doi: 10.1158/0008-5472.CAN-18-3962

71. Newman TM, Vitolins MZ, Cook KL. From the table to the tumor: The role of Mediterranean and Western dietary patterns in shifting microbial-mediated signaling to impact breast cancer risk. *Nutrients* (2019) 11(11):2565. doi: 10.3390/nu11112565

72. Schwabe RF, Jobin C. The microbiome and cancer. *Nat Rev Cancer* (2013) 13(11):800–12. doi: 10.1038/nrc3610

73. Hang S, Paik D, Yao L, Kim E, Trinath J, Lu J, et al. Bile acid metabolites control T. *Nature* (2019) 576(7785):143–8. doi: 10.1038/s41586-019-1785-z

74. Song X, Sun X, Oh SF, Wu M, Zhang Y, Zheng W, et al. Microbial bile acid metabolites modulate gut RORγ. *Nature* (2020) 577(7790):410–5. doi: 10.1038/s41586-019-1865-0

75. Nguyen TT, Ung TT, Kim NH, Jung YD. Role of bile acids in colon carcinogenesis. *World J Clin Cases* (2018) 6(13):577–88. doi: 10.12998/wjcc.v6.i13.577

76. Fu J, Yu M, Xu W, Yu S. Research progress of bile acids in cancer. *Front Oncol* (2021) 11:778258. doi: 10.3389/fonc.2021.778258

77. Corrêa-Oliveira R, Fachi JL, Vieira A, Sato FT, Vinolo MA. Regulation of immune cell function by short-chain fatty acids. *Clin Transl Immunol* (2016) 5(4): e73. doi: 10.1038/cti.2016.17

78. Mirzaei R, Afaghi A, Babakhani S, Sohrabi MR, Hosseini-Fard SR, Babolhavaeji K, et al. Role of microbiota-derived short-chain fatty acids in cancer development and prevention. *BioMed Pharmacother* (2021) 139:111619. doi: 10.1016/j.biopha.2021.111619

79. Sipe LM, Chaib M, Pingili AK, Pierre JF, Makowski L. Microbiome, bile acids, and obesity: How microbially modified metabolites shape anti-tumor immunity. *Immunol Rev* (2020) 295(1):220–39. doi: 10.1111/imr.12856

80. Singh V, Yeoh BS, Vijay-Kumar M. Feed your gut with caution! *Transl Cancer Res* (2016) 5(Suppl 3):S507–S13. doi: 10.21037/tcr.2016.09.13

81. Golonka RM, Vijay-Kumar M. Atypical immunometabolism and metabolic reprogramming in liver cancer: Deciphering the role of gut microbiome. *Adv Cancer Res* (2021) 149:171–255. doi: 10.1016/bs.acr.2020.10.004

82. Fong W, Li Q, Yu J. Gut microbiota modulation: a novel strategy for prevention and treatment of colorectal cancer. *Oncogene* (2020) 39(26):4925–43. doi: 10.1038/s41388-020-1341-1

83. Conlon MA, Bird AR. The impact of diet and lifestyle on gut microbiota and human health. *Nutrients* (2014) 7(1):17–44. doi: 10.3390/nu7010017

84. Cavalier-Smith T. Origins of secondary metabolism. In: DJ Chadwick and J Whelan, editors. *Secondary metabolites: Their function and evolution* (Chichester, Wiley) (1992). p. 64–80.

85. Sharon G, Garg N, Debelius J, Knight R, Dorrestein PC, Mazmanian SK. Specialized metabolites from the microbiome in health and disease. *Cell Metab* (2014) 20(5):719–30. doi: 10.1016/j.cmet.2014.10.016

86. Postler TS, Ghosh S. Understanding the holobiont: How microbial metabolites affect human health and shape the immune system. *Cell Metab* (2017) 26(1):110–30. doi: 10.1016/j.cmet.2017.05.008

87. Ferguson GP, Tötemeyer S, MacLean MJ, Booth IR. Methylglyoxal production in bacteria: suicide or survival? *Arch Microbiol* (1998) 170(4):209–18. doi: 10.1007/s002030050635

88. Cai M, Kandalai S, Tang X, Zheng Q. Contributions of human-associated archaeal metabolites to tumor microenvironment and carcinogenesis. *Microbiol Spectr* (2022) 10(2):e0236721. doi: 10.1128/spectrum.02367-21

89. Louis P, Hold GL, Flint HJ. The gut microbiota, bacterial metabolites and colorectal cancer. *Nat Rev Microbiol* (2014) 12(10):661–72. doi: 10.1038/nrmicro3344

90. Ernst L, Steinfeld B, Barayeu U, Klintzsch T, Kurth M, Grimm D, et al. Methane formation driven by reactive oxygen species across all living organisms. *Nature* (2022) 603:482–7. doi: 10.1038/s41586-022-04511-9

91. Gao FF, Quan JH, Lee MA, Ye W, Yuk JM, Cha GH, et al. Trichomonas vaginalis induces apoptosis *via* ROS and ER stress response through ER-mitochondria crosstalk in SiHa cells. *Parasit Vectors* (2021) 14(1):603. doi: 10.1186/s13071-021-05098-2

92. Ohnishi S, Ma N, Thanan R, Pinlaor S, Hammam O, Murata M, et al. DNA Damage in inflammation-related carcinogenesis and cancer stem cells. *Oxid Med Cell Longev* (2013) 2013:387014. doi: 10.1155/2013/387014

93. Aoyagi T, Takeuchi T, Matsuzaki A, Kawamura K, Kondo S. Leupeptins, new protease inhibitors from actinomycetes. *J Antibiot (Tokyo)* (1969) 22(6):283–6. doi: 10.7164/antibiotics.22.283

94. Guo CJ, Chang FY, Wyche TP, Backus KM, Acker TM, Funabashi M, et al. Discovery of reactive microbiota-derived metabolites that inhibit host proteases. *Cell* (2017) 168(3):517–26.e18. doi: 10.1016/j.cell.2016.12.021

95. Zheng Q, Wang Q, Wang S, Wu J, Gao Q, Liu W. Thiopeptide antibiotics exhibit a dual mode of action against intracellular pathogens by affecting both host and microbe. *Chem Biol* (2015) 22(8):1002–7. doi: 10.1016/j.chembiol.2015.06.019

96. Wang S, Zheng Q, Wang J, Zhao Z, Li Q, Yu Y, et al. Target-oriented design and biosynthesis of thiostrepton-derived thiopeptide antibiotics with improved pharmaceutical properties. *Org Chem Front* (2015) 2:106–9. doi: 10.1039/C4QO00288A

97. Bagley MC, Dale JW, Merritt EA, Xiong X. Thiopeptide antibiotics. *Chem Rev* (2005) 105(2):685–714. doi: 10.1021/cr0300441

98. Donia MS, Cimermancic P, Schulze CJ, Wieland Brown LC, Martin J, Mitreva M, et al. A systematic analysis of biosynthetic gene clusters in the human microbiome reveals a common family of antibiotics. *Cell* (2014) 158(6):1402–14. doi: 10.1016/j.cell.2014.08.032

99. Vinogradov AA, Suga H. Introduction to thiopeptides: Biological activity, biosynthesis, and strategies for functional reprogramming. *Cell Chem Biol* (2020) 27(8):1032–51. doi: 10.1016/j.chembiol.2020.07.003

100. Secher T, Samba-Louaka A, Oswald E, Nougayrède JP. Escherichia coli producing colibactin triggers premature and transmissible senescence in mammalian cells. *PLoS One* (2013) 8(10):e77157. doi: 10.1371/journal.pone.0077157

101. Silpe JE, Wong JWH, Owen SV, Baym M, Balskus EP. The bacterial toxin colibactin triggers prophage induction. *Nature* (2022) 603:315–20. doi: 10.1038/s41586-022-04444-3

102. Topping DL, Clifton PM. Short-chain fatty acids and human colonic function: roles of resistant starch and nonstarch polysaccharides. *Physiol Rev* (2001) 81(3):1031–64. doi: 10.1152/physrev.2001.81.3.1031

103. Boffa LC, Vidali G, Mann RS, Allfrey VG. Suppression of histone deacetylation *in vivo* and *in vitro* by sodium butyrate. *J Biol Chem* (1978) 253 (10):3364–6. doi: 10.1016/S0021-9258(17)34804-4

104. Cousens LS, Gallwitz D, Alberts BM. Different accessibilities in chromatin to histone acetylase. *J Biol Chem* (1979) 254(5):1716–23. doi: 10.1016/S0021-9258(17)37831-6

105. Waldecker M, Kautenburger T, Daumann H, Busch C, Schrenk D. Inhibition of histone-deacetylase activity by short-chain fatty acids and some polyphenol metabolites formed in the colon. *J Nutr Biochem* (2008) 19(9):587–93. doi: 10.1016/j.jnutbio.2007.08.002

106. Hinnebusch BF, Meng S, Wu JT, Archer SY, Hodin RA. The effects of short-chain fatty acids on human colon cancer cell phenotype are associated with histone hyperacetylation. *J Nutr* (2002) 132(5):1012–7. doi: 10.1093/jn/132.5.1012

107. Kiefer J, Beyer-Sehlmeyer G, Pool-Zobel BL. Mixtures of SCFA, composed according to physiologically available concentrations in the gut lumen, modulate histone acetylation in human HT29 colon cancer cells. *Br J Nutr* (2006) 96(5):803–10. doi: 10.1017/BJN20061948

108. Vander Heiden MG, Cantley LC, Thompson CB. Understanding the warburg effect: the metabolic requirements of cell proliferation. *Science* (2009) 324(5930):1029–33. doi: 10.1126/science.1160809

109. Vander Heiden MG, DeBerardinis RJ. Understanding the intersections between metabolism and cancer biology. *Cell* (2017) 168(4):657–69. doi: 10.1016/j.cell.2016.12.039

110. Goodwin ML, Gladden LB, Nijsten MW, Jones KB. Lactate and cancer: revisiting the warburg effect in an era of lactate shuttling. *Front Nutr* (2014) 1:27. doi: 10.3389/fnut.2014.00027

111. Zhang D, Tang Z, Huang H, Zhou G, Cui C, Weng Y, et al. Metabolic regulation of gene expression by histone lactylation. *Nature* (2019) 574(7779):575–80. doi: 10.1038/s41586-019-1678-1

112. Chen AN, Luo Y, Yang YH, Fu JT, Geng XM, Shi JP, et al. Lactylation, a novel metabolic reprogramming code: Current status and prospects. *Front Immunol* (2021) 12:688910. doi: 10.3389/fimmu.2021.688910

113. Chang PV, Hao L, Offermanns S, Medzhitov R. The microbial metabolite butyrate regulates intestinal macrophage function *via* histone deacetylase inhibition. *Proc Natl Acad Sci U S A* (2014) 111(6):2247–52. doi: 10.1073/pnas.1322269111

114. Yang W, Yu T, Huang X, Bilotta AJ, Xu L, Lu Y, et al. Intestinal microbiota-derived short-chain fatty acids regulation of immune cell IL-22 production and gut immunity. *Nat Commun* (2020) 11(1):4457. doi: 10.1038/s41467-020-18262-6

115. Furusawa Y, Obata Y, Fukuda S, Endo TA, Nakato G, Takahashi D, et al. Commensal microbe-derived butyrate induces the differentiation of colonic regulatory T cells. *Nature* (2013) 504(7480):446–50. doi: 10.1038/nature12721

116. Arpaia N, Campbell C, Fan X, Dikiy S, van der Veeken J, deRoos P, et al. Metabolites produced by commensal bacteria promote peripheral regulatory T-cell generation. *Nature* (2013) 504(7480):451–5. doi: 10.1038/nature12726

117. Smith PM, Howitt MR, Panikov N, Michaud M, Gallini CA, Bohlooly-Y M, et al. The microbial metabolites, short-chain fatty acids, regulate colonic treg cell homeostasis. *Science* (2013) 341(6145):569–73. doi: 10.1126/science.1241165

118. Vinolo MA, Hatanaka E, Lambertucci RH, Newsholme P, Curi R. Effects of short chain fatty acids on effector mechanisms of neutrophils. *Cell Biochem Funct* (2009) 27(1):48–55. doi: 10.1002/cbf.1533

119. Emenaker NJ, Basson MD. Short chain fatty acids inhibit human (SW1116) colon cancer cell invasion by reducing urokinase plasminogen activator activity and stimulating TIMP-1 and TIMP-2 activities, rather than *via* MMP modulation. *J Surg Res* (1998) 76(1):41–6. doi: 10.1006/jsre.1998.5279

120. Emenaker NJ, Calaf GM, Cox D, Basson MD, Qureshi N. Short-chain fatty acids inhibit invasive human colon cancer by modulating uPA, TIMP-1, TIMP-2, mutant p53, bcl-2, bax, p21 and PCNA protein expression in an *in vitro* cell culture model. *J Nutr* (2001) 131(11 Suppl):3041S–6S. doi: 10.1093/jn/131.11.3041S

121. Zeng H, Briske-Anderson M. Prolonged butyrate treatment inhibits the migration and invasion potential of HT1080 tumor cells. *J Nutr* (2005) 135(2):291–5. doi: 10.1093/jn/135.2.291

122. Matsushita M, Fujita K, Hayashi T, Kayama H, Motooka D, Hase H, et al. Gut microbiota-derived short-chain fatty acids promote prostate cancer growth *via* IGF1 signaling. *Cancer Res* (2021) 81(15):4014–26. doi: 10.1158/0008-5472.CAN-20-4090

123. Chirakkal H, Leech SH, Brookes KE, Prais AL, Waby JS, Corfe BM. Upregulation of BAK by butyrate in the colon is associated with increased Sp3 binding. *Oncogene* (2006) 25(54):7192–200. doi: 10.1038/sj.onc.1209702

124. Buda A, Qualtrough D, Jepson MA, Martines D, Paraskeva C, Pignatelli M. Butyrate downregulates alpha2beta1 integrin: a possible role in the induction of apoptosis in colorectal cancer cell lines. *Gut* (2003) 52(5):729–34. doi: 10.1136/gut.52.5.729

125. Fung KY, Brierley GV, Henderson S, Hoffmann P, McColl SR, Lockett T, et al. Butyrate-induced apoptosis in HCT116 colorectal cancer cells includes induction of a cell stress response. *J Proteome Res* (2011) 10(4):1860–9. doi: 10.1021/pr1011125

126. Comalada M, Bailón E, de Haro O, Lara-Villoslada F, Xaus J, Zarzuelo A, et al. The effects of short-chain fatty acids on colon epithelial proliferation and survival depend on the cellular phenotype. *J Cancer Res Clin Oncol* (2006) 132 (8):487–97. doi: 10.1007/s00432-006-0092-x

127. Zgouras D, Wächtershäuser A, Frings D, Stein J. Butyrate impairs intestinal tumor cell-induced angiogenesis by inhibiting HIF-1alpha nuclear translocation. *Biochem Biophys Res Commun* (2003) 300(4):832–8. doi: 10.1016/S0006-291X(02)02916-9

128. Terui T, Murakami K, Takimoto R, Takahashi M, Takada K, Murakami T, et al. Induction of PIG3 and NOXA through acetylation of p53 at 320 and 373

lysine residues as a mechanism for apoptotic cell death by histone deacetylase inhibitors. *Cancer Res* (2003) 63(24):8948–54.

129. Gope R, Gope ML. Effect of sodium butyrate on the expression of retinoblastoma (RB1) and P53 gene and phosphorylation of retinoblastoma protein in human colon tumor cell line HT29. *Cell Mol Biol (Noisy-le-grand)* (1993) 39(6):589–97.

130. Cook JW, Kennaway EL, Kennaway NM. Production of tumours in mice by deoxycholic acid. *Nature* (1940) 145(3677):627. doi: 10.1038/145627a0

131. Májer F, Sharma R, Mullins C, Keogh L, Phipps S, Duggan S, et al. New highly toxic bile acids derived from deoxycholic acid, chenodeoxycholic acid and lithocholic acid. *Bioorg Med Chem* (2014) 22(1):256–68. doi: 10.1016/j.bmc.2013.11.029

132. Narahara H, Tatsuta M, Iishi H, Baba M, Uedo N, Sakai N, et al. K-Ras point mutation is associated with enhancement by deoxycholic acid of colon carcinogenesis induced by azoxymethane, but not with its attenuation by all-trans-retinoic acid. *Int J Cancer* (2000) 88(2):157–61. doi: 10.1002/1097-0215(20001015)88:2<157::AID-IJC2>3.0.CO;2-B

133. Powolny A, Xu J, Loo G. Deoxycholate induces DNA damage and apoptosis in human colon epithelial cells expressing either mutant or wild-type p53. *Int J Biochem Cell Biol* (2001) 33(2):193–203. doi: 10.1016/S1357-2725(00)00080-7

134. Arvind P, Papavassiliou ED, Tsioulias GJ, Duceman BW, Lovelace CI, Geng W, et al. Lithocholic acid inhibits the expression of HLA class I genes in colon adenocarcinoma cells. differential effect on HLA-a, -b and -c loci. *Mol Immunol* (1994) 31(8):607–14. doi: 10.1016/0161-5890(94)90168-6

135. Gafar AA, Draz HM, Goldberg AA, Bashandy MA, Bakry S, Khalifa MA, et al. Lithocholic acid induces endoplasmic reticulum stress, autophagy and mitochondrial dysfunction in human prostate cancer cells. *PeerJ* (2016) 4:e2445. doi: 10.7717/peerj.2445

136. Martinez JD, Stratagoules ED, LaRue JM, Powell AA, Gause PR, Craven MT, et al. Different bile acids exhibit distinct biological effects: the tumor promoter deoxycholic acid induces apoptosis and the chemopreventive agent ursodeoxycholic acid inhibits cell proliferation. *Nutr Cancer* (1998) 31(2):111–8. doi: 10.1080/01635589809514689

137. Crowley-Weber CL, Payne CM, Gleason-Guzman M, Watts GS, Futscher B, Waltmire CN, et al. Development and molecular characterization of HCT-116 cell lines resistant to the tumor promoter and multiple stress-inducer, deoxycholate. *Carcinogenesis* (2002) 23(12):2063–80. doi: 10.1093/carcin/23.12.2063

138. Wu G, Morris SM. Arginine metabolism: nitric oxide and beyond. *Biochem J* (1998) 336(Pt 1):1–17. doi: 10.1042/bj3360001

139. Tabor CW, Tabor H. Polyamines in microorganisms. *Microbiol Rev* (1985) 49(1):81–99. doi: 10.1128/mr.49.1.81-99.1985

140. Di Martino ML, Campilongo R, Casalino M, Micheli G, Colonna B, Prosseda G. Polyamines: emerging players in bacteria-host interactions. *Int J Med Microbiol* (2013) 303(8):484–91. doi: 10.1016/j.ijmm.2013.06.008

141. Khan AU, Mei YH, Wilson T. A proposed function for spermine and spermidine: protection of replicating DNA against damage by singlet oxygen. *Proc Natl Acad Sci U S A* (1992) 89(23):11426–7. doi: 10.1073/pnas.89.23.11426

142. Linsalata M, Caruso MG, Leo S, Guerra V, D'Attoma B, Di Leo A. Prognostic value of tissue polyamine levels in human colorectal carcinoma. *Anticancer Res* (2002) 22(4):2465–9.

143. Linsalata M, Giannini R, Notarnicola M, Cavallini A. Peroxisome proliferator-activated receptor gamma and spermidine/spermine N1-acetyltransferase gene expressions are significantly correlated in human colorectal cancer. *BMC Cancer* (2006) 6:191. doi: 10.1186/1471-2407-6-191

144. Smith RC, Litwin MS, Lu Y, Zetter BR. Identification of an endogenous inhibitor of prostatic carcinoma cell growth. *Nat Med* (1995) 1(10):1040–5. doi: 10.1038/nm1095-1040

145. Kee K, Foster BA, Merali S, Kramer DL, Hensen ML, Diegelman P, et al. Activated polyamine catabolism depletes acetyl-CoA pools and suppresses prostate tumor growth in TRAMP mice. *J Biol Chem* (2004) 279(38):40076–83. doi: 10.1074/jbc.M406002200

146. Kee K, Vujcic S, Merali S, Diegelman P, Kisiel N, Powell CT, et al. Metabolic and antiproliferative consequences of activated polyamine catabolism in LNCaP prostate carcinoma cells. *J Biol Chem* (2004) 279(26):27050–8. doi: 10.1074/jbc.M403323200

147. Huang Y, Keen JC, Pledgie A, Marton LJ, Zhu T, Sukumar S, et al. Polyamine analogues down-regulate estrogen receptor alpha expression in human breast cancer cells. *J Biol Chem* (2006) 281(28):19055–63. doi: 10.1074/jbc.M600910200

148. Xu H, Chaturvedi R, Cheng Y, Bussiere FI, Asim M, Yao MD, et al. Spermine oxidation induced by helicobacter pylori results in apoptosis and DNA damage: implications for gastric carcinogenesis. *Cancer Res* (2004) 64(23):8521–5. doi: 10.1158/0008-5472.CAN-04-3511

149. Chaturvedi R, Cheng Y, Asim M, Bussière FI, Xu H, Gobert AP, et al. Induction of polyamine oxidase 1 by helicobacter pylori causes macrophage apoptosis by hydrogen peroxide release and mitochondrial membrane depolarization. *J Biol Chem* (2004) 279(38):40161–73. doi: 10.1074/jbc.M401370200

150. Bussière FI, Chaturvedi R, Cheng Y, Gobert AP, Asim M, Blumberg DR, et al. Spermine causes loss of innate immune response to helicobacter pylori by inhibition of inducible nitric-oxide synthase translation. *J Biol Chem* (2005) 280(4):2409–12. doi: 10.1074/jbc.C400498200

151. Gobert AP, Chaturvedi R, Wilson KT. Methods to evaluate alterations in polyamine metabolism caused by helicobacter pylori infection. *Methods Mol Biol* (2011) 720:409–25. doi: 10.1007/978-1-61779-034-8_26

152. Wang X, Feith DJ, Welsh P, Coleman CS, Lopez C, Woster PM, et al. Studies of the mechanism by which increased spermidine/spermine N1-acetyltransferase activity increases susceptibility to skin carcinogenesis. *Carcinogenesis* (2007) 28(11):2404–11. doi: 10.1093/carcin/bgm162

153. Coleman CS, Pegg AE, Megosh LC, Guo Y, Sawicki JA, O'Brien TG. Targeted expression of spermidine/spermine N1-acetyltransferase increases susceptibility to chemically induced skin carcinogenesis. *Carcinogenesis* (2002) 23(2):359–64. doi: 10.1093/carcin/23.2.359

154. Latour YL, Gobert AP, Wilson KT. The role of polyamines in the regulation of macrophage polarization and function. *Amino Acids* (2020) 52(2):151–60. doi: 10.1007/s00726-019-02719-0

155. Vander Jagt DL, Robinson B, Taylor KK, Hunsaker LA. Reduction of trioses by NADPH-dependent aldo-keto reductases. aldose reductase, methylglyoxal, and diabetic complications. *J Biol Chem* (1992) 267(7):4364–9. doi: 10.1016/S0021-9258(18)42844-X

156. Speer O, Morkunaite-Haimi S, Liobikas J, Franck M, Hensbo L, Linder MD, et al. Rapid suppression of mitochondrial permeability transition by methylglyoxal. role of reversible arginine modification. *J Biol Chem* (2003) 278(37):34757–63. doi: 10.1074/jbc.M301990200

157. Baskaran S, Rajan DP, Balasubramanian KA. Formation of methylglyoxal by bacteria isolated from human faeces. *J Med Microbiol* (1989) 28(3):211–5. doi: 10.1099/00222615-28-3-211

158. Richarme G, Mihoub M, Dairou J, Bui LC, Leger T, Lamouri A. Parkinsonism-associated protein DJ-1/Park7 is a major protein deglycase that repairs methylglyoxal- and glyoxal-glycated cysteine, arginine, and lysine residues. *J Biol Chem* (2015) 290(3):1885–97. doi: 10.1074/jbc.M114.597815

159. Richarme G, Liu C, Mihoub M, Abdallah J, Leger T, Joly N, et al. Guanine glycation repair by DJ-1/Park7 and its bacterial homologs. *Science* (2017) 357(6347):208–11. doi: 10.1126/science.aag1095

160. Zheng Q, Maksimovic I, Upad A, David Y. Non-enzymatic covalent modifications: a new link between metabolism and epigenetics. *Protein Cell* (2020) 11(6):401–16. doi: 10.1007/s13238-020-00722-w

161. Zheng Q, Prescott NA, Maksimovic I, David Y. (De)Toxifying the epigenetic code. *Chem Res Toxicol* (2019) 32(5):796–807. doi: 10.1021/acs.chemrestox.9b00013

162. Zheng Q, Maksimovic I, Upad A, Guber D, David Y. Synthesis of an alkynyl methylglyoxal probe to investigate nonenzymatic histone glycation. *J Org Chem* (2020) 85(3):1691–7. doi: 10.1021/acs.joc.9b02504

163. Zheng Q, Omans ND, Leicher R, Osunsade A, Agustinus AS, Finkin-Groner E, et al. Reversible histone glycation is associated with disease-related changes in chromatin architecture. *Nat Commun* (2019) 10(1):1289. doi: 10.1038/s41467-019-09192-z

164. Zheng Q, Osunsade A, David Y. Protein arginine deiminase 4 antagonizes methylglyoxal-induced histone glycation. *Nat Commun* (2020) 11(1):3241. doi: 10.1038/s41467-020-17066-y

165. Ray DM, Jennings EQ, Maksimovic I, Chai X, Galligan JJ, David Y, et al. Chemical labeling and enrichment of histone glyoxal adducts. *ACS Chem Biol* (2022) 17(4):756–61. doi: 10.1021/acschembio.1c00864

166. Schalkwijk CG, Stehouwer CDA. Methylglyoxal, a highly reactive dicarbonyl compound, in diabetes, its vascular complications, and other age-related diseases. *Physiol Rev* (2020) 100(1):407–61. doi: 10.1152/physrev.00001.2019

167. Bellahcène A, Nokin MJ, Castronovo V, Schalkwijk C. Methylglyoxal-derived stress: An emerging biological factor involved in the onset and progression of cancer. *Semin Cancer Biol* (2018) 49:64–74. doi: 10.1016/j.semcancer.2017.05.010

168. Nokin MJ, Durieux F, Peixoto P, Chiavarina B, Peulen O, Blomme A, et al. Methylglyoxal, a glycolysis side-product, induces Hsp90 glycation and YAP-mediated tumor growth and metastasis. *Elife* (2016) 5:e19375. doi: 10.7554/eLife.19375

169. Bollong MJ, Lee G, Coukos JS, Yun H, Zambaldo C, Chang JW, et al. A metabolite-derived protein modification integrates glycolysis with KEAP1-NRF2 signalling. *Nature* (2018) 562(7728):600–4. doi: 10.1038/s41586-018-0622-0

170. Maksimovic I, Finkin-Groner E, Fukase Y, Zheng Q, Sun S, Michino M, et al. Deglycase-activity oriented screening to identify DJ-1 inhibitors. *RSC Med Chem* (2021) 12(7):1232–8. doi: 10.1039/D1MD00062D

171. Garrett WS. Cancer and the microbiota. *Science* (2015) 348(6230):80–6. doi: 10.1126/science.aaa4972

172. Griffin ME, Espinosa J, Becker JL, Luo JD, Carroll TS, Jha JK, et al. E*nterococcus p*eptidoglycan remodeling promotes checkpoint inhibitor cancer immunotherapy. *Science* (2021) 373(6558):1040–6. doi: 10.1126/science.abc9113

173. Mager LF, Burkhard R, Pett N, Cooke NCA, Brown K, Ramay H, et al. Microbiome-derived inosine modulates response to checkpoint inhibitor immunotherapy. *Science* (2020) 369(6510):1481–9. doi: 10.1126/science.abc3421

174. Zheng DW, Deng WW, Song WF, Wu CC, Liu J, Hong S, et al. Biomaterial-mediated modulation of oral microbiota synergizes with PD-1 blockade in mice with oral squamous cell carcinoma. *Nat BioMed Eng* (2022) 6 (1):32–43. doi: 10.1038/s41551-021-00807-9

175. Geller LT, Barzily-Rokni M, Danino T, Jonas OH, Shental N, Nejman D, et al. Potential role of intratumor bacteria in mediating tumor resistance to the chemotherapeutic drug gemcitabine. *Science* (2017) 357(6356):1156–60. doi: 10.1126/science.aah5043

176. Kramer MG, Masner M, Ferreira FA, Hoffman RM. Bacterial therapy of cancer: Promises, limitations, and insights for future directions. *Front Microbiol* (2018) 9:16. doi: 10.3389/fmicb.2018.00016

177. Canale FP, Basso C, Antonini G, Perotti M, Li N, Sokolovska A, et al. Metabolic modulation of tumours with engineered bacteria for immunotherapy. *Nature* (2021) 598(7882):662–6. doi: 10.1038/s41586-021-04003-2

178. Chowdhury S, Castro S, Coker C, Hinchliffe TE, Arpaia N, Danino T. Programmable bacteria induce durable tumor regression and systemic antitumor immunity. *Nat Med* (2019) 25(7):1057–63. doi: 10.1038/s41591-019-0498-z

179. Gurbatri CR, Lia I, Vincent R, Coker C, Castro S, Treuting PM, et al. Engineered probiotics for local tumor delivery of checkpoint blockade nanobodies. *Sci Transl Med* (2020) 12(530):eaax0876. doi: 10.1126/scitranslmed.aax0876

180. Zhou S, Gravekamp C, Bermudes D, Liu K. Tumour-targeting bacteria engineered to fight cancer. *Nat Rev Cancer* (2018) 18(12):727–43. doi: 10.1038/s41568-018-0070-z

181. Russell SJ, Peng KW, Bell JC. Oncolytic virotherapy. *Nat Biotechnol* (2012) 30(7):658–70. doi: 10.1038/nbt.2287

182. Sze DY, Reid TR, Rose SC. Oncolytic virotherapy. *J Vasc Interv Radiol* (2013) 24(8):1115–22. doi: 10.1016/j.jvir.2013.05.040

183. Li L, Liu S, Han D, Tang B, Ma J. Delivery and biosafety of oncolytic virotherapy. *Front Oncol* (2020) 10:475. doi: 10.3389/fonc.2020.00475

184. Lin Y, Zhang H, Liang J, Li K, Zhu W, Fu L, et al. Identification and characterization of alphavirus M1 as a selective oncolytic virus targeting ZAP-defective human cancers. *Proc Natl Acad Sci U S A* (2014) 111(42):E4504–12. doi: 10.1073/pnas.1408759111

185. Wang G, Kang X, Chen KS, Jehng T, Jones L, Chen J, et al. An engineered oncolytic virus expressing PD-L1 inhibitors activates tumor neoantigen-specific T cell responses. *Nat Commun* (2020) 11(1):1395. doi: 10.1038/s41467-020-15229-5

186. Mondal M, Guo J, He P, Zhou D. Recent advances of oncolytic virus in cancer therapy. *Hum Vaccin Immunother* (2020) 16(10):2389–402. doi: 10.1080/21645515.2020.1723363

187. Fukuhara H, Takeshima Y, Todo T. Triple-mutated oncolytic herpes virus for treating both fast- and slow-growing tumors. *Cancer Sci* (2021) 112(8):3293–301. doi: 10.1111/cas.14981

188. Starnes CO. Coley's toxins in perspective. *Nature* (1992) 357(6373):11–2. doi: 10.1038/357011a0

189. Wiemann B, Starnes CO. Coley's toxins, tumor necrosis factor and cancer research: a historical perspective. *Pharmacol Ther* (1994) 64(3):529–64. doi: 10.1016/0163-7258(94)90023-X

190. Salomon BL, Leclerc M, Tosello J, Ronin E, Piaggio E, Cohen JL. Tumor necrosis factor α and regulatory T cells in oncoimmunology. *Front Immunol* (2018) 9:444. doi: 10.3389/fimmu.2018.00444

191. Chen AY, Wolchok JD, Bass AR. TNF in the era of immune checkpoint inhibitors: friend or foe? *Nat Rev Rheumatol* (2021) 17(4):213–23. doi: 10.1038/s41584-021-00584-4

192. Iida N, Dzutsev A, Stewart CA, Smith L, Bouladoux N, Weingarten RA, et al. Commensal bacteria control cancer response to therapy by modulating the tumor microenvironment. *Science* (2013) 342(6161):967–70. doi: 10.1126/science.1240527

193. Luu M, Riester Z, Baldrich A, Reichardt N, Yuille S, Busetti A, et al. Microbial short-chain fatty acids modulate CD8. *Nat Commun* (2021) 12(1):4077. doi: 10.1038/s41467-021-24331-1

194. Zheng DW, Dong X, Pan P, Chen KW, Fan JX, Cheng SX, et al. Phage-guided modulation of the gut microbiota of mouse models of colorectal cancer augments their responses to chemotherapy. *Nat BioMed Eng* (2019) 3(9):717–28. doi: 10.1038/s41551-019-0423-2

195. Song W, Tiruthani K, Wang Y, Shen L, Hu M, Dorosheva O, et al. Trapping of lipopolysaccharide to promote immunotherapy against colorectal cancer and attenuate liver metastasis. *Adv Mater* (2018) 30(52):e1805007. doi: 10.1002/adma.201805007

196. Li L, Yang Z, Chen X. Recent advances in stimuli-responsive platforms for cancer immunotherapy. *Acc Chem Res* (2020) 53(10):2044–54. doi: 10.1021/acs.accounts.0c00334

197. Seitz I, Shaukat A, Nurmi K, Ijäs H, Hirvonen J, Santos HA, et al. Prospective cancer therapies using stimuli-responsive DNA nanostructures. *Macromol Biosci* (2021) 21(12):e2100272. doi: 10.1002/mabi.202100272

198. Davis ME, Chen ZG, Shin DM. Nanoparticle therapeutics: an emerging treatment modality for cancer. *Nat Rev Drug Discovery* (2008) 7(9):771–82. doi: 10.1038/nrd2614

199. Ye QN, Wang Y, Shen S, Xu CF, Wang J. Biomaterials-based delivery of therapeutic antibodies for cancer therapy. *Adv Healthc Mater* (2021) 10(11): e2002139. doi: 10.1002/adhm.202002139

200. Smith TT, Stephan SB, Moffett HF, McKnight LE, Ji W, Reiman D, et al. *In situ* programming of leukaemia-specific T cells using synthetic DNA nanocarriers. *Nat Nanotechnol* (2017) 12(8):813–20. doi: 10.1038/nnano.2017.57

201. Grosskopf AK, Labanieh L, Klysz DD, Roth GA, Xu P, Adebowale O, et al. Delivery of CAR-T cells in a transient injectable stimulatory hydrogel niche improves treatment of solid tumors. *Sci Adv* (2022) 8(14):eabn8264. doi: 10.1126/sciadv.abn8264

202. Pan H, Zheng M, Ma A, Liu L, Cai L. Cell/Bacteria-based bioactive materials for cancer immune modulation and precision therapy. *Adv Mater* (2021) 33(50):e2100241. doi: 10.1002/adma.202100241

203. Liu Y, Li Z, Wu Y, Jing X, Li L, Fang X. Intestinal bacteria encapsulated by biomaterials enhance immunotherapy. *Front Immunol* (2020) 11:620170. doi: 10.3389/fimmu.2020.620170

204. Moghimipour E, Abedishirehjin S, Baghbadorani MA, Handali S. Bacteria and archaea: A new era of cancer therapy. *J Control Release* (2021) 338:1–7. doi: 10.1016/j.jconrel.2021.08.019

frontiers | Frontiers in Oncology

ORIGINAL RESEARCH
published: 25 July 2022
doi: 10.3389/fonc.2022.903033

Metabolic Reprogramming Helps to Define Different Metastatic Tropisms in Colorectal Cancer

Ana Montero-Calle[1†], Marta Gómez de Cedrón[2†], Adriana Quijada-Freire[2], Guillermo Solís-Fernández[3], Victoria López-Alonso[4], Isabel Espinosa-Salinas[5], Alberto Peláez-García[6], María Jesús Fernández-Aceñero[7], Ana Ramírez de Molina[2*] and Rodrigo Barderas[1*]*

[1] Functional Proteomics Unit, Chronic Disease Programme, UFIEC, Instituto de Salud Carlos III, Madrid, Spain, [2] Precision Nutrition and Cancer Program, Molecular Oncology Group, IMDEA Food Institute, Campus of International Excellence (CEI) University Autonomous of Madrid (UAM) + Consejo Superior de Investigaciones Científicas (CSIC), Madrid, Spain, [3] Molecular Imaging and Photonics Division, Chemistry Department, Faculty of Sciences, KU Leuven, Leuven, Belgium, [4] Unidad de Biología Computacional, Chronic Disease Programme, UFIEC, Instituto de Salud Carlos III, Madrid, Spain, [5] Platform for Clinical Trials in Nutrition and Health (GENYAL), IMDEA Food Institute, Campus of International Excellence (CEI) University Autonomous of Madrid (UAM) + Consejo Superior de Investigaciones Científicas (CSIC), Madrid, Spain, [6] Molecular Pathology and Therapeutic Targets Group, La Paz University Hospital (IdiPAZ), Madrid, Spain, [7] Servicio de Anatomía Patológica Hospital Clínico San Carlos, Departamento de Anatomía Patológica, Facultad de Medicina, Complutense University of Madrid, Madrid, Spain

OPEN ACCESS

Edited by:
Jose Luis Izquierdo-Garcia, Complutense University of Madrid, Spain

Reviewed by:
Mara De Martino, NewYork-Presbyterian, United States
Deepanshi Dhar, Johnson & Johnson, United States

***Correspondence:**
Rodrigo Barderas
r.barderasm@isciii.es
Ana Ramírez de Molina
ana.ramirez@imdea.org
Marta Gómez de Cedrón
marta.gomezdecedron@imdea.org

†These authors have contributed equally to this work

Specialty section:
This article was submitted to Cancer Metabolism, a section of the journal Frontiers in Oncology

Received: *23 March 2022*
Accepted: *09 June 2022*
Published: *25 July 2022*

Citation:
Montero-Calle A, Gómez de Cedrón M, Quijada-Freire A, Solís-Fernández G, López-Alonso V, Espinosa-Salinas I, Peláez-García A, Fernández-Aceñero MJ, Ramírez de Molina A and Barderas R (2022) Metabolic Reprogramming Helps to Define Different Metastatic Tropisms in Colorectal Cancer. Front. Oncol. 12:903033. doi: 10.3389/fonc.2022.903033

Approximately 25% of colorectal cancer (CRC) patients experience systemic metastases, with the most frequent target organs being the liver and lung. Metabolic reprogramming has been recognized as one of the hallmarks of cancer. Here, metabolic and functional differences between two CRC cells with different metastatic organotropisms (metastatic KM12SM CRC cells to the liver and KM12L4a to the lung when injected in the spleen and in the tail vein of mice) were analysed in comparison to their parental non-metastatic isogenic KM12C cells, for a subsequent investigation of identified metabolic targets in CRC patients. Meta-analysis from proteomic and transcriptomic data deposited in databases, qPCR, WB, *in vitro* cell-based assays, and *in vivo* experiments were used to survey for metabolic alterations contributing to their different organotropism and for the subsequent analysis of identified metabolic markers in CRC patients. Although no changes in cell proliferation were observed between metastatic cells, KM12SM cells were highly dependent on oxidative phosphorylation at mitochondria, whereas KM12L4a cells were characterized by being more energetically efficient with lower basal respiration levels and a better redox management. Lipid metabolism-related targets were found altered in both cell lines, including *LDLR*, *CD36*, *FABP4*, *SCD*, *AGPAT1*, and *FASN*, which were also associated with the prognosis of CRC patients. Moreover, CD36 association

with lung metastatic tropism of CRC cells was validated *in vivo*. Altogether, our results suggest that *LDLR*, *CD36*, *FABP4*, *SCD*, *FASN*, *LPL*, and *APOA1* metabolic targets are associated with CRC metastatic tropism to the liver or lung. These features exemplify specific metabolic adaptations for invasive cancer cells which stem at the primary tumour.

Keywords: CRC (colorectal cancer), metabolic reprograming, tropism of metastasis, obesity, fatty acids (FA), organotropism

INTRODUCTION

Colorectal cancer (CRC) is the third most common cancer and the second leading cause of cancer-related deaths worldwide. Metastasis is the last step of cancer, being the main responsible factor for morbidity and mortality. Moreover, more than 90% of mortality associated with CRC is due to metastasis (1). In CRC, approximately 25% of patients experience systemic metastases, with liver being the most common metastatic tropism followed by the lung (2). Despite major research efforts and clinical progress, there is still a great need for predictable biomarkers for metastasis and therapeutics for advanced CRC.

Cancer energy relies on metabolic editing to drive malignant transformation (3). Great effort has been made to characterize tumour metabolic phenotypes, and new oncometabolites are constantly being described. To support the high energy and macromolecule demands for rapid proliferation of cancer cells (4), in addition to the Warburg effect and known alterations in carbohydrate metabolism, it is recognized that tumours use a wide range of metabolic adaptations to sustain their growth and dissemination (5–7).

Metabolic changes in cancer cells are often related to growth and survival pathways that drive different aspects of tumorigenesis. For instance, glycolytic behaviour is associated with Akt and Erk pathways (8, 9), while the Myc oncogene governs glutamine addiction (10). Catabolic and anabolic alterations in lipid metabolism are also part of the metabolic reprogramming that occurs in tumour cells in response to gene mutations, loss of tumour suppressors, and/or epigenetic modifications (11). The cross talk between metabolic and tumorigenic pathways can lead to the activation of new metabolic cascades that may affect cell cycle regulation, redox management, and other changes, which in turn would enable different characteristics of tumoural cells (12). For example, ROS production, aerobic glycolysis metabolites, and the accumulation of other by-products from cancer metabolism have been shown to enhance the dissemination of cancer cells through the activation of the epithelial to mesenchymal transition (EMT) program (13–15).

In the context of cancer dissemination, a shift to a more mesenchymal state within the EMT program is thought to contribute to the early stages of metastatic translocation, i.e., tumour invasion, extravasation, release of circulating tumour cells (CTCs), and survival in the bloodstream and formation of metastatic niches. In contrast, the reverse process (mesenchymal to epithelial transition, MET) has been associated with an increased ability to proliferate and metastasize to secondary organs, which contribute to the fatal late stages of metastatic development (16). Lastly, the existence of a phenotypic plasticity is suggested to, together with the characteristics of stem cells, favour not only dissemination but also subsequent metastatic colonization (17).

Multiple studies support a good correlation between the findings observed in the KM12 cell system of CRC metastasis and patient samples, indicating that isogenic KM12 cell lines effectively recapitulate the critical steps of CRC metastasis (18–20). The in-depth proteomic characterization of the KM12 cell system, composed of the low metastatic KM12C cells and the metastatic to liver KM12SM cells, showed differences in multiple proteins, complexes, and pathways (21–23), including many metabolic pathways (22, 23). Furthermore, it was also suggested, based on the protein profile comparison of KM12SM and KM12C cells, that a partial EMT reversion could be observed in the liver metastatic CRC cells contributing to the liver colonization of these cells (22–24). Here, we aim to dive into the metabolic profile, cell bioenergetics, and metabolic genes of the two isogenic KM12 cell lines with organ-specific tropisms compared to their non-metastatic isogenic parental cell line KM12C, together with the analysis of specific alterations in EMT markers that could also contribute to the different tropisms. After being injected in spleen, KM12SM cells produce liver metastasis and KM12L4a cells show lung and liver metastasis. Furthermore, when metastatic KM12 cells are injected through the tail vein, only KM12L4a cells can metastasize to the lung.

Herein, we describe differences in the metabolic pathways and bioenergetic profiles of KM12SM and KM12L4a cells that appear to help define intrinsic protumorigenic features associated with differences in their organ-specific tropism. We found that metastatic dysregulation of *LDLR*, *CD36*, *FABP4*, *SCD*, *FASN*, *LPL*, and *APOA1* shows concordance with CRC cell tropism toward the liver versus lung, whereas *LDLR*, *CD36*, *FABP4*, *SCD*,

Abbreviations: ABCA1, phospholipid-transporting ATPase ABCA1; AGPAT, 1-acyl-sn-glycerol-3-phosphate acyltransferase beta; APOA1, apolipoprotein A-I; BIP (HSPA5), endoplasmic reticulum chaperone BiP; CD29, integrin beta-1; CD36, platelet glycoprotein 4; CD44, CD44 antigen; CD133, prominin-1; CHOP (DDIT3), DNA damage-inducible transcript 3 protein; COX2 (PTGS2), prostaglandin G/H synthase 2; FABP1, fatty acid-binding protein, liver; FABP4, fatty acid-binding protein, adipocyte; FASN, fatty acid synthase; SCD, stearoyl-CoA desaturase 5; ILR6, interleukin-6 receptor subunit alpha; LDLR, low-density lipoprotein receptor; Lgr5, leucine-rich repeat-containing G-protein coupled receptor 5; LPL, lipoprotein lipase; MSI1, RNA-binding protein Musashi homolog 1; SREBF1, sterol regulatory element-binding protein 1; TNFα, tumour necrosis factor.

AGPAT1, and *FASN* alterations are associated with CRC patients' prognosis. In conclusion, we describe metabolic differences, which not only could help dictate the different tropism of cancer cells but also are associated with prognosis of CRC patients.

MATERIALS AND METHODS

Proteomic Data Analysis

SILAC experiment datasets of the subcellular fractions and secretome analysis of KM12C and KM12SM cells were obtained from previous reports (22, 23). Data analysis of proteins related to metabolism and MET was performed using Gene Ontology (http://geneontology.org), STRING (https://string-db.org), and DAVID (https://david.ncifcrf.gov) databases (**Table S1**).

Cell Culture and Reagents

Cell lines, obtained from ATCC (ATCC, Manassas, VA, USA), were cultured in Dulbecco's Modified Eagle's Medium (DMEM, Lonza) supplemented with 10% foetal bovine serum (FBS, Saint Louis, Missouri, USA), 1× L-glutamine (Lonza, Basel, Switzerland), and 1× penicillin/streptavidin (Lonza), and maintained under standard conditions. N-Acetyl cysteine (NAC) and metformin were purchased form Sigma-Aldrich (Sigma-Aldrich, St. Louis, MO, USA). Images were captured using a Leica DM IL microscope (Leica Microsystems, Wetzlar, Germany), with a 10× Plan Fluotar objective and registered using Leica Application Suite (LAS).

Analysis of Superoxide Anion and Membrane Potential

SO* levels were determined with MitoSOX Red (Invitrogen Molecular Probes, Madrid, Spain; M36008) and the membrane potential quantified after staining with a TMRN probe, as previously described (25). Briefly, 10^5 cells were seeded in a 12-well plate and treated with the probes for 30 min. After washing with PBS, cells were harvested and stained with propidium iodide to identify dead cells.

Quantitative Real-Time PCR

RNA (1 μg) was reverse-transcribed using the High Capacity RNA-to-cDNA Master Mix system (Life Technologies, Carlsbad CA, USA) and the corresponding forward and reverse oligonucleotides (**Table S2**). Quantitative real-time PCR (qPCR) was performed with VeriQuest SYBR Green qPCR Master Mix (Affymetrix, Santa Clara, CA, USA) on the 7900HT Real-Time PCR System (Life Technologies). Relative gene expression was calculated using the $2^{-\Delta\Delta Ct}$ method.

Cell-Based Assays

For proliferation analysis, MTT reagent (Sigma-Aldrich) was used for cell proliferation assays. CRC cells were harvested with Trypsin-EDTA (Lonza), and 1×10^4 cells per well were seeded in 96-well plates (Corning) in 10% FBS DMEM, for 24 h at 37°C and 5% CO_2. Then, the culture medium was removed and 150 μl of 10% FBS DMEM was added to each well. Next, cells were treated with the corresponding drugs, including control wells without any drug, in quadruplicate. For NAC assays, final NAC concentrations of 5, 10, 15, and 20 mM were tested from a 0.5-M NAC solution in H_2O. For metformin assays, final metformin concentrations of 5 and 10 mM from a 100-mM solution in H_2O were tested. Cells were incubated for 72 h at 37°C and 5% CO_2, and the culture media with the corresponding drugs were changed every 24 h. After 72 h of incubation, the growth medium was removed, and wells were washed three times with 200 μl of PBS 1× (Lonza) to remove traces of drugs that may interact with the MTT reagent. Next, 100 μl of DMEM was added and, subsequently, 50 μl of 3 mg/ml MTT solution in DMEM was added to each well to a final concentration of 1 mg/ml of MTT per well. Plates were then incubated at 37°C and 5% CO_2 for 1 h to allow cells to take up the MTT. Next, DMEM was removed and cells were lysed with 50 μl of 100% DMSO (Darmstadt, Germany). Plates were incubated with shaking during 15 min at room temperature, and finally, the absorbance at 570 nm was read with the Spark multimode microplate (TECAN, Mannedorf, Switzerland).

The migratory potential of the cells was assessed by wound-healing assays using two-well silicone inserts (Ibidi, Gräfelfing, Germany), which form a wound (gap) in the well of 500-μm width. First, silicone inserts were placed over the wells of a 24-well plate (Corning, Tewksbury, MA, USA). Then, CRC cells were harvested with Trypsin-EDTA (Lonza), and 2×10^5 cells were resuspended in 70 μl of 10% FBS DMEM, seeded into each well of the silicone inserts, and incubated overnight at 37°C and 5% CO_2. The next day, the silicone inserts were removed and 1 ml of 10% FBS DMEM was added to each well. At this point, cells were treated with or without NAC at 5 or 10 mM from a 1-M NAC solution in H_2O, or 5 and 10 mM of metformin from a 100-mM solution in H_2O, in duplicate. Then, the 24-well plate was placed on the TCS SP5 Confocal microscope (Leica) at 37°C and 5% CO_2, and the size of the wound was monitored by taking photos every 2 for 62 h of each well. Finally, the images were processed with the ImageJ program (Fiji) and the MRI Wound Healing Tool.

The adhesion capacity of CRC cells was evaluated using a Matrigel matrix (Sigma-Aldrich). First, CRC cells were incubated in DMEM without FBS for 24 h at 37°C and 5% CO_2. At the same time, 96-well plates (Corning) were coated with 100 μl Matrigel matrix (0.4 μg/mm^2), diluted in 0.1 M $NaHCO_3$, and incubated at 4°C O/N. Then, 96-well plates were blocked with 200 μl of sterile adhesion medium (DMEM 0.5% BSA) for 2 h at 37°C and CRC cells were fluorescently stained with 10 μl of 1 mg/ml BCEBF (Sigma-Aldrich) per 1 ml of DMEM for 30 min at 37°C and 5% CO_2. Then, cells were harvested with 4 mM EDTA–PBS, and 1×10^5 cells were resuspended in 50 μl of sterile adhesion medium and transferred to each precoated well, previously removing the adhesion medium. At this point, cells were treated with or without 5 or 10 mM of NAC and 5 or 10 mM of metformin from a 0.5-M and 100-mM solution of NAC or metformin, respectively, diluted in H_2O, in quadruplicate.

Subsequently, the cells were incubated for 2 h at 37°C and 5% CO_2, and non-adhered cells were removed by decantation. Wells were washed twice with 100 µl PBS 1× to adequately remove all non-adhered cells, and finally, adhered cells were lysed with 50 µl of 10% SDS in PBS. Plates were incubated on shake for 20 min at room temperature and in the dark. The fluorescence signal was read with the Spark multimode microplate (TECAN), at 436–535-nm excitation–emission, respectively.

The invasion potential of CRC cells was evaluated using 6.5-mm transwells with 8-µm Pore Polycarbonate Membrane Inserts (Corning). First, transwells were settled onto 24-well plates (Corning) and coated with 50 µl of Matrigel matrix diluted in DMEM (1:3) and incubated at 37°C for 1 h. CRC cells were harvested with Trypsin-EDTA (Lonza), and 1×10^6 cells were resuspended in 100 µl sterile adhesion medium and transferred to a precoated transwell. One milliliter of 10% FBS DMEM was added to each well as chemoattractant. At this point, cells were treated with or without 5 or 10 mM of NAC and 5 or 10 mM of metformin. Subsequently, plates were incubated for 22 h at 37°C and 5% CO_2. Then, non-invaded cells and Matrigel were removed from the upper membrane surface of the transwells with cotton swabs, and invaded cells on the lower membrane surface were fixed by adding 2 ml of 4% paraformaldehyde to each well for 1 h at room temperature (RT). Next, transwells were transferred to new 24-well plates and stained with 2 ml of 0.2% crystal violet and 25% methanol for 30 min at RT. Finally, transwells were washed with H_2Omq to remove dye traces and photographed with the DMi1 Microscope (Leica), and cells were counted with the ImageJ program (Fiji).

Protein Extract and Western Blot

Protein expression was analyzed by Coomassie Blue staining and Western blot (WB). First, CRC cells were harvested with Trypsin-EDTA (Lonza). Cells were lysed in 500 µl of lysis buffer (RIPA, Sigma-Aldrich) supplemented with 1× protease and phosphatase inhibitors (MedChemExpress, Princeton, NJ, USA) by mechanical disaggregation using 16- and 18-G needle syringes. Then, the protein extracts were centrifuged for 10 min at 4°C at 10,000 g, and supernatants were transferred to new tubes. The protein concentration was determined by tryptophan quantification (22, 26, 27) and confirmed by Coomassie blue staining. Five micrograms of each protein extract was separated by 10% sodium dodecyl sulphate-polyacrylamide gel electrophoresis (SDS-PAGE) under reducing conditions and transferred to nitrocellulose membranes. Membranes were then blocked with 0.1% Tween PBS supplemented with 3% skimmed milk for 1 h at room temperature. Subsequently, membranes were incubated with a mouse monoclonal anti-LDLR (1/2,000, Elabscience, Houston, TX, USA, E-AB-27729), a rabbit polyclonal anti-CD36 (1/1,000, NeoBiotech, Las Vegas, NV, USA, NB-22-37760), a rabbit polyclonal anti-FASN (1/1,000, Elabscience, E-AB-31416), and a rabbit polyclonal anti-GAPDH (1/2,000, Rockland, Pottstown, PA, USA, 800-656-7625) O/N at 4°C. The next day, membranes were washed three times with 0.1% Tween PBS and incubated with the secondary antibody HRP-conjugated goat anti-rabbit IgG (GAR, 1/3,000, Sigma-Aldrich) or HRP-conjugated goat anti-mouse IgG (GAM, 1/3,000, Sigma-Aldrich) for 1 h at room temperature. Finally, the membranes were washed three times with 0.1% Tween PBS and the signal developed using the ECL Pico Plus Chemiluminescent Reagent (Thermo Fisher Scientific, Waltham, MA, USA).

In Silico Analysis of Prognostic Value

The COAD (colon adenocarcinoma) TCGA dataset was used to analyse the prognostic value of LDLR, CD36, FABP4, FASN, FABP1, APOA1, ABCA1, AGPAT1, SCD, LPL, and SREBF1. The prognostic value of these genes was evaluated by Kaplan–Meier curves using the median as the best cutoff to separate high- and low-expression populations. The significance of the difference in survival between both populations was estimated using the log-rank test. The GSE68468 database with transcript data from patients with primary colon cancer was used to analyse the association of these genes with metastasis using 47 metastatic samples to the liver, 20 metastatic samples to the lung, 186 CRC tumour samples, and 55 normal colon samples. Data were normalized using Bioconductor's Affymetrix package and transformed into z-scores. Data and p values were calculated with ggplot2. For a proper visualization of the data, box-plots were made with GraphPad Prism 8.

Analysis of Cell Bioenergetics

The oxygen consumption rate (OCR) and extracellular acidification rate (ECAR) were monitored to quantify the oxidative phosphorylation and aerobic glycolysis, respectively, using the extracellular flux bioanalyzer Seahorse (Seahorse Biosciences, North Billerica, MA, USA).

Prior to experiments, cell density and drug concentration were optimized. For the Mito Stress test, cells were seeded in DMEM 10% FBS, and the next day, the media were changed to 10 mM glucose, 2 mM glutamine, and 2 mM pyruvate in non-buffered DMEM base media adjusted to pH 7.4. Cells were then kept for 1 h in an incubator at 37°C, without CO_2. The assay was performed as previously described (25), with minor modifications. In brief, basal OCR was first measured, and then different modulators of the respiration chain complexes were injected, following the specifications of the Mito Stress kit (2 µM oligomycin, 0.8 µM FCCP, and 0.5 µM rotenone/antimycin A). For Glyco Stress analysis, cells were seeded in DMEM base media in the absence of glucose with 1 mM pyruvate and 2 mM glutamine. Following the specifications of the Glycolysis Stress kit, 10 mM glucose was injected first, then 0.5 µM oligomycin, and finally, 50 mM 2-deoxy-D-glucose (2-DG). OCR and ECAR were measured three times after injection of each drug. Three independent experiments were performed, with six replicates per condition.

Alternatively, experiments were performed in the presence or absence of plasma from individuals with morbid obesity (body mass index, BMI >30 kg/m^2—obese) and individuals with normal weight (BMI <25 kg/m^2—NW) as a control of the assay. To this end, media were supplemented with 5% of plasma from these individuals instead of 10% FBS, as above indicated, in KM12C, KM12SM, and KM12L4a cells.

Plasma From Volunteers

Plasma samples used in this study were provided by the Platform for Clinical Trials in Nutrition and Health (GENYAL) of the IMDEA Food Institute (Madrid, Spain). Informed consent was obtained from the subjects to conserve their sample for scientific studies within the line of research in nutrition and health. This informed consent was included in the IMD PI:030 clinical trial protocol approved by the IMDEA Food ethics committee.

Eight plasma samples were divided in two groups: A, plasma of volunteers with a body mass index (BMI) <25 kg/m^2 (normal-weight NW), and group B, with a BMI >30 kg/m^2 (Obese OB) (**Table S3**). The main parameters considered from anthropometric and biochemical data were sex, BMI, %total fat, %muscle mass, visceral fat classification, waist contour, systolic blood pressure, diastolic blood pressure, heart rate, total cholesterol, HDL cholesterol, LDL cholesterol, triglycerides, creatinine, liver health-related enzymes (aspartate aminotransferase, alanine aminotransferase), and ultrasensitive CRP.

Transient CD36 Silencing

For transient CD36 silencing, transfection was performed in six-well plates using the jetPRIME reagent (PolyPlus Transfection) with, alternatively, MISSION esiRNAs targeting CD36 (EHU089321; Sigma-Aldrich) or control siRNAs (SIC001; Sigma-Aldrich) following the manufacturer's instructions. Briefly, 2.5 × 10^5 cells were transfected with 22 pmol siRNA using 2 µl of jetPRIME transfection reagent and 100 µl of jetPRIME buffer. Then, 48 h after transfection, cells were analyzed by semiquantitative PCR or Western blot (WB). Alternatively, transfected cells were used for cell-based assays as above or for *in vivo* analysis.

In Vivo Animal Experiments

The Ethical Committee of the Instituto de Salud Carlos III (Spain) approved the protocols used for the experimental work with mice after approval by the OEBA ethical committee (Proex 285/19).

For marker analysis in tumour metastasis, 1 × 10^6 KM12SM or KM12L4a cells were injected intrasplenically in nude mice (Charles River n = 3) in 0.1 ml PBS and distal metastasis collected at endpoint. For liver homing analysis, nude mice were inoculated intrasplenically with 1 × 10^6 KM12SM or KM12L4a cells after 24 h of transient transfection with CD36 or control siRNAs (n = 2) in 0.1 ml PBS. Mice were euthanized 24 h after intrasplenical cell inoculation, and RNA from the liver, lung, and spleen was isolated using TRIzol Reagent. RNA was analyzed by RT-PCR to amplify human GAPDH and murine β-actin as loading control using specific primers (**Table S2**).

Statistical Analysis

Significance between groups was determined by Student's t-test. All reported p values were two-sided. Statistical significance was defined as $p < 0.05$. The statistical analyses were done with GraphPad Prism8.

RESULTS

Meta-Analysis of Proteomics Data of KM12SM and KM12C Cell Lines Reveal Metabolic and EMT Differences Associated With Progression and Metastasis

An in-depth quantitative SILAC proteomics analysis of KM12SM in comparison to KM12C cells was previously performed (22, 23). Secretome protein analysis was subsequently followed by the subcellular fractionation of these cells to spatially analyse cytoplasmic, membrane, nuclear, chromatin-bound, and cytoskeletal proteins (22, 23). In these reports, dysregulated proteins in metastatic to liver CRC cells were quantified and their localization mapped. The data highlighted the importance of protein localization to distinguish proteins and complexes that behave differently in various organelles and locations to identify underlying mechanisms of CRC metastasis to the liver.

Here, we first surveyed these proteomic data for the identification of protein alterations related to metabolism, EMT, and/or stemness (**Figure 1**), which would support increased plasticity and stemness of metastatic cells to facilitate metastasis and further colonization. Interestingly, gene ontology annotation of proteins altered between KM12C and KM12SM cells revealed 868 dysregulated proteins related to metabolism, with 334 of them differentially upregulated in KM12SM metastatic to liver cells (**Figure 1A** and **Table S1A**). These proteomic alterations affected several cellular metabolic processes. Among the altered pathways, we found oxidative phosphorylation and lipid- and protein-related metabolic processes, which were mostly upregulated in liver metastasis. On the other hand, metabolic pathways of nitrogen compounds and small molecules were mainly downregulated in liver metastasis (**Figure 1A** and **Figure S1**). In addition, we found 45 dysregulated proteins related to EMT and stemness such as Cadherin-17, metalloproteases, integrins, or proteins related to actin cytoskeleton. Most of these proteins, mainly integrins, cytokines, and chemokines, were involved in the remodelling of cytoskeleton and the extracellular matrix, as well as in the configuration of the local tumour and the premestastatic tumour microenvironment (**Table S1B** and **Figure 1B**).

Several studies have already described an association between alterations in metabolism and bioenergetics and the appearance of intrinsic protumorigenic features (12, 12, 16, 17). Hence, we hypothesized that the metabolic alterations along with additional changes in the proteome may coordinate signal cascades to sustain cell proliferation, survival, chemoresistance, and metastatic formation and thus might have prognostic potential for CRC patients. Furthermore, these mediators may target different cellular components in the tumour microenvironment including adipocytes, fibroblasts, and endothelial and immune cells, which can also help define specific organs of dissemination.

Then, to get further insights into metabolic differences associated with the organotropic dissemination, we

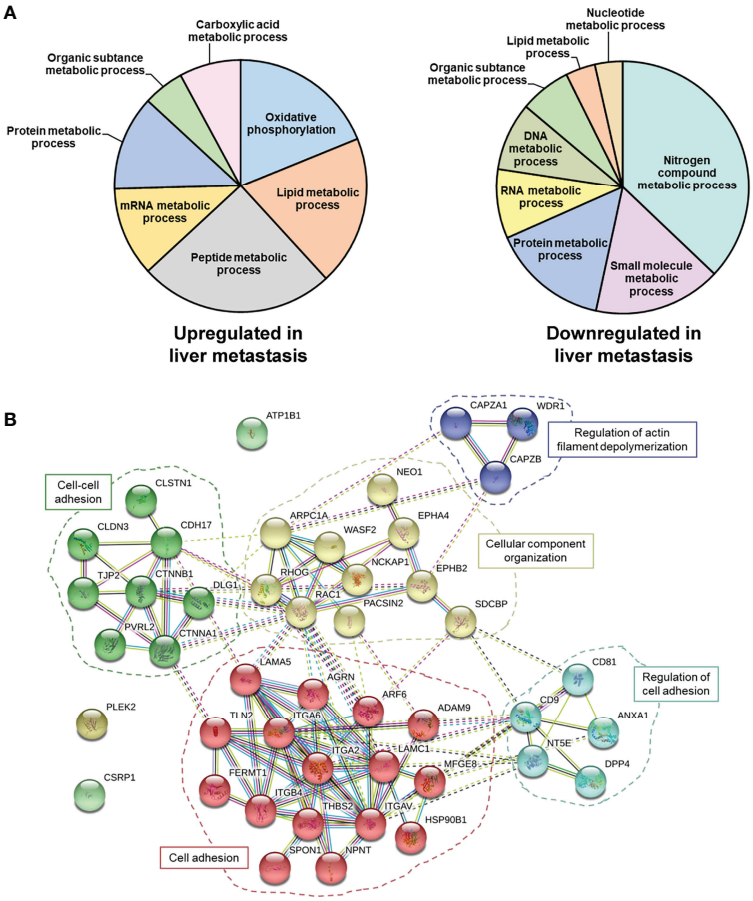

FIGURE 1 | Meta-analysis of proteomics data of liver metastatic KM12SM in comparison to parental non-metastatic KM12C CRC cells. **(A)** Metabolic processes altered in liver metastasis of CRC cells. A total of 868 dysregulated proteins 334 upregulated and 534 downregulated—in KM12SM cells in comparison to KM12C CRC cells were associated with metabolism. **(B)** Forty-five dysregulated proteins related to EMT and stemness in CRC liver metastasis were also involved in processes related to cell-cell contacts.

interrogated the well-established KM12 cell model system of CRC metastasis by means of cell-based *in vitro* functional experiments, qPCR, WB analysis, extracellular flux bioenergetic analysis, and *in vivo* assays. Lipid metabolic specificities have been identified associated with their differential metastatic organotropism, and validated *in vitro* and *in vivo*. Importantly, these differences may constitute potential prognostic biomarkers in CRC patients as revealed by meta-analysis on the COAD TCGA database and help dictate metastatic foci as revealed by meta-analysis on the GSE68468 database containing information regarding RNA expression data of CRC patients (primary colon cancer, metastases, and matched normal mucosa).

KM12SM and KM12L4a CRC Cells Display Increased Invasiveness *In Vitro* Compared to Their Control Isogenic Parental KM12C Cells

The EMT program confers critical properties for proliferation, adhesion, extracellular matrix remodelling, invasion, and metastatic dissemination (28).

First, we corroborated by qPCR the statistically significant dysregulation of EMT markers, *E-cadherin*, *NaKATPase*, and *Vimentin*, in the KM12 cell system. Furthermore, although not significant, the opposite dysregulation of *N-cadherin* in the KM12 cell system in comparison to *E-cadherin* was also observed. These results confirmed the upregulation of mesenchymal markers and the downregulation of epithelial markers in both metastatic CRC cells compared to KM12C parental cells (**Figure 2A**). The initial acquisition of an EMT phenotype in the primary tumour and the reversion to a MET phenotype in secondary niches are crucial for the establishment of metastasis and cancer progression.

As illustrated in **Figures 2B–E**, KM12SM and KM12L4a cells showed increased tumorigenic and metastatic properties in comparison to non-metastatic KM12C CRC cells. KM12L4a and KM12SM metastatic CRC cell lines proliferated (**Figure 2B**) and invaded through Matrigel-coated chambers (**Figure 2C**) to a higher extent than the parental KM12C cell line. Furthermore, KM12SM and KM12L4a showed higher migratory capacity (wound closure speed) than KM12C

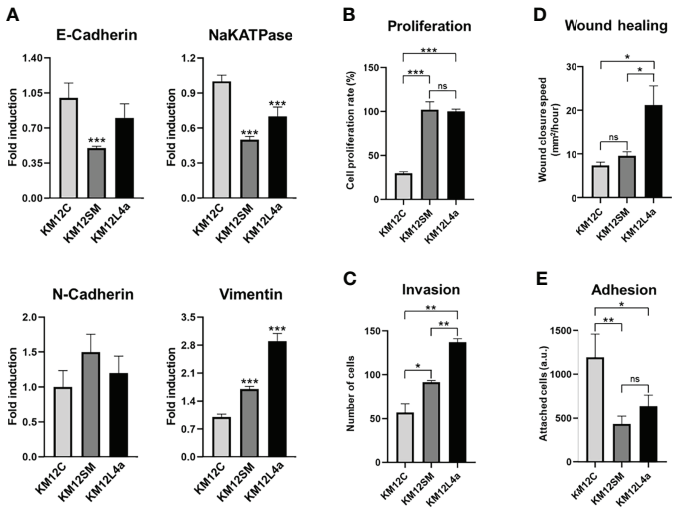

FIGURE 2 | Characterization of metastatic KM12SM and KM12L4a CRC cells in comparison to the isogenic non-metastatic KM12C CRC cells. **(A)** qPCR analysis showed the upregulation of mesenchymal markers (N-cadherin and vimentin) and the downregulation of epithelial markers (E-cadherin and NaKATPase) in both metastatic CRC cells compared to KM12C cells. **(B–E)** *In vitro* functional cell-based assays showed that metastatic CRC cells possessed increased tumorigenic and metastatic properties than non-metastatic KM12C CRC cells. **(B)** Proliferation. **(C)** Invasion. **(D)** Wound healing. **(E)** Adhesion. *p value < 0.05; **p value < 0.01; ***p value < 0.001.

control cells, with KM12L4a showing statistically higher migratory capacity than control and KM12SM cells (**Figure 2D**). In contrast, the adhesion abilities of KM12L4a and KM12SM highly metastatic cells were reduced compared to KM12C cells, supporting their increased ability for cell dissemination (**Figure 2E**). Moreover, the analysis of stemness markers showed increased phenotypic plasticity in metastatic KM12SM and KM12L4a cells, supporting not only dissemination but also the potential for subsequent metastatic colonization (**Figure S2**).

Collectively, these data validated our previous findings showing dysregulation in EMT and stemness in highly metastatic CRC cells.

Metastatic KM12SM and KM12L4a CRC Cells Have Higher Levels of SO* and Ψm at Mitochondria

In carcinoma cells, the EMT program can be triggered by heterotypic signals, such as somatic mutations sustained during primary tumour formation, intracellular and extracellular signalling pathways, and even signals from the tumour-associated stroma.

Increased levels of reactive oxygen species (ROS) have been shown to promote survival and dissemination of cancer cells (13). ROS produced as by-products of metabolism have been shown to play a critical role in cancer initiation and progression (29). For this reason, we interrogated the KM12 CRC cell system for the levels of mitochondrial membrane potential (Ψm)—TMRE staining—and the levels of the mitochondrial derived superoxide anions (SO*)—MitoSOX staining. We found that KM12SM and KM12L4a metastatic cells showed increased levels of Ψm, suggesting a mitochondrial switch favouring anabolism, in line with the increased cell proliferation compared to KM12C control cells (**Figure 3A**). Interestingly, only KM12SM cells displayed increased levels of SO* produced in mitochondria compared to control cells (**Figure 3B**). These results indicate that metastatic CRC cells have differences in the performance of the oxidative phosphorylation in mitochondria.

To further confirm these results, we analysed the effect of N-acetylcysteine (NAC) on cell proliferation, migration, invasion, and adhesion assays (**Figures 3C–F** and **Figure S3A**). NAC has been described as an exogenous antioxidant that mimics the effects of natural antioxidants. It is an aminothiol whose anti-ROS activity results from its free radical scavenging capacity, which originates from the redox potential of thiols and from the increase it induces in the cellular levels of cysteine and intracellular glutathione (GSH), a substrate of ROS scavenging enzymes (30, 31). Analysis of the tumorigenic capacities of high and low metastatic KM12 cells in the presence of different amounts of NAC revealed differences in metastatic KM12SM and KM12L4a cells at 5 and 10 mM of NAC treatment, whereas higher NAC concentrations induced cellular death. We observed that in the presence of NAC, the proliferation, migration, and invasion capacity of KM12SM and KM12L4a cells were statistically significant delayed, with KM12SM being the most affected cell line, while their adhesion capacity was increased. In contrast, higher concentrations of NAC (between 15 and 20 mM NAC) were needed to significantly affect the capabilities of KM12C cells. These results support the idea that KM12SM and KM12L4a cells require higher levels of ROS than KM12C

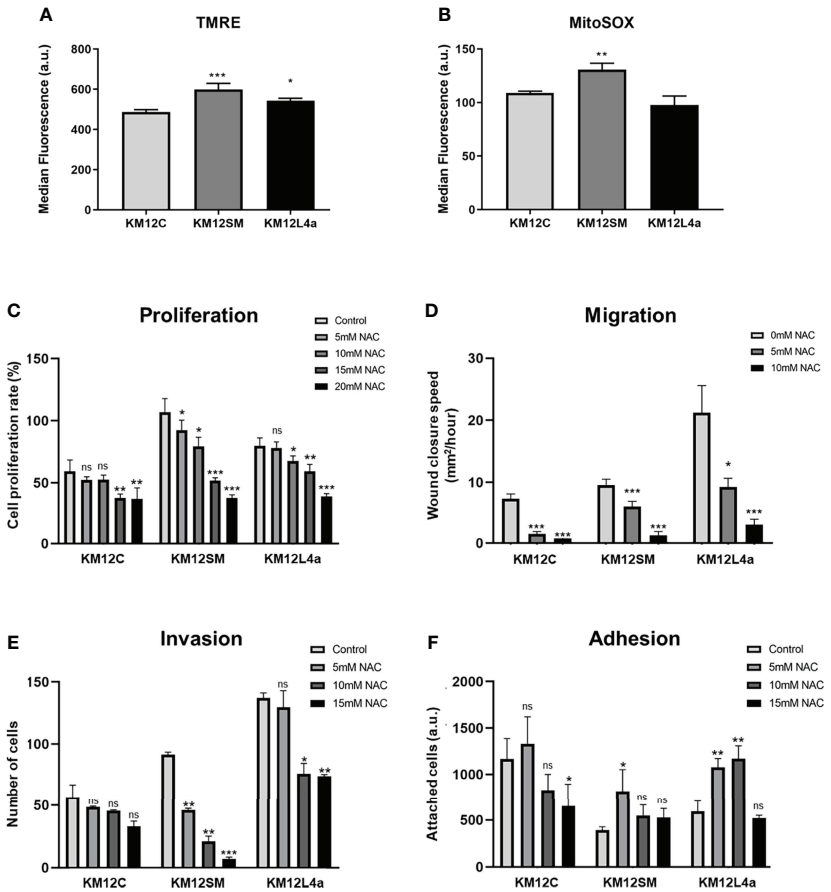

FIGURE 3 | Reactive oxygen species effects on CRC cells. **(A, B)** Quantification by FACS analysis of Ψm at mitochondria and ROS species. Statistical analysis is referred to the comparisons with KM12C cells. **(A)** A TMRM probe was used to quantify the mitochondrial membrane potential (Ψm). **(B)** A MitoSOX-Red probe was used to determine the levels of mitochondrial superoxide anions (SO•). Analysis of the effect of NAC (0–20 mM) on proliferation **(C)**, migration **(D)**, invasion **(E)**, and adhesion **(F)** ability of metastatic and non-metastatic KM12 CRC cells. Wound closure speed is referred to wound size differences between 0 and 62 h of each experiment. Metastatic CRC cells were more dependent on the high levels of ROS to maintain their properties, with KM12SM cells being the most dependent of ROS. **(C–F)** Statistical analysis is referred to the cells without NAC treatment. *p value < 0.05; **p value < 0.01; ***p value < 0.001.

cells to activate signalling pathways to support their tumorigenic abilities.

In addition, we also analysed the effects of metformin treatment by means of cell proliferation, invasion, adhesion, and wound healing assays (**Figure 4** and **Figure S3B**). Metformin disrupts mitochondrial respiration by interfering with mitochondrial complex I, which decreases ATP synthesis and activates AMPK, inducing cell metabolic stress and increasing the levels of intracellular ROS (32, 33). Here, we observed that this AMPK activator mainly delayed the proliferation and invasion capacity of KM12SM cells (**Figures 4A, B**), whereas KM12L4a and KM12C cells did not show significant differences in its presence or absence. In addition, the adhesion capacity of KM12SM cells was increased in the presence of metformin (**Figure 4C**), while the adhesion capacity of KM12L4a and KM12C cells was unaffected. On the other hand, metformin produced a significant decrease in the migration capacity of KM12L4a and KM12SM cells (**Figure 4D**), while the migration of KM12C cells remained unaltered. Remarkably, KM12L4a migrated 33% less than control cells without drugs, while KM12SM migratory capacity was reduced by more than 50%.

Collectively, these data show that metastatic KM12SM and KM12L4a cells are more dependent on intracellular ROS levels than non-metastatic KM12C cells, with KM12SM cells requiring the highest amount of ROS to maintain their metastatic properties. Furthermore, we observed that KM12SM cells were unable to respond to the increased cellular stress after metformin treatment compared to KM12L4a cells, highlighting the high dependence of KM12SM cells on oxidative phosphorylation.

Cell Bioenergetics of Main Energetic Pathways

Then, to gain insights into functional bioenergetics and determine whether metabolic differences in the metastatic CRC cells may contribute to their different metastatic tropism, we

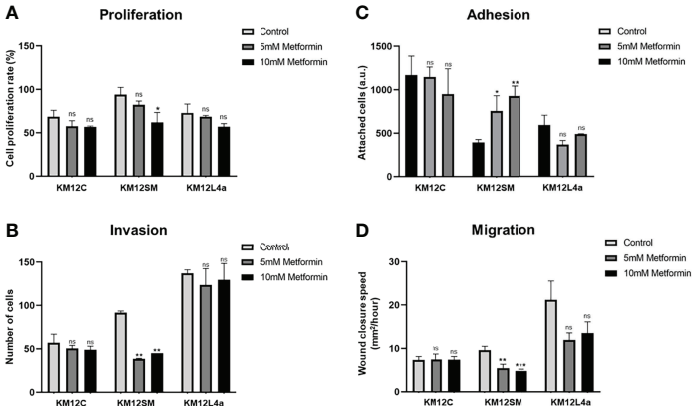

FIGURE 4 | Analysis of the effect of metformin on the tumorigenic and metastatic properties of CRC isogenic cells with metastatic and non-metastatic properties. **(A)** Proliferation, **(B)** invasion, **(C)** adhesion, and **(D)** migration abilities of KM12 cells in the presence or absence of 10–15 mM metformin are represented. Wound closure speed is referred to wound size differences between 0 and 62 h of each experiment. KM12SM metastatic cells were the most affected by this complex I inhibitor compound, suggesting that these cells are not able to respond to increased cellular stress. *p value < 0.05; **p value < 0.01; ***p value < 0.001.

proceeded to analyse in detail the bioenergetic profile of KM12C, KM12SM, and KM12L4a cells. To this end, aerobic glycolysis and mitochondrial respiration were analysed by monitoring ECAR and OCR rates (**Figure 5**).

Aerobic Glycolysis

After 1 h of glucose starving, basal ECAR, which is an indirect readout of L-lactate production by aerobic glycolysis, was measured. Interestingly, basal ECAR of KM12SM cells was higher than that observed in parental cells. In contrast, KM12L4a cell basal ECAR was decreased compared to parental cells (**Figure 5A**). Next, we injected glucose into the media to determine the cells' ability to increase the glycolytic pathway. KM12SM cells showed the highest response associated with increased levels of ECAR. In contrast, although capable of responding to glucose, KM12L4a cells showed reduced levels of ECAR compared to KM12C cells. Finally, KM12SM cells continued to increase glycolysis to a higher maximum ECAR than parental cells when oligomycin was injected to block ATP production from mitochondria. In contrast, the maximum ECAR for KM12L4a cells was the lowest compared to parental cells.

Then, to further confirm that the observed differences were due to changes in aerobic glycolysis, we analysed glycoPER. In this assay, cells were maintained in complete media (10 mM glucose, 1 mM pyruvate, and 2 mM glutamine) to apply an experimentally determined buffer (provided by Seahorse Bioscience) which allows to determine the contribution of H^+ to the Proton Extrusion Rate (PE) from aerobic glycolysis (L-lactate and H^+) or mitochondrial oxidative phosphorylation (CO_2+H_20-HCO_3^- +H^+). As shown in **Figure 5B**, basal glycolysis was higher in KM12SM and lower in KM12L4a compared to control parental cells. Next, we injected rotenone/antimycin A to shut down mitochondrial complexes I and III and induce a compensatory upregulation of aerobic glycolysis. Furthermore, compensatory stressed glycolysis of KM12SM cells was higher than that of control cells. In contrast, KM12L4a cells showed the lowest levels of compensatory ECAR. Finally, we injected 2-deoxyglucose, a competitive inhibitor of glucokinase, to demonstrate that ECAR was associated with aerobic glycolysis.

These results clearly show that KM12SM and KM12L4a cells have different performances associated with aerobic glycolysis compared to control non-metastatic KM12C parental CRC cells.

Mitochondrial Oxidative Phosphorylation

Due to the differences observed independently of aerobic glycolysis, and the fact that KM12SM cells displayed increased levels of ROS species, we wanted to interrogate KM12 cells regarding mitochondrial oxidative phosphorylation (**Figure 5C**).

Therefore, OCR levels were measured after the sequential injection of drugs that modulate the oxidative phosphorylation in mitochondria. KM12SM cells showed the highest basal respiration rates (BRR) in comparison to KM12C cells. In contrast, KM12L4a cells showed the lowest BRR. When oligomycin (1 μM) was injected to inhibit the V-ATPase complex, the OCR levels of KM12SM cells were reduced to the OCR levels of KM12L4a and parental cells. Interestingly, after injection of FCCP (0.4 μM) to uncouple the electron transport chain (ETC) from ATP synthesis, the maximal respiration rate (MRR) of KM12SM cells was lower than that of KM12L4a and parental cells. These results suggest that the respiration rate of KM12SM cells is compromised under stress conditions, indicating that they are at their maximal respiratory capacity. This is in agreement with the higher levels of ROS and membrane potential at mitochondria (Ψm) observed in KM12SM cells. To confirm this result, we conducted a Mito Stress test by adding 10 mM galactose, which is a substrate that generates higher levels of ROS compared to glucose. All cell lines

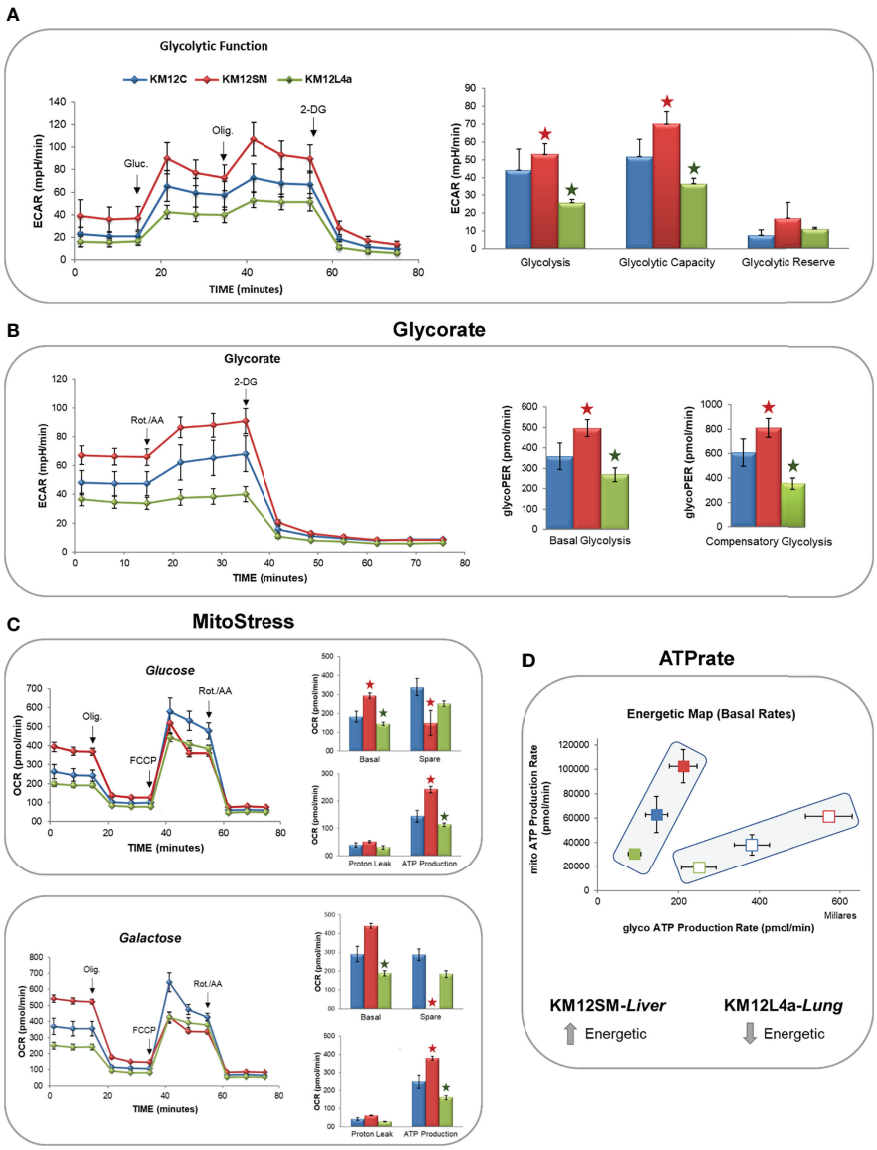

FIGURE 5 | Monitorization by flux analysis of aerobic glycolysis and mitochondrial oxidative phosphorylation. **(A)** Analysis of ECAR glycolysis stress. Cells were incubated overnight in low-glucose media (5 mM glucose). The next day, the medium was changed to DMEM base media in the absence of glucose for 1 h, and the basal levels of ECAR were determined. After the injection of 10 mM glucose (Gluc), the increase in ECAR was used to quantify aerobic glycolysis. Next, after the injection of oligomycin, the increased ECAR allowed the determination of the maximal glycolytic capacity. **(B)** GlycoRate test. **(C)** Mito Stress test in the presence of glucose or galactose. **(D)** Basal OCR (BRR), ATP production, and maximal OCR are shown after the sequential injections of oligomycin (Olig.), FCCP, and rotenone/antimycin A (Rot./AA). 2-DG: 2-deoxy-D-glucose. *p value < 0.05.

increased their basal respiration rate compared to that observed in the glucose condition. Again, KM12SM showed the highest BRR and KM12L4a the lowest BRR. Interestingly, KM12SM cells showed similar rates of basal and maximal respiration, suggesting that they are highly oxidative cells under basal conditions and that this oxidative capacity cannot be augmented under stress conditions. In contrast, KM12L4a cells showed the lowest levels of both BRR and MRR. In conclusion, these results indicate that KM12SM cells are energetically very active, while KM12L4a are the least energetic cells.

ATP Rate and Energetic Phenotype

Finally, ATP rate analysis of KM12SM and KM12L4a cells showed interesting bioenergetic differences among KM12 cells. While parental isogenic non-metastatic KM12C cells showed an intermediate cell bioenergetics, liver metastatic KM12SM cells showed the highest ATP production under basal or stressed conditions. In contrast, KM12L4a showed the lowest levels of ATP production (**Figure 5D**). These results are in agreement with the increased glycolytic and oxidative phosphorylation observed in KM12SM cells (the highest bioenergetic profile)

and the lower bioenergetic profile of KM12L4a cells, both independent of aerobic glycolysis and oxidative phosphorylation.

Metastatic KM12L4a CRC Cells Display Higher Dependency on Exogenous Fatty Acid Uptake

The mechanisms whereby some tumour cells detach from the primary lesion to colonize distant sites are still largely unknown, as well as pro-metastatic events occurring in the majority of solid tumours. As the proliferation rates in KM12SM and KM12L4a cell lines were similar, metabolic differences, regardless of cell bioenergetics, may contribute to differences in other cell signalling and protumorigenic features. Changes in lipid metabolism have been recognized as crucial players affecting cancer cell survival, progression, and therapy response. Furthermore, since tumour cells are often exposed to a metabolically challenging environment, mediators of lipid metabolism are key players in controlling the associated metabolic stress and in shaping the stroma and the cellular components of the tumour microenvironment.

Then, to functionally confirm the dependence of metastatic CRC cells on exogenous fatty acid supply, we monitored, using the Seahorse bioanalyzer, the mitochondrial oxidative phosphorylation response to extracellular fatty acid (FA) supplementation. Briefly, after an O/N starvation (low glucose —0.5 mM glucose, 1% FBS, 0.5 mM carnitine), we challenged cells to a palmitic acid-BSA (PA) input and monitored OCR. Control-BSA was also included as a negative control. Interestingly, we found that KM12L4a and KM12SM cell lines only increased their basal OCR compared to control cells when PA was added, especially KM12L4a cells (**Figure 6A**). Furthermore, we observed that KM12SM exhibited a lower spare respiratory capacity after PA supplementation, being unable to respond to the additional energy demand under stress conditions (after FCCP injection), as previously shown in glucose enriched media. On the other hand, the spare respiratory capacity of KM12L4a cells was significantly increased with PA, compared to control-BSA, suggesting that KM12L4a cells are more dependent on the exogenous FA uptake to increase their cell bioenergetic capacity.

In summary, KM12SM cells showed an increased Warburg effect, increased oxidative phosphorylation, and increased ROS, and, as weakness, reduced spare respiratory capacity (in complete media, or in FA-supplemented media), related to a low capacity to respond to additional energy demand, while KM12L4a cells showed a reduced Warburg effect, reduced oxidative phosphorylation, high respiratory capacity, and, as weakness, high dependence on exogenous FA (**Figure 6B**).

Next, to further investigate the FA dependence of metastatic CRC cells compared to parental KM12C CRC cells, we analyzed the expression of genes related to lipid metabolism. We focused on genes involved in *de novo* fatty acid synthesis (*SREBF1*, *FASN*, *SCD*); exogenous lipid uptake (*LDLR*, *CD36*, *LPL*, *FABP1*, *FABP4*); remodelling of cholesterol and membrane lipids (*ABCA1*, *APOA1*, *AGPAT1*); and inflammation (*PTGS2*, 5*LOX*, *IL6R*, and *TNFA*), which could explain, at least partially, the observed differences in cell bioenergetics in KM12SM and KM12L4a cells compared to KM12C parental cells (**Figures 6C–E**). Strikingly, both metastatic CRC cells, KM12SM and KM12L4a, showed reduced expression levels of *SREBF1* (master transcription factor involved in *de novo* synthesis of fatty acids) and its downstream molecular targets *FASN* and *SCD* compared to control cells (**Figure 6C**). In contrast, metastatic KM12SM and KM12L4a CRC cells showed an increased expression of genes related to exogenous lipid uptake. More specifically, KM12L4a cells had increased gene expression levels of *LDLR*, *CD36*, and *LPL* and reduced gene expression levels of *FABP4* compared to KM12C cells, whereas KM12SM cells showed increased *LDLR* and *CD36* gene expression levels and reduced *FABP4* gene expression levels compared to parental KM12C control cells (**Figure 6D**).

Interestingly, the analysis of genes involved in plasma membrane lipid remodelling showed the upregulation of *ABCA1* and *AGPAT1* in KM12L4a cells compared to parental KM12C control cells, whereas KM12SM cells showed increased expression levels of *ABCA1* and reduced expression levels of *APOA1* compared to KM12C cells (**Figure 6E**). Furthermore, analysis of inflammatory lipid mediators also highlighted specific differences between the two metastatic CRC cell lines compared to KM12C cells. KM12L4a cells showed increased expression levels of *PTGS2* along with decreased 5*LOX*. Given that both enzymes have arachidonic acid (AA) as substrate, these results suggest that KM12L4a cells favour inflammatory mediators downstream of the prostaglandin pathway, as evidenced by the increase in the downstream mediator *IL6R*, which was also upregulated in KM12L4a cells (**Figure 6E**). In addition, although not significant, the increase of another downstream mediator (*TNFA*) was also observed, supporting the results observed for *IL6R* regarding inflammatory mediators.

Finally, *BIP* and *CHOP* were found upregulated in both metastatic cell lines, but the differences were statistically significant only in KM12SM cells, suggesting an increased metabolic stress in these cell lines (**Figure 6F**).

Collectively, the analysis of a panel of enzymes related to lipid metabolism has allowed for the identification of three metabolic axes associated with the differential organotropic dissemination involved in (i) the extracellular uptake of FAs and cholesterol vs. *de novo* lipogenesis, (ii) lipid-associated inflammatory networks, and (iii) lipid enzymes that affect plasma membrane remodelling, plasticity, and fluidity. Furthermore, these results highlight the role of *SREBF1*, *FASN*, *SCD*, *LDLR*, *CD36*, *FABP1*, *FABP4*, *LPL*, *PGCTS2*, *LOX5*, *IL6R*, *ABCA1*, *APOA1*, and *AGPAT1*, as differential lipid metabolism biomarkers of lung or liver tropism.

Effect of Exogenous Fatty Acids From Plasma of Morbid Obesity and Normal-Weight Individuals on the KM12 Cell System

Several retrospective studies analysing large cohorts of CRC patients highlight the impact of obesity on overall survival (34). In addition, the mortality of CRC patients with a BMI between 25 and 50 kg/m^2 increases linearly, while in patients

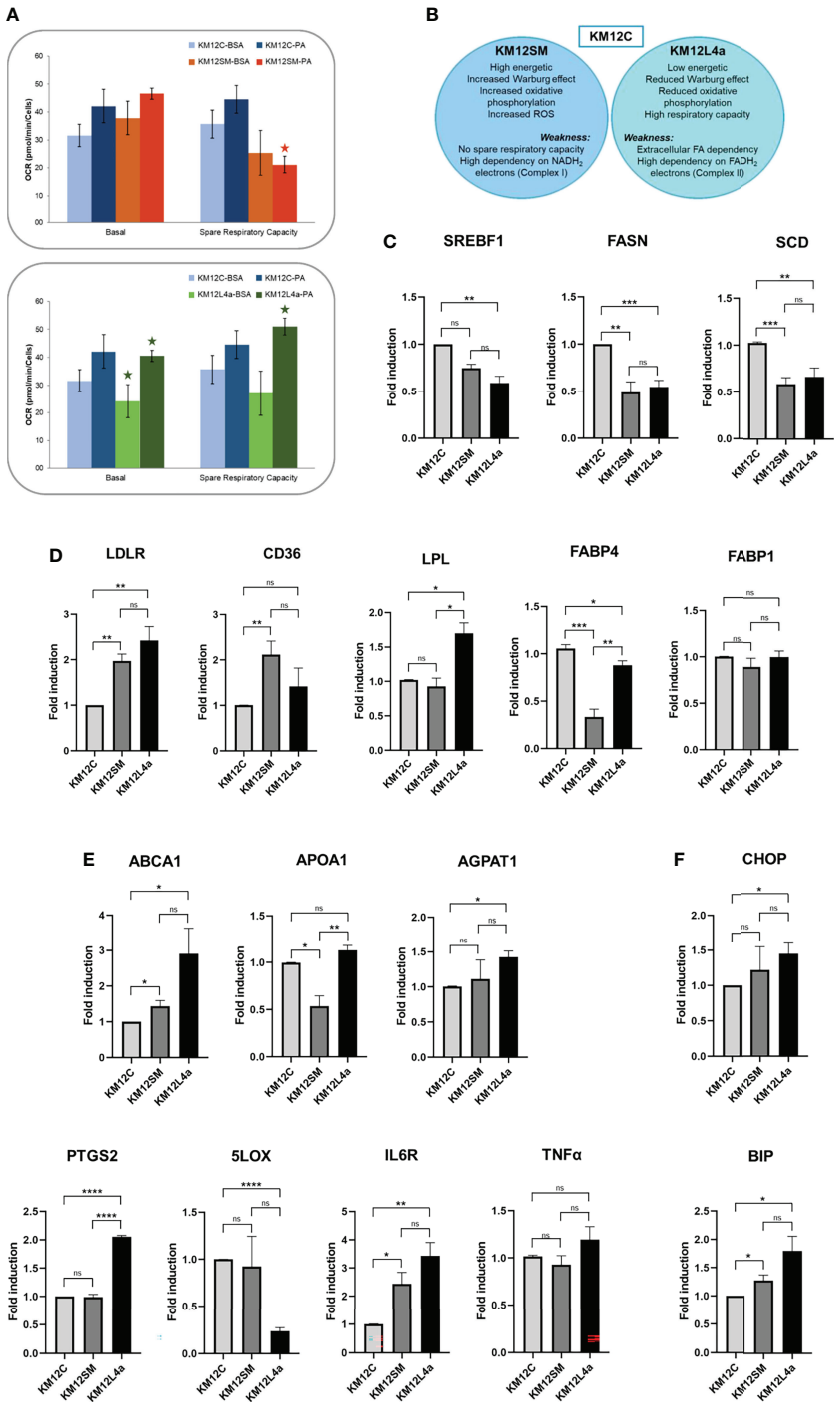

FIGURE 6 | Analysis of the expression levels of lipid metabolism genes in KM12C and KM12SM and KM12L4a. **(A)** Exogenous uptake of FAs and cholesterol. The mitochondrial oxidative phosphorylation response to FA supplementation was analysed with the Seahorse bioanalyzer. **(B)** Schematic of the strengths and weaknesses of the metastatic isogenic KM12SM and KM12L4a cells as observed from the analyses. qPCR analysis of the expression levels of lipid metabolism genes related to **(C)** *de novo* synthesis of FA, **(D)** intracellular cholesterol homeostasis and plasmatic membrane lipid remodeling-related genes, **(E)** cholesterol and membrane lipid remodeling and of lipid metabolism-related inflammatory markers, and **(F)** cellular stress mediators in KM12SM and KM12L4a referring to KM12C parental cells. **p* value < 0.05; ***p* value < 0.01; ****p* value < 0.001; *****p* value < 0.0001.

with a BMI between 15 and 25 kg/m^2 the risk of mortality does not vary.

Given that lipid metabolism targets related to extracellular lipid uptake were found to be upregulated in metastatic KM12SM and KM12L4a cells compared to KM12C control cells, we next wanted to evaluate the effect of obesity on the biological behaviour of the tumoural cells. Since obesity is characterized by increased levels of circulating free fatty acids that promote low-grade chronic inflammation (35), we hypothesized that incubation of KM12 cells with plasma from volunteers with a BMI <25 (group A: NW), or volunteers with a BMI >30 (group B: OB), would affect the behaviour of the cells differently.

The supplementation with 5% of plasma from OB volunteers significantly enhanced the basal respiration and the ATP production of KM12C cells compared to that in the presence of plasma from NW volunteers, suggesting that plasma from OB volunteers is enriched on FAs and/or growth factors. In a similar way, plasma from OB volunteers significantly enhanced the basal respiration and the ATP production of KM12SM cells compared to that in the presence of plasma from NW volunteers but not their spare respiratory capacity (**Figure 7A**). Importantly, supplementation with 5% of plasma from OB volunteers significantly enhanced the basal and spare respiratory capacity and the ATP production of KM12L4a cells compared to that of supplementation with plasma from NW volunteers (**Figure 7B**). Furthermore, the data collected with NW plasma were in agreement with the response obtained at the basal state (**Figure 5C**).

These data indicate that obesity may stimulate cell migration capacity, stemness, and/or angiogenesis. Furthermore, obesity can remodel the tumour microenvironment leading to a chronic inflammatory state to stimulate dissemination, which will decrease the overall survival of CRC patients (36).

Analysis of CD36 Lipid Metabolism Biomarker in Lung and Liver Tropism

Next, the ability of the KM12 CRC cell system to take up extracellular fatty acids was blocked by siRNAs to CD36 to determine whether it would have any effect on their metastatic ability, and to analyse whether the markers could be functionally important for the metastatic phenotypes.

Transient CD36 silencing followed by adhesion, proliferation, and wound healing assays was performed on KM12SM and KM12L4a cells compared to scrambled cells to assess the influence of CD36 on the tumorigenic and metastatic properties of cells. First, CD36 depletion by transient silencing was efficiently achieved as observed by PCR and WB analyses (**Figure 8A**). In proliferation assays, CD36-depleted KM12L4a cells proliferated less than control cells transfected with the scrambled siRNA (p value < 0.05), while KM12SM cells were mostly unaffected (**Figure 8B**). Wound healing assays were then used to analyze the role of CD36 in cell migration. Both CD36-silenced cell lines closed the wound at a slower rate than their control cells transfected with scramble siRNA with a significantly higher effect on KM12SM cells. Regarding the effect of CD36 on adhesive properties, cells transfected with CD36 siRNA showed opposite properties. KM12SM upon CD36 depletion showed a significant 20% higher adhesion than control cells, while KM12L4a cells showed a significant 32% lower adhesion ability to Matrigel than control cells.

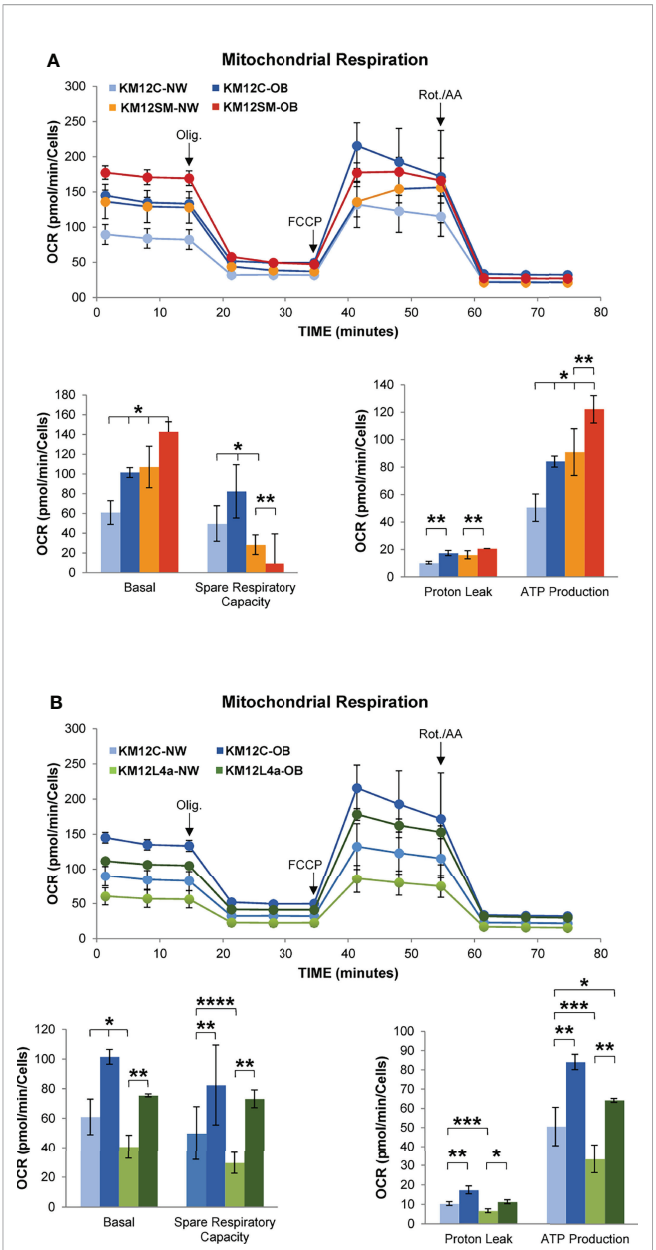

FIGURE 7 | Investigation by flux analysis of mitochondrial respiration of KM12 cells incubated with plasma from volunteers. **(A)** Analysis of mitochondrial respiration of KM12C and KM12SM cells incubated with 5% plasma of volunteers with BMI <25 (NW) or BMI >30 (OB). Basal OCR and spare respiratory capacity, proton leak, and ATP production are shown. **(B)** Analysis of mitochondrial respiration of KM12C and KM12L4a cells incubated with 5% plasma of volunteers with BMI <25 (NP) or BMI >30 (OB). Basal OCR and spare respiratory capacity, proton leak, and ATP production are shown. Olig, oligomycin; Rot./AA, rotenone/antimycin **(A)** *p value < 0.05; **p value < 0.01; ***p value < 0.001; ****p value < 0.0001.

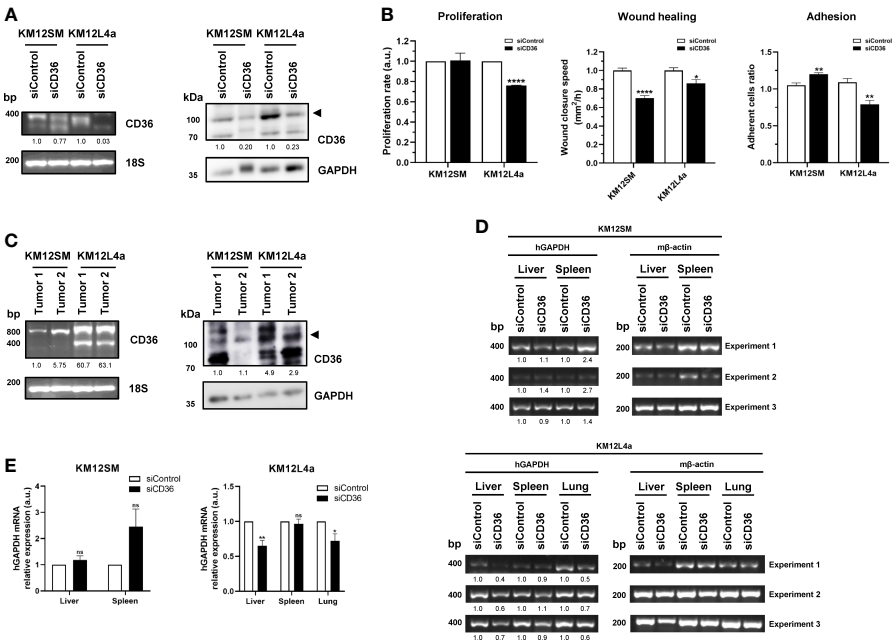

FIGURE 8 | *In vitro* and *in vivo* effect of CD36 depletion in the tumorigenic and metastatic properties of KM12SM and KM12L4a cells or derived tumours. **(A)** Evaluation by PCR and WB of the transient silencing of CD36 after 48 h post-transfection in KM12SM and KM12L4a cell lines. As control, we transfected the cell lines with a scramble siRNA. By PCR, 18S was used as internal control. By WB, GAPDH was used as loading control. **(B)** Proliferation, wound healing, and adhesion properties of KM12SM and KM12L4a transiently transfected with CD36 siRNA in comparison to scramble siRNA were investigated, showing that CD36 plays a role in the tumorigenic and metastatic properties of metastatic colorectal cancer cell lines. **(C)** Analysis of the CD36 mRNA and protein expression levels in actual metastatic tumoral samples (n = 2) derived from KM12SM and KM12L4a cells. By PCR, 18S was used as internal control. By WB, GAPDH was used as loading control. **(D)** Nude mice intrasplenically inoculated with KM12SM or KM12L4a cells transiently transfected with siScramble and CD36 siRNA were sacrificed 24 h after inoculation for analysis of *in vivo* liver and lung homing (n = 3). RNA was isolated from the liver, lung, and spleen (as control) and directly subjected to RT-PCR to amplify human GAPDH (hGAPDH). Murine β-actin (mβ-actin) was amplified as control. **(E)** Statistically significant lower mRNA levels of hGAPDH were found for liver and lung homing of KM12L4a cells. **(A–D)** mRNA or protein abundance was quantified by densitometry using ImageJ, and data were normalized with the expression levels of 18S or mβ-actin for mRNA and GAPDH for protein abundance. *p value < 0.05; **p value < 0.01; ****p value < 0.0001.

These results suggest that CD36 silencing preferentially affects KM12L4a cells to a greater extent than KM12SM cells. For further confirmation, *in vivo* experiments were performed. First, the differential expression of CD36 was analyzed by PCR and WB in samples of metastatic tumours derived from intrasplenic injection of KM12SM and KM12L4a cells (**Figure 8C**). Metastatic tissue showed an enhanced CD36 expression in KM12L4a cell-derived metastatic tumour than in KM12SM cell-derived metastatic tumour, which would support the higher significant changes in the *in vitro* cell-based assays for KM12L4a cells than for KM12SM cells. Next, the *in vivo* effects on lung and liver homing of transient CD36 depletion were investigated in KM12SM and KM12L4a CRC metastatic cells. KM12SM and KM12L4a cells were inoculated into the spleens of nude mice to examine the effect of CD36 on the capacity for liver and lung homing. As a surrogate marker for homing, human GAPDH was detected by PCR, using mβ-actin as a control. Scramble and CD36 siRNA-transfected KM12SM cells were detected at similar extents in the liver, suggesting that CD36 had no effect on the homing of KM12SM cells. However, KM12L4a cells were significantly detected at a lower extent in the liver and lung upon CD36 depletion in comparison to control cells transfected with scramble siRNA (**Figures 8D, E**).

Collectively, as the bioenergetics-derived results suggested, CD36 depletion preferentially impaired homing produced by KM12L4a cells, whereas liver homing was unaffected by CD36-deficient KM12SM cells.

Exogenous FA Transporters as Prognostic Markers of CRC

Finally, we hypothesized that these findings may be reflected in actual CRC samples from patients. To address this question, we analysed the mRNA levels of the lipid metabolism biomarkers *SREBF1*, *FASN*, *SCD*, *LDLR*, *CD36*, *LPL*, *FABP1*, *FABP4*, *ABCA1*, *APOA1*, and *AGPAT1* in actual tumoural tissue samples by meta-analysis of the COAD TCGA dataset, to determine their usefulness as prognostic markers. Additionally, we used the GSE68468 database to analyse their association to different CRC metastatic foci (**Figure 9**).

Remarkably, we observed statistically significant differences in patient survival according to *FASN*, *AGPAT1*, *LDLR*, *CD36*, *FABP4*, and *SCD* expression levels (**Figure 9A**). The 5-year survival rate decreases to 60% with a high expression of *LDLR*, while it increases to 73% with a low expression of this receptor (p value < 0.05). Similarly, high expression levels of *CD36*, *FABP4*, *SCD*, and *AGPAT1* decrease this rate to 49%–55%, while the rate

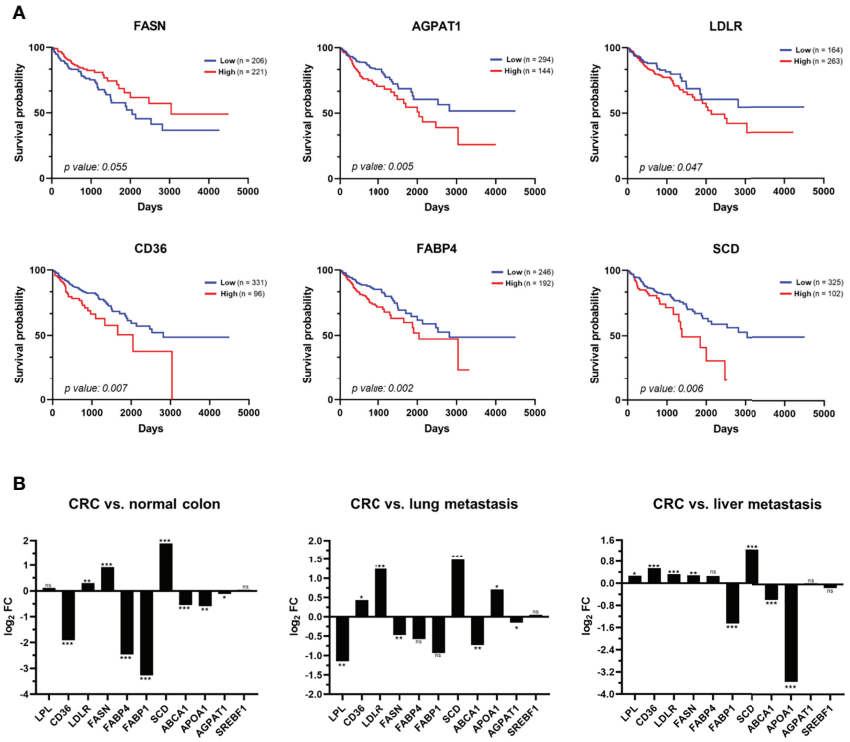

FIGURE 9 | Analysis of the clinical relevance of the metabolic alterations in CRC patients. **(A)** Meta-analysis of mRNA levels of *FASN*, *AGPAT1*, *LDLR*, *CD36*, *FABP4*, and *SCD* in tissue samples of CRC patients using TCGA data related to colon adenocarcinoma (COAD). Kaplan–Meier analyses of overall survival of patients with colon cancer showed that a high expression of *AGPAT1*, *LDLR*, *CD36*, *FABP4*, and *SCD* are prognostic factors of worst prognosis for CRC patients. **(B)** The dataset from the NCBI Gene Expression Omnibus GSE68468 was used to analyse 47 metastatic samples to the liver and 20 metastatic samples to the lung from patients with primary colon cancer in comparison to 186 CRC primary tumour samples and 55 normal colon samples. Box-plots in $\log_2$ revealed a dysregulation of nine of the 11 proteins analysed in CRC primary tumour in comparison with normal colon mucosa (left panel). In addition, a statistically significant upregulation of *LPL*, *FASN*, *AGPAT1*, and *ABCA1* in lung metastasis in comparison with primary CRC tumour (middle panel) was found, whereas *FABP1*, *ABCA1*, and *APOA1* were found statistically upregulated in liver metastasis in comparison with primary CRC tumour (right panel). FC, fold change; ns, not-significant; **p* value < 0.05; ***p* value < 0.01; ****p* value < 0.001.

increases to 67%–71% with their low expression (p value < 0.05). On the other hand, a low expression of *FASN* decreases the 5-year survival rate to 60%, while it increases to 70% with its high expression (p value < 0.05). In conclusion, the expression levels of these proteins are prognostic factors of colon cancer, which could be associated with a more or less aggressive phenotype of CRC (**Figure 9A**).

Then, we analysed their potential association with metastatic foci. First, nine out of the 11 genes analysed were found statistically dysregulated in CRC in comparison to normal colon mucosa (**Figure 9B**). Furthermore, *ABCA1* and *FABP1* were found to be statistically upregulated in liver and lung metastasis compared to CRC tumour, while *SCD*, *CD36*, and *LDLR* were downregulated in both CRC metastastic foci (**Figure 9B**). Interestingly, *APOA1*, *FASN*, *FABP4*, and *LPL* were oppositely dysregulated in liver and lung metastasis compared to the primary CRC tumour, whereas *AGPAT1* was found to be significantly upregulated in lung metastasis (**Figure 9B**). Finally, the expression levels of these genes were compared between lung CRC metastasis and liver CRC metastasis. We found an upregulation of *LPL*, *CD36*, *LDLR*, *FASN*, *FABP4*, *SCD*, *ABCA1*, and *AGPAT1* and a downregulation of *FABP1*, *APOA1*, and *SREBF1* in lung CRC metastasis compared with liver CRC metastasis (**Figure S4A**). Remarkably, the protein expression levels of *CD36*, *LDLR*, and *FASN* in KM12SM and KM12L4a cells with different metastatic abilities were in agreement with data from CRC patients from the GSE68468 database (**Figure S4B**). These results further support the usefulness of the CRC metastasis KM12 cell system, which recapitulates quite effectively critical issues of CRC metastasis.

Collectively, these data indicate that the metabolic alterations found in isogenic CRC cells with different metastatic organotropisms partially resemble alterations in CRC patients that are associated with prognosis. The concordance observed between the expression levels of the indicated genes associated with organotropism of CRC cells and their expression in metastatic tissue of CRC patients suggests that these metabolic alterations—among others—help to dictate metastatic tropisms. Specifically, we have demonstrated here the role of *CD36*, *FASN*, *LDLR*, *FABP4*, *LPL*, *SCD*, and *APOA1* as markers of metastatic

CRC tropism and validated *in vivo* the association of CD36 with the lung tropism of CRC cells.

DISCUSSION

It is well known that oncogenic transformation alters tumour metabolism to sustain cell growth and dissemination. Furthermore, cancer cells need to control metabolic stress to avoid cell death by activating pro-survival pathways (37). Moreover, by-products of cancer metabolism, such as ROS production, may support the EMT program to promote dissemination (13, 14). Thus, the exposition to matrix metalloproteinases (MMPs) (38), local inflammation (39), and aerobic glycolysis metabolites have been shown to activate the EMT program (15). In addition, the relevance of alterations in lipid metabolism in cancer dissemination has been recently highlighted (40).

Herein, we have identified and validated *in vitro* and *in vivo* lipid metabolism features implicated in the differential dissemination of CRC cells to specific niches—mainly to the liver for KM12SM cells and to the lung for KM12L4a cells. Importantly, some of the metabolic differences are worst prognostic factors of CRC patients.

In addition to the Warburg effect and increased glutaminolysis, the role of lipid metabolism in cancer has been recognized. Fatty acids are key structural components of cell membranes. They are substrates for ATP production and key mediators of oncogenic signalling pathways. Our results indicate that changes in lipid metabolism are associated with functional differences between the two metastatic CRC cells and that these changes demand further attention. KM12SM preferentially promotes a higher bioenergetic activity (**Figures 5–7**) as demonstrated by the increased levels of aerobic glycolysis and oxidative phosphorylation in mitochondria (**Figure 5**). In contrast, KM12L4a is characterized by reduced oxidative phosphorylation and glycolytic performance compared to parental KM12 cells (**Figures 5**, **6**). Nevertheless, when KM12L4a cells are exposed to exogenous FAs, they can increase oxidative phosphorylation to levels similar to those of parental KM12 cells.

In a previous work (40), we compared the cell bioenergetic performance of the isogenic pair non-metastatic SW480 CRC cells and the metastatic SW620 CRC cells with lymph node tropism. SW620 cells showed reduced mitochondrial oxidative phosphorylation without glycolytic changes compared to SW480 cells, indicating an overall energetic advantage. Metastatic SW620 cells had higher levels of reduced glutathione (GSH) compared to isogenic SW480 cells. Interestingly, the increased dependence of KM12L4a cells on extracellular FA uptake could explain the lower oxidative stress observed in this metastatic cell line, as fatty acid oxidation (FAO) can provide NADH and $FADH_2$ for reduced glutathione regeneration. In this sense, KM12L4a cells were almost unaffected by metformin, which inhibits respiratory chain complex I, suggesting that this cell line is highly dependent on respiratory chain complex II to obtain energy through lipid metabolism using $FADH_2$ obtained during β-oxidation.

Moreover, specialized transporters facilitate the uptake of exogenous FA across the plasma membrane. Whereas normal cells rely on exogenous FA uptake, cancer cells promote *de novo* FA synthesis, independently of the extracellular circulating lipid levels, highlighting the relevance of the crucial role played by FA synthesis in tumorigenesis (41). Here, we have observed, in addition to a dysregulation in the EMT and stemness markers, that metastatic CRC cells differentially reactivated FA uptake to get different metastatic niches in comparison to non-metastatic CRC cells, suggesting that metabolic reprogramming helps dictate metastatic organ colonization. The best-characterized FA receptors/transporters include CD36, also known as fatty acid translocase (FAT), fatty acid transport protein family (FATPs), also known as solute carrier protein family 27 (SLC27), and plasma membrane fatty acid-binding proteins (FABPpm), along with low-density lipoprotein receptor LDLR. Importantly, most of them showed increased gene and protein expression in tumours. These results are also in agreement with the fact that obesity and metabolic disorders increase the risk and worse prognosis of certain types of cancer, including CRC (42).

One of the goals of the study was to determine whether the different FA uptake detected also plays a relevant role in the prognosis of CRC patients. First, through meta-analysis we observed a correlation with worst prognosis of *CD36*, *LDLR*, *FABP4*, *AGPAT1*, and *SCD* overexpression and *FASN* reduction in CRC. High CD36 expression has been correlated with poor prognosis in several tumour types, including breast, ovarian, gastric, and prostate (43, 44). Regarding LDLR, an elevated tumour expression of this protein has been shown to accelerate LDL cholesterol-mediated breast cancer growth in mouse models of hyperlipidaemia (45). Furthermore, LDLR expression and its transcriptional regulation in tumours have been largely unexplored (46). Remarkably, no other studies linking these metabolic abnormalities to CRC prognosis have been previously reported. Furthermore, experiments with plasma from obese volunteers reinforced this idea, further supporting the link between metabolic alterations and CRC prognosis. Remarkably, plasma from obese volunteers produced a significantly increased basal, but not spare, respiratory capacity of metastatic cells, as well as increased tumorigenic and metastatic properties of metastatic cells in contrast to KM12C cells.

Second, through meta-analysis of primary CRC and metastatic *foci*, we also confirmed that *LPL*, *CD36*, *LDLR*, *FASN*, *FABP1*, *SCD*, *ABCA1*, *APOA1*, *AGPAT1*, and *SREBF1* expression levels were associated with lung or liver tropisms, suggesting that metabolic alterations help dictate, among other alterations, specific organotropisms in CRC patients. In this sense, the depletion of CD36 in KM12SM and KM12L4a cells helped to confirm its association to lung metastasis *in vitro*, where a decrease in tumorigenic and metastatic properties was observed, and *in vivo* with a partial impairment of lung metastasis homing of KM12L4a cells in contrast to KM12SM cells, where no alterations in homing were observed. In addition,

the comparison of the expression levels of these genes between lung and liver metastatic foci indicated that *LPL*, *CD36*, *LDLR*, *FASN*, *FABP4*, *SCD*, *ABCA1*, and *AGPAT1* were associated with metastatic lung foci; whereas the expression of *FABP1*, *APOA1*, and *SREBF1* was associated with metastatic liver foci (**Figure S4**).

CONCLUSION

Here, we have identified metabolic and functional differences in metastatic CRC cells with different tropisms, reflecting the relevance of distinct metabolic adaptations of metastatic CRC cells that may help dictate the organ of colonization. Importantly, the identified dysregulated metabolic proteins have also been shown to be prognostic factors of CRC and potential metastatic markers that show differential correlation with the organs of colonization.

DATA AVAILABILITY STATEMENT

The datasets presented in this study can be found in online repositories. The names of the repository/repositories and accession number(s) can be found in the article/**Supplementary Material**.

ETHICS STATEMENT

The studies involving human participants were reviewed and approved by the Platform for Clinical Trials in Nutrition and Health (GENYAL) at IMDEA Food Institute (Madrid, Spain). Volunteers included in the GENYAL database were contacted to participate in this study (IMD PI:030). The patients/participants provided their written informed consent to participate in this study. The Ethical Committee of the Instituto de Salud Carlos III (Spain) approved the protocols used for experimental work with mouse after approval for the ethical committee OEBA (Proex 285/19).

AUTHOR CONTRIBUTIONS

Conception and design: MG, AM-C, AR, and RB. Development of methodology: AM-C, AQ-F, AP-G, GS-F, and MF-A, IE-S. Performing of research: AM-C, AQ-F, AP-G, GS-F, MF-A, VL-A IE-S and MG. Analysis and interpretation of data: AM-C, AQ-F, AP-G, GS-F, MF-A, VL-A, and MG, AR, and RB. Writing and review of the manuscript: AM-C, MG, AR, and RB. Revision of the manuscript: all authors. Technical, obtaining and processing of samples, or material support: MG, AR, RB, VL-A, and MF-A. All authors contributed to the article and approved the submitted version.

FUNDING

This work was supported by grants cofounded by Fondo Europeo de Desarrollo Regional -FEDER- PI17CIII/00045 and PI20CIII/00019 from the AES-ISCIII program to RB from the Instituto de Salud Carlos III (ISCIII) and grants from Spanish Ministry of Science (Plan Nacional I+D+i PID2019-110183RB-C21), Regional Government of Community of Madrid (P2018/BAA-4343-ALIBIRD2020-CM, and Y2020/BIO-6350), and Ramón Areces Foundation (CIVP19A5937) to AR. AM-C FPU predoctoral contract is supported by the Spanish Ministerio de Educación, Cultura y Deporte. AQ-F acknowledges Comunidad de Madrid for the Garantía Juvenil PEJD-2017-PRE/BMD-3394 contract. GS-F is a recipient of a predoctoral contract (grant number 1193818N) supported by the Flanders Research Foundation (FWO).

SUPPLEMENTARY MATERIAL

The Supplementary Material for this article can be found online at: https://www.frontiersin.org/articles/10.3389/fonc.2022.903033/full#supplementary-material

REFERENCES

1. Chaffer CL, Weinberg RA. A Perspective on Cancer Cell Metastasis. *Science* (2011) 331:1559–64. doi: 10.1126/science.1203543
2. Obenauf AC, Massague J. Surviving at a Distance: Organ-Specific Metastasis. *Trends Cancer* (2015) 1:76–91. doi: 10.1016/j.trecan.2015.07.009
3. Hanahan D, Weinberg RA. Hallmarks of Cancer: The Next Generation. *Cell* (2011) 144:646–74. doi: 10.1016/j.cell.2011.02.013
4. Lunt SY, Vander Heiden MG. Aerobic Glycolysis: Meeting the Metabolic Requirements of Cell Proliferation. *Annu Rev Cell Dev Biol* (2011) 27:441–64. doi: 10.1146/annurev-cellbio-092910-154237
5. Boroughs LK, DeBerardinis RJ. Metabolic Pathways Promoting Cancer Cell Survival and Growth. *Nat Cell Biol* (2015) 17:351–9. doi: 10.1038/ncb3124
6. Metallo CM, Gameiro PA, Bell EL, Mattaini KR, Yang J, Hiller K, et al. Reductive Glutamine Metabolism by IDH1 Mediates Lipogenesis Under Hypoxia. *Nature* (2011) 481:380–4. doi: 10.1038/nature10602
7. Schug ZT, Peck B, Jones DT, Zhang Q, Grosskurth S, Alam IS, et al. Acetyl-CoA Synthetase 2 Promotes Acetate Utilization and Maintains Cancer Cell Growth Under Metabolic Stress. *Cancer Cell* (2015) 27:57–71. doi: 10.1016/j.ccell.2014.12.002
8. Elstrom RL, Bauer DE, Buzzai M, Karnauskas R, Harris MH, Plas DR, et al. Akt Stimulates Aerobic Glycolysis in Cancer Cells. *Cancer Res* (2004) 64:3892–9. doi: 10.1158/0008-5472.CAN-03-2904
9. Yang W, Zheng Y, Xia Y, Ji H, Chen X, Guo F, et al. ERK1/2-Dependent Phosphorylation and Nuclear Translocation of PKM2 Promotes the Warburg Effect. *Nat Cell Biol* (2012) 14:1295–304. doi: 10.1038/ncb2629
10. Wise DR, DeBerardinis RJ, Mancuso A, Sayed N, Zhang XY, Pfeiffer HK, et al. Myc Regulates a Transcriptional Program That Stimulates Mitochondrial Glutaminolysis and Leads to Glutamine Addiction. *Proc Natl Acad Sci USA* (2008) 105:18782–7. doi: 10.1073/pnas.0810199105
11. Carracedo A, Cantley LC, Pandolfi PP. Cancer Metabolism: Fatty Acid Oxidation in the Limelight. *Nat Rev Cancer* (2013) 13:227–32. doi: 10.1038/nrc3483
12. Ou J, Miao H, Ma Y, Guo F, Deng J, Wei X, et al. Loss of Abhd5 Promotes Colorectal Tumor Development and Progression by Inducing Aerobic

Glycolysis and Epithelial-Mesenchymal Transition. *Cell Rep* (2018) 24:2795–7. doi: 10.1016/j.celrep.2018.08.050
13. Gupta SC, Hevia D, Patchva S, Park B, Koh W, Aggarwal BB. Upsides and Downsides of Reactive Oxygen Species for Cancer: The Roles of Reactive Oxygen Species in Tumorigenesis, Prevention, and Therapy. *Antioxidants Redox Signaling* (2012) 16:1295–322. doi: 10.1089/ars.2011.4414
14. Cichon MA, Radisky DC. ROS-Induced Epithelial-Mesenchymal Transition in Mammary Epithelial Cells is Mediated by NF-kB-Dependent Activation of Snail. *Oncotarget* (2014) 5:2827–38. doi: 10.18632/oncotarget.1940
15. Lin CC, Cheng TL, Tsai WH, Tsai HJ, Hu KH, Chang HC, et al. Loss of the Respiratory Enzyme Citrate Synthase Directly Links the Warburg Effect to Tumor Malignancy. *Sci Rep* (2012) 2:785. doi: 10.1038/srep00785
16. Gunasinghe NP, Wells A, Thompson EW, Hugo HJ. Mesenchymal-Epithelial Transition (MET) as a Mechanism for Metastatic Colonisation in Breast Cancer. *Cancer Metastasis Rev* (2012) 31:469–78. doi: 10.1007/s10555-012-9377-5
17. Jolly MK, Jia D, Boareto M, Mani SA, Pienta KJ, Ben-Jacob E, et al. Coupling the Modules of EMT and Stemness: A Tunable 'Stemness Window' Model. *Oncotarget* (2015) 6:25161–74. doi: 10.18632/oncotarget.4629
18. Kuniyasu H, Ohmori H, Sasaki T, Sasahira T, Yoshida K, Kitadai Y, et al. Production of Interleukin 15 by Human Colon Cancer Cells is Associated With Induction of Mucosal Hyperplasia, Angiogenesis, and Metastasis. *Clin Cancer Res* (2003) 9:4802–10.
19. Li A, Varney ML, Singh RK. Constitutive Expression of Growth Regulated Oncogene (Gro) in Human Colon Carcinoma Cells With Different Metastatic Potential and its Role in Regulating Their Metastatic Phenotype. *Clin Exp Metastasis* (2004) 21:571–9. doi: 10.1007/s10585-004-5458-3
20. Calon A, Espinet E, Palomo-Ponce S, Tauriello DV, Iglesias M, Cespedes MV, et al. Dependency of Colorectal Cancer on a TGF-Beta-Driven Program in Stromal Cells for Metastasis Initiation. *Cancer Cell* (2012) 22:571–84. doi: 10.1016/j.ccr.2012.08.013
21. Morikawa K, Walker SM, Nakajima M, Pathak S, Jessup JM, Fidler IJ. Influence of Organ Environment on the Growth, Selection, and Metastasis of Human Colon Carcinoma Cells in Nude Mice. *Cancer Res* (1988) 48:6863–71.
22. Barderas R, Mendes M, Torres S, Bartolome RA, Lopez-Lucendo M, Villar-Vazquez R, et al. In-Depth Characterization of the Secretome of Colorectal Cancer Metastatic Cells Identifies Key Proteins in Cell Adhesion, Migration, and Invasion. *Mol Cell Proteomics* (2013) 12:1602–20. doi: 10.1074/mcp.M112.022848
23. Mendes M, Pelaez-Garcia A, Lopez-Lucendo M, Bartolome RA, Calvino E, Barderas R, et al. Mapping the Spatial Proteome of Metastatic Cells in Colorectal Cancer. *Proteomics* (2017) 17:1700094. doi: 10.1002/pmic.201700094
24. Luque-Garcia JL, Martinez-Torrecuadrada JL, Epifano C, Canamero M, Babel I, Casal JI. Differential Protein Expression on the Cell Surface of Colorectal Cancer Cells Associated to Tumor Metastasis. *Proteomics* (2010) 10:940–52. doi: 10.1002/pmic.200900441
25. Gomez de Cedron M, Acin Perez R, Sanchez-Martinez R, Molina S, Herranz J, Feliu J, et al. MicroRNA-661 Modulates Redox and Metabolic Homeostasis in Colon Cancer. *Mol Oncol* (2017) 11:1768–87. doi: 10.1002/1878-0261.12142
26. Pelaez-Garcia A, Barderas R, Batlle R, Vinas-Castells R, Bartolome RA, Torres S, et al. A Proteomic Analysis Reveals That Snail Regulates the Expression of the Nuclear Orphan Receptor Nuclear Receptor Subfamily 2 Group F Member 6 (Nr2f6) and Interleukin 17 (IL-17) to Inhibit Adipocyte Differentiation. *Mol Cell Proteomics* (2015) 14:303–15. doi: 10.1074/mcp.M114.045328
27. Solis-Fernandez G, Montero-Calle A, Martinez-Useros J, Lopez-Janeiro A, de Los Rios V, Sanz R, et al. Spatial Proteomic Analysis of Isogenic Metastatic Colorectal Cancer Cells Reveals Key Dysregulated Proteins Associated With Lymph Node, Liver, and Lung Metastasis. *Cells* (2022) 11:447. doi: 10.3390/cells11030447
28. Nguyen DX, Bos PD, Massague J. Metastasis: From Dissemination to Organ-Specific Colonization. *Nat Rev Cancer* (2009) 9:274–84. doi: 10.1038/nrc2622
29. Costa A, Scholer-Dahirel A, Mechta-Grigoriou F. The Role of Reactive Oxygen Species and Metabolism on Cancer Cells and Their Microenvironment. *Semin Cancer Biol* (2014) 25:23–32. doi: 10.1016/j.semcancer.2013.12.007
30. Sun SY. N-Acetylcysteine, Reactive Oxygen Species and Beyond. *Cancer Biol Ther* (2010) 9:109–10. doi: 10.4161/cbt.9.2.10583
31. Halasi M, Wang M, Chavan TS, Gaponenko V, Hay N, Gartel AL. ROS Inhibitor N-Acetyl-L-Cysteine Antagonizes the Activity of Proteasome Inhibitors. *Biochem J* (2013) 454:201–8. doi: 10.1042/BJ20130282
32. Vial G, Detaille D, Guigas B. Role of Mitochondria in the Mechanism(s) of Action of Metformin. *Front Endocrinol (Lausanne)* (2019) 10. doi: 10.3389/fendo.2019.00294
33. Jackson AL, Sun W, Kilgore J, Guo H, Fang Z, Yin Y, et al. Phenformin has Anti-Tumorigenic Effects in Human Ovarian Cancer Cells and in an Orthotopic Mouse Model of Serous Ovarian Cancer. *Oncotarget* (2017) 8:100113–27. doi: 10.18632/oncotarget.22012
34. Bhaskaran K, Dos-Santos-Silva I, Leon DA, Douglas IJ, Smeeth L. Association of BMI With Overall and Cause-Specific Mortality: A Population-Based Cohort Study of 3.6 Million Adults in the UK. *Lancet Diabetes Endocrinol* (2018) 6:944–53. doi: 10.1016/S2213-8587(18)30288-2
35. Ouchi N, Parker JL, Lugus JJ, Walsh K. Adipokines in Inflammation and Metabolic Disease. *Nat Rev Immunol* (2011) 11:85–97. doi: 10.1038/nri2921
36. Weidinger C, Ziegler JF, Letizia M, Schmidt F, Siegmund B. Adipokines and Their Role in Intestinal Inflammation. *Front Immunol* (2018) 9. doi: 10.3389/fimmu.2018.01974
37. Jeon SM, Chandel NS, Hay N. AMPK Regulates NADPH Homeostasis to Promote Tumour Cell Survival During Energy Stress. *Nature* (2012) 485:661–5. doi: 10.1038/nature11066
38. Radisky DC, Levy DD, Littlepage LE, Liu H, Nelson CM, Fata JE, et al. Rac1b and Reactive Oxygen Species Mediate MMP-3-Induced EMT and Genomic Instability. *Nature* (2005) 436:123–7. doi: 10.1038/nature03688
39. Coussens LM, Werb Z. Inflammation and Cancer. *Nature* (2002) 420:860–7. doi: 10.1038/nature01322
40. Sanchez-Martinez R, Cruz-Gil S, Gomez de Cedron M, Alvarez-Fernandez M, Vargas T, Molina S, et al. A Link Between Lipid Metabolism and Epithelial-Mesenchymal Transition Provides a Target for Colon Cancer Therapy. *Oncotarget* (2015) 6:38719–36. doi: 10.18632/oncotarget.5340
41. Chen M, Huang J. The Expanded Role of Fatty Acid Metabolism in Cancer: New Aspects and Targets. *Precis Clin Med* (2019) 2:183–91. doi: 10.1093/pcmedi/pbz017
42. Garcia-Jimenez C, Gutierrez-Salmeron M, Chocarro-Calvo A, Garcia-Martinez JM, Castano A, de la Vieja A. From Obesity to Diabetes and Cancer: Epidemiological Links and Role of Therapies. *Br J Cancer* (2016) 114:716–22. doi: 10.1038/bjc.2016.37
43. Calvo D, Gomez-Coronado D, Suarez Y, Lasuncion MA, Vega MA. Human CD36 is a High Affinity Receptor for the Native Lipoproteins HDL, LDL, and VLDL. *J Lipid Res* (1998) 39:777–88. doi: 10.1016/S0022-2275(20)32566-9
44. Ladanyi A, Mukherjee A, Kenny HA, Johnson A, Mitra AK, Sundaresan S, et al. Adipocyte-Induced CD36 Expression Drives Ovarian Cancer Progression and Metastasis. *Oncogene* (2018) 37:2285–301. doi: 10.1038/s41388-017-0093-z
45. Gallagher EJ, Zelenko Z, Neel BA, Antoniou IM, Rajan L, Kase N, et al. Elevated Tumor LDLR Expression Accelerates LDL Cholesterol-Mediated Breast Cancer Growth in Mouse Models of Hyperlipidemia. *Oncogene* (2017) 36:6462–71. doi: 10.1038/onc.2017.247
46. Huang J, Li L, Lian J, Schauer S, Vesely PW, Kratky D, et al. Tumor-Induced Hyperlipidemia Contributes to Tumor Growth. *Cell Rep* (2016) 15:336–48. doi: 10.1016/j.celrep.2016.03.020

Conflict of Interest: The authors declare that the research was conducted in the absence of any commercial or financial relationships that could be construed as a potential conflict of interest.

The handling editor JI-G declared a shared parent affiliation with the author MF-A at the time of review.

this article, or claim that may be made by its manufacturer, is not guaranteed or endorsed by the publisher.

frontiers | Frontiers in Oncology

TYPE Original Research
PUBLISHED 10 October 2022
DOI 10.3389/fonc.2022.1004014

OPEN ACCESS

EDITED BY
Dan Lindholm,
University of Helsinki, Finland

REVIEWED BY
Terence Kin Wah Lee,
Hong Kong Polytechnic University,
Hong Kong SAR, China
Vesa Olkkonen,
Minerva Foundation, Finland

*CORRESPONDENCE
Liza Barki-Harrington
Lbarki@psy.haifa.ac.il

SPECIALTY SECTION
This article was submitted to Cancer Metabolism, a section of the journal Frontiers in Oncology

RECEIVED 26 July 2022
ACCEPTED 05 September 2022
PUBLISHED 10 October 2022

CITATION
Hartal-Benishay LH, Saadi E, Toubiana S, Shaked L, Lalzar M, Abu Hatoum O, Tal S, Selig S and Barki-Harrington L (2022) MBTPS1 regulates proliferation of colorectal cancer primarily through its action on sterol regulatory element-binding proteins. *Front. Oncol.* 12:1004014. doi: 10.3389/fonc.2022.1004014

MBTPS1 regulates proliferation of colorectal cancer primarily through its action on sterol regulatory element-binding proteins

Liat H. Hartal-Benishay[1], Esraa Saadi[1], Shir Toubiana[2], Lior Shaked[1], Maya Lalzar[3], Ossama Abu Hatoum[4,5], Sharon Tal[1], Sara Selig[2,6] and Liza Barki-Harrington[1]*

[1]Department of Human Biology, Faculty of Natural Sciences, University of Haifa, Haifa, Israel, [2]Department of Genetics and Developmental Biology, Rappaport Faculty of Medicine and Research Institute, Technion, Haifa, Israel, [3]Bioinformatics Service Unit, Faculty of Natural Sciences, University of Haifa, Haifa, Israel, [4]Department of Surgery, Ha'emek Medical Center, Afula, Israel, [5]Department of Medicine, Rappaport Faculty of Medicine and Research Institute, Technion, Haifa, Israel, [6]Laboratory of Molecular Medicine, Rambam Health Care Campus, Haifa, Israel

Among the main metabolic pathways implicated in cancer cell proliferation are those of cholesterol and fatty acid synthesis, both of which are tightly regulated by sterol regulatory element-binding proteins (SREBPs). SREBPs are activated through specific cleavage by membrane-bound transcription factor protease 1 (MBTPS1), a serine protease that cleaves additional substrates (ATF6, BDNF, CREBs and somatostatin), some of which are also implicated in cell proliferation. The goal of this study was to determine whether MBTPS1 may serve as a master regulator in proliferation of colorectal cancer (CRC). Tumors from CRC patients showed variable levels of MBTPS1 mRNA, which were in positive correlation with the levels of SREBPs and ATF6, and in reverse correlation with BDNF levels. Chemical inhibition of MBTPS1 activity in two CRC-derived cell lines resulted in a marked decrease in the levels of SREBPs, but not of its other substrates and a marked decrease in cell proliferation, which suggested that MBTPS1 activity is critical for proliferation of these cells. In accordance, CRISPR/Cas9 targeted knockout (KO) of the *MBTPS1* gene resulted in the survival of only a single clone that presented a phenotype of severely attenuated proliferation and marked downregulation of several energy metabolism pathways. We further showed that survival of the MBTPS1 KO clone was dependent upon significant upregulation of the type-1 interferon pathway, the inhibition of which halted proliferation entirely. Finally, rescue of the MBTPS1 KO cells, resulted in partial restoration of MBTPS1 levels, which was in accordance with partial recovery in proliferation and in SREBP levels. These finding suggest that MBTPS1 plays a critical role in regulating colon cancer

proliferation primarily through SREBP-associated lipid metabolism, and as such may serve as a possible therapeutic target in CRC.

KEYWORDS

MBTPS1, SKI-1/S1P, site-1 protease, colon cancer, SREBP, CRISPR/Cas9, HT-29, lipid metabolism

Introduction

Proliferation of cancer cells is dependent upon activation or enhancement of specific metabolic pathways in order to supply their growing energetic needs. Two major pathways that are often deregulated in cancers cells are those of cholesterol and fatty acid synthesis (1). Cholesterol is an essential molecule for membrane and hormone biosynthesis and multiple *in vitro* studies have demonstrated that inhibition of HMG-reductase, the rate limiting enzyme of cholesterol synthesis, is detrimental to cancer cell growth (Reviewed in (2). However, clinical studies that tested the effect of statins-HMG CoA reductase inhibitors as potential anti-cancer drugs have so far been inconclusive (3). Increased fatty acid synthesis and uptake have also been identified as promoting tumor growth and several inhibitors of enzymes in these pathways are being tested, with no clear results thus far (1).

One of the most important regulators of synthesis and uptake of cholesterol, fatty acids, triglycerides and phospholipids are a family of sterol regulatory element-binding proteins (SREBPs) transcription factors (4). Two main isoforms of SREBPs, SREBP1 and SREBP2 (encoded by the genes *SREBF1* and *SREBF2*, respectively) are synthesized as inactive precursors that are anchored to the membranes of the ER and nuclear envelope, and activated through cleavage by MBTPS1 (membrane-bound transcription factor protease, also known as site-1 protease or SKI-1). The cleavage of SREBPs facilitates their localization to the nucleus where they activate transcription of target genes such as the low density lipoprotein (LDL) receptor and 3-hydroxy-3-methylglutaryl-CoA (HMG-CoA) reductase - the rate limiting enzyme in cholesterol synthesis (4).

MBTPS1 is a calcium-dependent serine protease that is encoded by the *MBTPS1* gene, synthesized in the endoplasmic reticulum (ER) as an inactive precursor that becomes active upon autocatalytic processing in the Golgi apparatus (5–8). Two MBTPS1 substrates, MBTPS1 itself, and the membrane-bound precursor of N-acetylglucosamine (GlcNac)-1 phosphotransferase (9), are constitutively cleaved by MBTPS1, while its other substrates are cleaved upon intracellular signals. In addition to SREBPs, MBTPS1 cleaves and activates several transcription factors that are critical for various cellular functions. These include ATF6 (10), cyclic AMP-responsive element-binding proteins (CREB) 3 and 4 (11, 12), the pro-form of the secretory brain-derived neurotrophic factor (BDNF) (8, 13) and pro-somatostatin (14). ATF6 is one of the three ER-resident proteins that regulate the unfolded protein response (UPR) and is activated upon ER stress signaling [reviewed in (15)]. ATF6 is also activated directly by specific lipids (16), and interacts with activated peroxisome proliferator-activated receptor a (PPARα), a key transcription factor that controls fatty acid oxidation in the liver (17). Like SREBPs and ATF6, CREB3 is also cleaved by MBTPS1 in the Golgi apparatus, and its subsequent translocation to the nucleus has multiple tissue-dependent roles including acute cell response, lipid metabolism, survival and differentiation [reviewed in (18)]. In contrast to SREBPs, ATF6 and CREBs the physiological significance of BDNF and somatostatin cleavage by MBTPS1 remains unclear.

Previous studies indicate that several of MBTPS1 downstream targets are implicated in growth of colorectal cancer (CRC) cells. Knockdown of SREBPs in CRC-derived cells was shown to significantly hamper the rate of fatty acid synthesis (19), cell proliferation and the ability of the cells to form spheroids, as well as to inhibit xenograft tumor growth and decrease the expression of genes associated with cancer stemness (20). In another study, inhibition of the SREBP1 pathway suppressed growth and lipogenesis of colon cancer xenografts (21). ATF6 was also found to be linked to CRC by upregulating the inhibitor of protein phosphatase 2A (CIP2A), an oncogene that increases cancer cell survival (22, 23). Mice with intestinal epithelial expression of the active form of ATF6 developed spontaneous colon adenomas at 12 weeks of age, and in CRC patients increased ATF6 expression was associated with reduced time of disease-free survival (23). The levels of another MBTPS1 target, BDNF, were also found to be elevated in human CRC samples where its presence was associated with reduced apoptosis of cancer cells (24). Increased BDNF levels also enhanced migration of colon cancer cells (25).

MBTPS1 belongs to the family of proprotein convertases (PCs), some of which have been implicated in cancer cell proliferation. PC members PC2 and PC3 were found to be expressed in adrenal tumors (26), and elevated in small cell lung carcinoma (SCLC), while the PCs furin and PACE4 were

described as highly expressed in non-small lung carcinoma (NSCLC) (27). Several studies also showed that the expression of some PCs correlates with rapid growth, invasiveness or metastatic potential of several tumor-derived cell lines [reviewed in (28)]. However, to date, only a few studies specifically link MBTPS1 to tumorigenesis. Weiss et al. demonstrated that inhibition of MBTPS1 by a small peptide inhibitor suppressed the growth of melanoma cells (29), and Caruana et al. found that treatment of glioblastoma cells with a chemical MBTPS1 inhibitor decreased cell viability, induced apoptosis and downregulated cholesterol and fatty acid biosynthesis pathways (30). Since MBTPS1 is upstream to numerous factors implicated in CRC prosperity, we used a combined chemical and genetic approach to examine its specific role in regulating CRC proliferation.

Materials and methods

Materials

The MBTPS1 inhibitor PF-429242 dihydrochloride (Cat. # SML0667) and Poly(I:C) (Cat #. P1038) were purchased from Sigma Aldrich (Merck, Israel). STAT1 inhibitor Fludarabine (Cat. # 14128), gift of Prof. Amiram Ariel, was from Cayman Chemical (Ann Arbor, MI, USA). Apoptosis was measured using the MEBCYTO-Apoptosis kit (Annexin V-FITC Kit) from Medical & Biological Laboratories (Nagano, Japan). All cell culture media, fetal bovine serum and antibiotics were from Biological Industries (Beit HaEmek, Israel). All other materials were standard laboratory grade.

Patients and RNA extraction

Biopsies were obtained from patients diagnosed with adenocarcinoma of the colon or rectum at Ha'Emek Medical Center, Afula, Israel. Surgery was performed on all patients prior to any neoadjuvant treatment by radiation, and samples were obtained according to the Declaration of Helsinki as revised in 2008 (Ha'Emek Medical Center- 0049–19). Samples were submerged in approximately 5-10 volumes of RNA SAVE solution (Cat. # 01-891-1A, Sartorius, Israel) and kept at room temperature for 24 hours, after which they were frozen at -80°C pending analysis. For RNA extraction, the tissue was placed on top of a closed ice-filled glass Petri dish, washed with ice-cold PBS and cut into small pieces. RNA was then extracted using Quick-RNA™ Miniprep Plus Kit (Cat. # R1058, Zymo Research), according to the manufacturer's instructions. The concentration of RNA was determined using Nanodrop-1000 (Thermo Scientific), and cDNA was synthesized using High-Capacity cDNA Reverse Transcription Kit (Cat. #4374966, Applied Biosystems).

Quantitative RT- PCR

RT-qPCR was carried out on an Applied Biosystems StepOnePlus Real-Time PCR system with Fast SYBR Green Master Mix (Cat # 4385612, Applied Biosystems). Analysis was carried out by the ΔΔCt method using the β2 microglobulin as the reference gene. Results were analyzed using StepOne software (Applied Biosystems). Average relative quantification (RQ) values were calculated for each tumor and compared to the levels obtained from the same patient's normal tissue.

List of RT-qPCR primers

Gene	Forward	Reverse
ATF6	5'-GGAGCCACTGA AGGAAGATAA G-3'	5'-GTGCTGCTGGA AGCAATAAAG-3'
BDNF	5'-GGTGCTGTTG TCAT GCT TTA C-3'	5'-CTCTACTCCCTG TGGGAACTAA-3'
CREB3	5'-GTAGAGGGA CAGTGGATAGGT-3'	5'-TTGGGACAACTA CGGAAAGG-3'
HMGCS1	5'-AAGAAAACAC TCCAATTCTCTTCC CT-3'	5'-GTACACATCTTCAG TATATGGTTCCC-3'
HMGCS2	5'-CACCAACAA GGACCTGGATAA-3'	5'-CCATTGTGAGTG GAGAGGTAAA-3'
MBTPS1	5'-GGGAGTGCCA AGGATTTG C-3'	5'-GCGTCCAAAAAC CAAGATGTG-3'
PPRG	5'-GCCTGCATCTC CACCTTATTA-3'	5'-ATCTCCACAGAC ACGACATTC-3'
PPRGC1A	5'-TGAACTGAGGG ACAGTGATITTC-3'	5'-CCCAAGGGTAGC TCAGTTTAT C-3
SREBF1	5'-GAGCCATGG ATTGCACTTTC-3'	5'-AGCATAGGGTGG GTCAAATAG-3'
SREBF2	5'-CTGTAGCGTC TTGATTCTCTCC-3'	5'-CCTGGCTGTCCT GTGTAATAA-3'
SST	5'-TGGAAGACT TTCACATCCTGTT-3'	5'-CGCTGAAGACTT GGAGGATTAG-3'

Cell culture

Human epithelial adenocarcinoma HT-29 and HCT-116 cells, obtained from the American Type Culture Collection repository (HTB-38, Manass, VA, USA). HT-29 cells were cultured in RPMI medium and HCT-116 in DMEM and both were supplemented with 10% heat-inactivated fetal bovine serum and 100 U/mL penicillin and streptomycin (Biological Industries, Beit HaEmek, Israel).

Microscopy

30,000 cells were seeded on 13-mm^2 glass coverslips, grown for 72 h prior to imaging, and mounted onto glass slides using Mowiol (Cat. # 81381 Sigma Aldrich, Saint Louis, MI, USA) for visualization by the Nikon Eclipse Ti2-E inverted wide-field fluorescent/

brightfield microscope with a Differential Interference Contrast (DIC) module. All images were acquired using the same exposure conditions at the Bioimaging Unit, University of Haifa.

Proliferation and apoptosis assays

For live cell tracking experiments, 30,000 HT-29 cells were seeded into 24-well dishes that were placed in the IncuCyte® ZOOM live-cell analysis system (Essen Bioscience, Ann Arbor, MI, USA) or the Cytation 5 Cell imaging Multi-Mode Reader (Agilent Bio Tek Imaging, Santa Clara CA, USA) for various durations, and snapshots were taken every 60 min. Percent confluency was analyzed over time using the IncuCyte® ZOOM Software or the Gene 5 software, respectively at the Biomedical Core Facility, Rappaport Faculty of Medicine, or the RBNI both in the Technion Israel Institute of Technology, Israel. Each experimental condition contained three repeats and was carried out in a minimum of two biological repeats (number of biological repeats for each experiment is indicated in the respective figure legends). Cell proliferation was also assessed under the same conditions using the 3-bis-(2-methoxy-4-nitro-5-sulfophenyl)-(2*H*)-tetrazolium-5-carboxanilide (XTT) kit (Biological Industries, Beit HaEmek, Israel). Each experimental point contained 4–8 technical repeats and was performed in a minimum of three biological repeats.

Apoptosis measurements were done using IncuCyte® ZOOM live tracking system. 10,000 or 5,000 cells were seeded in 96-well dishes and cells were treated with or without PF-429242 immediately before tracking commenced. Apoptosis was measured using the IncuCyte® Caspase3/7 Green Apoptosis Reagent (Cat. # 4440, Essen Bioscience).

Western blotting

Total cell lysates were processed for western blotting as described (31). Nitrocellulose membranes were incubated with primary antibodies at a dilution of 1:500–1000. The following antibodies were used: Rabbit polyclonal anti phospho-STAT-1 (Cat. #9167, clone 58D6) from Cell Signaling Technology, and Mouse monoclonal anti-Actin (clone 4) from MP Biomedicals, and Mouse monoclonal anti-SREBP1 (2A4, Cat# SC-13551) from Santa Cruz Biotechnology Inc. Proteins were visualized by a WesternBright ECL (AdvanstaMenlo Park, CA, USA), quantified using Amersham Imager 600 (GE, Buckinghamshire, UK) and analyzed using Quantity One -1D analysis software.

Gene editing

CRISPR/cas9 mediated knockout of the *MBTPS1* gene in HT-29 cells was carried out as following: a guide RNA (gRNA) targeting a coding region in exon 5 of *MBTPS1* (5'-ATCGTCCAGCGTTCGCTCGT-3') was designed using the Optimized CRISPR Design online tool (http://crispr.mit.edu) and cloned into pSpCas9(BB)−2A-GFP (PX458), a gift from Feng Zhang (Addgene plasmid #48138) (32). This plasmid was introduced into HT-29 cells by electroporation. GFP-positive single cells were sorted the following day into 96-well plates using the FACS Aria IIIu cell sorter, and expanded to obtain individual clones. Genomic DNA, extracted from multiple clones, was subjected to PCR using *MBTPS1*-specific primers (Fwd 5'- TTTTCTGTGGGTCCCAGG -3' and Rev 5'- TCCTGAAGTGCTACCTCC -3'), designed to amplify a 385bp region including the gRNA target site. PCR products were Sanger-sequenced to detect clones in which the open reading frame (ORF) of all *MBTPS1* alleles was disrupted by non-homologous end joining (NHEJ).

Fluorescent *in situ hybridization (FISH)*

HT-29 cells were treated with colcemid, harvested by trypsinization, treated with hypotonic solution and fixed with methanol/acetic acid (3:1). Cells were then dropped on slides and hybridized by a standard FISH protocol to a probe generated from BAC clone RP11-274I19 (BACPAC Genomics, Emeryville, California) which overlaps with the *MBTPS1* gene. Probe DNA was labeled with dUTP-digoxigenin and detected with anti-Dig-Rhodamine. DNA was stained with DAPI. Nuclei and chromosomes were visualized on a BX50 microscope (Olympus). Images were captured with an Olympus DP70 camera controlled by DP controller software (Olympus).

Viral infection

A lentiviral plasmid containing the ORF of the *MBTPS1* gene (Cat# 2819001, abm) was introduced by transduction into the HT-29 MBTPS1 KO clone according to manufacturer's instructions. In short, the viral packaging cell line HEK-293T was used to generate lentiviral particles by co-transfection of the expression vector together with VSVG and pMD2 plasmids. Transfection was performed using Lipofectamine™ 3000 Reagent (L3000-008, Invitrogen). Forty-eight hours post transfection the supernatant containing the viruses was collected and filtered through a 0.45-µm PVDF filter. Viruses were used to infect the HT-29 cells in the presence of 6µg/ml polybrene (Millipore, TR-1003-G). Selection for cells that incorporated the viral sequence was performed with puromycin.

CXCL1 ELISA

100,000 HT-29 or MBTPS1 KO cells were seeded in 6-well dishes. One day after seeding, cells were washed twice with warm

PBS and fresh media containing 50 μg/ml Poly(I:C) was added for 24h. The amount of CXCL1 was determined using the Human CXCL1/GROα DuoSet Elisa (# DY275-05, R&D Systems) according to the manufacturer's instructions.

Transcriptome analyses and statistics

Total RNA was prepared in three biological repeats using the Quick-RNA MiniPrep kit (Cat. # ZR-R10554, Zymo Research). Library preparation was performed using NEBNext Ultra RNA library Prep kit for Illumina (Cat. # E7530L, ThermoFischer Scientific, Waltham, MA USA), according to the manufacturer's protocol. Sequencing (single-read, 50bp) was carried out using the Illumina HiSeq 2500 at the TGC-Technion Genome center (Technion, Haifa, Israel). Sequence reads were aligned to the human reference genome version GRCh37 using Tophat (2.0.9). Gene expression levels were quantified using Htseq-count (0.6.1-py2.7) and differential expression was analyzed using EdgeR (3.2.4). Differential expression was considered significant for *P*-value< 0.05. The differentially expressed (DE) gene set was subjected to gene-set enrichment analysis using ENRICHR [accessed Jan 2022 (33)] considering gene ontology biological processes database. Cutoff for significant enrichment was adjusted based on *P* value<0.05 (Table S1). For each significantly enriched pathway, the percentage of DE genes in the pathway was calculated. In addition, the trend toward up or down regulation was expressed as a z-score, calculated as $^{up-down}/_{\sqrt{total\ DE}}$.

A network describing the overlap in genes between significantly enriched pathways was calculated using R package 'igraph' (version 1.2.7) based on pairwise Jaccard distances matrix between pathways. Pathways selected for network analysis included those for which the z-score value was >|2|. The resulting network was exported and visualized in Cytoscape (version 3.9.0).

For the correlation studies, Pearson's correlation coefficient (r) was used to measure the strength of correlations between the different variables, *P*<0.05 was considered significant.

Results

Correlation between mRNA expression of MBTPS1 and its downstream targets in tumors of CRC patients

In order to test the hypothesis that MBTPS1 is directly involved in CRC proliferation, we first determined its expression in colorectal tumors in comparison to normal surrounding tissue from patients diagnosed with low or moderate colorectal adenocarcinoma. Due to the lack of satisfactory commercial antibodies against MBTPS1, we were unable to adequately assess its protein levels and therefore measured mRNA levels. Three categories of *MBTPS1* expression were noticeable among the tumor samples (Figure 1A). In some patients, *MBTPS1* expression was comparable between tumor samples and normal surrounding tissue (Figure 1A, green dots). In the remaining tumor samples, we found that *MBTPS1* levels were either significantly decreased (Figure 1A, light blue dots) or significantly increased (Figure 1A, red dots).

We next sought to determine whether the variability in *MBTPS1* expression affects the mRNA levels of its known downstream targets. As depicted in Figure 1, we found a positive correlation between the levels of *MBTPS1* and *SREBF1*, *SREBF2* (the SREBP genes), and *ATF6* (Figures 1B–D), i.e. samples with low levels of *MBTPS1* mRNA showed low expression levels of SREPBs and ATF6 and vice versa. In addition, a significant positive correlation between the levels of *SREBF1* and *SREBF2* was also evident in the tumor samples (P=0.0011, Figure S1). In contrast, our analysis revealed no significant correlation between *MBTPS1* and somatostatin (*SST*) or *CREB3* genes (Figures 1E, F), and a negative correlation between *MBTPS1* and *BDNF* (Figure 1G). Thus far, these data suggest that in the human CRC, MBTPS1 expression levels vary considerably among patients and that this variability is associated with changes in the expression levels of some, but not all of the genes encoding MBTPS1 target proteins.

Given the positive correlation between the expression of *MBTPS1* and the SREBP encoding genes, we next examined the transcript levels of downstream gene targets of SREBPs within the same tumor samples. As depicted in Figure 2A, we found a positive correlation between *SREBF1* and the cytosolic enzyme 3-Hydroxy-3-Methylglutaryl-CoA Synthase 1 (*HMGCS1*), which catalyzes the synthesis of HMG-CoA, a precursor for cholesterol and other products of the mevalonate pathway (3). In contrast, as expected, no correlation was found between the expression levels of *SREBF1* and *HMGCS2*, an HMGSC1 paralog that catalyzes the first step of ketogenesis in the mitochondria to provide lipid-derived energy during starvation (34) (Figure 2B). A positive correlation was additionally found between the levels of *SREBF1* and PPARG Coactivator 1 Alpha (*PPARGC1A*) (Figure 2C), a transcriptional coactivator of *PPARG* involved in coordination of fatty acid metabolism (35), but not between *SREBF1* and *PPARG* itself (Figure 2D). No correlations were found between *SREBF2* and *HMGCS1*, *HMGCS2* (Figures 2E, F), or with *PPARG* (Figure 2H), but a highly significant correlation was found with *PPARGC1A* (Figure 2G, *P*< 0.0001).

MBTPS1 and its downstream targets regulate the proliferation of colon cancer-derived cells

To determine whether MBTPS1 is directly involved in proliferation of colon cancer cells, we treated two human-

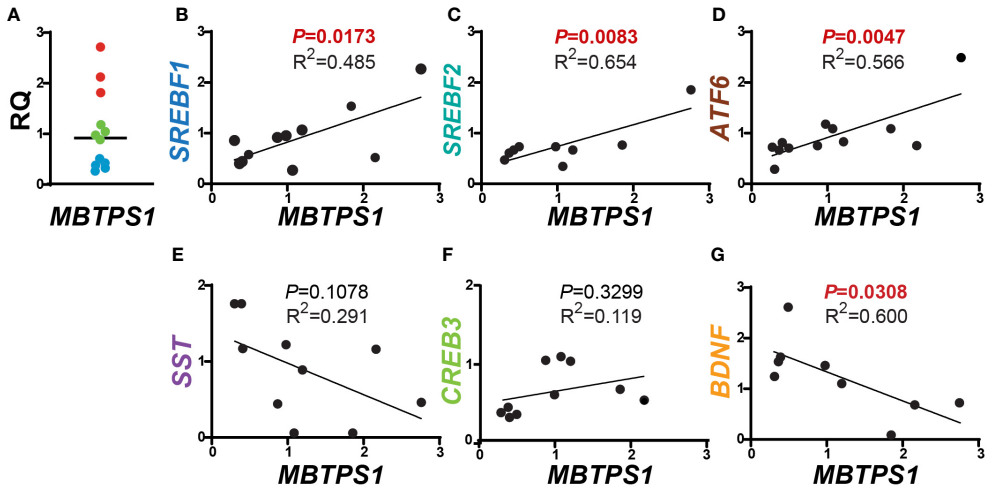

FIGURE 1
Correlations between *MBTPS1* levels and its downstream targets in human CRC. **(A)** Relative *MBTPS1* mRNA levels in tumors compared to normal surrounding tissue obtained from the same patient (*n*=12 patients). Note that while in some patients the levels of *MBTPS1* are unchanged (green circles), in others the levels are markedly elevated (red circles) or markedly reduced (light blue circles). **(B–D)** Positive correlation between *MBTPS1* and three MBTPS1 targets: *SREBF1* (r = 0.6963, *P* = 0.0173), *SREBF2* (r = 0.8086, *P* =0.0083) and *ATF6* (r = 0.7526, *P* = 0.0047). **(E, F)** No correlation between *MBTPS1* and *SST* (r = -0.5691, *P* = 0.1078) or *CREB3* (r = 0.3443, *P* = 0.3299). **(G)** A negative correlation between *MBTPS1* and *BDNF* (r = -0.7138, *P* = 0.0308).

derived epithelial adenocarcinoma cells, HT-29 and HCT-116, with a MBTPS1 chemical inhibitor (PF-429242) (36) and measured the effect on cell proliferation. We utilized a concentration of PF-429242 reported as non-toxic to other mammalian cells (37, 38). As shown in Figure 3A, attenuation of cell proliferation was evident within approximatly 48 hours of exposure to the MBTPS1 inhibitor and reached 50% at 69.5 and 83 h for HCT-116 and HT-29, respectively. 96 hours after

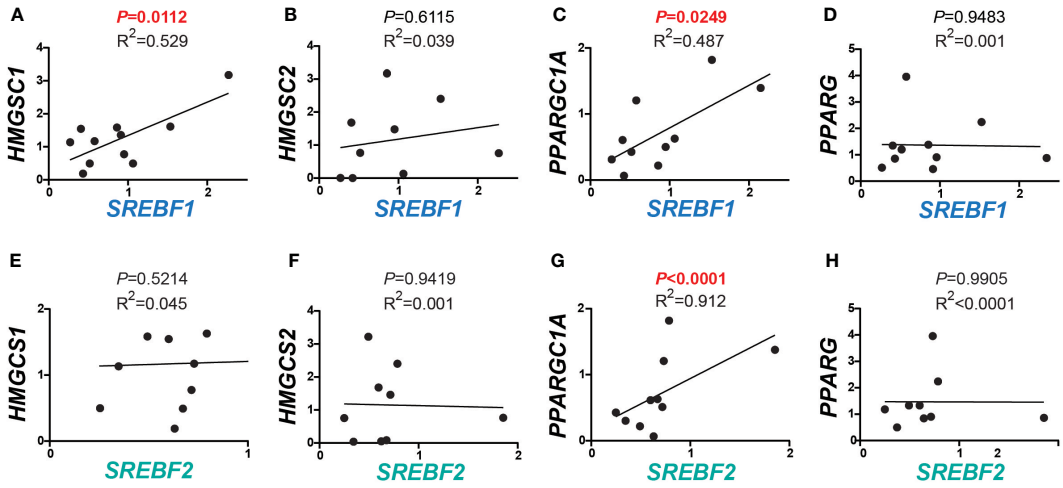

FIGURE 2
Correlations between expression of SREBFs and their downstream targets in human CRC. **(A–D)** Correlations between *SREBF1* and downstream target genes involved in lipid metabolism. *HMGCS1* and *PPARGC1A* correlated significantly with *SREBF1* (r = 0.7273, *P* = 0.0112, and 0.6978, *P* = 0.0249), while no correlations were detected with *HMGCS2* (r = 0.1970, *P* = 0.6115) and PPARG (r = -0.0236, *P* = 0.9483). **(E–H)** *SREBF2* levels were in correlation with PPARGC1A (r = 0.9552, *P*< 0.0001). No correlations were found between any of *HMGCS1* (r = 0.2127, *P* = 0.4855), *HMGCS2* (r = -0.0285, *P* = 0.9419) and *PPARG* (r = -0.0046, *P* = 0.9905) with *SREBF2*.

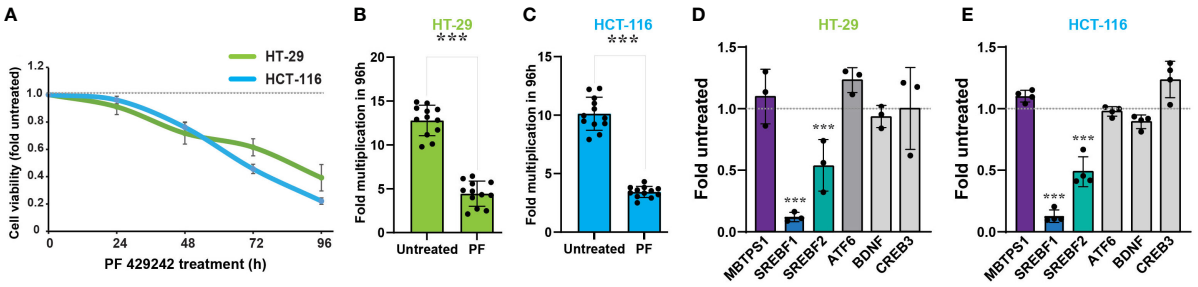

FIGURE 3
MBTPS1 is involved in proliferation of colon cancer-derived HT-29 and HCT-116 cells. **(A)** Inhibition of MBTPS1 enzymatic activity attenuates cell proliferation. Proliferation of HT-29 cells (green line) and HCT-116 (light blue line) treated with either vehicle or 10 μM PF-429242 for the entire duration of the experiment was measured using the XTT proliferation assay. Shown is an average ± SD of *n*=5 for each condition from four independent experiments. Dotted line represents proliferation of the untreated cells. **(B, C)** Rate of cell multiplication 96h after treatment of HT-29 **(B)** or HCT-116 **(C)** treated with either vehicle or 10 μM PF-429242. *n*=12 Student's *t*-test ***p<0.0001. **(D)** Relative mRNA levels of *MBTPS1* and its downstream targets 24 hours following treatment with 10 μM PF-429242 in HT-29 cells **(D)** and HCT-116 cells **(E)**. The levels of each gene were compared between PF-429242-treated cells to vehicle. The experiment was conducted in *n*=3 biological repeats with three technical repeats in each experiment. Student's *t*-test ***p<0.0001.

exposure, the rate of cell multiplication was 3-2.5 fold lower in the HT-29 and HCT-116 cells treated with PF-429242 compared to their controls, respectively (Figures 3B, C).

We next measured the transcript levels of *MBTPS1* and its downstream gene targets in HT-29 and HCT-116 cells following 24 hours of treatment with PF-429242, reasoning that the change in gene expression preceeds that of proliferation. As depicted in Figures 3D, E, inhibition of MBTPS1 did not cause a significant change in its mRNA levels in neither cell line, nor was there a change in the mRNA levels of *CREB3*, *BDNF* and *ATF6*. The most significant effect of PF-429242 treatment was observed on the mRNA levels of *SREBF1* (12% compared to the vehicle-treated cells in both lines) and in *SREBF2* (54- and 45% compared to the vehicle-treated HT-29 and HCT-116 cells, respectively). Of note is the finding that SST levels in both cell lines were below detection, suggesting that this gene does not play a significant role in the effect of MBTPS1 inhibition on proliferation of either cell line.

The dramatic effect of the MBTPS1 inhibitor, PF-429242, on proliferation of CRC cell lines suggested that elimination of the *MBTPS1* gene may slow down cell proliferation, or even halt it completely. However, we could not rule out that PF-429242 has also MBTPS1-independent effects on cell division. To this end, we attempted a CRISPR/Cas9-mediated knockout (KO) of the three alleles of the *MBTPS1* gene in HT-29 cells (Figure S2). Following this intervention and despite analysis of hundreds of clones, we succeeded in identifying only one clone in which the three allelic copies of *MBTPS1* were disrupted (Figure S2C). Accordingly, *MBTPS1* mRNA levels in this clone were reduced to less than 10% of the original cell line (Figure S2D). Consistent with the effect of the chemical inhibitor, KO of *MBTPS1* expression resulted in marked retardation of approximately 5-fold in cell proliferation rate (Figures 4A–C). The MBTPS1 KO cells showed similar levels of annexin V-positive cells as control cells (6-7%) (Figure 4D), suggesting that the retarded proliferation in cells lacking *MBTPS1* expression is not due to cell death. Furthermore, SREBP1 protein levels were significantly reduced by MBTPS1 KO (Figure 4E). Collectivity, genetic and pharmacological inhibition in colon cancer-derived HT-29 and HCT-116 cells indicate that MBTPS1 plays an essential role in proliferation of cells of this cancer type.

Pharmacological inhibition and genetic manipulation independently and consistently show that MBTPS1 plays a critical role in CRC-derived cell proliferation. Therefore, we postulated that the single *MBTPS1*-KO clone isolated following our CRISPR/Cas9 manipulation could serve to uncover both the cellular pathways affected by the absence of *MBTPS1* as well as pathways that may be upregulated to enable survival of this single KO clone. To that end, we first performed RNA-seq analysis on the control and MBTPS1 KO HT-29, which identified 3,391 genes that were differentially expressed (DE) between the two lines (FDR threshold $P<0.05$). Among these genes, 1,671 (49%) were upregulated and 1,720 (51%) were downregulated in the *MBTPS1*-KO cells compared to the unmanipulated HT-29 cells (Benjamini-Hochberg adjusted P value<0.05) (Table S1) SREBF1 and SREBF2 were among the downregulated genes, confirming the observations in (Figures 3, 4) that inhibition of MBTPS1 leads to a significant reduction in SREBFs transcript and protein levels.

We then applied a z-score cutoff of 2 (absolute value) and performed a gene ontology (GO) analysis, which resulted in a list of 87 pathways. Since many of the genes are common to more than one pathway, we calculated a pathway network describing this overlap, which resulted in eight network modules (Figure 5). In such a depiction, a positive z score reflects GO terms in which most of the genes were elevated, and vice versa for a negative z

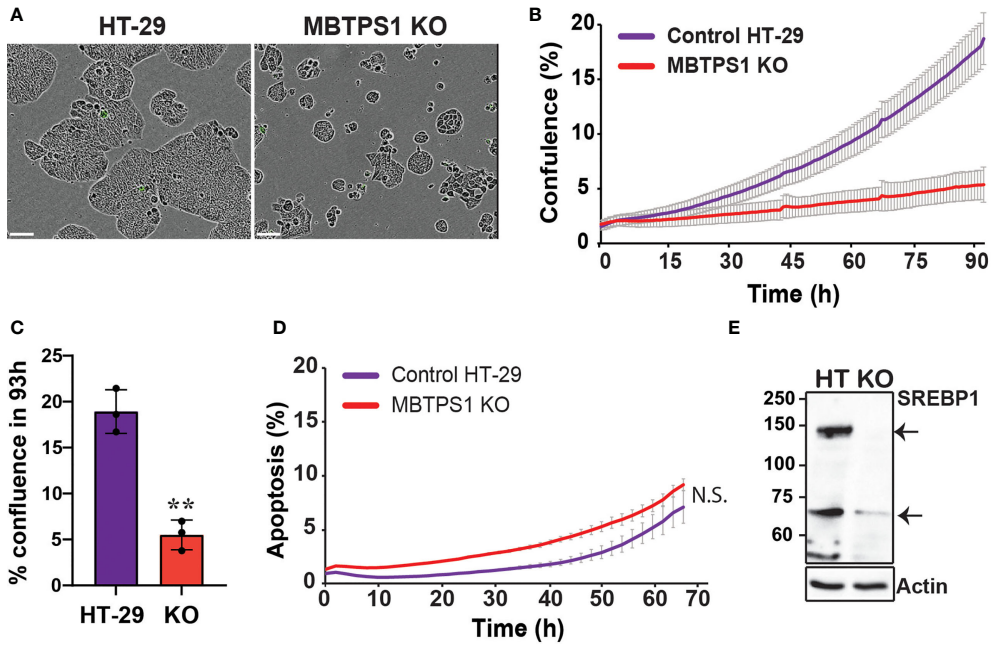

FIGURE 4
CRISPR/Cas9-mediated knockout of the MBTPS1 gene attenuates cell proliferation of colon cancer-derived HT-29 cells. **(A)** Representative images of original HT-29 and MBTPS1 KO cells. Scale bar represents 300 mm. **(B)** Knockout of MBTPS1 in HT-29 cells leads to attenuated proliferation. Shown is a representative of six independent experiments tracking the growth of original HT-29 and MBTPS1 KO cells, average ± SD of *n*=3 for each condition. **(C)** % confluence of original HT-29 and MBTPS1 KO cells 96 h after seeding (*n*=3, t-test, **P<0.001). **(D)** Staining of original HT-29 and MBTPS1 KO cells with the active caspase 3/7 reagent did not show significant differences in the percentage of apoptosis between the two cell lines. Shown is an average ± SD of *n*=2 for each condition. **(E)** A representative immunoblot of control HT-29 and MBTPS1 KO cells stained for SREBP1 showing a significant reduction in the expression of SREBP1 precursor (125 kD, top arrow) and mature SREBP1 (68 kD, bottom arrow)

score. *MBTPS1*, whose level is significantly reduced in the KO cells (Figure S2), appears in the "cellular protein modification process" term (GO:0006464), a large term that contains 1,025 genes, 223 of which are affected in the KO cells. Since this term contains slightly more upregulated than down regulated terms, it is depicted as having a positive z score. This module interconnects the largest identified modules (lipid metabolism, translation and type-1 interferon), and consistent with the patient data, MBTPS1 KO also has a marked effect on modules that include SPEBFs and ATF6 (GO:0045944).

MBTPS1 knockout upregulates the type-1 interferon pathway

In our analysis, the most dramatic effect of MBTPS1 KO appears in the form of upregulation of the type-1 interferon (type-1 IFN) pathway (Figure 5). For example, in the cellular response to type-1 IFN (GO:0071357), 34 of the 65 genes (52%) in the pathway were differentially expressed, all of which were upregulated. Similarly, in the regulation of type-1 IFN production (GO:0032479), 32 of the 89 genes (36%) in the pathway were affected, 25 of which were upregulated (Figure 5 and Table S1).

Since several studies have indicated the existence of type-1 IFN pathway in HT-29 cells (39, 40), we first tested whether inhibition of STAT1, one of the key downstream components of this pathway upregulated in the MBTPS1 KO transcriptome, affects the proliferation of the original HT-29 cells. As depicted in Figure 6A, inhibition of STAT1 caused a significant arrest in proliferation, indicating that the type-1 IFN pathway is critical for proliferation of these cells. Next, we tested whether inhibition of MBTPS1 activates the type-1 IFN pathway, by measuring the transcript levels of STAT1 in the presence of the MBTPS1 inhibitor. As shown in Figure 6B, MBTPS1 inhibition did not affect the levels of STAT1 mRNA during the first 24 hours of treatment. Notably, at that time point the levels of SREBFs were already markedly downregulated by PF-429242 (Figure 3), but there was still no apparent effect on proliferation (Figure 3A). However, by 48 hours of treatment, proliferation was already affected (Figure 3A), many cell died and the remaining ones showed marked upregulation of STAT1 (Figure 6). This confirmed that MBTPS1 inhibition leads to activation of the IFN pathway, which occurs after its effect on SREBPs.

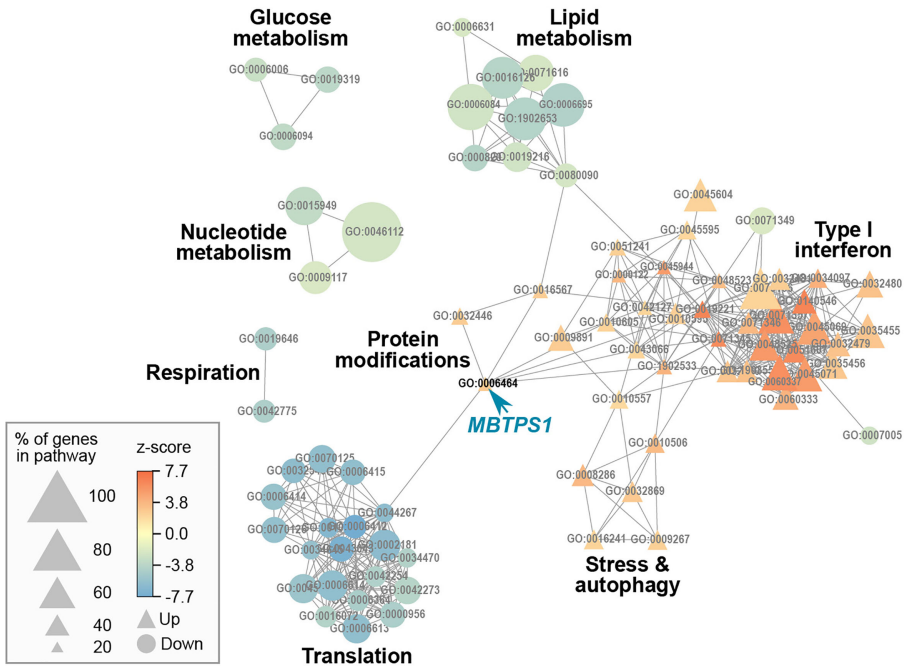

FIGURE 5
Gene ontology network of MBTPS1 KO. Overlap between pathways that are significantly enriched in the DE gene set of MBTPS1 KO compared to original HT-29 cells. GO terms are represented as nodes. The size of the node indicates the percentage of genes in the pathway that are DE. The node color represents the z-score, which calculates the trend of DE genes toward increased (Up ▲) or decreased (Down ●) expression.

Given the above findings, we tested the hypothesis that the sole MBTPS1 KO clone survived due to permanent upregulation of type-1 IFN pathway. In support, we found that STAT1 mRNA levels increased by almost 3-fold in the MBTPS1 KO cells compared to the control HT-29 cells (Figure 6C). Accordingly, the protein levels of phospho-STAT1 were markedly elevated in the knockout cells (Figure 6D). To confirm that the increase in STAT-1 mRNA and protein levels reflects an increase in a functional interferon system, we challenged control and MBTPS1 KO HT-29 cells with polyinosinic:polycytidylic acid (Poly(I:C)), an immune-stimulant that mimics viral infection (41), and measured the levels of CXCL1, one of the chemokines generated in response to this type of challenge. Measurement of CXCL1 following exposure to Poly(I:C) revealed that the original HT-29 cells lack the ability to respond to Poly(I:C) stimulation. In contrast, MBTPS1 KO cells had a significantly higher basal level of CXCL1 compared to the original HT-29 line and responded by further elevation of its levels in response to the Poly(I:C) stimulation (Figure 6E). Finally, the application of the STAT1 inhibitor arrested the proliferation of the MBTPS1 KO cells entirely (Figure 6F), providing additional support to the hypothesis that the MBTPS1 KO clone indeed survived due to upregulation of the type-1 IFN pathway.

MBTPS1 affects cell proliferation primarily through the SREBP pathway

In addition to upregulation of the type-1 IFN pathway, MBTPS1 KO was accompanied by a marked reduction in the expression of genes in five modules: glucose metabolism, lipid metabolism, nucleotide metabolism, respiration and translation (Figure 5). Of the modules that are known to be directly linked to MBTPS1, the cholesterol biosynthetic process (GO:0006695) is highlighted as the functional group with the highest changes in expression: 63% of the genes in this module are altered in the MBTPS1 KO cells, 95% of which are downregulated. In order to verify that these phenotypes are directly related to MBTPS1 KO, we reintroduced the wildtype MBTPS1 gene into the MBTPS1 KO cells and examined whether the abnormal phenotypes in these cells are rescued. Ectopic expression of *MBTPS1* in MBTPS1 KO cells only partially restored *MBTPS1* transcript levels, albeit, not to that of the original HT-29 cells (Figure 7A). In accordance with the partial rescue in MBTPS1 expression, the proliferation rate of the rescued cells was also partially restored to an intermediate level between the original and KO HT-29 cells (Figure 7B). Subsequent measurements of MBTPS1 targets revealed that *CREB3* and *ATF6* mRNA levels were not

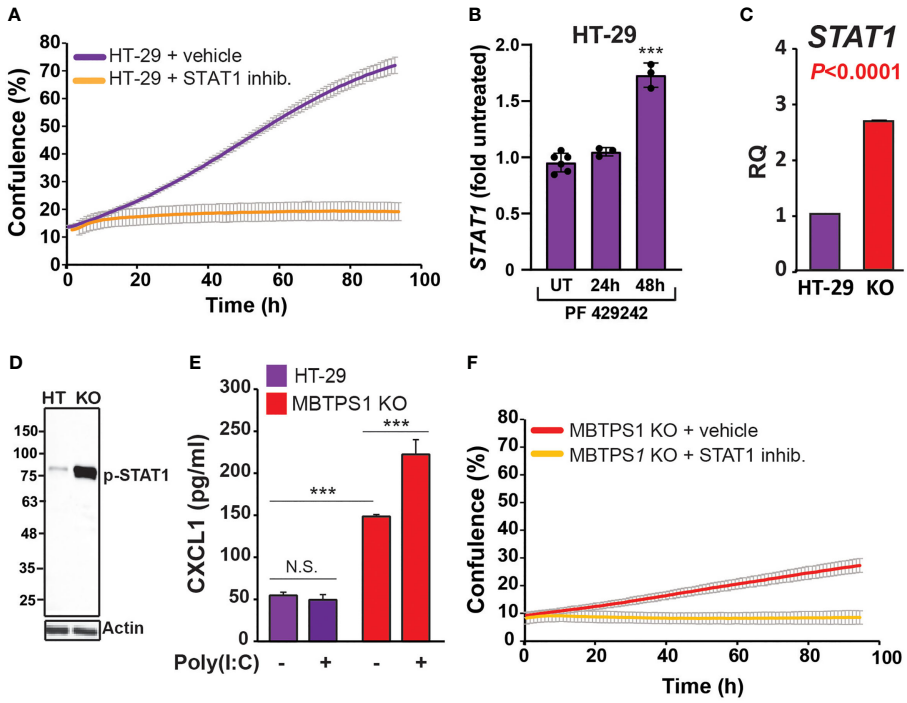

FIGURE 6
MBTPS1 knockout upregulates the type-1 interferon pathway. **(A)** STAT1 activity is critical for proliferation of HT-29 cells. Proliferation of HT-29 cells treated with either vehicle or 25 mM STAT1 inhibitor fludarabine was tracked over 96 h using time-laps microscopy. Shown is an average ± SD *n*=3 for each condition. **(B)** Relative STAT1 mRNA levels 24 and 48 hours following treatment with 10 mM PF-429242 in HT-29 cells. *n*=3-6 One –Way ANOVA ***p<0.0001. **(C)** Relative mRNA levels of STAT1 in the original and MBTPS1 knockout HT-29 cells (*n*=3, t-test, P<0.0001). The levels of STAT1 in the knockout are markedly elevated, in accordance with the transcriptome data. **(D)** Immunoblot of control HT-29 and MBTPS1 KO cells show elevated levels of phosphorylated STAT1 (p-STAT1). Representative blots of n=3. **(E)** MBTPS1 KO cells show a functional response to poly(I:C) stimulation. Shown is CXCL1 production in response to stimulation of HT-29 or MBTPS1 KO cells with 50 mg/ml poly(I:C) overnight (*n*=4 repeats). **(F)** Proliferation of MBTPS1 KO cells treated with either vehicle or 25 mM STAT1 inhibitor fludarabine. Shown is an average ± SD n=3 for each condition. N.S., not significant.

significantly affected by re-expression of *MBTPS1* (Figures 7C, D). *BDNF* levels were eliminated almost completely in the MBTPS1 KO cells but since they recovered completely upon reintroduction of *MBTPS1* (Figure 7E), they probably do not play a significant role in MBTPS1-mediated regulation of HT-29 cell divisions, or their role is not reflected in changes in mRNA levels.

In agreement with the transcriptome analysis, RT-qPCR analysis revealed that the levels of both SREBFs were significantly reduced by MBTPS1 KO. In particular, *SREBF1* expression was completely lost in MBTPS1 KO cells. Despite the partial recovery in *MBTPS1* levels, the recovery of *SREBF1* expression was minor but significant (Figure 7F). *SREBF2* levels were also markedly affected by MBTPS*1* knockout and recovered partially, albeit to higher levels than *SREBF1* (Figure 7G). Partial recovery was also observed in mRNA levels of the downstream affected genes *HMGCS1* and *PPARGC1A* (Figures 7H, I). Remarkably, knockout of *MBTPS1* caused a marked elevation in *HMGCS2* levels (Figure 7J), which was not reduced back to normal levels following the reintroduction of *MBTPS1*, suggesting that despite the partial re-expression of *MBTPS1*, the cells continued to display an energy-deprived phenotype.

Discussion

Here, we investigated the direct involvement of MBTPS1 in colon cancer by integrating data from human CRC tumors and *in vitro* models of CRC-derived cell lines. The dataset obtained from patients with colorectal cancer provided valuable information regarding significant correlations between MBTPS1 expression and some, but not all, of its downstream targets. However, it did not offer mechanistic information regarding the role of MBTPS1 in proliferation. Conversely, manipulating MBTPS1 activity in the CRC-derived cell lines provided insights into its role in CRC proliferation. A previous study has indicated that other PCs, furin and PC5A enhance

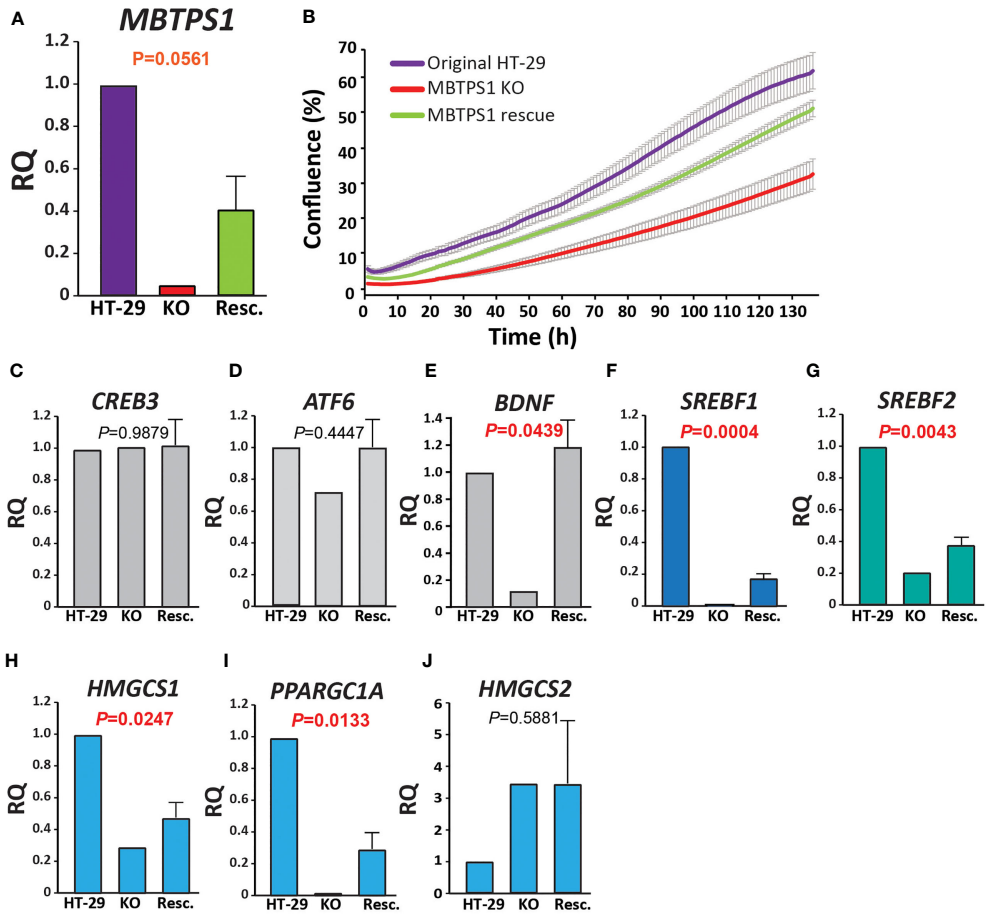

FIGURE 7
MBTPS1-mediated effect on proliferation is dependent mainly upon the SREBP pathway. **(A)** Relative mRNA levels of *MBTPS1* in original (HT-29), MBTPS1 KO and re-expression of MBTPS1 (Rescue) HT-29 cells. *P*-values indicate a significant difference between KO and Resc. HT-29 cells Reintroduction of the *MBTPS1* gene into the KO cells resulted in partial recovery of its mRNA levels (n=4). **(B)** Proliferation of HT-29, MBTPS1 KO and MBTPS1 rescued cells was tracked using time-lapse microscopy. Shown is an average ± SD of n=3 for each condition from four independent experiments. In accordance with the partial recovery in MBTPS1 expression, the rate of proliferation of the cells with ectopic MBTPS1 expression was intermediate between the original and the KO cells. **(C, D)** No significant effect of MBTPS1 rescue on the relative mRNA expression of MBTPS1 targets *CREB3* and *ATF6* (*P*=0.09879 and 0.4447, respectively). **(E)** Significant reduction in the expression of *BDNF* in MBTPS1 KO cells and its complete recovery in the cells with ectopic MBTPS1 expression (*P*=0.0439). **(F, G)** Significant effect of MBTPS1 expression on its downstream targets *SREBF1* (*P*=0.0004) and *SREBF2* (*P*=0.0043). The levels of both targets drop significantly and show a small but significant recovery. **(H, I)** Significant reduction and partial recovery of the SREBP downstream targets *HMGCS1* (*P*=0.0247) and *PPARGC1A* (*P*=0.0133). **(J)** The absence of MBTPS1 causes a marked elevation in *HMGSC2* that is not restored to normal levels after partial recovery of MBTPS1 (*P*=0.5881), suggesting that part of the transcriptional changes that occurred in the MBTPS1 KO cells are irreversible. n=2-4 repeats, One-Way ANOVA, *P*<0.05 significant.

proliferation of HT-29 cells by cleavage of the IGF-1 receptor (42). By combining the information derived from the two datasets herein, we conclude that another PC, MBTPS1 plays a significant role in regulating proliferation of colorectal cancer cells.

MBTPS1 has several known substrates. In order to identify which of them may be involved in CRC proliferation we used a combined strategy of patient and cell-derived data. Using this approach we found that while CREB3, SST and BDNF may be involved in CRC, they are not the downstream mediators of MBTPS1 on proliferation. Surprisingly, ATF6, a well-known target of MBTPS1 whose expression levels were found to be in strong correlation with those of MBTPS1 in the patient samples, does not play a significant role in the MBTPS1-mediated regulation of CRC-derived cell proliferation (Figures 3, 7). However, studies show that ATF6 may also be activated by specific lipids (16), which may explain the correlation between ATF6 and MBTPS1 levels in CRC tumors.

The SREBP1/2 pathway was the only one that showed similar trends in the tumors and the MBTPS1 KO cells, results

which are in agreement with earlier findings which showed that downregulation of SREBPs inhibits tumor growth in colon cancer (20). In the tumors, there was a strong positive correlation between the expression of *MBTPS1* and both *SREBPs* (Figures 1A, B), and between *SREBP1* and its downstream targets (Figures 2A, C). Interestingly, despite the strong correlation between expression levels of *SREBP1* and *SREBP2* (Figure S1), no correlation was detected between expression of *SREBP2* and *HMGCS1* in tumors (Figure 2E), suggesting that the effect on *HMGCS1* is mediated *via* SREBP1, but not SREBP2. Furthermore, no correlations were evident between either SREBPs and HMGCS2, that regulates ketogenesis (43), or with PPARG, that is activated by PPARGC1A (44). The most significant change in the MBTPS1 KO cells also occurred in the SREBP pathway. The expression of both SREBPs, and especially SREBP1, was significantly reduced in the absence of MBTPS1 (Figures 7F, G), and the transcript levels of downstream targets of SREBPs, HMGCS1 and PPARGC1A, were also downregulated to a great extent (Figures 7G–I). Interestingly, MBTPS1 KO upregulated HMGCS2 mRNA levels by more than 3-fold, suggesting that the MBTPS1 KO cells display a phenotype of fasting cells. In contrast to partial recovery of other downstream targets following ectopic expression of MBTPS1, HMGCS2 expression remained elevated (Figure 7J), suggesting that part of the changes in the MBTPS1 KO cells are secondary to MBTPS1 elimination and are irreversible.

The results presented in this study demonstrate that impairment of MBTPS1 activity or KO of its gene is detrimental to CRC cells. This is best illustrated by the fact that despite our vast attempts, we obtained only one clone that proliferated following the KO of the three *MBTPS1* alleles in HT-29 CRC cells. Based on findings from the gene expression analysis of this KO clone as well as additional experiments, we showed that the survival of this clone is most likely due to upregulation of the type-1 IFN pathway. Importantly, HT-29 cells depend on this pathway for their proliferation (Figures 6A, B), but in the MBTPS1 KO cells this pathway was upregulated even further. An interplay between the immune system and lipid synthesis was reported previously, although in contrast to our system, it involved signaling between more than a single cell type. A prominent study identified a crucial role for SREBPs in regulating the intra-tumor response of Regulatory T cells (Treg), which drive immunosuppression in the tumor microenvironment (45). In this latter study, inhibition of SREBP-dependent lipid synthesis caused reprogramming of Treg cells such that it enabled an effective anti-tumor immune response by other cells within the tumor environment. In our study, the reduction or absence of MBTPS1 in CRC cells downregulated SREBPs and upregulated the intracellular type-1 IFN system. Furthermore, the levels of STAT1, which increased significantly in the KO cells (Figure 6A), remained high even after re-introduction of MBTPS1 into the cells (2.38 + 0.7 fold). Together these findings suggest that upregulation of type-1 interferon response enabled the proliferation of CRC cells despite the loss of MBTPS1. Further studies are required to understand how the mechanistic relationship between these two pathways.

MBTPS1 KO cells were grown in a nutrient-rich environment that contains high glucose levels and is supplemented with fetal bovine serum that includes lipids, carbohydrates, protein and cholesterol (46). Nonetheless, these cells presented with a phenotype of hunger and low energy, reflected by high HMGSC2 levels that provide lipid-derived energy during carbohydrate deprivation (Figure 7J). Since cholesterol synthesis and uptake are regulated at the transcriptional level by SREBPs, it is plausible that the levels of key enzymes such as HMG CoA reductase (the rate-limiting enzyme for cholesterol biosynthesis) and LDLR, which mediates endocytosis of cholesterol-rich LDLs (47), are affected by MBTPS1 KO, thus causing imbalance in lipid metabolism that affects additional central metabolic pathways including glycolysis and the respiratory electron transport chain.

In conclusion, using a combined chemical and CRISPR/Cas9 – gene knockout approach we show that MBTPS1 plays a pivotal role in proliferation of colon cancer cells. Furthermore, by comparing data from human CRC samples to that of CRC-derived cell lines we were able to rule out the involvement of certain downstream MBTPS1 targets in regulating proliferation, and to identify the SREBP pathway as most likely responsible for this effect. Nonetheless, the data herein only studies the effect of MBTPS1 KO on cell proliferation. Thus, we cannot completely rule out the possibility that the other MBTPS1 targets affect additional cellular functions that may have an indirect effect on cell survival. Whether MBTPS1 inhibition may serve as an additional therapeutic target in CRC remains to be determined.

Data availability statement

The datasets presented in this study can be found in online repositories. The names of the repository/repositories and accession number(s) can be found in the article/Supplementary Material.

Ethics statement

The studies involving human participants were reviewed and approved by Institutional Review Board of Ha'Emek Medical Center (protocol code 0049–19-EMC 6 January 2022). The patients/participants provided their written informed consent to participate in this study.

Author contributions

Conceptualization, SS and LB-H; Data curation, ML; Formal analysis, LH-B, ES, STo, ML, OAH, STa, SS, and LB-H; Funding

acquisition, OAH and LB-H; Investigation, LH-B, ES, STo, LS, OAH, STa, and SS; Methodology, SS and LB-H; Project administration, STa and LB-H; Resources, LB-H; Supervision, SS and LB-H; Validation, ML; Visualization, STa and LB-H; Writing – original draft, SS and LB-H; Writing – review & editing, LH-B, STo, SS, and LB-H. All authors contributed to the article and approved the submitted version.

Funding

This work was supported by the Israel Science foundation [#1445/15 & 2240/19] and by the Israel Cancer Association [#20210063] to LB-H.

Acknowledgments

We thank Ms. Liran Giladi for technical assistance, Dr. Amiram Ariel for materials and discussion regarding the type-1 interferon pathway, and Drs. Martin Mikl, Amir Sapir and Hila Toledano for critical manuscript comments.

Conflict of interest

The authors declare that the research was conducted in the absence of any commercial or financial relationships that could be construed as a potential conflict of interest.

Publisher's note

Supplementary material

The Supplementary Material for this article can be found online at: https://www.frontiersin.org/articles/10.3389/fonc.2022.1004014/full#supplementary-material

References

1. Vazquez A, Kamphorst JJ, Markert E, Schug ZT, Tardito S, Gottlieb E. Cancer metabolism at a glance. *J Cell Sci* (2016) 129:3367–73. doi: 10.1242/jcs.181016

2. Snaebjornsson MT, Janaki-Raman S, Schulze A. Greasing the wheels of the cancer machine: The role of lipid metabolism in cancer. *Cell Metab* (2020) 31:62–76. doi: 10.1016/j.cmet.2019.11.010

3. Mullen PJ, Yu R, Longo J, Archer MC, Penn LZ. The interplay between cell signalling and the mevalonate pathway in cancer. *Nat Rev Cancer* (2016) 16:718–31. doi: 10.1038/nrc.2016.76

4. Horton JD, Shah NA, Warrington JA, Anderson NN, Park SW, Brown MS, et al. Combined analysis of oligonucleotide microarray data from transgenic and knockout mice identifies direct SREBP target genes. *P Natl Acad Sci USA* (2003) 100:12027–32. doi: 10.1073/pnas.1534923100

5. Brown MS, Goldstein JL. A proteolytic pathway that controls the cholesterol content of membranes, cells, and blood. *P Natl Acad Sci USA* (1999) 96:11041–8. doi: 10.1073/pnas.96.20.11041

6. Brown MS, Ye J, Rawson RB, Goldstein JL. Regulated intramembrane proteolysis: a control mechanism conserved from bacteria to humans. *Cell* (2000) 100:391–8. doi: 10.1016/S0092-8674(00)80675-3

7. Sakai J, Rawson RB, Espenshade PJ, Cheng D, Seegmiller AC, Goldstein JL, et al. Molecular identification of the sterol-regulated luminal protease that cleaves SREBPs and controls lipid composition of animal cells. *Mol Cell* (1998) 2:505–14. doi: 10.1016/S1097-2765(00)80150-1

8. Seidah NG, Mowla SJ, Hamelin J, Mamarbachi AM, Benjannet S, Toure BB, et al. Mammalian subtilisin kexin isozyme SKI-1: A widely expressed proprotein convertase with a unique cleavage specificity and cellular localization. *P Natl Acad Sci USA* (1999) 96:1321–6. doi: 10.1073/pnas.96.4.1321

9. Marschner K, Kollmann K, Schweizer M, Braulke T, Pohl S. A key enzyme in the biogenesis of lysosomes is a protease that regulates cholesterol metabolism. *Science* (2011) 333:87–90. doi: 10.1126/science.1205677

10. Ye J, Rawson RB, Komuro R, Chen X, Dave UP, Prywes R, et al. ER stress induces cleavage of membrane-bound ATF6 by the same proteases that process SREBPs. *Mol Cell* (2000) 6:1355–64. doi: 10.1016/S1097-2765(00)00133-7

11. Raggo C, Rapin N, Stirling J, Gobeil P, Smith-Windsor E, O'Hare P, et al. Luman, the cellular counterpart of herpes simplex virus VP16, is processed by regulated intramembrane proteolysis. *Mol Cell Biol* (2002) 22:5639–49. doi: 10.1128/MCB.22.16.5639-5649.2002

12. Stirling J, O'Hare P. CREB4, a transmembrane bZip transcription factor and potential new substrate for regulation and cleavage by S1P. *Mol Biol Cell* (2006) 17:413–26. doi: 10.1091/mbc.e05-06-0500

13. Toure BB, Munzer JS, Basak A, Benjannet S, Rochemont J, Lazure C, et al. Biosynthesis and enzymatic characterization of human SKI-1/S1P and the processing of its inhibitory prosegment. *J Biol Chem* (2000) 275:2349–58. doi: 10.1074/jbc.275.4.2349

14. Mouchantaf R, Watt HL, Sulea T, Seidah NG, Alturaihi H, Patel YC, et al. Prosomatostatin is proteolytically processed at the amino terminal segment by subtilase SKI-1. *Regul Peptides*. (2004) 120:133–40. doi: 10.1016/j.regpep.2004.02.022

15. Chakrabarti A, Chen AW, Varner JD. A review of the mammalian unfolded protein response. *Biotechnol Bioeng*. (2011) 108:2777–93. doi: 10.1002/bit.23282

16. Tam AB, Roberts LS, Chandra V, Rivera IG, Nomura DK, Forbes DJ, et al. The UPR activator ATF6 responds to proteotoxic and lipotoxic stress by distinct mechanisms. *Dev Cell*. (2018) 46(3):327–343.e7. doi: 10.1016/j.devcel.2018.04.023

17. Chen XQ, Zhang FF, Gong Q, Cui AY, Zhuo S, Hu ZM, et al. Hepatic ATF6 increases fatty acid oxidation to attenuate hepatic steatosis in mice through peroxisome proliferator-activated receptor alpha. *Diabetes* (2016) 65:1904–15. doi: 10.2337/db15-1637

18. Sampieri L, Di Giusto P, Alvarez C. CREB3 transcription factors: ER-golgi stress transducers as hubs for cellular homeostasis. *Front Cell Dev Biol* (2019) 7. doi: 10.3389/fcell.2019.00123

19. Li JN, Mahmoud MA, Han WF, Ripple M, Pizer ES. Sterol regulatory element-binding protein-1 participates in the regulation of fatty acid synthase expression in colorectal neoplasia. *Exp Cell Res* (2000) 261:159–65. doi: 10.1006/excr.2000.5054

20. Wen YA, Xiong XP, Zaytseva YY, Napier DL, Vallee E, Li AT, et al. Downregulation of SREBP inhibits tumor growth and initiation by altering cellular metabolism in colon cancer. *Cell Death Dis* (2018) 9, 265. doi: 10.1038/s41419-018-0330-6

21. Liu YX, Hua WW, Li Y, Xian XR, Zhao Z, Liu C, et al. Berberine suppresses colon cancer cell proliferation by inhibiting the SCAP/SREBP-1 signaling pathway-mediated lipogenesis. *Biochem Pharmacol* (2020) 174. doi: 10.1016/j.bcp.2019.113776

22. Liu CY, Hsu CC, Huang TT, Lee CH, Chen JL, Yang SH, et al. ER stress-related ATF6 upregulates CIP2A and contributes to poor prognosis of colon cancer. *Mol Oncol* (2018) 12:1706–17. doi: 10.1002/1878-0261.12365

23. Coleman OI, Lobner EM, Bierwirth S, Sorbie A, Waldschmitt N, Rath E, et al. Activated ATF6 induces intestinal dysbiosis and innate immune response to promote colorectal tumorigenesis. *Gastroenterology* (2018) 155:1539. doi: 10.1053/j.gastro.2018.07.028

24. Yang XM, Martin TA, Jiang WG. Biological influence of brain-derived neurotrophic factor (BDNF) on colon cancer cells. *Exp Ther Med* (2013) 6:1475–81. doi: 10.3892/etm.2013.1330

25. Huang SM, Lin CJ, Lin HY, Chiu CM, Fang CW, Liao KF, et al. Brain-derived neurotrophic factor regulates cell motility in human colon cancer. *Endocr-Relat Cancer* (2015) 22:455–64. doi: 10.1530/ERC-15-0007

26. Konoshita T, Gasc JM, Villard E, Takeda R, Seidah NG, Corvol P, et al. Expression of Pc2 and Pc1/Pc3 in human pheochromocytomas. *Mol Cell Endocrinol* (1994) 99:307–14. doi: 10.1016/0303-7207(94)90022-1

27. Mbikay M, Sirois F, Yao J, Seidah NG, Chretien M. Comparative analysis of expression of the proprotein convertases furin, PACE4, PC1 and PC2 in human lung tumours. *Brit J Cancer* (1997) 75:1509–14. doi: 10.1038/bjc.1997.258

28. Bassi DE, Fu J, de Cicco RL, Klein-Szanto AJP. Proprotein convertases: "Master switches" in the regulation of tumor growth and progression. *Mol Carcinogen.* (2005) 44:151–61. doi: 10.1002/mc.20134

29. Weiss N, Stegemann A, Elsayed MAT, Schallreuter KU, Luger TA, Loser K, et al. Inhibition of the prohormone convertase subtilisin-kexin isoenzyme-1 induces apoptosis in human melanoma cells. *J Invest Dermatol* (2014) 134:168–75. doi: 10.1038/jid.2013.282

30. Caruana BT, Skoric A, Brown AJ, Lutze-Mann LH. Site-1 protease, a novel metabolic target for glioblastoma. *Biochem Bioph. Res Co* (2017) 490:760–6. doi: 10.1016/j.bbrc.2017.06.114

31. Saadi E, Sood R, Dromi I, Srouji R, Hatoum OA, Tal S, et al. Limited proteolysis of cyclooxygenase-2 enhances cell proliferation. *Int J Mol Sci* (2020) 21 (9):3195. doi: 10.3390/ijms21093195

32. Ran FA, Hsu PD, Wright J, Agarwala V, Scott DA, Zhang F. Genome engineering using the CRISPR-Cas9 system. *Nat Protoc* (2013) 8:2281–308. doi: 10.1038/nprot.2013.143

33. Xie Z, Bailey A, Kuleshov MV, Clarke DJB, Evangelista JE, Jenkins SL, et al. Gene set knowledge discovery with enrichr. *Curr Protoc* (2021) 1:e90. doi: 10.1002/cpz1.90

34. Hegardt FG. Mitochondrial 3-hydroxy-3-methylglutaryl-CoA synthase: a control enzyme in ketogenesis. *Biochem J* (1999) 338:569–82. doi: 10.1042/bj3380569

35. Oberkofler H, Schraml E, Krempler F, Patsch W. Restoration of sterol-regulatory-element-binding protein-1c gene expression in HepG2 cells by peroxisome-proliferator-activated receptor-gamma co-activator-1 alpha. *Biochem J* (2004) 381:357–63. doi: 10.1042/BJ20040173

36. Hay BA, Abrams B, Zumbrunn AY, Valentine JJ, Warren LC, Petras SF, et al. Aminopyrrolidineamide inhibitors of site-1 protease. *Bioorganic Medicinal Chem Lett* (2007) 17:4411–4. doi: 10.1016/j.bmcl.2007.06.031

37. Machado PD, Gomes PS, Midlej V, Coimbra ES, Guedes HLD. PF-429242, a subtilisin inhibitor, is effective *in vitro* against leishmania infantum. *Front Microbiol 12* (2021) 17(16):4411–4414. doi: 10.3389/fmicb.2021.583834

38. Pasquato A, Rochat C, Burri DJ, Pasqual G, de la Torre JC, Kunz S. Evaluation of the anti-arenaviral activity of the subtilisin kexin isozyme-1/site-1 protease inhibitor PF-429242. *Virology* (2012) 423:14–22. doi: 10.1016/j.virol.2011.11.008

39. Frias AH, Jones RM, Fifadara NH, Vijay-Kumar M, Gewirtz AT. Rotavirus-induced IFN-beta promotes anti-viral signaling and apoptosis that modulate viral replication in intestinal epithelial cells. *Innate Immun* (2012) 18:294–306. doi: 10.1177/1753425911401930

40. Mukherjee S, Biswas R, Biswas T. Alternative TLRs are stimulated by bacterial ligand to induce TLR2-unresponsive colon cell response. *Cell Signal* (2013) 25:1678–88. doi: 10.1016/j.cellsig.2013.04.008

41. Matsumoto M, Seya T. TLR3: Interferon induction by double-stranded RNA including poly(I : C). *Adv Drug Deliver Rev* (2008) 60:805–12. doi: 10.1016/j.addr.2007.11.005

42. Khatib AM, Siegfried G, Prat A, Luis J, Chretien M, Metrakos P, et al. Inhibition of proprotein convertases is associated with loss of growth and tumorigenicity of HT-29 human colon carcinoma cells - importance of insulin-like growth factor-1 (IGF-1) receptor processing in IGF-1-mediated functions. *J Biol Chem* (2001) 276:30686–93. doi: 10.1074/jbc.M101725200

43. Puchalska P, Crawford PA. Multi-dimensional roles of ketone bodies in fuel metabolism, signaling, and therapeutics. *Cell Metab* (2017) 25:262–84. doi: 10.1016/j.cmet.2016.12.022

44. Vega RB, Huss JM, Kelly DP. The coactivator PGC-1 cooperates with peroxisome proliferator-activated receptor alpha in transcriptional control of nuclear genes encoding mitochondrial fatty acid oxidation enzymes. *Mol Cell Biol* (2000) 20:1868–76. doi: 10.1128/MCB.20.5.1868-1876.2000

45. Lim SA, Wei J, Nguyen TLM, Shi H, Su W, Palacios G, et al. Lipid signalling enforces functional specialization of T-reg cells in tumours. *Nature* (2021) 591 (7849):306–311. doi: 10.1038/s41586-021-03235-6

46. Zidovetzki R, Levitan I. Use of cyclodextrins to manipulate plasma membrane cholesterol content: Evidence, misconceptions and control strategies. *Bba-Biomembranes* (2007) 1768:1311–24. doi: 10.1016/j.bbamem.2007.03.026

47. Shimano H, Sato R. SREBP-regulated lipid metabolism: convergent physiology - divergent pathophysiology. *Nat Rev Endocrinol* (2017) 13:710–30. doi: 10.1038/nrendo.2017.91

frontiers | Frontiers in Oncology

TYPE Review
PUBLISHED 17 October 2022
DOI 10.3389/fonc.2022.994672

OPEN ACCESS

EDITED BY
Federica Sotgia,
University of Salford, United Kingdom

REVIEWED BY
Diego Gabriel Ogando,
Indiana University, United States
Martina Chiu,
University of Parma, Italy
Jun-Jen Liu,
Taipei Medical University, Taiwan

*CORRESPONDENCE
Yehui Duan
duanyehui@isa.ac.cn
Wei Liu
weiliupro@hunau.edu.cn

SPECIALTY SECTION
This article was submitted to Cancer Metabolism, a section of the journal Frontiers in Oncology

RECEIVED 26 July 2022
ACCEPTED 30 September 2022
PUBLISHED 17 October 2022

CITATION
Gong T, Zheng C, Ou X, Zheng J, Yu J, Chen S, Duan Y and Liu W (2022) Glutamine metabolism in cancers: Targeting the oxidative homeostasis. *Front. Oncol.* 12:994672. doi: 10.3389/fonc.2022.994672

Glutamine metabolism in cancers: Targeting the oxidative homeostasis

Tengfang Gong[1], Changbing Zheng[2], Xidan Ou[1], Jie Zheng[2,3], Jiayi Yu[2,3], Shuyu Chen[1], Yehui Duan[2,3]* and Wei Liu[1]*

[1]Research Center for Parasites & Vectors, College of Veterinary Medicine, Hunan Agricultural University, Changsha, China, [2]CAS Key Laboratory of Agro-ecological Processes in Subtropical Region, Hunan Provincial Key Laboratory of Animal Nutritional Physiology and Metabolic Process, National Engineering Laboratory for Pollution Control and Waste Utilization in Livestock and Poultry Production, Institute of Subtropical Agriculture, Chinese Academy of Sciences, Changsha, China, [3]College of Advanced Agricultural Sciences, University of Chinese Academy of Sciences, Beijing, China

Glutamine is the most abundant amino acid in blood and tissues, and the most important nutrient except for glucose in cancer cells. Over the past years, most studies have focused on the role of Gln metabolism in supporting energy metabolism rather than maintaining oxidative homeostasis. In fact, Gln is an important factor in maintaining oxidative homeostasis of cancer cells, especially in "Glutamine addicted" cancer cells. Here, this paper will review the recent scientific literature about the link between Gln metabolism and oxidative homeostasis, with an emphasis on the potential role of Gln metabolism in different cancers. Given that oxidative homeostasis is of critical importance in cancer, understanding the impacts of a Gln metabolism on oxidative homeostasis, gaining great insights into underlying molecular mechanisms, and developing effective therapeutic strategies are of great importance.

KEYWORDS

Gln metabolism, oxidative homeostasis, cancer cells, ROS, health

Introduction

The reactive oxygen species (ROS), which mainly comes from the mitochondrial membrane as a byproduct of OXPHOS and nicotinamide adenine dinucleotide oxidases (NOXs), cannot avoid being produced in cellular metabolism (1–4). Cancer cells usually show higher levels of ROS, which acts as a signaling molecule in cancer, contributing to their growth and metastasis (5–8). Notably, when the levels of ROS in cancer cells are in excess, it will destroy oxidative homeostasis, subsequently damaging effects on macromolecules such as enzyme inactivation, DNA and protein damage (Figure 1) (9, 10). Thus, maintaining oxidative homeostasis in cancer cells is of great importance and loss of balance has profound pathophysiology consequences (11).

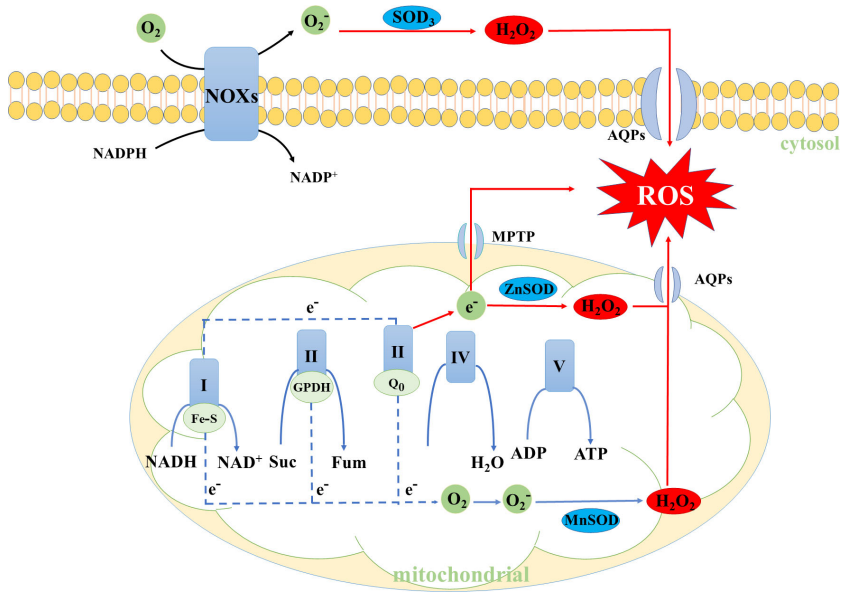

FIGURE 1
The primary generation mechanisms of intracellular ROS. SOD, Superoxide dismutase.

Glutamine (Gln), a non-essential amino acid, is essential for the survival of most cancer cells. The "Glutamine addiction" is a good description of the importance of Gln in cancer cells. When Gln is deprived of the medium, most cancer cells will be in a stagnant state or even die (12, 13). Gln metabolism, which could promote the biosynthesis of Glutathione (GSH) and nicotinamide adenine dinucleotide phosphate (NADPH), is involved in the maintenance of oxidative homeostasis in cancer cells (14). In light of the importance of Gln metabolism in oxidative homeostasis, a comprehensive understanding of the mechanics is vital for developing of tumor therapies. This review will elaborate on the functions of Gln and its products in the oxidative homeostasis of cancer cells, including roles in the biosynthesis of GSH and NADPH, and will explore the roles of Gln metabolism in different cancers *via* regulating oxidative homeostasis.

Gln metabolism in oxidative homeostasis

The Gln metabolism could maintain oxidative homeostasis through many pathways. One of the most important pathways is through promoting the biosynthesis of GSH. Glutamate (Glu), cysteine, and glycine are required amino acids for *de novo* biosynthesis of GSH (15–17). Notably, the conversion of Gln to Glu is required to maintain the large intracellular pools of Glu (13). Typically, Gln is first taken in by cancer cells through the transporters (such as ASCT2, $ATB^{0,+}$, System L, System A), and then converted to Glu (18–20). The Gln-converted Glu subsequently generates GSH in two ways (Figure 2). On the one hand, Glu can be polymerized with cysteine in an ATP-dependent manner to form γ-glutamylcysteine, and further condense with glycine to produce GSH (21–24). On the other hand, Glu is transported *via* cystine/glutamate antiporter xCT (also commonly known as SLC7A11) to the extracellular for exchanging cystine and a subsequent conversion of cystine to cysteine through a NADPH-consuming reduction reaction. The generated cysteine is subsequently used to form GSH (25, 26). GSH is a powerful reducing agent that acts as a free radical scavenger. Maintaining high levels of GSH in cancer cells can eliminate excessive ROS and detoxify xenobiotics to avoid oxidative damage.

Besides the role in the *de novo* biosynthesis of GSH, Gln also contributes to NADPH production. First, Gln enters the TCA cycle, and directly generates malate, or indirectly forms malate from the conversion of Asp *via* the Asp transporter mitochondrial uncoupling protein 2 (UCP2) and the enzymes aspartate transaminase (GOT1) and malate dehydrogenase 1 (MDH1). Then, malate crosses the mitochondrial membrane to the cytoplasm and is further catalyzed to pyruvate *via* the malic enzyme 1 (ME1), accompanied by reducing NADP to NADPH (27–29). Importantly, NADPH can reduce glutathione disulfide (GSSG) to GSH, an essential cofactor maintaining the reduced form of GSH (30, 31). On the other hand, NADPH can reduce cystine to cysteine for *de novo* biosynthesis of GSH (32, 33). Therefore, NADPH plays a role in the production of GSH, thus contributing to the maintenance of redox balance.

Overall, the Gln metabolism in this review refers to the metabolic pathway of the formation of GSH and NADPH from

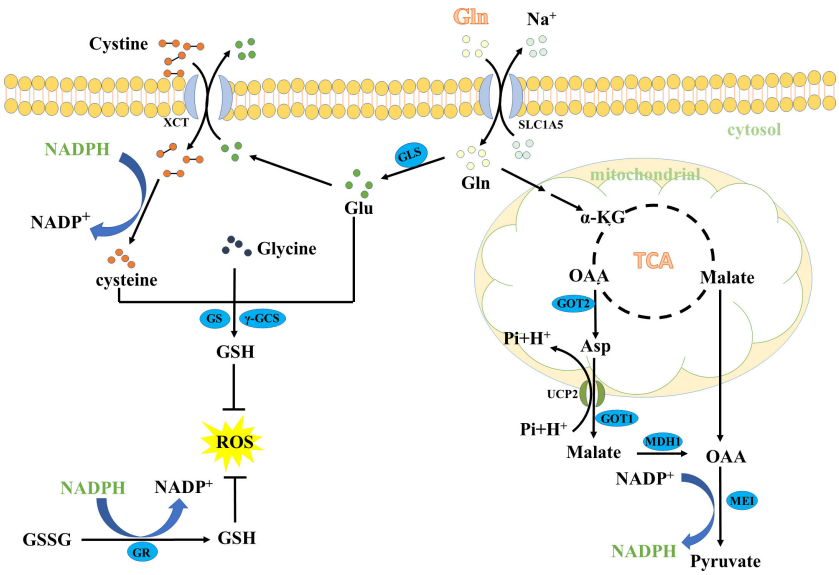

FIGURE 2
The key role of glutamine in GSH and NADPH biosynthesis. MDH1, malate dehydrogenase 1; SLC1A5, the solute carrier family 1, member 5.

Gln, which could help maintain oxidative homeostasis of cancer cells and hence promote their progression.

The potential role of Gln metabolism in different cancers

Gln metabolism has different potential roles in different cancer cells by maintaining oxidative homeostasis and is crucial for cancer development. In the following sections, we describe in detail the role of Gln metabolism in different cancer cells (Figure 3).

Pancreatic ductal adenocarcinoma

Pancreatic ductal adenocarcinoma (PADC) is common malignant and poor prognosis tumors with a 5-year survival rate of approximately 10% in the USA (34–36). Multiple pieces of evidence have demonstrated that Gln metabolism implicates the progression of PADC induced by internal or external factors.

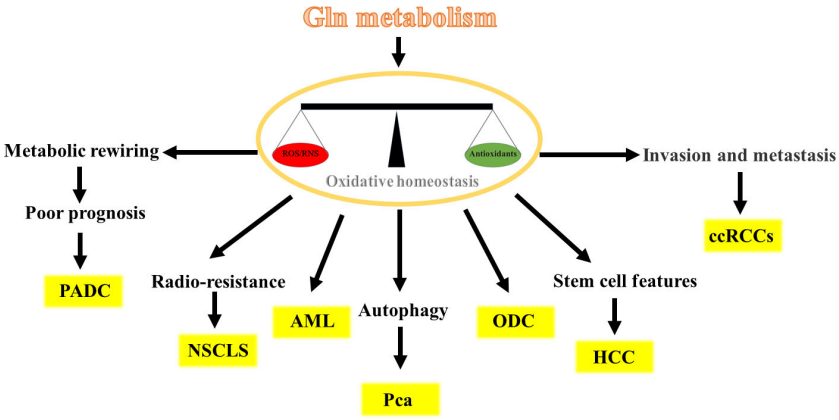

FIGURE 3
Different potential roles of Gln metabolism in different cancer cells.

For instance, Gln-metabolism is required for the hypoxia-inducible factor-2a-promoted PDAC progression (37). Moreover, the oncogenic *KRAS*-triggered PDAC growth is accompanied by the metabolic rewiring of Gln metabolism, which fulfills the NADPH need and balances cellular oxidative homeostasis (29). Similar increased production of Gln-derived NADPH is observed upon oxidative stress, accompanied by the survival and growth of PADC (38). These findings present us with intriguing evidence that the Gln-derived NADPH may positively associate with the poor prognosis of PDAC (39, 40). In addition, it has been demonstrated that PADC development-required NADPH strongly relies on Gln metabolism rather than on the pentose phosphate (PP) pathway. Evidence to support this hypothesis is that the Gln-derived NADPH markedly decreased after the knockdown of GOT1 or ME1 in PADC cells, which caused a significant increase in the ratio of GSSG/GSH, whereas glucose deprivation or knockdown of the limiting enzyme G6PD in the PP pathway had only a modest impact on NADPH (29, 41). Further evidence comes from the finding that the knockdown of UCP2 (the Asp transporter) decreased Gln-derived NADPH levels and increased ROS levels in PDAC cells, thus suppressing PDAC cell growth (42). Taken together, Gln-derived NADPH is required for the progression of PADC, and targeting this distinct pathway represents a novel prognostic biomarker and therapeutic target for patients with PDAC.

Acute myeloid leukemia

Several recent studies have demonstrated that Gln metabolism is implicated in the progression of acute myeloid leukemia (AML), as evidenced by exerting antileukemic effects (43–47). However, most of these studies focus on the role of Gln in supporting energy metabolism rather than maintaining oxidative homeostasis. Therefore, to better understand the role and regulatory mechanism of Gln metabolism in oxidative homeostasis of AML, one study using a FLT3-mutated AML cell model found that impaired Gln metabolism by FLT3 inhibitors could lead to depletion of GSH and accumulation of mitochondrial reactive oxygen species (mitoROS), subsequently leading to apoptosis of AML cell (48). A similar reduction of GSH levels and elevation of mitoROS and apoptosis were observed when AML cell lines were treated with the glutaminase inhibitor CB-839 for 24 h, which led to an inhibition of Gln metabolism (49).. These findings suggest that depletion of GSH is a universal consequence of inhibition of Gln metabolism in AML. In addition, inhibition of Gln metabolism makes AML cells susceptible to adjunctive drugs that further impair oxidative homeostasis. For example, combination of arsenic trioxide (ATO) and homoharringtonine (HHT) (the potent inducers of mitoROS) with CB-839 the exacerbates accumulation of mitoROS and apoptosis, which leads to complete cell death in AML cell lines, primary AML patient samples and *in vivo* mouse models of AML (49). Overall, Gln metabolism is implicated in promoting the development of AML, and the use of a Gln metabolism inhibitor in combination with drugs that further induces mitoROS and apoptosis may represent an effective and widely applicable therapeutic strategy for treating multiple types of AML.

Non-small cell lung cancer

In general, radiotherapy alone or in combination with chemotherapy and adjuvant durvalumab are mainly therapeutic methods for patients with locally advanced non-small cell lung cancer (NSCLC) (50, 51). However, after radiotherapy, the patient is prone to loco-regional recurrence, which remains a major clinical challenge for the cure for NSCLC (52–55). Existing evidences has linked Gln metabolism to the radio-resistance in NSCLC. For instance, a recently published article showed that the liver kinase B1-deficient NSCLC cells strongly depend on Gln-derived GSH to reduce ionizing radiation-derived ROS generation and to alleviate radiation-derived cytotoxic effects under radiotherapy. On the contrary, inhibition of Gln metabolism using knockdown of GLS could impair oxidative homeostasis, resulting in radio-sensitization of NSCLC (56). Another study also showed that the knockdown of GLS could increase response to radiotherapy of NSCLC by 30% *in vitro* and *in vivo* (57). Consistently, other studies also show that inhibition of Gln metabolism could suppress the GSH levels and enhanced radiosensitivity of NSCLC (58–60). These results indicate that NSCLC relies on Gln-derived GSH to maintain oxidative homeostasis to resist radiotherapy. All in all, inhibition of Glu metabolism may serve as a potential therapeutic strategy to cure this highly refractory subgroup of NSCLC patients.

Hepatocellular carcinoma

Liver cancer stem cells (CSCs), a subset of liver cells with stem cell features, are considered to be responsible for hepatocellular carcinoma (HCC) recurrence, metastasis, and chemoresistance (61, 62). These cells are heavily implicated in the Wnt/β-catenin pathway which is identified as one of the most frequent events occurring in CSCs (63, 64). It has been recognized that Gln metabolism is strongly correlated with Wnt/β-catenin pathway activation, contributing to liver carcinogenesis, hampering patient prognosis, and treatment stratification (65–67). Up to further investigations, the researchers found that the stemness properties in HCC were regulated by Gln metabolism through a ROS/Wnt/β-catenin signaling positive-feedback loop. More specifically, Gln metabolism could maintain low amounts of ROS and Wnt/β-catenin activation, which causes accumulation of β-catenin in the cytoplasm and then promotes the translocation of β-catenin

to the nucleus. β-catenin in the nucleus activates the expression of CSC markers, such as NANOG, OCT4, KLF4, SOX2, and c-MYC and other Wnt target genes in HCC cell lines, thus promoting the progression of HCC (68). Interestingly, this study has also shown that the activated Wnt/β-catenin pathway *via* its agonist SKL2001 could upregulate the mRNA and protein levels of GLS1, and then promote Gln metabolism, which means that activated Wnt/β-catenin pathway could promote GLS expression with positive feedback (68). A similar study has shown that the high expression of GLS1 in HCC had a markedly shorter overall survival time than its low expression (69). Taken together, Gln metabolism can increase the stemness properties in HCC through activating ROS/Wnt/β-catenin pathway, and targeting Gln metabolism, especially GLS1, may be a therapeutic target for the elimination of CSCs.

Prostate cancer

Prostate cancer (Pca) treatments, such as radiation, chemotherapy, and hormone therapy, can induce autophagy that improves therapeutic resistance (70–72). Existing evidence has linked the Gln metabolism to autophagy through oxidative homeostasis in Pca. For instance, a recently published article showed that the radio-resistant Pca cells strongly rely on Gln metabolism to maintain oxidative homeostasis. However, Pca cells could trigger autophagy upon Gln withdrawal and do not exhibit significant radio-sensitization (73). Upon further investigations, the researchers found that the ionizing radiation-derived ROS can induce autophagy as a stress response of Pca cells, but it is neutralized by GSH and NADPH produced by Gln metabolism. When blocking Gln metabolism, Pca cells could activate the ATG -mediated autophagy as a survival strategy to withstand radiation-induced damage due to GSH depletion and ROS accumulation (73, 74). Consistently, other studies also confirmed that autophagy inhibition increases ROS production in Pca cells (75–77). Overall, Gln metabolism affects the autophagy of Pca cells by affecting the level of ROS.

Kidney cancer

Kidney cancer, the ideal model of metabolic reprogramming among all cancers, has been duly named as a "Metabolic Disease" (78–81). There is growing evidence that clear cell renal cell carcinoma cells (ccRCCs) are Gln-addicted that is reprogrammed to feed an intrinsic antioxidant system (82–84). For instance, combined proteomics and metabolomics studies have shown that the ccRCC largely uses Gln to feed the GSH/GSSG antioxidant system to attenuate oxidative stress, rather than to generate energy and cellular components through the TCA cycle (85). To further confirm the role of Gln as a source for the GSH pathway, absolute quantitative GSH and GSSG levels in cells grown with and without Gln were compared. The result showed that GSH and GSSG levels were markedly reduced in the Gln-depleted group, which confirms the necessity of Gln for maintaining oxidative homeostasis of ccRCCs (85). Similar findings were obtained in another study, showing that inhibition of Gln metabolism *via* CB-839 led to decreased GSH/GSSG ratio, and furtherly increased oxidative stress and ccRCCs apoptosis (86). In addition, an interesting study shows that the suppression of fatty acid metabolism by inhibition of β-oxidation lead to the RCC cells dependent on the Gln-GSH pathway to prevent lipid peroxidation and ferroptosis (87). Notably, high GSH levels have proven to be a key feature of high-grade, high-stage and metastatic ccRCCs (81, 88). All in all, these data suggest that Gln-dependent antioxidant effects may provide ccRCCs with a critical mechanism for their survival.

Oligodendroglioma

In general, Gln is an antioxidant defense only in Gln addicted cancers, but not in all cases. Oligodendroglioma cells lack Gln synthetase (a marker of Gln-addicted cancers), but are independent of extracellular Gln (thus are not Gln addicted) (89, 90). However, a previous study showed that small amounts of extracellular Gln are sufficient for oligodendroglioma cells growth. Gln starvation does not significantly affect the cell content of anaplerotic substrates, but causes a significant decrease in the intracellular content of GSH in oligodendroglioma cells (91). This result means that Gln addiction and Gln roles as antioxidants are not correlated. In addition, Gln starvation causes hindrance of the Wnt/β-catenin pathway and protein synthesis attenuation in oligodendroglioma cells, which means that Gln may stimulate Wnt/beta-catenin pathways by ROS levels to affect the activity of cells, as in HCC (68, 91).

ROS production and ferroptosis

In light of the findings mentioned above, it would seem reasonable to expect that Gln metabolism plays an important role in maintaining ROS levels in cancer cells. However, we noted that most of the above-mentioned studies have mainly focused on the effects of Gln metabolism on maintaining oxidative homeostasis of cancer cells, whereas these effects were not suitable for every situation. Some studies have shown that the anaplerotic role of Gln metabolism in replenishing the TCA cycle intermediates could enhance ROS production under the blocking of GSH synthesis (92–94). For instance, a recently published article showed that Gln metabolism was crucial to maintaining cystine starvation-induced mitochondrial membrane potential (MMP) hyperpolarization, accompanied by an increase in electron transfer chain (ETC) activity and lipid ROS generation to promote ferroptosis (95). In support of

this notion, data from various studies showed that inhibiting the glutaminolysis can suppress TCA cycle and MMP hyperpolarization, and reduce lipid ROS production, thus enhancing ferroptosis resistance (95–98). Similarly, various studies showed that inhibiting xCT activities could suppress Gln-derived Glu export and enhance Glu to replenish the TCA cycle intermediates (99–101). Therefore, it has been theorized that inhibition of xCT activities could promote Glu to replenish the TCA cycle intermediates, which could promote ROS production (102) (Figure 4). All in all, increasing ROS levels by Gln metabolism under blocking of GSH synthesis promoted ferroptosis, which may provide a novel treatment guideline for ferroptosis-based tumor therapy.

Therapeutic strategies targeting Gln metabolism in cancer

The demonstration of the link between Gln metabolism and oxidative homeostasis of cancer has prompted research into strategies to target Gln metabolism to damage oxidative homeostasis of cancer. In this regard, GLS inhibitors aimed at decreasing Gln metabolism and impairing oxidative homeostasis are attracting increasing clinical interest. Many small molecules have been assayed to block GLS isoenzymes after the first attempt and failure to use 6-diazo-5-oxo-L-norleucine (DON) as an anti-cancer drug (103, 104). The bis-2-(5-phenylacetamido-1,2,4-thiadiazol-2-yl) ethyl sulfide (BPTES) and CB-839 are the specific inhibitors most frequently (86). Notably, CB-839 is currently being administered to humans in phase 1 clinical trials for some types of cancers (49, 103–106).

However, because of the plasticity of adaptive metabolic reprogramming in cancer cells, successful single treatments against cancers are scarce (4, 107–109). Therefore, some specific inhibitor of Gln metabolism has reached better results in sensitizing cancer cells to other treatments (110). Targeting Gln metabolism combined with drugs that are strong inducers of mitochondrial ROS, is widely used for treating multiple cancers (Table 1). For instance, dihydroartemisinin cooperatively induces excessive intracellular ROS resulting in profound apoptosis when combined with CB-839 in HCC (111). In a similar study, Gregory et al. demonstrated that a combination of GLS inhibition with ATO or HHT showed great activity against AML (49). Preclinical studies have also reported a benefit when combined with Gln metabolism inhibitors and radiotherapy. For example, the inhibitor CB-839 increased GSH depletion, and enhanced the radiation sensitivity of lung tumor cells xenografts in mice (57). Interestingly, one recent study showed that the combination of Gln metabolism inhibitors with radiotherapy could activate the ATG5-mediated autophagy of Prostate cancer, and proposes a strategy that a combination with autophagy inhibition and the blockade of Gln metabolism makes Pca radio-sensitization (73, 74, 122). Notably, the chemotherapy and/or radiation can also cause cellular damage in normal organs and tissues by generating free radicals (123). Antioxidants such as vitamins, minerals, and polyphenols can quench ROS activity alleviate the adverse effects of chemotherapy and/or radiotherapy (124, 125). Combining inhibition of Gln metabolism with antioxidant supplementation may enhance

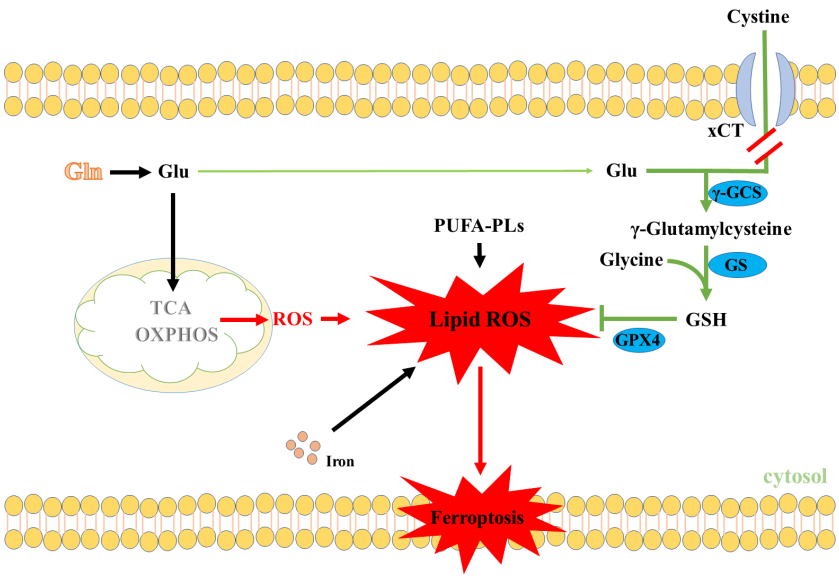

FIGURE 4
Gln metabolism promotes ROS production through the TCA cycle. PUFA-PLs, Polyunsaturated fatty acid chain(s).

TABLE 1 Combined treatments: targeting glutaminolysis in combination with drugs that unbalance mitochondrial redox state.

Type of cancer	Target Gln metabolism		Combined treatment	Drug mechanism	References
	Site	Type of inhibition			
AML	GLS	CB-839	ATO; HHT	Inducing excessive ROS	(49)
HCC			Dihydroartemisinin	Inducing excessive ROS	(111)
NSCLC			Radiotherapy	Radiosensitization	(56)
Pca		GLS siRNA silencing	ATG5 siRNA silencing; Radiotherapy	Inhibition of autophagy; Radiosensitization	(74)
PDAC			ß-lapachone	Inducing excessive ROS	(112)
GBM			ATO, H2O2	Inducing excessive ROS	(113)
TNBC		Compound 968	CQ	Inhibition of autophagy; inducing excessive ROS	(114)
NSCLC					(115)
LCLC			Apigenin	Inducing excessive ROS	(116)
GBM	GLS2	GLS2 overexpression	ATO; H2O2	Inducing excessive ROS	(113)
BC	SLC1A5	V9302	anti-PD-1 monoclonal antibody (mAb)	Enhancing antitumor immunity	(117)
HNSCC		Cetuximab	Dichloroacetate	Inducing excessive ROS	(118, 119)
CC	SLC1A5/ GDH1	CB-839/R162	CAI	Inducing excessive ROS	(120)
BC	/	Glutamine deprivation	Vorinostat	Inducing excessive ROS	(121)
CC					

BC, Breast cancer; CAI, Carboxyamidotriazole; CQ, chloroquine; CC, Colon cancer; GBM, glioblastoma; GDH1, glutamate dehydrogenase 1; HNSCC, head and neck squamous cell carcinoma; LCLC, large cell lung carcinoma; TNBC, triple-negative breast cancer; V9302, glutamine metabolism inhibitor.

the chemotherapy and/or radiation sensitivity while preventing cellular damage of normal organs and tissues, which may be an effective strategy for the treatment of cancer. However, it remains controversial whether antioxidants affect treatment outcomes or whether antioxidants ameliorate adverse effects induced by chemotherapy and radiotherapy, which needs further investigations in the future (126). In conclusion, combination therapy, including inhibitors of Gln metabolism, may be a promising strategy for cancer cells.

Conclusion

The antioxidant capacity of tumor cells is required for rapidly proliferating and aggressive cancer cells to adapt to hypoxia and excessive ROS levels. The literature reviewed here suggests that Gln has been established as an important factor in maintaining the oxidative homeostasis of cancer cells. Targeting Gln metabolism impaired oxidative homeostasis of cancer cells and may provide effective approaches for therapies against cancer. In addition, more research is urgently needed to implement multiple synergistic targeting (including Gln metabolism inhibitors) to block tumor proliferation and increase cancer cells' sensitivity of cancer cells to other therapies. Future studies on Gln metabolism in maintaining oxidative homeostasis may provide novel and effective therapeutic strategies to treat a subset of cancer patients.

Author contributions

Conceptualization, YD, WL, and TG; writing—original draft preparation, TG, CZ, XO, JZ, JY, and SC; writing—review and editing, YD and WL; visualization, YD. All authors have read and agreed to the published version of the manuscript.

Funding

This study was jointly supported by the Natural Science Foundation of the Hunan Province, China (2021JJ30335, 2021JJ20044), the National Natural Science Foundation of China (U19A2037), the Changsha Natural Science Funds for Distinguished Young Scholar (kq2009020), Young Elite Scientists Sponsorship Program by CAST (2020-2022QNRC003), the Natural Science Foundation of Guangxi Province (2020JJA130102), China Agriculture Research System of MOF and MARA (CARS-35), and the 'Strategic Priority Research Program' of the Chinese Academy of Sciences (XDA24030204), the Scientific Research Fund of Hunan Provincial Education Department, China (21A0141).

Conflict of interest

The authors declare that the research was conducted in the absence of any commercial or financial relationships that could be construed as a potential conflict of interest.

Publisher's note

References

1. Kussmaul L, Hirst J. The mechanism of superoxide production by NADH: ubiquinone oxidoreductase (complex I) from bovine heart mitochondria. *Proc Natl Acad Sci USA* (2006) 103:7607–12. doi: 10.1073/pnas.0510977103

2. Lambeth JD. NOX enzymes and the biology of reactive oxygen. *Nat Rev Immunol* (2004) 4:181–9. doi: 10.1038/nri1312

3. Quinlan CL, Orr AL, Perevoshchikova IV, Treberg JR, Ackrell BA, Brand MD. Mitochondrial complex II can generate reactive oxygen species at high rates in both the forward and reverse reactions. *J Biol Chem* (2012) 287:27255–64. doi: 10.1074/jbc.M112.374629

4. Gorrini C, Harris IS, Mak TW. Modulation of oxidative stress as an anticancer strategy. *Nat Rev Drug Discovery.* (2013) 12:931–47. doi: 10.1038/nrd4002

5. Panieri E, Santoro MM. ROS homeostasis and metabolism: a dangerous liason in cancer cells. *Cell Death Disease.* (2016) 7:e2253. doi: 10.1038/cddis.2016.105

6. Kröller-Schön S, Steven S, Kossmann S, Scholz A, Daub S, Oelze M, et al. Molecular mechanisms of the crosstalk between mitochondria and NADPH oxidase through reactive oxygen species-studies in white blood cells and in animal models. *Antioxidants Redox Signaling* (2014) 20:247–66. doi: 10.1089/ars.2012.4953

7. Warburg O. On the origin of cancer cells. *Sci (New York NY).* (1956) 123:309–14. doi: 10.1126/science.123.3191.309

8. Sosa V, Moliné T, Somoza R, Paciucci R, Kondoh H, Lleonart ME. Oxidative stress and cancer: An overview. *Ageing Res Rev* (2013) 12:376–90. doi: 10.1016/j.arr.2012.10.004

9. Herraiz C, Crosas-Molist E, Sanz-Moreno V. Reactive oxygen species and tumor dissemination: Allies no longer. *Mol Cell Oncol* (2016) 3:e1127313. doi: 10.1080/23723556.2015.1127313

10. Maryanovich M, Gross A. A ROS rheostat for cell fate regulation. *Trends Cell Biol* (2013) 23:129–34. doi: 10.1016/j.tcb.2012.09.007

11. Hayes JD, Dinkova-Kostova AT, Tew KD. Oxidative stress in cancer. *Cancer Cell* (2020) 38:167–97. doi: 10.1016/j.ccell.2020.06.001

12. Kodama M, Oshikawa K, Shimizu H, Yoshioka S, Takahashi M, Izumi Y, et al. A shift in glutamine nitrogen metabolism contributes to the malignant progression of cancer. *Nat Commun* (2020) 11:1320. doi: 10.1038/s41467-020-15136-9

13. DeBerardinis RJ, Cheng T. Q's next: the diverse functions of glutamine in metabolism, cell biology and cancer. *Oncogene* (2010) 29:313–24. doi: 10.1038/onc.2009.358

14. Altman BJ, Stine ZE, Dang CV. From Krebs to clinic: glutamine metabolism to cancer therapy. *Nat Rev Cancer.* (2016) 16:619–34. doi: 10.1038/nrc.2016.71

15. Franklin CC, Backos DS, Mohar I, White CC, Forman HJ, Kavanagh TJ. Structure, function, and post-translational regulation of the catalytic and modifier subunits of glutamate cysteine ligase. *Mol aspects Med* (2009) 30:86–98. doi: 10.1016/j.mam.2008.08.009

16. Kennedy L, Sandhu JK, Harper ME, Cuperlovic-Culf M. Role of glutathione in cancer: From mechanisms to therapies. *Biomolecules* (2020) 10:1429. doi: 10.3390/biom10101429

17. Lu SC. Regulation of glutathione synthesis. *Mol aspects Med* (2009) 30:42–59. doi: 10.1016/j.mam.2008.05.005

18. van Geldermalsen M, Wang Q, Nagarajah R, Marshall AD, Thoeng A, Gao D, et al. ASCT2/SLC1A5 controls glutamine uptake and tumour growth in triple-negative basal-like breast cancer. *Oncogene* (2016) 35:3201–8. doi: 10.1038/onc.2015.381

19. Jiang H, Zhang N, Tang T, Feng F, Sun H, Qu W. Target the human Alanine/Serine/Cysteine transporter 2(ASCT2): Achievement and future for novel cancer therapy. *Pharmacol Res* (2020) 158:104844. doi: 10.1016/j.phrs.2020.104844

20. Bhutia YD, Ganapathy V. Glutamine transporters in mammalian cells and their functions in physiology and cancer. *Biochim Biophys Acta* (2016) 1863:2531–9. doi: 10.1016/j.bbamcr.2015.12.017

21. Gao P, Tchernyshyov I, Chang TC, Lee YS, Kita K, Ochi T, et al. C-myc suppression of miR-23a/b enhances mitochondrial glutaminase expression and glutamine metabolism. *Nature* (2009) 458:762–5. doi: 10.1038/nature07823

22. Hu W, Zhang C, Wu R, Sun Y, Levine A, Feng Z. Glutaminase 2, a novel p53 target gene regulating energy metabolism and antioxidant function. *Proc Natl Acad Sci USA* (2010) 107:7455–60. doi: 10.1073/pnas.1001006107

23. Lukey MJ, Greene KS, Erickson JW, Wilson KF, Cerione RA. The oncogenic transcription factor c-jun regulates glutaminase expression and sensitizes cells to glutaminase-targeted therapy. *Nat Commun* (2016) 7:11321. doi: 10.1038/ncomms11321

24. Suzuki S, Tanaka T, Poyurovsky MV, Nagano H, Mayama T, Ohkubo S, et al. Phosphate-activated glutaminase (GLS2), a p53-inducible regulator of glutamine metabolism and reactive oxygen species. *Proc Natl Acad Sci USA* (2010) 107:7461–6. doi: 10.1073/pnas.1002459107

25. Zhang J, Pavlova NN, Thompson CB. Cancer cell metabolism: the essential role of the nonessential amino acid, glutamine. *EMBO J* (2017) 36:1302–15. doi: 10.15252/embj.201696151

26. Koppula P, Zhang Y, Zhuang L, Gan B. Amino acid transporter SLC7A11/xCT at the crossroads of regulating redox homeostasis and nutrient dependency of cancer. *Cancer Commun (London England).* (2018) 38:12. doi: 10.1186/s40880-018-0288-x

27. DeBerardinis RJ, Mancuso A, Daikhin E, Nissim I, Yudkoff M, Wehrli S, et al. Beyond aerobic glycolysis: transformed cells can engage in glutamine metabolism that exceeds the requirement for protein and nucleotide synthesis. *Proc Natl Acad Sci USA* (2007) 104:19345–50. doi: 10.1073/pnas.0709747104

28. Ying M, You D, Zhu X, Cai L, Zeng S, Hu X. Lactate and glutamine support NADPH generation in cancer cells under glucose deprived conditions. *Redox Biol* (2021) 46:102065. doi: 10.1016/j.redox.2021.102065

29. Son J, Lyssiotis CA, Ying H, Wang X, Hua S, Ligorio M, et al. Glutamine supports pancreatic cancer growth through a KRAS-regulated metabolic pathway. *Nature* (2013) 496:101–5. doi: 10.1038/nature12040

30. Moreno-Sánchez R, Gallardo-Pérez JC, Rodríguez-Enríquez S, Saavedra E, Marín-Hernández Á. Control of the NADPH supply for oxidative stress handling in cancer cells .*Free Radic Biol Med.* (2017) 112:149–61 doi: 10.1016/j.freeradbiomed.2017.07.018

31. Bansal A, Simon MC. Glutathione metabolism in cancer progression and treatment resistance. *J Cell Biol* (2018) 217:2291–8. doi: 10.1083/jcb.201804161

32. Jaganjac M, Milkovic L, Sunjic SB, Zarkovic N. The NRF2, thioredoxin, and glutathione system in tumorigenesis and anticancer therapies. *Antioxidants (Basel Switzerland).* (2020) 9:1151. doi: 10.3390/antiox9111151

33. Palde PB, Carroll KS. A universal entropy-driven mechanism for thioredoxin-target recognition. *Proc Natl Acad Sci USA* (2015) 112:7960–5. doi: 10.1073/pnas.1504376112

34. Mizrahi JD, Surana R, Valle JW, Shroff RT. Pancreatic cancer. *Lancet (London England).* (2020) 395:2008–20. doi: 10.1016/s0140-6736(20)30974-0

35. Siegel RL, Miller KD, Fuchs HE, Jemal A. Cancer statistics, 2022. *CA: Cancer J Clin* (2022) 72:7–33. doi: 10.3322/caac.21708

36. Park W, Chawla A, O'Reilly EM. Pancreatic cancer: A review. *Jama* (2021) 326:851–62. doi: 10.1001/jama.2021.13027

37. Li W, Chen C, Zhao X, Ye H, Zhao Y, Fu Z, et al. HIF-2α regulates non-canonical glutamine metabolism *via* activation of PI3K/mTORC2 pathway in human pancreatic ductal adenocarcinoma. *J Cell Mol Med* (2017) 21:2896–908. doi: 10.1111/jcmm.13202

38. Tong Y, Guo D, Lin SH, Liang J, Yang D, Ma C, et al. SUCLA2-coupled regulation of GLS succinylation and activity counteracts oxidative stress in tumor cells. *Mol Cell* (2021) 81:2303–2316.e8. doi: 10.1016/j.molcel.2021.04.002

39. Hu T, Shukla SK, Vernucci E, He C, Wang D, King RJ, et al. Metabolic rewiring by loss of Sirt5 promotes kras-induced pancreatic cancer progression. *Gastroenterology* (2021) 161:1584–600. doi: 10.1053/j.gastro.2021.06.045

40. Wang YP, Zhou W, Wang J, Huang X, Zuo Y, Wang TS, et al. Arginine methylation of MDH1 by CARM1 inhibits glutamine metabolism and suppresses pancreatic cancer. *Mol Cell* (2016) 64:673–87. doi: 10.1016/j.molcel.2016.09.028

41. Ying H, Kimmelman AC, Lyssiotis CA, Hua S, Chu GC, Fletcher-Sananikone E, et al. Oncogenic kras maintains pancreatic tumors through regulation of anabolic glucose metabolism. *Cell* (2012) 149:656–70. doi: 10.1016/j.cell.2012.01.058

42. Raho S, Capobianco L, Malivindi R, Vozza A, Piazzolla C, De Leonardis F, et al. KRAS-regulated glutamine metabolism requires UCP2-mediated aspartate transport to support pancreatic cancer growth. *Nat Metab* (2020) 2:1373–81. doi: 10.1038/s42255-020-00315-1

43. Jacque N, Ronchetti AM, Larrue C, Meunier G, Birsen R, Willems L, et al. Targeting glutaminolysis has antileukemic activity in acute myeloid leukemia and synergizes with BCL-2 inhibition. *Blood* (2015) 126:1346–56. doi: 10.1182/blood-2015-01-621870

44. Willems L, Jacque N, Jacquel A, Neveux N, Maciel TT, Lambert M, et al. Inhibiting glutamine uptake represents an attractive new strategy for treating acute myeloid leukemia. *Blood* (2013) 122:3521–32. doi: 10.1182/blood-2013-03-493163

45. Gallipoli P, Giotopoulos G, Tzelepis K, Costa ASH, Vohra S, Medina-Perez P, et al. Glutaminolysis is a metabolic dependency in FLT3(ITD) acute myeloid leukemia unmasked by FLT3 tyrosine kinase inhibition. *Blood* (2018) 131:1639–53. doi: 10.1182/blood-2017-12-820035

46. Matre P, Velez J, Jacamo R, Qi Y, Su X, Cai T, et al. Inhibiting glutaminase in acute myeloid leukemia: metabolic dependency of selected AML subtypes. *Oncotarget* (2016) 7:79722–35. doi: 10.18632/oncotarget.12944

47. Gregory MA, Nemkov T, Reisz JA, Zaberezhnyy V, Hansen KC, D'Alessandro A, et al. Glutaminase inhibition improves FLT3 inhibitor therapy for acute myeloid leukemia. *Exp hematology.* (2018) 58:52–8. doi: 10.1016/j.exphem.2017.09.007

48. Gregory MA, D'Alessandro A, Alvarez-Calderon F, Kim J, Nemkov T, Adane B, et al. ATM/G6PD-driven redox metabolism promotes FLT3 inhibitor resistance in acute myeloid leukemia. *Proc Natl Acad Sci USA* (2016) 113:E6669–e6678. doi: 10.1073/pnas.1603876113

49. Gregory MA, Nemkov T, Park HJ, Zaberezhnyy V, Gehrke S, Adane B, et al. Targeting glutamine metabolism and redox state for leukemia therapy. *Clin Cancer Res* (2019) 25:4079–90. doi: 10.1158/1078-0432.ccr-18-3223

50. Bezjak A, Temin S, Franklin G, Giaccone G, Govindan R, Johnson ML, et al. Definitive and adjuvant radiotherapy in locally advanced non-Small-Cell lung cancer: American society of clinical oncology clinical practice guideline endorsement of the American society for radiation oncology evidence-based clinical practice guideline. *J Clin Oncol* (2015) 33:2100–5. doi: 10.1200/jco.2014.59.2360

51. Cheema PK, Rothenstein J, Melosky B, Brade A, Hirsh V. Perspectives on treatment advances for stage III locally advanced unresectable non-small-cell lung cancer. *Curr Oncol (Toronto Ont).* (2019) 26:37–42. doi: 10.3747/co.25.4096

52. Cassidy RJ, Zhang X, Patel PR, Shelton JW, Escott CE, Sica GL, et al. Next-generation sequencing and clinical outcomes of patients with lung adenocarcinoma treated with stereotactic body radiotherapy. *Cancer* (2017) 123:3681–90. doi: 10.1002/cncr.30794

53. Jeong Y, Hoang NT, Lovejoy A, Stehr H, Newman AM, Gentles AJ, et al. Role of KEAP1/NRF2 and TP53 mutations in lung squamous cell carcinoma development and radiation resistance. *Cancer Discovery.* (2017) 7:86–101. doi: 10.1158/2159-8290.cd-16-0127

54. Gurtner K, Kryzmien Z, Koi L, Wang M, Benes CH, Hering S, et al. Radioresistance of KRAS/TP53-mutated lung cancer can be overcome by radiation dose escalation or EGFR tyrosine kinase inhibition in vivo. *Int J Cancer* (2020) 147:472–7. doi: 10.1002/ijc.32598

55. Mak RH, Hermann G, Lewis JH, Aerts HJ, Baldini EH, Chen AB, et al. Outcomes by tumor histology and KRAS mutation status after lung stereotactic body radiation therapy for early-stage non-small-cell lung cancer. *Clin Lung cancer.* (2015) 16:24–32. doi: 10.1016/j.cllc.2014.09.005

56. Sitthideatphaiboon P, Galan-Cobo A, Negrao MV, Qu X, Poteete A, Zhang F, et al. STK11/LKB1 mutations in NSCLC are associated with KEAP1/NRF2-dependent radiotherapy resistance targetable by glutaminase inhibition. *Clin Cancer Res* (2021) 27:1720–33. doi: 10.1158/1078-0432.ccr-20-2859

57. Boysen G, Jamshidi-Parsian A, Davis MA, Siegel ER, Simecka CM, Kore RA, et al. Glutaminase inhibitor CB-839 increases radiation sensitivity of lung tumor cells and human lung tumor xenografts in mice. *Int J Radiat Biol* (2019) 95:436–42. doi: 10.1080/09553002.2018.1558299

58. Sappington DR, Siegel ER, Hiatt G, Desai A, Penney RB, Jamshidi-Parsian A, et al. Glutamine drives glutathione synthesis and contributes to radiation sensitivity of A549 and H460 lung cancer cell lines. *Biochim Biophys Acta* (2016) 1860:836–43. doi: 10.1016/j.bbagen.2016.01.021

59. Fujimoto M, Higashiyama R, Yasui H, Yamashita K, Inanami O. Preclinical studies for improving radiosensitivity of non-small cell lung cancer cell lines by combining glutaminase inhibition and senolysis. *Trans Oncol* (2022) 21:101431. doi: 10.1016/j.tranon.2022.101431

60. Meijer TWH, Peeters WJM, Dubois LJ, van Gisbergen MW, Biemans R, Venhuizen JH, et al. Targeting glucose and glutamine metabolism combined with radiation therapy in non-small cell lung cancer. *Lung Cancer (Amsterdam Netherlands).* (2018) 126:32–40. doi: 10.1016/j.lungcan.2018.10.016

61. Zhu Z, Hao X, Yan M, Yao M, Ge C, Gu J, et al. Cancer stem/progenitor cells are highly enriched in CD133+CD44+ population in hepatocellular carcinoma. *Int J cancer.* (2010) 126:2067–78. doi: 10.1002/ijc.24868

62. Chiba T, Zheng YW, Kita K, Yokosuka O, Saisho H, Onodera M, et al. Enhanced self-renewal capability in hepatic stem/progenitor cells drives cancer initiation. *Gastroenterology* (2007) 133:937–50. doi: 10.1053/j.gastro.2007.06.016

63. Yamashita T, Budhu A, Forgues M, Wang XW. Activation of hepatic stem cell marker EpCAM by wnt-beta-catenin signaling in hepatocellular carcinoma. *Cancer Res* (2007) 67:10831–9. doi: 10.1158/0008-5472.can-07-0908

64. Yang W, Yan HX, Chen L, Liu Q, He YQ, Yu LX, et al. Wnt/beta-catenin signaling contributes to activation of normal and tumorigenic liver progenitor cells. *Cancer Res* (2008) 68:4287–95. doi: 10.1158/0008-5472.can-07-6691

65. Cadoret A, Ovejero C, Terris B, Souil E, Lévy L, Lamers WH, et al. New targets of beta-catenin signaling in the liver are involved in the glutamine metabolism. *Oncogene* (2002) 21:8293–301. doi: 10.1038/sj.onc.1206118

66. Sekine S, Lan BY, Bedolli M, Feng S, Hebrok M. Liver-specific loss of beta-catenin blocks glutamine synthesis pathway activity and cytochrome p450 expression in mice. *Hepatol (Baltimore Md).* (2006) 43:817–25. doi: 10.1002/hep.21131

67. Liao J, Liu PP, Hou G, Shao J, Yang J, Liu K, et al. Regulation of stem-like cancer cells by glutamine through β-catenin pathway mediated by redox signaling. *Mol cancer.* (2017) 16:51. doi: 10.1186/s12943-017-0623-x

68. Li B, Cao Y, Meng G, Qian L, Xu T, Yan C, et al. Targeting glutaminase 1 attenuates stemness properties in hepatocellular carcinoma by increasing reactive oxygen species and suppressing wnt/beta-catenin pathway. *EBioMedicine* (2019) 39:239–54. doi: 10.1016/j.ebiom.2018.11.063

69. Yu D, Shi X, Meng G, Chen J, Yan C, Jiang Y, et al. Kidney-type glutaminase (GLS1) is a biomarker for pathologic diagnosis and prognosis of hepatocellular carcinoma. *Oncotarget* (2015) 6:7619–31. doi: 10.18632/oncotarget.3196

70. Farrow JM, Yang JC, Evans CP. Autophagy as a modulator and target in prostate cancer. *Nat Rev Urology.* (2014) 11:508–16. doi: 10.1038/nrurol.2014.196

71. Ashrafizadeh M, Paskeh MDA, Mirzaei S, Gholami MH, Zarrabi A, Hashemi F, et al. Targeting autophagy in prostate cancer: preclinical and clinical evidence for therapeutic response. *J Exp Clin Cancer Res CR.* (2022) 41:105. doi: 10.1186/s13046-022-02293-6

72. Luo S, Shao L, Chen Z, Hu D, Jiang L, Tang W. NPRL2 promotes docetaxel chemoresistance in castration resistant prostate cancer cells by regulating autophagy through the mTOR pathway. *Exp Cell Res* (2020) 390:111981. doi: 10.1016/j.yexcr.2020.111981

73. Mukha A, Kahya U, Linge A, Chen O, Löck S, Lukiyanchuk V, et al. GLS-driven glutamine catabolism contributes to prostate cancer radiosensitivity by regulating the redox state, stemness and ATG5-mediated autophagy. *Theranostics* (2021) 11:7844–68. doi: 10.7150/thno.58655

74. Mukha A, Kahya U, Dubrovska A. Targeting glutamine metabolism and autophagy: the combination for prostate cancer radiosensitization. *Autophagy* (2021) 17:3879–81. doi: 10.1080/15548627.2021.1962682

75. Kim KY, Park KI, Kim SH, Yu SN, Park SG, Kim YW, et al. Inhibition of autophagy promotes salinomycin-induced apoptosis *via* reactive oxygen species-mediated PI3K/AKT/mTOR and ERK/p38 MAPK-dependent signaling in human prostate cancer cells. *Int J Mol Sci* (2017) 18:1088. doi: 10.3390/ijms18051088

76. Jangamreddy JR, Ghavami S, Grabarek J, Kratz G, Wiechec E, Fredriksson BA, et al. Salinomycin induces activation of autophagy, mitophagy and affects mitochondrial polarity: differences between primary and cancer cells. *Biochim Biophys Acta* (2013) 1833:2057–69. doi: 10.1016/j.bbamcr.2013.04.011

77. Kim KY, Yu SN, Lee SY, Chun SS, Choi YL, Park YM, et al. Salinomycin-induced apoptosis of human prostate cancer cells due to accumulated reactive oxygen species and mitochondrial membrane depolarization. *Biochem Biophys Res Commun* (2011) 413:80–6. doi: 10.1016/j.bbrc.2011.08.054

78. Rathmell WK, Rathmell JC, Linehan WM. Metabolic pathways in kidney cancer: current therapies and future directions. *J Clin Oncol* (2018) JCO2018792309. doi: 10.1200/JCO.2018.79.2309

79. Weiss RH. Metabolomics and metabolic reprogramming in kidney cancer. *Semin Nephrol* (2018) 38(2):175–82. doi: 10.1016/j.semnephrol.2018.01.006

80. Wettersten HI. Reprogramming of metabolism in kidney cancer. *Semin Nephrol* (2020) 40(1):2–13. doi: 10.1016/j.semnephrol.2019.12.002

81. Wettersten HI, Aboud OA, Lara PN, Weiss RH. Metabolic reprogramming in clear cell renal cell carcinoma. *Nat Rev Nephrol.* (2017) 13:410–9. doi: 10.1038/nrneph.2017.59

82. Shroff EH, Eberlin LS, Dang VM, Gouw AM, Gabay M, Adam SJ, et al. MYC oncogene overexpression drives renal cell carcinoma in a mouse model through

glutamine metabolism. *Proc Natl Acad Sci USA* (2015) 112:6539–44. doi: 10.1073/pnas.1507228112

83. Gameiro PA, Yang J, Metelo AM, Pérez-Carro R, Baker R, Wang Z, et al. *In vivo* HIF-mediated reductive carboxylation is regulated by citrate levels and sensitizes VHL-deficient cells to glutamine deprivation. *Cell Metab* (2013) 17:372–85. doi: 10.1016/j.cmet.2013.02.002

84. Chakraborty S, Balan M, Sabarwal A, Choueiri TK, Pal S. Metabolic reprogramming in renal cancer: Events of a metabolic disease. *Biochim Biophys Acta Rev cancer.* (2021) 1876:188559. doi: 10.1016/j.bbcan.2021.188559

85. Wettersten HI, Hakimi AA, Morin D, Bianchi C, Johnstone ME, Donohoe DR, et al. Grade-dependent metabolic reprogramming in kidney cancer revealed by combined proteomics and metabolomics analysis. *Cancer Res* (2015) 75:2541–52. doi: 10.1158/0008-5472.can-14-1703

86. Abu Aboud O, Habib SL, Trott J, Stewart B, Liang S, Chaudhari AJ, et al. Glutamine addiction in kidney cancer suppresses oxidative stress and can be exploited for real-time imaging. *Cancer Res* (2017) 77:6746–58. doi: 10.1158/0008-5472.can-17-0930

87. Miess H, Dankworth B, Gouw AM, Rosenfeldt M, Schmitz W, Jiang M, et al. The glutathione redox system is essential to prevent ferroptosis caused by impaired lipid metabolism in clear cell renal cell carcinoma. *Oncogene* (2018) 37:5435–50. doi: 10.1038/s41388-018-0315-z

88. Hakimi AA, Reznik E, Lee CH, Creighton CJ, Brannon AR, Luna A, et al. An integrated metabolic atlas of clear cell renal cell carcinoma. *Cancer Cell* (2016) 29:104–16. doi: 10.1016/j.ccell.2015.12.004

89. Zhuang Z, Qi M, Li J, Okamoto H, Xu DS, Iyer RR, et al. Proteomic identification of glutamine synthetase as a differential marker for oligodendrogliomas and astrocytomas. *J Neurosurg* (2011) 115:789–95. doi: 10.3171/2011.5.jns11451

90. Pilkington GJ, Lantos PL. The role of glutamine synthetase in the diagnosis of cerebral tumours. *Neuropathol Appl Neurobiol* (1982) 8:227–36. doi: 10.1111/j.1365-2990.1982.tb00277.x

91. Chiu M, Taurino G, Bianchi MG, Ottaviani L, Andreoli R, Ciociola T, et al. Oligodendroglioma cells lack glutamine synthetase and are auxotrophic for glutamine, but do not depend on glutamine anaplerosis for growth. *Int J Mol Sci* (2018) 19:1099. doi: 10.3390/ijms19041099

92. Gao M, Monian P, Quadri N, Ramasamy R, Jiang X. Glutaminolysis and transferrin regulate ferroptosis. *Mol Cell* (2015) 59:298–308. doi: 10.1016/j.molcel.2015.06.011

93. Weinberg F, Hamanaka R, Wheaton WW, Weinberg S, Joseph J, Lopez M, et al. Mitochondrial metabolism and ROS generation are essential for kras-mediated tumorigenicity. *Proc Natl Acad Sci USA* (2010) 107:8788–93. doi: 10.1073/pnas.1003428107

94. Anderson NM, Mucka P, Kern JG, Feng H. The emerging role and targetability of the TCA cycle in cancer metabolism. *Protein Cell* (2018) 9:216–37. doi: 10.1007/s13238-017-0451-1

95. Gao M, Yi J, Zhu J, Minikes AM, Monian P, Thompson CB, et al. Role of mitochondria in ferroptosis. *Mol Cell* (2019) 73:354–363.e3. doi: 10.1016/j.molcel.2018.10.042

96. Shin D, Lee J, You JH, Kim D, Roh JL. Dihydrolipoamide dehydrogenase regulates cystine deprivation-induced ferroptosis in head and neck cancer. *Redox Biol* (2020) 30:101418. doi: 10.1016/j.redox.2019.101418

97. Luo M, Wu L, Zhang K, Wang H, Zhang T, Gutierrez L, et al. miR-137 regulates ferroptosis by targeting glutamine transporter SLC1A5 in melanoma. *Cell Death Differ.* (2018) 25:1457–72. doi: 10.1038/s41418-017-0053-8

98. Zhang K, Wu L, Zhang P, Luo M, Du J, Gao T, et al. miR-9 regulates ferroptosis by targeting glutamic-oxaloacetic transaminase GOT1 in melanoma. *Mol carcinogenesis.* (2018) 57:1566–76. doi: 10.1002/mc.22878

99. Huang Y, Dai Z, Barbacioru C, Sadée W. Cystine-glutamate transporter SLC7A11 in cancer chemosensitivity and chemoresistance. *Cancer Res* (2005) 65:7446–54. doi: 10.1158/0008-5472.can-04-4267

100. Lim JKM, Delaidelli A, Minaker SW, Zhang HF, Colovic M, Yang H, et al. Cystine/glutamate antiporter xCT (SLC7A11) facilitates oncogenic RAS transformation by preserving intracellular redox balance. *Proc Natl Acad Sci USA* (2019) 116:9433–42. doi: 10.1073/pnas.1821323116

101. Ogiwara H, Takahashi K, Sasaki M, Kuroda T, Yoshida H, Watanabe R, et al. Targeting the vulnerability of glutathione metabolism in ARID1A-deficient cancers. *Cancer Cell* (2019) 35:177–190.e8. doi: 10.1016/j.ccell.2018.12.009

102. Yao X, Li W, Fang D, Xiao C, Wu X, Li M, et al. Emerging roles of energy metabolism in ferroptosis regulation of tumor cells. *Adv. Sci (Weinheim Baden-Wurttemberg Germany).* (2021) 8:e2100997. doi: 10.1002/advs.202100997

103. Matés JM, Campos-Sandoval JA, de Los Santos-Jiménez J, Segura JA, Alonso FJ, Márquez J. Metabolic reprogramming of cancer by chemicals that target glutaminase isoenzymes. *Curr Med. Chem* (2020) 27:5317–39. doi: 10.2174/0929867326666190416165004

104. Matés JM, Di Paola FJ, Campos-Sandoval JA, Mazurek S, Márquez J. Therapeutic targeting of glutaminolysis as an essential strategy to combat cancer. *Semin Cell Dev Biol* (2020) 98:34–43. doi: 10.1016/j.semcdb.2019.05.012

105. Lee P, Malik D, Perkons N, Huangyang P, Khare S, Rhoades S, et al. Targeting glutamine metabolism slows soft tissue sarcoma growth. *Nat Commun* (2020) 11:498. doi: 10.1038/s41467-020-14374-1

106. Meric-Bernstam F, Tannir NM, Mier JW, DeMichele A, Telli ML, Fan AC, et al. Phase 1 study of CB-839, a small molecule inhibitor of glutaminase (GLS), alone and in combination with everolimus (E) in patients (pts) with renal cell cancer (RCC). *Am Soc Clin Oncol* (2016) 69:12–13. doi: 10.1016/S0959-8049(16)32626-0

107. Wondrak GT. Redox-directed cancer therapeutics: molecular mechanisms and opportunities. *Antioxidants Redox Signaling* (2009) 11:3013–69. doi: 10.1089/ars.2009.2541

108. Trachootham D, Alexandre J, Huang P. Targeting cancer cells by ROS-mediated mechanisms: a radical therapeutic approach? *Nat Rev Drug Discovery* (2009) 8:579–91. doi: 10.1038/nrd2803

109. Kalyanaraman B, Cheng G, Hardy M, Ouari O, Bennett B, Zielonka J. Teaching the basics of reactive oxygen species and their relevance to cancer biology: Mitochondrial reactive oxygen species detection, redox signaling, and targeted therapies. *Redox Biol* (2018) 15:347–62. doi: 10.1016/j.redox.2017.12.012

110. Matés JM, Campos-Sandoval JA, Santos-Jiménez JL, Márquez J. Dysregulation of glutaminase and glutamine synthetase in cancer. *Cancer letters.* (2019) 467:29–39. doi: 10.1016/j.canlet.2019.09.011

111. Wang D, Meng G, Zheng M, Zhang Y, Chen A, Wu J, et al. The glutaminase-1 inhibitor 968 enhances dihydroartemisinin-mediated antitumor efficacy in hepatocellular carcinoma cells. *PloS One* (2016) 11:e0166423. doi: 10.1371/journal.pone.0166423

112. Chakrabarti G, Moore ZR, Luo X, Ilcheva M, Ali A, Padanad M, et al. Targeting glutamine metabolism sensitizes pancreatic cancer to PARP-driven metabolic catastrophe induced by ß-lapachone. *Cancer Metab* (2015) 3:12. doi: 10.1186/s40170-015-0137-1

113. Martín-Rufián M, Nascimento-Gomes R, Higuero A, Crisma AR, Campos-Sandoval JA, Gómez-García MC, et al. Both GLS silencing and GLS2 overexpression synergize with oxidative stress against proliferation of glioma cells. *J Mol Med (Berl).* (2014) 92:277–90. doi: 10.1007/s00109-013-1105-2

114. Halama A, Kulinski M, Dib SS, Zaghlool SB, Siveen KS, Iskandarani A, et al. Accelerated lipid catabolism and autophagy are cancer survival mechanisms under inhibited glutaminolysis. *Cancer letters.* (2018) 430:133–47. doi: 10.1016/j.canlet.2018.05.017

115. Han T, Guo M, Zhang T, Gan M, Xie C, Wang JB. A novel glutaminase inhibitor-968 inhibits the migration and proliferation of non-small cell lung cancer cells by targeting EGFR/ERK signaling pathway. *Oncotarget* (2017) 8:28063–73. doi: 10.18632/oncotarget.14188

116. Lee YM, Lee G, Oh TI, Kim BM, Shim DW, Lee KH, et al. Inhibition of glutamine utilization sensitizes lung cancer cells to apigenin-induced apoptosis resulting from metabolic and oxidative stress. *Int J Oncol* (2016) 48:399–408. doi: 10.3892/ijo.2015.3243

117. Li Q, Zhong X, Yao W, Yu J, Wang C, Li Z, et al. Inhibitor of glutamine metabolism V9302 promotes ROS-induced autophagic degradation of B7H3 to enhance antitumor immunity. *J Biol Chem* (2022) 298:101753. doi: 10.1016/j.jbc.2022.101753

118. Tao X, Lu Y, Qiu S, Wang Y, Qin J, Fan Z. AP1G1 is involved in cetuximab-mediated downregulation of ASCT2-EGFR complex and sensitization of human head and neck squamous cell carcinoma cells to ROS-induced apoptosis. *Cancer letters.* (2017) 408:33–42. doi: 10.1016/j.canlet.2017.08.012

119. Lu H, Lu Y, Xie Y, Qiu S, Li X, Fan Z. Rational combination with PDK1 inhibition overcomes cetuximab resistance in head and neck squamous cell carcinoma. *JCI Insight* (2019) 4:e131106. doi: 10.1172/jci.insight.131106

120. Shi J, Ju R, Gao H, Huang Y, Guo L, Zhang D. Targeting glutamine utilization to block metabolic adaptation of tumor cells under the stress of carboxyamidotriazole-induced nutrients unavailability. *Acta Pharm Sin B* (2022) 12:759–73. doi: 10.1016/j.apsb.2021.07.008

121. Miyamoto K, Watanabe M, Boku S, Sukeno M, Morita M, Kondo H, et al. xCT inhibition increases sensitivity to vorinostat in a ROS-dependent manner. *Cancers (Basel).* (2020) 12:827. doi: 10.3390/cancers12040827

122. Zannella VE, Dal Pra A, Muaddi H, McKee TD, Stapleton S, Sykes J, et al. Reprogramming metabolism with metformin improves tumor oxygenation and radiotherapy response. *Clin Cancer Res* (2013) 19:6741–50. doi: 10.1158/1078-0432.ccr-13-1787

123. Ziech D, Franco R, Georgakilas AG, Georgakila S, Malamou-Mitsi V, Schoneveld O, et al. The role of reactive oxygen species and oxidative stress in environmental carcinogenesis and biomarker development. *Chem Biol Interact* (2010) 188:334–9. doi: 10.1016/j.cbi.2010.07.010

124. Fuchs-Tarlovsky V. Role of antioxidants in cancer therapy. *Nutrition* (2013) 29:15–21. doi: 10.1016/j.nut.2012.02.014

125. Lamson DW, Brignall MS. Antioxidants in cancer therapy; their actions and interactions with oncologic therapies. *Altern Med Rev* (1999) 4:304–29.

126. Yasueda A, Urushima H, Ito T. Efficacy and interaction of antioxidant supplements as adjuvant therapy in cancer treatment: A systematic review. *Integr Cancer Ther* (2016) 15:17–39. doi: 10.1177/1534735415610427

frontiers | Frontiers in Oncology

TYPE Original Research
PUBLISHED 24 October 2022
DOI 10.3389/fonc.2022.979537

OPEN ACCESS

EDITED BY
Jose Luis Izquierdo-Garcia,
Complutense University of Madrid,
Spain

REVIEWED BY
Carla Carrera,
University of Turin, Italy
Aleš Dvořák,
Charles University, Czechia

*CORRESPONDENCE
Mioara Larion
mioara.larion@nih.gov

SPECIALTY SECTION
This article was submitted to Cancer Metabolism, a section of the journal Frontiers in Oncology

RECEIVED 27 June 2022
ACCEPTED 03 October 2022
PUBLISHED 24 October 2022

CITATION
Ruiz-Rodado V, Dowdy T, Lita A, Kramp T, Zhang M, Shuboni-Mulligan D, Herold-Mende C, Armstrong TS, Gilbert MR, Camphausen K and Larion M (2022) Metabolic biomarkers of radiotherapy response in plasma and tissue of an IDH1 mutant astrocytoma mouse model.
Front. Oncol. 12:979537.
doi: 10.3389/fonc.2022.979537

Metabolic biomarkers of radiotherapy response in plasma and tissue of an IDH1 mutant astrocytoma mouse model

Victor Ruiz-Rodado[1], Tyrone Dowdy[1], Adrian Lita[1], Tamalee Kramp[2], Meili Zhang[1], Dorela Shuboni-Mulligan[1], Christel Herold-Mende[3], Terri S. Armstrong[1], Mark R. Gilbert[1], Kevin Camphausen[2] and Mioara Larion[1]*

[1]Neuro-Oncology Branch, Center for Cancer Research, National Cancer Institute, National Institutes of Health, Bethesda, MD, United States, [2]Radiation Oncology Branch, Center for Cancer Research, National Institutes of Health, Bethesda, MD, United States, [3]Division of Neurosurgical Research, Department of Neurosurgery, University Hospital Heidelberg, Heidelberg, Germany

Astrocytomas are the most common subtype of brain tumors and no curative treatment exist. Longitudinal assessment of patients, usually *via* Magnetic Resonance Imaging (MRI), is crucial since tumor progression may occur earlier than clinical progression. MRI usually provides a means for monitoring the disease, but it only informs about the structural changes of the tumor, while molecular changes can occur as a treatment response without any MRI-visible change. Radiotherapy (RT) is routinely performed following surgery as part of the standard of care in astrocytomas, that can also include chemotherapy involving temozolomide. Monitoring the response to RT is a key factor for the management of patients. Herein, we provide plasma and tissue metabolic biomarkers of treatment response in a mouse model of astrocytoma that was subjected to radiotherapy. Plasma metabolic profiles acquired over time by Liquid Chromatography Mass Spectrometry (LC/MS) were subjected to multivariate empirical Bayes time-series analysis (MEBA) and Receiver Operating Characteristic (ROC) assessment including Random Forest as the classification strategy. These analyses revealed a variation of the plasma metabolome in those mice that underwent radiotherapy compared to controls; specifically, fumarate was the best discriminatory feature. Additionally, Nuclear Magnetic Resonance (NMR)-based ^{13}C-tracing experiments were performed at end-point utilizing [U-^{13}C]-Glutamine to investigate its fate in the tumor and contralateral tissues. Irradiated mice displayed lower levels of glycolytic metabolites (e.g. phosphoenolpyruvate) in tumor tissue, and a higher flux of glutamine towards succinate was observed in the radiation cohort. The plasma biomarkers provided herein could be

validated in the clinic, thereby improving the assessment of brain tumor patients throughout radiotherapy. Moreover, the metabolic rewiring associated to radiotherapy in tumor tissue could lead to potential metabolic imaging approaches for monitoring treatment using blood draws.

KEYWORDS

Astrocytoma, metabolomics, biomarker, radiotherapy, 13C-tracing

Introduction

Lower grade gliomas (LGGs) that harbor IDH1^{mut} are the less aggressive form of gliomas; however, malignant transformation towards a more aggressive phenotype occurs (1, 2). For example, astrocytomas harboring an IDH1 mutation progress towards a highly aggressive phenotype (3). These malignancies tend to spread into neighboring healthy tissue; thus, surgical interventions present limitations, which makes radiotherapy (RT) a critical component of the therapeutic approach to these tumors. Monitoring the response to RT and other treatments is generally performed through Magnetic Resonance Imaging (MRI) and symptomatic evaluation. While these approaches are the current standard of care, an earlier distinction between radiation-induced necrosis and tumor progression than is currently offered by MRI would be beneficial for patient treatment (1). Therefore, plasma-based biomarkers represent attractive alternatives to monitor treatment response. Plasma-based metabolomics has been utilized to provide markers of CNS (Central Nervous System) tumors in the past (4, 5), as well as a reporter of progression and response to treatment in mouse models of cancer and patients (6). Typically, Liquid Chromatography Mass Spectrometry (LC/MS) and Nuclear Magnetic Resonance (NMR) are the techniques utilized to profile the blood fraction of choice for analysis. Datasets arising therefrom are subsequently examined for biomarkers or trends that allow the classification of subjects according to a disease, treatment, etc. Metabolomics investigations can experience the deleterious effects arising from multicollinearity and overfitting due to the nature of the experiments, i.e. few subjects and hundreds of variables. Accordingly, data analysis strategies have been implemented to overcome related challenges in the metabolomic studies of bio-fluids (7, 8). Additionally, metabolic profiling of brain tissue can also serve as an in-situ reporter of RT response as it carries the metabolic signature derived from the treatment. Metabolic information contained in different blood fractions have been previously utilized in diagnosis of gliomas (9) and in investigations involving the response to radiotherapy in cancer (10, 11). However, the assessment of response to RT in an animal model of astrocytoma in both tissue and plasma have not been reported yet. Studies addressing the metabolic profiling of bio-samples for radiotherapy monitoring are still severely limited (12–14). Herein, we report the plasma metabolic profiling of a grade III astrocytoma mouse model undergoing radiotherapy in addition to providing a series of time-related biomarkers associated with treatment response. Furthermore, we dissected the metabolic pathways affected from the treatment through the LC/MS and NMR analysis of tumor tissue and ^{13}C-tracing experiments utilizing uniformly labeled ^{13}C Glutamine, [U-^{13}C]-Glutamine. ^{13}C flux from glutamine towards succinate was significantly increased in the treated cohort whilst total lactate levels were decreased, which may indicate a potential rewiring of the metabolism within the tumor due to radiotherapy.

Materials and methods

Animal work

NCH1681 cell line was originated from an IDH1 mutant grade III astrocytoma patient (33 years old) (15). The treatment of primary tumor involved temozolomide and treatment of progressive disease by proton therapy before surgery of first recurrence. NCH1681 cells were maintained in DMEM:F12 Glutamax, supplemented with EGF, FGF, antibiotics and BIT (PeloBiotech, Martinsried, Germany) (16). Once cells reached the required number in culture, they were harvested, washed with phosphate buffered saline (PBS) and counted. The resulting pellets were resuspended in Hank's Balanced Salt Solution, and 5 µL of this cell suspension (500,000 cells/mouse) were injected stereotactically into the striatum of 6–8 weeks old female SCID (severe combined immunodeficient) mice (Charles River Frederick Research Model Facility) using a stereotactic device. The intracranial orthotopic mouse model with the IDH1 mutant glioma cell line NCH1681 was established according to approved animal study proposal NOB-008 by the National Cancer Institute–Animal Use and Care Committee. Tumor growth was monitored for neurological symptoms daily. To determine

endpoint, an independent researcher performed health assessment of the mice twice a day without previous knowledge of the experiment in course. Once this researcher determined that a mouse was reaching end point in view of previously defined symptoms, that mouse was euthanized. Symptoms include animal experiencing rapid weight loss (>15%, monitored daily), debilitating diarrhea, rough hair coat, hunched posture, labored breathing, lethargy, persistent recumbence, significantly abnormal neurological signs, bleeding from any orifice, self-induced trauma, impaired mobility, becomes moribund or otherwise becomes unable to obtain food or water. For comparison of survival curves, the log-rank (Mantel–Cox) test has been used (GraphPad Prism 7).

To examine the effects of radiation in control mice, we used 5 C57BL/6 mice obtained from Charles River Laboratories (CRL, Dublin, VA). Mice were sampled across 7 time points, one day before radiation and 6 timepoints after radiation (3 hrs, 6 hrs, 1 day, 4 days, 12 days and 24 days). Blood samples were taken 2 hrs before lights off for all time points except 6 hrs-post radiation which was sampled 2hr after light off. Micro sample tubes coated with lithium heparin (Sarstedt AG & Co., Germany) were used to collect 100 uL of blood from the mandibular vein, samples were centrifuged at 3,500 g for 15 min at 4°C to collect plasma and flash frozen with dry ice then stored at -80°C until analysis. Radiation was given using a small animal Pentax x-ray irradiator to anesthetized mice (ketamine: 80–120 mg/kg and xylazine: 5–25 mg/kg) restrained in a lead shielded apparatus designed to isolate radiation to only the brain. Mice were allowed to recover from anesthesia on heated pads for a maximum of two hours and returned to home cages after recovery.

Animal radiotherapy

Radiation was performed on mice intracranially injected with the NCH1681 cell line. 30 days after injection, the mice were randomized in two groups, one undergoing RT (n=9 mice) and the other one as control (n=9 mice). Mice were irradiated with a total of 12 Gy; specifically, animals were treated on Monday and Friday for 2 consecutive weeks at 3Gy/session. Radiation was performed in a Pantek machine an orthovoltage radiotherapy unit. The mice were anesthetized with a cocktail of ketamine/rompun/saline mixture, i.e. ketamine (100 mg/ml), rompun (20 mg/ml) and diluted with saline to give the mice a 100 mg/kg dose of ketamine and 10 mg/kg rompun. The mice were injected with the cocktail at a dose of 0.01 µL per gram of half of the mouse's body weight. Animals were then placed in a custom-made jig that only exposes the mouse brain to radiation while sheilding the body, including the eyes, ears, the oral cavity, and the spinal cord. The non-irradiated control mice were administrated both anesthesia and atipamezole. The radiated mice were observed for how much time they would have to be sedated for radiation and how long time passed until they received atipamezole, approximately. Those same parameters were used on the non-irradiated control mice. After radiation, the mice were given atipamezole, a reversal agent, to aid in the recovery.

^{13}C tracing *in vivo*

When mice reached endpoint, they were injected with [U-^{13}C]-glutamine and tumor was harvested for both quantification of ^{13}C incorporation by NMR and metabolic profiling through LC/MS. [U-^{13}C]-glutamine was injected to mice reaching endpoint at similar time points to improve consistency, i.e. mice undergoing radiotherapy utilized for ^{13}C tracing analysis have an average survival of 92 days and control animal 82 days. Injections were performed as previously described (17, 18); briefly, [U-^{13}C]-glutamine (Cambridge Isotopes) was prepared as a 36.2 mg/ml stock solution in sterile PBS and injected (200 µL, 7.24 mg) through the tail vein at 15 min intervals for 3 times (total = 142 µmol) just prior to mice reaching endpoint. Mice were euthanized 15 min after the last injection (45 min from the first injection). Tumors were separated from the brain and both tissues were gently blotted and flash-frozen in liquid nitrogen.

Plasma processing for metabolic profiling

Blood was collected approximately every 10 days from the tail vein of the mice in Li-heparin collection tubes; subsequently, the sample was separated into plasma and packed cells by centrifugation at 3,500 g for 15 min at 4°C and stored at -80°C until extraction. 35 µL of plasma were extracted in a 1:2:1 water: methanol:chloroform mixture. Centrifuged for 20 min at 4°C and 13,000 rpm and the resulting upper hydrophilic phase was then transferred to a clean vial and dried under a stream of N_2 gas. Dried sediments were resuspended in 60% methanol (aq.) and injected into the LC/MS system for global profiling. Blood samples were collected from all the mice at each time point, although 5 mice were selected for each group for biomarker discovery in order to account for blood samples at all the time points for the same animal, since mice deceased over time.

Tissue processing for metabolomics

When mice reached endpoint, malignant tissue and contralateral regions were collected. Tumor tissue was first weighted as frozen for metabolite quantification purposes and to normalize the metabolite levels computed by LC/MS; subsequently, the sample was stored at -80°C for further processing. Tissue samples were mechanically lysed utilizing a

bullet blender, and metabolite extraction was performed in a 1:2:1 water:methanol:chloroform solution. Then, samples were centrifuged at 12,000 rpm, for 20 min. at 4°C. The two resulting phases (upper aqueous polar and lower organic lipid) were separated, and the polar one was split in 2 (for NMR and LC/MS analyses) and dried under a stream of N_2. Samples were resuspended in methanol for LC/MS analysis or in 180 µL of pH 7 phosphate buffer (100 mM) in D_2O (containing d-TSP) and 0.1% NaN_3 for NMR experiments. These tissue extracts were utilized for both quantification of ^{13}C incorporation into metabolites *via* NMR and metabolic profiling by LC/MS.

NMR acquisition and processing

NMR spectra were acquired on a 700 MHz Bruker Avance Neo (US National Cancer Institute, Bethesda, US). For 1D ^1H experiments we utilized the noesygppr1d pulse sequence for water suppression involving 64 scans with a relaxation delay of 3 s, a spectral width of 12,000 Hz and 32,000 data points. Spectra were zero-filled to 64K points and we applied an exponential line broadening function of 0.3 Hz. 1D HSQC experiments for ^{13}C tracing were acquired using the hsqcetgpsisp2.2 pulse sequence over 400 scans, 3,500 data points and a spectral width of 8,200 Hz. We applied an exponential line broadening function of 4 Hz and a Gaussian function of 7.5 Hz. All data were referenced to the TSP internal standard signal (s, $\delta = 0.00$ ppm), phased and baseline corrected using ACD Labs Spectrus Processor 2016. For quantification, data was normalized to the TSP singlet and tissue weight and corrected for natural abundance of ^{13}C (1.1%). Assignment of metabolites was done on the basis of literature values (19, 20) and available databases (21). The formula utilized to compute the nmol/mg of tissue from a 1d-hsqc is:

$$C = \frac{A}{A_{TSP}} \; x \; \frac{nH^+_{TSP}}{nH^+} \; x \; C_{TSP} x \; \frac{V}{m}$$

where: A are the areas under the peak of interest, nH^+ are the number of protons attributable to each resonance signal, C_{TSP} is concentration of the TSP reference corrected for the natural abundance of ^{13}C (1.11%), V is the volume of the sample and m the tumor mass.

LC/MS global profiling of plasma and tissue

LC/MS analysis was conducted with the Agilent 6545 QTOF-MS combined with 1290 Infinity II UHPLC system (Agilent Technologies, Wilmington, DE, USA). Only LC/MS grade solvents and additives purchased from Covachem (CovaChem, LLC., Loves Park, IL, USA) were used to prepare mobile phases and wash solutions. Wash cycles consisting of strong wash (50% Methanol, 25% Isopropanol, and 25% Water), weak wash (90% Acetonitrile and 10% Water), and seal wash (10% Isopropanol and 90% water) were implemented to eliminate carryover between injections. Dried extracts were reconstituted in 80 µL 60:40 $MeOH/H_2O$ and samples were injected (8 µL) to resolve analytes using Infinity 1290 in-line filter combined with AdvanceBio Glycan Map 2.1 x 100mm, 2.7µm column (Agilent Technologies, Wilmington, DE., USA) set at 35^0C. The solvent buffers were composed of mobile phase A (10 mM ammonium acetate in 88% water/12% acetonitrile) and mobile phase B (10 mM ammonium acetate in 90% Acetonitrile) titrated with formic acid and ammonium hydroxide to pH 6.85. The linear gradient was executed at flow rate 0.2 mL/min, as follows: 100% B, 0.5 min; 95% B, 2.0 min; 60% B, 3.0 min; 35% B, 5 min; hold 0.25 min; 0% B, 6 min; hold 0.5 min; 100% B, 7.8 min; equilibrate for 1.7 min. The mass analyzer acquisition parameters include drying gas temperature, 250^0C; drying gas flow, 9 L/min; sheath gas temperature, 325^0C; sheath gas flow, 11 L/min; nebulizer, 45 psig. Mass spectra were acquired at 3.0 spectra/s in negative electrospray ionization (ESI-) mode for a mass range from 72 to 1200 m/z using a voltage gradient of capillary 3000 V, nozzle 2000 V, fragmentor 80 V, skimmer 50 V, and octopole radio frequency 750 V.

LC/MS data analysis

Prior to preprocessing datasets, pooled QC samples were inspected for consistency of retention time shifts and signal degradation. Following acquisition, m/z spectra binning was performed by partitioning the m/z vs retention time (RT) matrices into fixed width using Agilent Masshunter Profinder B.08.00. Bins were manually inspected to confirm consistent integration for all analytes detected across all samples. Targeted TOF-MS extraction of precursor ions was performed using in-house compound library. Ion selection and alignment parameters were restricted to proton loss (H-) in ESI-, H+ gain in ESI+, 5.0 mDa mass range, and retention time span ± 0.4 min. Following pre-processing, the areas for each analyte from each sample was corrected by area of sample-specific internal standard, p-nitrobenzoate and debrisoquine. Same acquisition procedure was followed for the ^{13}C isotopically labeled samples. After alignment and identification of analytes of interest retention times a PCDL card was constructed using PCDL Manager B.07.00 (Agilent). The chromatograms were introduced in Agilent MassHunter Profinder B.08.00 and the PCDL card was used in the Batch Isotopologue Extraction routine with the following parameters: 99% ^{13}C labeling, 20% peak height ion abundance criteria, mass tolerance of ± 15ppm +2 mDa with a threshold of 250 counts for anchor and 1000 counts for the sum of ion heights with a minimum correlation coefficient bigger then 0.5. Total levels of metabolites of interest included both the unlabeled and all the labeled isotopologues.

Statistical analysis

MetaboAnalyst 4.0 (22) was employed for multivariate analysis including MEBA (multivariate empirical Bayes time-series analysis) (23) and multivariate ROC (receiver operating characteristic) curve analysis. MEBA was utilized to select the metabolites according to their correlation with the treatment over time. Top 15 ranked metabolites were evaluated as biomarkers by ROC curve analysis in a multivariate fashion that involved Random Forest as a classification strategy. The area under the curve (AUC) was the measure of separability as a function of treatment. GraphPad Prism 7 was employed to perform ANOVA for repeated measures and outliers were removed if >5 times the standard deviation.

Results

Radiotherapy for a mouse model of IDH1 mutant glioma

Radiotherapy was applied to the intracranial IDH1 mutant glioma model in 2 consecutive weeks at 3 Gy per dose, 2 days per week (Figure 1A). Cox-Mantel test was utilized to assess the efficacy of the treatment delivering a significant p-value of 0.0018 and median survival values of 50 and 96 days for the control and RT groups respectively (Figure 1B). These results reveal a beneficial effect of RT on survival for our glioma mouse model. We also evaluated if the presence of IDH1 mutation in this model was translated to 2HG formation *in vivo*. 2HG levels were assessed by LC/MS in the different tissues, i.e. contralateral (CL) and tumor, revealing the expected higher levels of 2HG in the malignant tissue compared to the CL region in both treated and untreated mice (Figure 1C). In addition, we validated the presence of IDH1 in NCH1681 using DNA sequencing, DNA methylation profiling, and Western Blot analysis of IDH1 mutant protein (Figure S3).

Plasma biomarkers of radiation in a glioma mouse model

Since the NCH1681 model responded positively to radiotherapy, we conducted a plasma metabolomics investigation to evaluate the effect of RT in the plasma metabolome over time in 5 mice per cohort. Plasma metabolomics can provide a snapshot of the overall metabolic status of an organism and reveal potential metabolic biomarkers of RT response. The importance of the temporal changes of metabolites was assessed by MEBA, which is based on multivariate empirical Bayes statistic (23). The Hotelling's T^2 parameter arising from this test was employed to select the top-15 metabolites which displayed differential levels over time (Table S1). These top 15 features were further assessed as plasma markers of radiation through multivariate ROC curve analysis (Figure 2A). The best performance was obtained with RF models including only 2 metabolites (AUC=0.878, CI=0.689-1) and the addition of more features did not improve the outcome of the classifier. Fumarate, glucose 1,6 biphosphate, PEP, UMP and taurine were those metabolites most frequently included in the models for samples classification (Figure 2B); although only fumarate levels attained statistical significance (from the multiple comparison test) at the last time point (Figure 2C), i.e. 24 days after last dose of radiation, similarly to glutamate (Figure S1). As a control, we irradiated normal mice and collected plasma pre-treatment 3 hours, 6 hours, 1 day, 4 days, 12 days and 24 days post-RT. Interestingly, fumarate levels did not change significantly in normal mice that underwent radiotherapy (Figure S2).

Two-way ANOVA revealed that glutamate, PEP and fumarate levels changed significantly between both cohorts (Table S1) and glutamate, dihydroxyacetone phosphate

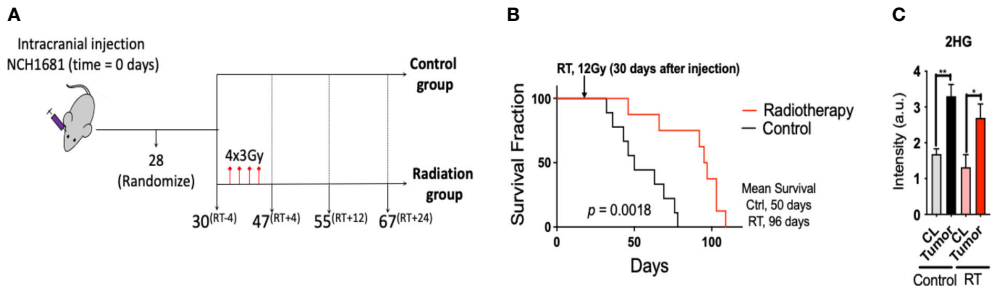

FIGURE 1
Radiotherapy for a mouse model of IDH1 mutant astrocytoma: **(A)**, Diagram of the experimental set up of the investigation (superscripts indicating the time in days relative to radiotherapy). **(B)**, Survival curves for the glioma mouse model under radiation and control (RT, radiotherapy) (n=9). **(C)**, 2HG levels obtained by LC/MS analysis in the tissues indicated (n=4 samples/group). Statistical significance from a two way-ANOVA followed by Sidak's multiple comparison test displayed as **, p<0.005; *, p<0.05 (only significant differences are indicated).

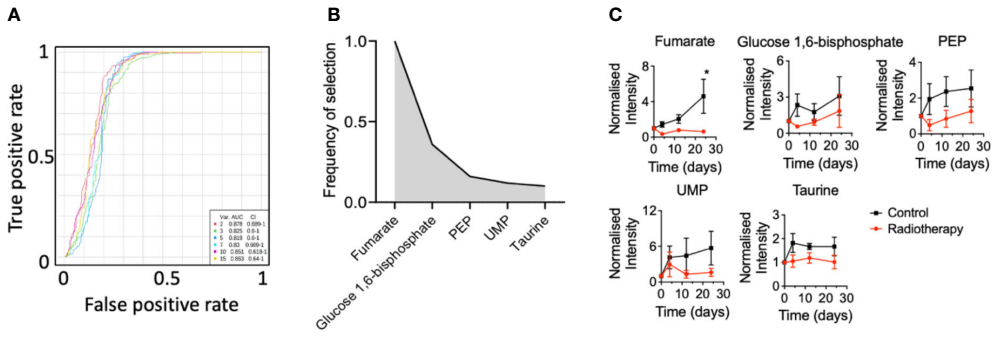

FIGURE 2
Plasma biomarkers of radiation for an astrocytoma mouse model: **(A)**, Multivariate ROC curve diagram for those metabolites selected by MEBA with the highest potential as plasma biomarkers based on the area under the curve. **(B)**, Top-5 ranked variables included in the multivariate ROC curve analysis and **(C)** their levels over time (n=5 mice per group, metabolites levels are displayed as mean ± SEM, significance assessed by a two-way ANOVA for repeated measures followed by Sidak's test for multiple comparisons. *, p<0.05).

(DHAP), inosine and dUMP levels displayed a significant correlation with the factor 'time' (Table S1).

Radiotherapy modifies the metabolic profile of glioma tissue

In order to explore the metabolic signature of radiotherapy within the tumor, we analyzed malignant tissue collected from both groups (treated and untreated) at end point by LC/MS (Figure S4) and NMR (Figure 3). From the 88 metabolites detected by LC/MS in profiling experiment, we observed a dysregulation of the glycolytic pathway in view of the number of metabolites associated to this metabolic route that were affected after radiation (Figure S4A). Levels of phosphoenolpyruvate (PEP) and glyceraldehyde-3P, both glycolytic intermediates, were downregulated in addition to lactate; contrarily, 1,3-biphosphoglycerate levels were higher for the radiation group. Hence, glucose metabolism was highlighted as a key metabolic pathway affected from treatment (Figure S4B). Energetic metabolites such as ATP and GTP were also upregulated in the treated cohort as well as further intermediates such as UDP and GDP; however, deoxy nucleotides including dUMP and dTMP were both downregulated in the radiation group. Indeed, pathway analysis (Figure S4B) revealed pyrimidine metabolism as one of the main pathways affected from radiation.

Additionally, we performed ^{13}C tracing experiments by bolus injection of [U-^{13}C]-glutamine through the mouse tail vein, since this amino acid has been revealed as a key metabolite in gliomas metabolism and contributes to fuel the TCA cycle, especially under hypoxic conditions (24–26) (Figure 3). Indeed, the utilization of inhibitors of glutaminase, the enzyme that converts glutamine to glutamate, has been proposed as a potential target in tumors that harbor the IDH1 mutant gene (27, 28). NMR analysis of the tissue extracts obtained from treated and control mice allow to quantify the incorporation of ^{13}C units derived from [U-^{13}C]-glutamine into downstream metabolites including lactate, alanine, GABA, glutamate, GSH and aspartate (Figures 3A-C). We observed downregulation of lactate production from ^{13}C glutamine in the RT-treated cohort ($p<0.05$ for 'treatment' factor from two-way ANOVA), although these changes did not attain statistical significance for individual comparisons Figure 3C).

Tumor tissue displays a higher uptake of [U-^{13}C]-glutamine in the control group, although the differences found through the ^{13}C tracing experiment did not attain statistical significance. Previous investigations have reported ^{18}F-Glutamine as an imaging marker of glioma (29) in view of its higher uptake by tumor tissue. Under RT, CL region displays similar levels to those encountered in the control mice. Lower levels of glutamine were found in tumor tissue compared to the CL region in those mice that underwent RT as well as the tumor from the control cohort. GABA synthesis was also downregulated in the tumor compared to the CL region for both groups ($p<0.05$ for 'tissue' factor CL vs tumor from the two-way ANOVA), and this effect was more intense under RT as glutamine is a major precursor for this neurotransmitter (30). The flux from [U-^{13}C]-glutamine to succinate, a TCA cycle intermediate, was upregulated in the treated cohort (both interaction, 'tissue x treatment', and 'tissue' factors attained a $p<0.05$ from the two-way ANOVA); however, ^{13}C succinate levels were similar to both CL regions and tumor tissue within the control group.

Discussion

Radiotherapy is known to generate DNA damage and compromise its repair in addition to triggering radiolysis of cellular water that can originate free radicals that may cause

chemical modifications in the DNA, proteins, and tumor microenvironment (31–33).

Tumors harboring a mutation in the IDH1 gene have been reported to present an enhanced sensitivity to radiation due to the modification of the epigenetic landscape by 2HG that affects the DNA damage responses (34). In addition, *de novo* pyrimidine pathway which contributes precursors to DNA synthesis has been recently reported to be a vulnerability of IDH1-mutated astrocytoma (35). The RT vulnerability has been exploited in IDH1-mutant tumors revealing a beneficial effect in response to radiation (36), as observed in our model as well (Figure 1B).

Interestingly, a recent investigation including a longitudinal study of brain tumor patients harboring the IDH1 mutation that received RT reported how 2HG levels decreased over time in oligodendroglioma patients under treatment. Astrocytoma patients experienced a comparable trend, although it was less pronounced (37). In our study, 2HG levels in tumors experienced a slight (non-significant) decrease in the treated cohort compared to the non-treated group (Figure 1C, black bars versus red bars). Together, these studies suggest the need to identify other biomarkers that could report on RT response.

Herein, we report biomarkers associated with RT in plasma of mice harboring an IDH1-mutated astrocytoma and which experienced a significant increase in survival as a result of RT. We discovered that glutamate and fumarate, were top-ranked by MEBA analysis, therefore, serving as biomarkers of RT. These metabolites are closely related since fumarate is one of the TCA cycle intermediates for which one of the entries involves the deamination of glutamate that produces α-ketoglutarate. Glutamate has been reported as downregulated in serum collected from GBM patients under RT (38). A recent investigation including human plasma from brain tumor patients and healthy individuals also highlighted the TCA cycle as a major dysregulated pathway in gliomas (39). Interestingly, a urinary metabolomics investigation

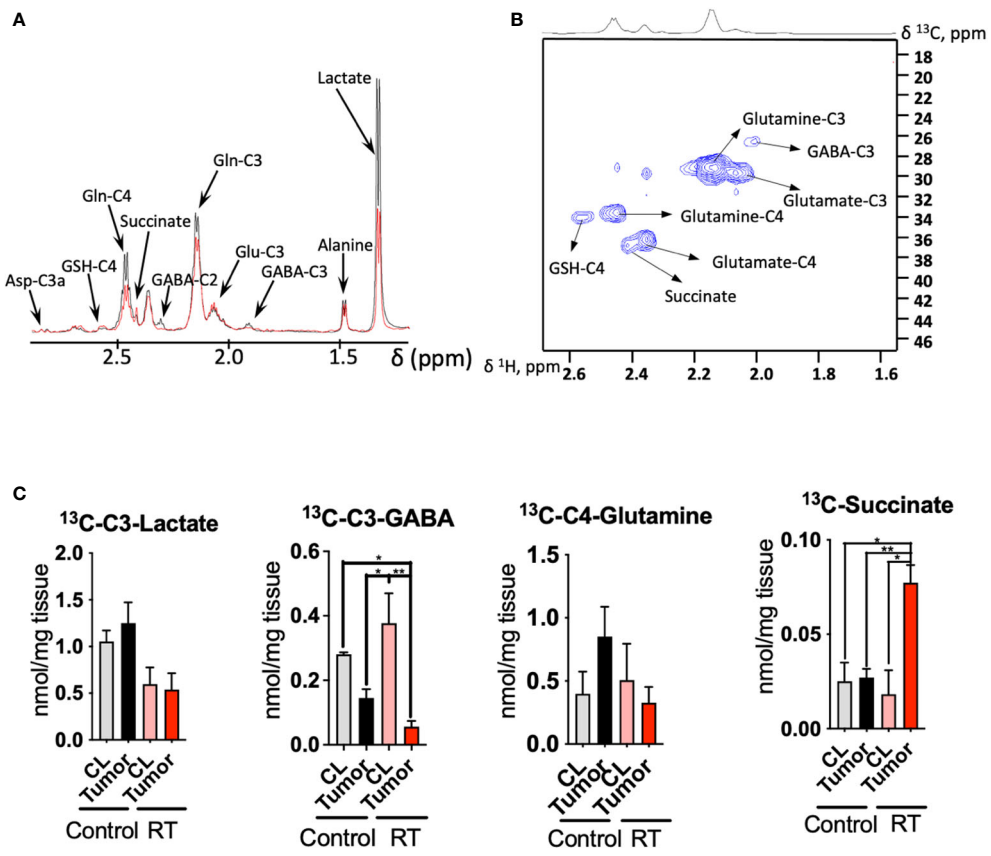

FIGURE 3
Radiotherapy enhances the 13C incorporation of glutamine to succinate in astrocytoma tissue: **(A)**, 1D HSQC NMR stack plot of spectra acquired on tumor tissue from a mouse from the control group (black) and undergoing radiotherapy (RT, red) displaying the resonances arising from ^{13}C labeling from [U-^{13}C]-glutamine tracing experiments. Typical spectra are shown (resonance intensities normalized to tumor weight). **(B)**, 2D ^{1}H-^{13}C HSQC Representative spectrum of a tumor sample from a mouse infused with [U-^{13}C]-glutamine displaying the region between 1.6-2.6 ppm (^{1}H) and 18-46 ppm (^{13}C). **(C)**, Quantification of the [U-^{13}C]-glutamine labeling on those metabolites showing a different degree of ^{13}C incorporation after radiation in tumor and contralateral regions. (data displayed as bar plots ± SEM, n=3, statistical significance assessed through a two-way ANOVA followed by Tukey HSD test, *, p<0.05; **, p<0.005). Only significant differences are indicated. RT was 12Gy.

including non-human primates subjected to radiation found fumarate to be downregulated in the urine collected from treated animals (40).

Next, we undertook a steady state analysis of tumor tissue. We observed that pyrimidine metabolism was significantly affected from RT (Figure S4B). This pathway is mainly involved in the synthesis of nucleic acids required for cell division and further proliferation. In fact, dTMP levels were also lower in tumor tissue collected from mice that underwent radiotherapy. This metabolite is a major metabolic component of proliferative processes including DNA synthesis. Therefore, reduced levels of dTMP may indicate reduced proliferation attributable to radiation, which may be reflected in the increased survival of the cohort undergoing RT. These results are interesting since *de novo* pyrimidine synthesis has been recently reported as a novel vulnerability in the IDH1-mutant astrocytoma models and suggests the potential for combining RT with *de novo* pyrimidine synthesis inhibitors (35).

Since the glutamate and fumarate were altered in plasma, we further looked at the [U-^{13}C] glutamine incorporation into various tissue metabolites. Interestingly, ^{13}C labeling of succinate was upregulated, reflecting an increased flux from the [U-^{13}C] glutamine. Since succinate is part of many pathways we speculated where succinate might be needed. Succinate can be produced within the nucleus through TET enzymes, although this process is known to be inhibited by 2HG, that acts as a competitive inhibitor of α-ketoglutarate-dependent dioxygenases (41). Notably, GABA is a precursor of succinate through the activities of GABA transaminase and succinic semialdehyde dehydrogenase (SSADH). Therefore, the decrease in ^{13}C-labeled GABA in tumor tissue under RT along with the significant increase in ^{13}C-succinate levels may indicate a higher flux of GABA towards succinate as a response to treatment. Interestingly, increased succinic semialdehyde dehydrogenase (SSADH) levels, the enzyme that converts GABA into succinate were found in highly proliferative areas within the glioblastoma (42). This is one hypothesis, however, the fate of ^{13}C labeled succinate is not very clear, since we were not able to detect fumarate ^{13}C peaks with our NMR approach.

Taking all these changes together, a dysregulated glutamine metabolism in tumor tissue is observed as a consequence of RT treatment. The increased levels of ATP and GTP in the radiation group can be attributed to an increased transference of energy carriers from the microenvironment in order to maintain the proliferation levels despite the deleterious effects of RT (43). However, we have also observed an increase in the total levels of oxoglutarate and a higher flux from [U-^{13}C]-glutamine to succinate which may indicate an upregulation of the succinyl CoA synthase which yields GTP; intriguingly, the following metabolites, such as fumarate and oxaloacetate, within the TCA cycle, display lower levels in the radiation group which may indicate downregulation of succinate dehydrogenase due to RT.

We have previously reported that the IDH1-mutant mouse model of NCH1681 exhibits an active glycolytic pathway that yields lactate *in vivo* (1), similarly to other aggressive IDH1 mutant glioma models (44). This observation indicates the utilization of this metabolic route to meet the high energetic demands for the enhanced proliferation characteristic of tumors. Lower levels of lactate reported in this investigation in the radiation group may serve as additional evidence for this metabolite to be employed as a marker of RT response in the gliomas (45). Indeed, a recent investigation revealed a decreased glycolytic activity in radiation-induced necrotic tissue based on lower lactate formation in brain tumors and metastasis including CL regions of irradiated mice as controls (46). Additionally, our ^{13}C tracing experiment revealed a significant increase in glutamine-derived succinate levels in tumor tissue after RT and not in the CL of mice from the same cohort. This metabolic response may highlight a potential marker of specific metabolic rewiring in gliomas subjected to radiation. However, the results presented herein are obtained by utilizing one animal model; therefore, preclinical and clinical validation including other glioma models and plasma obtained from patients must be conducted.

Conclusions

Herein, we have reported how plasma metabolomics could be employed as an alternative strategy for assessing response to radiotherapy in glioma. We observed significant changes in the plasma metabolic profile throughout the course of the mice lifespan after treatment which could be validated in the clinic in human patients. Additionally, we describe the radiation-induced changes in tumor tissue, and more specifically, those attributable to the utilization of glutamine which can be further explored by molecular imaging approaches in clinical settings.

Data availability statement

The LC-MS plasma metabolomic dataset generated is available at the NIH Common Fund's National Metabolomics Data Repository (NMDR) website, the Metabolomics Workbench, https://www.metabolomicsworkbench.org where it has been assigned Project ID PR001096. The data can be accessed directly *via* it's Project DOI: 10.21228/M81M6P.

Ethics statement

The animal study was reviewed and approved by Approved animal study proposal NOB-008 by the National Cancer Institute–Animal Use and Care Committee.

Author contributions

VR-R and ML: Conceptualization. ML: Project administration, supervision and funding acquisition. TD, AL, TK, MZ: Formal analysis. CH-M, KC, MG, and ML: Resources. VR-R: Writing—original draft preparation. VR-R, TD, AL, TK, MZ: Formal analysis. TD, AL, TK, MZ, CH-M, KC, TA, DS-M, MG, and ML: Writing—review and editing. All authors have read and agreed to the published version of the manuscript All authors contributed to the article and approved the submitted version.

Funding

This work was supported by the Intramural Research Program, Center for Cancer Research, National Cancer Institute, National Institutes of Health. This work is supported by NIH grant U2C-DK119886.

Acknowledgments

We would like to thank Hua Song, Dionne Davis and Wei Zhang for their help with the animal work.

Conflict of interest

The authors declare that the research was conducted in the absence of any commercial or financial relationships that could be construed as a potential conflict of interest.

Publisher's note

All claims expressed in this article are solely those of the authors and do not necessarily represent those of their affiliated organizations, or those of the publisher, the editors and the reviewers. Any product that may be evaluated in this article, or claim that may be made by its manufacturer, is not guaranteed or endorsed by the publisher.

Supplementary material

The Supplementary Material for this article can be found online at: https://www.frontiersin.org/articles/10.3389/fonc.2022.979537/full#supplementary-material

References

1. Ruiz-Rodado V, Malta TM, Seki T, Lita A, Dowdy T, Celiku O, et al. Metabolic reprogramming associated with aggressiveness occurs in the G-CIMP-High molecular subtypes of IDH1mut lower grade gliomas. *Neuro Oncol* (2019) 22 (4):480–92. doi: 10.1093/neuonc/noz207

2. Louis DN, Perry A, Reifenberger G, von Deimling A, Figarella-Branger D, Cavenee WK, et al. The 2016 world health organization classification of tumors of the central nervous system: a summary. *Acta Neuropathol* (2016) 131(6):803–20. doi: 10.1007/s00401-016-1545-1

3. Li ZH, Guan YL, Liu Q, Wang Y, Cui R, Wang YJ. Astrocytoma progression scoring system based on the WHO 2016 criteria. *Sci Rep* (2019) 9(1):96. doi: 10.1038/s41598-018-36471-4

4. Ivanisevic J, Siuzdak G. The role of metabolomics in brain metabolism research. *J Neuroimmune Pharmacol* (2015) 10(3):391–5. doi: 10.1007/s11481-015-9621-1

5. Zhao H, Heimberger AB, Lu Z, Wu X, Hodges TR, Song R, et al. Metabolomics profiling in plasma samples from glioma patients correlates with tumor phenotypes. *Oncotarget* (2016) 7(15):20486–95. doi: 10.18632/oncotarget.7974

6. Hou Y, Yin M, Sun F, Zhang T, Zhou X, Li H, et al. A metabolomics approach for predicting the response to neoadjuvant chemotherapy in cervical cancer patients. *Mol Biosyst* (2014) 10(8):2126–33. doi: 10.1039/C4MB00054D

7. Ruiz-Rodado V, Luque-Baena RM, te Vruchte D, Probert F, Lachmann RH, Hendriksz CJ, et al. H-1 NMR-linked urinary metabolic profiling of niemann-pick class C1 (NPC1) disease: Identification of potential new biomarkers using correlated component regression (CCR) and genetic algorithm (GA) analysis strategies. *Curr Metabolomics* (2014) 2(2):88–121. doi: 10.2174/2213235X02666141112215616

8. Worley B, Powers R. Multivariate analysis in metabolomics. *Curr Metabolomics* (2013) 1(1):92–107. doi: 10.2174/2213235X11301010092

9. Moren L, Bergenheim AT, Ghasimi S, Brannstrom T, Johansson M, Antti H. Metabolomic screening of tumor tissue and serum in glioma patients reveals diagnostic and prognostic information. *Metabolites* (2015) 5(3):502–20. doi: 10.3390/metabo5030502

10. Jelonek K, Krzywon A, Jablonska P, Slominska EM, Smolenski RT, Polanska J, et al. Systemic effects of radiotherapy and concurrent chemo-radiotherapy in head and neck cancer patients-comparison of serum metabolome profiles. *Metabolites* (2020) 10(2):60. doi: 10.3390/metabo10020060

11. Jelonek K, Pietrowska M, Widlak P. Systemic effects of ionizing radiation at the proteome and metabolome levels in the blood of cancer patients treated with radiotherapy: the influence of inflammation and radiation toxicity. *Int J Radiat Biol* (2017) 93(7):683–96. doi: 10.1080/09553002.2017.1304590

12. Laiakis EC, Pannkuk EL, Chauthe SK, Wang YW, Lian M, Mak TD, et al. A serum small molecule biosignature of radiation exposure from total body irradiated patients. *J Proteome Res* (2017) 16(10):3805–15. doi: 10.1021/acs.jproteome.7b00468

13. Laiakis EC, Nishita D, Bujold K, Jayatilake MM, Bakke J, Gahagen J, et al. Salivary metabolomics of total body irradiated nonhuman primates reveals long-term normal tissue responses to radiation. *Int J Radiat Oncol Biol Physics* (2019) 105(4):843–51. doi: 10.1016/j.ijrobp.2019.07.017

14. Wibom C, Surowiec I, Moren L, Bergstrom P, Johansson M, Antti H, et al. Metabolomic patterns in glioblastoma and changes during radiotherapy: A clinical microdialysis study. *J Proteome Res* (2010) 9(6):2909–19. doi: 10.1021/pr901088r

15. Dao Trong P, Jungwirth G, Yu T, Pusch S, Unterberg A, Herold-Mende C, et al. Large-Scale drug screening in patient-derived IDH(mut) glioma stem cells identifies several efficient drugs among FDA-approved antineoplastic agents. *Cells* (2020) 9(6):1389–404. doi: 10.3390/cells9061389

16. Dettling S, Stamova S, Warta R, Schnolzer M, Rapp C, Rathinasamy A, et al. Identification of CRKII, CFL1, CNTN1, NME2, and TKT as novel and frequent T-cell targets in human IDH-mutant glioma. *Clin Cancer Res* (2018) 24(12):2951–62. doi: 10.1158/1078-0432.CCR-17-1839

17. Ren L, Ruiz-Rodado V, Dowdy T, Huang S, Issaq SH, Beck J, et al. Glutaminase-1 (GLS1) inhibition limits metastatic progression in osteosarcoma. *Cancer Metab* (2020) 8:4. doi: 10.1186/s40170-020-0209-8

18. Lane AN, Yan J, Fan TW. (13)C tracer studies of metabolism in mouse tumor xenografts. *Bio Protoc* (2015) 5(22):1–11. doi: 10.21769/bioprotoc.1650

19. Quansah E, Ruiz-Rodado V, Grootveld M, Probert F, Zetterstrom TSC. (1)H NMR-based metabolomics reveals neurochemical alterations in the brain of adolescent rats following acute methylphenidate administration. *Neurochem Int* (2017) 108:109–20. doi: 10.1016/j.neuint.2017.03.003

20. Fan TW, Lane AN. Applications of NMR spectroscopy to systems biochemistry. *Prog Nucl Magn Reson Spectrosc* (2016) 92-93:18–53. doi: 10.1016/j.pnmrs.2016.01.005

21. Wishart DS, Feunang YD, Marcu A, Guo AC, Liang K, Vazquez-Fresno R, et al. HMDB 4.0: the human metabolome database for 2018. *Nucleic Acids Res* (2018) 46(D1):D608–D17. doi: 10.1093/nar/gkx1089

22. Chong J, Xia J. Using MetaboAnalyst 4.0 for metabolomics data analysis, interpretation, and integration with other omics data. *Methods Mol Biol* (2020) 2104:337–60. doi: 10.1007/978-1-0716-0239-3_17

23. Tai YC, Speed TP. A multivariate empirical bayes statistic for replicated microarray time course data. *Ann Statistics* (2006) 34(5):2387–412. doi: 10.1214/009053606000000759

24. Marquez J, Alonso FJ, Mates JM, Segura JA, Martin-Rufian M, Campos-Sandoval JA. Glutamine addiction in gliomas. *Neurochem Res* (2017) 42(6):1735–46. doi: 10.1007/s11064-017-2212-1

25. Obara-Michlewska M, Szeliga M. Targeting glutamine addiction in gliomas. *Cancers (Basel)* (2020) 12(2):310. doi: 10.3390/cancers12020310

26. Grassian AR, Parker SJ, Davidson SM, Divakaruni AS, Green CR, Zhang X, et al. IDH1 mutations alter citric acid cycle metabolism and increase dependence on oxidative mitochondrial metabolism. *Cancer Res* (2014) 74(12):3317–31. doi: 10.1158/0008-5472.CAN-14-0772-T

27. Seltzer MJ, Bennett BD, Joshi AD, Gao P, Thomas AG, Ferraris DV, et al. Inhibition of glutaminase preferentially slows growth of glioma cells with mutant IDH1. *Cancer Res* (2010) 70(22):8981–7. doi: 10.1158/0008-5472.CAN-10-1666

28. McBrayer SK, Mayers JR, DiNatale GJ, Shi DD, Khanal J, Chakraborty AA, et al. Transaminase inhibition by 2-hydroxyglutarate impairs glutamate biosynthesis and redox homeostasis in glioma. *Cell* (2018) 175(1):101–16. doi: 10.1016/j.cell.2018.08.038

29. Venneti S, Dunphy MP, Zhang H, Pitter KL, Zanzonico P, Campos C, et al. Glutamine-based PET imaging facilitates enhanced metabolic evaluation of gliomas in vivo. *Sci Transl Med* (2015) 7(274):274ra17. doi: 10.1126/scitranslmed.aaa1009

30. Altman BJ, Stine ZE, Dang CV. From Krebs to clinic: glutamine metabolism to cancer therapy. *Nat Rev Cancer* (2016) 16(10):619–34. doi: 10.1038/nrc.2016.71

31. Sultana N, Sun C, Katsube T, Wang B. Biomarkers of brain damage induced by radiotherapy. *Dose Response* (2020) 18(3):1559325820938279. doi: 10.1177/1559325820938279

32. Zhang P, Chen Y, Zhu H, Yan L, Sun C, Pei S, et al. The effect of gamma-Ray-Induced central nervous system injury on peripheral immune response: An *In vitro* and *In vivo* study. *Radiat Res* (2019) 192(4):440–50. doi: 10.1667/RR15378.1

33. Raviraj R, Nagaraja SS, Selvakumar I, Mohan S, Nagarajan D. The epigenetics of brain tumors and its modulation during radiation: A review. *Life Sci* (2020) 256:117974. doi: 10.1016/j.lfs.2020.117974

34. Sulkowski PL, Corso CD, Robinson ND, Scanlon SE, Purshouse KR, Bai H, et al. 2-hydroxyglutarate produced by neomorphic IDH mutations suppresses homologous recombination and induces PARP inhibitor sensitivity. *Sci Transl Med* (2017) 9(375):1–15. doi: 10.1126/scitranslmed.aal2463

35. Shi DD, Savani MR, Levitt MM, Wang AC, Endress JE, Bird CE, et al. *De novo* pyrimidine synthesis is a targetable vulnerability in IDH mutant glioma. *Cancer Cell* (2022) 40(9):939–56.e16. doi: 10.1016/j.ccell.2022.07.011

36. Wang Y, Wild AT, Turcan S, Wu WH, Sigel C, Klimstra DS, et al. Targeting therapeutic vulnerabilities with PARP inhibition and radiation in IDH-mutant gliomas and cholangiocarcinomas. *Sci Adv* (2020) 6(17):eaaz3221. doi: 10.1126/sciadv.aaz3221

37. Choi CH, Raisanen JM, Ganji SK, Zhang S, McNeil SS, An ZX, et al. Prospective longitudinal analysis of 2-hydroxyglutarate magnetic resonance spectroscopy identifies broad clinical utility for the management of patients with IDH-mutant glioma. *J Clin Oncol* (2016) 34(33):4030–U157. doi: 10.1200/JCO.2016.67.1222

38. Moren L, Wibom C, Bergstrom P, Johansson M, Antti H, Bergenheim AT. Characterization of the serum metabolome following radiation treatment in patients with high-grade gliomas. *Radiat Oncol* (2016) 11:51. doi: 10.1186/s13014-016-0626-6

39. Kelimu A, Xie R, Zhang K, Zhuang Z, Mamtimin B, Sheyhidin I. Metabonomic signature analysis in plasma samples of glioma patients based on (1)H-nuclear magnetic resonance spectroscopy. *Neurol India* (2016) 64(2):246–51. doi: 10.4103/0028-3886.177606

40. Pannkuk EL, Laiakis EC, Girgis M, Dowd SE, Dhungana S, Nishita D, et al. Temporal effects on radiation responses in nonhuman primates: Identification of biofluid small molecule signatures by gas chromatography(-)Mass spectrometry metabolomics. *Metabolites.* (2019) 9(5):98. doi: 10.3390/metabo9050098

41. Xu W, Yang H, Liu Y, Yang Y, Wang P, Kim SH, et al. Oncometabolite 2-hydroxyglutarate is a competitive inhibitor of alpha-ketoglutarate-dependent dioxygenases. *Cancer Cell* (2011) 19(1):17–30. doi: 10.1016/j.ccr.2010.12.014

42. El-Habr EA, Dubois LG, Burel-Vandenbos F, Bogeas A, Lipecka J, Turchi L, et al. A driver role for GABA metabolism in controlling stem and proliferative cell state through GHB production in glioma. *Acta Neuropathol* (2017) 133(4):645–60. doi: 10.1007/s00401-016-1659-5

43. Gupta K, Vuckovic I, Zhang S, Xiong Y, Carlson BL, Jacobs J, et al. Radiation induced metabolic alterations associate with tumor aggressiveness and poor outcome in glioblastoma. *Front Oncol* (2020) 10:535. doi: 10.3389/fonc.2020.00535

44. Ruiz-Rodado V, Seki T, Dowdy T, Lita A, Zhang M, Han S, et al. Metabolic landscape of a genetically engineered mouse model of IDH1 mutant glioma. *Cancers (Basel)* (2020) 12(6):1633. doi: 10.3390/cancers12061633

45. Day SE, Kettunen MI, Cherukuri MK, Mitchell JB, Lizak MJ, Morris HD, et al. Detecting response of rat C6 glioma tumors to radiotherapy using hyperpolarized [1-C-13]Pyruvate and c-13 magnetic resonance spectroscopic imaging. *Magnetic Resonance Med* (2011) 65(2):557–63. doi: 10.1002/mrm.22698

46. Park I, Kim S, Pucciarelli D, Song J, Choi JM, Lee KH, et al. Differentiating radiation necrosis from brain tumor using hyperpolarized carbon-13 MR metabolic imaging. *Mol Imaging Biol* (2021) 23(3):417–26. doi: 10.1007/s11307-020-01574-w

frontiers | Frontiers in Oncology

TYPE Original Research
PUBLISHED 16 May 2023
DOI 10.3389/fonc.2023.1125855

OPEN ACCESS

EDITED BY
Jaroslav Truksa,
Institute of Biotechnology (ASCR), Czechia

REVIEWED BY
Marco Sciacovelli,
University of Liverpool, United Kingdom
Shivani Bansal,
Georgetown University, United States

*CORRESPONDENCE
Ferdinando Chiaradonna
ferdinando.chiaradonna@unimib.it

RECEIVED 16 December 2022
ACCEPTED 26 April 2023
PUBLISHED 16 May 2023

CITATION
Zerbato B, Gobbi M, Ludwig T, Brancato V, Pessina A, Brambilla L, Wegner A and Chiaradonna F (2023) PGM3 inhibition shows cooperative effects with erastin inducing pancreatic cancer cell death *via* activation of the unfolded protein response.
Front. Oncol. 13:1125855.
doi: 10.3389/fonc.2023.1125855

PGM3 inhibition shows cooperative effects with erastin inducing pancreatic cancer cell death *via* activation of the unfolded protein response

Barbara Zerbato[1], Maximilian Gobbi[1], Tobias Ludwig[2], Virginia Brancato[1,3], Alex Pessina[1], Luca Brambilla[1], Andre Wegner[2] and Ferdinando Chiaradonna[1]*

[1]Tumor Biochemistry, Biotechnology and Biosciences, University of Milano Bicocca, Milan, Italy, [2]Pathometabolism, Department of Bioinformatics and Biochemistry, Braunschweig Integrated Centre of Systems Biology (BRICS), Technische Universität Braunschweig, Braunschweig, Germany, [3]Center for Genomic Science IIT@SEMM, Italian Institute of Technology, Milan, Italy

Background: Pancreatic ductal adenocarcinoma (PDAC) is a highly aggressive cancer with a poor patient prognosis. Remarkably, PDAC is one of the most aggressive and deadly tumor types and is notorious for its resistance to all types of treatment. PDAC resistance is frequently associated with a wide metabolic rewiring and in particular of the glycolytic branch named Hexosamine Biosynthetic Pathway (HBP).

Methods: Transcriptional and bioinformatics analysis were performed to obtain information about the effect of the HBP inhibition in two cell models of PDAC. Cell count, western blot, HPLC and metabolomics analyses were used to determine the impact of the combined treatment between an HBP's Phosphoglucomutase 3 (PGM3) enzyme inhibitor, named FR054, and erastin (ERA), a recognized ferroptosis inducer, on PDAC cell growth and survival.

Results: Here we show that the combined treatment applied to different PDAC cell lines induces a significant decrease in cell proliferation and a concurrent enhancement of cell death. Furthermore, we show that this combined treatment induces Unfolded Protein Response (UPR), NFE2 Like BZIP Transcription Factor 2 (NRF2) activation, a change in cellular redox state, a greater sensitivity to oxidative stress, a major dependence on glutamine metabolism, and finally ferroptosis cell death.

Conclusion: Our study discloses that HBP inhibition enhances, via UPR activation, the ERA effect and therefore might be a novel anticancer mechanism to be exploited as PDAC therapy.

KEYWORDS

hexosamine biosynthetic pathway, unfolded protein response, pancreatic cancer cells, cell death, erastin, ferroptosis

Introduction

Pancreatic ductal adenocarcinoma (PDAC) is a highly aggressive cancer with a poor patient prognosis (1). Conventional therapy, for both resectable and unresectable PDAC, relies mainly on the use of the chemotherapeutic agent gemcitabine (GEM) either alone or in combination with adjuvant therapies such as paclitaxel conjugated to albumin, 5-FU, capecitabine, and erlotinib, which can increase median OS as compared with GEM monotherapy (2). Despite the fact that drug combinations improve the median survival rate compared to GEM alone, these novel combinations elicit resistance within weeks and hence fail to bring tumor regression. For this reason, there is an urgent need to search for new pharmacological targets that will boost the sensibility to current treatments and reduce drug resistance.

Tumor metabolic rewiring and metabolic adaptation following drug treatments are typical clues of PDAC (3). Indeed, different reports indicate that reprogrammed metabolism closely regulates PDAC development and chemoresistance (4, 5). Among the different metabolic alterations observed in PDAC, the increased flux through the hexosamine biosynthetic pathway (HBP) tightly linked with glucose and glutamine metabolism has been found as a key metabolic change (6, 7). Worthy of note, the final metabolite generated by the HBP is the uridine 5′-diphospho-*N*-acetyl-D-glucosamine (UDP-GlcNAc), the main substrate for O- and N-protein glycosylation. Both post-translational modifications (PTMs) play critical roles in protein folding, stability, activity, macromolecular interactions, function, and nuclear translocation. Therefore, enhancement of HBP flux, responsible for the aberrant protein glycosylation often observed in different types of tumors including PDAC (8, 9), could represent a new target for tumor therapy.

In this regard, we have recently developed and tested in breast and pancreatic cancer cells as well as *in vivo* models a novel compound, FR054. This molecule is an N-acetyl-glucosamine 6-phosphate analogue capable of diminishing the HBP flux by targeting the HBP enzyme PGM3, leading first to a cell proliferation inhibition and then to cell death (10, 11), underlining the fundamental role of this pathway in breast and pancreatic cancer cell proliferation and survival. Importantly, FR054, if combined with GEM (12) or the pan-KRAS inhibitor BI-2852 (13), significantly enhances PDAC cancer cells' sensitivity to both drugs, also suggesting a role of HBP in drug resistance.

Our previous findings indicated that the death mechanism induced by FR054 is dependent on the acute activation of the unfolded protein response (UPR). Indeed, HBP flux reduction, decreasing UDP-GlcNAc availability, causes a reduction in protein N-glycosylation, an accumulation of misfolded proteins, and finally irremediable cell damage, which drives CHOP-dependent apoptotic signaling (11, 12). Worthy of note, previous reports propose that the UPR is constitutively active in PDAC and it may contribute to the disease progression and the acquisition of resistance to therapy (14). Thus, these different findings highlight a dual role for UPR in correlation with its level of activation. In particular, it is either an adaptive cellular mechanism to weaken protein and metabolic stresses created by a hypoxic environment and to induce chemoresistance, or it is an apoptotic inducer when prolonged in time (15). For this reason, some authors have suggested that targeting UPR in cancer including in PDAC may be highly beneficial, especially in combinatorial treatments that could provide an effective anti-tumorigenic response in patients.

Therefore, in this study, we aimed to further detail the mechanism of FR054-induced cell death, in order to verify whether its pro-apoptotic ability could be enhanced by co-targeting a specific protein or cellular pathway. For this purpose, we performed an RNA-seq analysis in two different PDAC cell lines, namely, MiaPaCa-2 and BxPC3, treated with FR054 to provide unbiased mechanistic insights. Results demonstrate that FR054 treatment induces expression of genes related to UPR, to the NRF2 pathway, and to glutathione biosynthesis and ferroptosis. Consequently, we show that inhibition of glutathione biosynthesis, by using the specific inhibitor for the Solute Carrier Family 7 Member 11/xCT (SLC7A11), ERA, in combination with FR054, significantly enhanced the FR054 effect causing a noteworthy increase in cancer cell proliferation arrest and death. Remarkably, the latter effect was tightly associated with a higher expression of the pro-apoptotic protein DNA Damage Inducible Transcript 3/CHOP (CHOP), reduced activity of SLC7A11 transporter, an alteration of intracellular glutathione (GSH) and glutathione disulfide (GSSG) levels, and a strengthening of lipid peroxidation, indicating that SLC7A11 inhibition is synthetic lethal with FR054. Notably, the metabolic analysis supported the role of FR054 in favoring glutamine metabolism over glycolysis. Therefore, our work reveals that simultaneous inhibition of HBP with FR054 and GSH metabolism could have therapeutic benefits in the treatment of pancreatic cancer.

Materials and methods

Materials

N-Acetyl-L-cysteine (NAC), DL-Buthionine-sulfoximine (BSO), and BPTES were purchased from Sigma-Aldrich (Merck Life Science, Milan, Italy), while erastin (ERA) was purchased from Selleckchem (Planegg, Germany). FR054 was synthesized either by our laboratories or by WuXi AppTec Co., Ltd. (Tianjin, China) (10, 11).

Cell lines

Human pancreatic ductal adenocarcinoma cell lines MiaPaCa-2 and PANC1 were routinely cultured in high glucose Dulbecco's medium Eagle's medium (DMEM), while the BxPC3 cell line was cultured in RPMI (Euroclone, Milan, Italy). Both media were supplemented with 2 mM L-glutamine, 100 U/ml penicillin, 100 µg/ml streptomycin (Sigma-Aldrich, Merck Life Science, Milan, Italy), and 10% fetal bovine serum (FBS; Euroclone, Milan, Italy). The cells were grown and maintained according to standard cell culture protocols and kept at 37°C with 5% CO_2. The medium was replaced every 2–3 days and cells were split or seeded for experiments when they reached the sub-confluence. MiaPaCa-2,

PANC1, and BxPC-3 were originally obtained from the American Type Culture Collection (ATCC).

Trypan blue vital assay

Where not differently specified, for experiments, cells were seeded in the complete growth medium, and after 24 h, cells were washed twice with phosphate buffer saline 1X (PBS 1X, Euroclone, Milan, Italy) and incubated in a complete medium with or without FR054. Twenty-four hours later, cells were also treated with or without 10 μM ERA.

Trypan blue vital assay was performed by seeded 4×10^4 (MiaPaCa-2 and PANC1) and 8×10^4 (BxPC3) viable cells per well in 12-well dishes, respectively. Inhibition of proliferation and cell death were assessed at different time points (48 and 72 h), counting harvested cells with Burker chamber after staining with trypan blue 0.4% (Life Technologies–Thermo Fisher Scientific, Waltham, MA, USA). In particular, cells were incubated in a complete medium with or without 350 μM FR054 for 24 h and then, after further 24 h, were also treated with or without 10 μM BPTES or 10 μM erastin. The MiaPaCa-2 cell line was also tested with two different concentrations of FR054, namely, 350 μM or 500 μM, to define an optimal concentration for all the other experiments in all PDAC cell lines. Cell death was also measured at 72 h of treatments as previously described, using a different treatment scheme: 24 h after seeding, cells were incubated in a complete medium with or without 350 μM FR054, and at 48 h post-seeding, cells were also treated with or without 10 μM ERA and 5 mM NAC or 5 mM BSO.

Western blot analysis

MiaPaCa-2 (6×10^5 cells) and BxPC3 (1.2×10^6 cells) were seeded onto 100-mm dishes in the complete growth medium. After 48 and 72 h, cells were harvested and disrupted in a buffer containing 50 mM Tris-HCl, pH 7.6, 150 mM NaCl, 1% (v/v) Triton X-100, 0.2% (v/v) sodium dodecyl sulfate (SDS), 0.5% (v/v) sodium deoxycholate, 1 mM $MgCl_2$, 1 mM EDTA, protease inhibitor cocktail, and phosphatase inhibitors (Sigma-Aldrich, Milan); 20 μg of total proteins was resolved by SDS-PAGE and transferred to the nitrocellulose membrane, which was incubated overnight with specific primary antibodies: cleaved caspase-3 (#9662S, 1:500), GRP78 (BiP, #3177, 1:1,000), phospho-eIF2α Ser 51 (#3398, 1:1,000) from Cell Signaling Technology Inc. (Euroclone, Milan, Italy), eIF2α (sc-133127, 1:1,000) from Santa Cruz Biotechnology Inc. (DBA Italia, Milan, Italy), ATF4 (#11815, 1:800), CHOP (#2895, 1:1,000) from Cell Signaling Technology Inc. (Euroclone, Milan, Italy), NRF2 (sc-13032, 1:1,000) from Santa Cruz Biotechnology Inc. (DBA Italia, Milan, Italy), SLC7A11 (ab175186, 1:5,000) from Abcam (Cambridge, UK), HO-1 (HMOX1; #86806, 1:500) from Cell Signaling Technology Inc. (Euroclone, Milan, Italy), and Keap1 (sc-365626, 1:1,000) and Vinculin (#sc-5573, 1:10,000) from Santa Cruz Biotechnology Inc. (DBA Italia, Milan, Italy). Levels of protein expression on Western blots were quantified by densitometry analysis using ImageJ software.

Glutamic acid and cystine determination

Cells were plated at a density of 4×10^4 (MiaPaCa-2 and PANC1) and 8×10^4 (BxPC3) per well in 12-well dishes. The media used for subsequent HPLC analyses were collected after 48 h and 72 h of treatment. Glutamic acid and cystine concentrations were determined by chromatographic analysis using a Jasco HPLC system (Jasco Europe, Cremella, Lecco, Italy) under the control of the ChromNAV 2.0 software. The analyses were carried out using the method described by Henderson et al. with some modifications. The derivatized amino acids were separated using a Waters (Milford, MA, USA) XTerra RP18 Column (4.6 mm × 250 mm i.d., 5 μm particle size) equipped with a precolumn Security Guard (Phenomenex, Macclesfield, UK). The flow rate was set at 1 ml/min with the column oven at 40°C. Twenty microliters of the sample, appropriately diluted, was injected into the system and the chromatogram was monitored at 338 nm. The pre-column derivatizing reagent o-Phtalaldehyde (OPA) was prepared by dissolving 25 mg of OPA and 25 mg of 3-Mercaptopropionic acid in 5 ml of 0.2 M borate buffer, pH 10.2, and stored at 4°C until any sign of degradation. The samples were prepared by adding 5.5 μl of the derivatization reagent to 5.5 μl of the samples and bringing the volume up to 200 μl with water. HPLC separation employed mobile phases A (40 mM sodium phosphate buffer, pH 7.8) and B (30% acetonitrile:60% methanol:10% H_2O). The column was equilibrated with 94.5%/5.5% (v/v) mobile phase A/B for 10 min before each sample analysis. The elution gradient consisted of 94.5%/5.5% (A/B) for 0.85 min; 2.15-min linear gradient to 13% phase B; 23-min linear gradient to 54% phase B; 94.5%/5.5% (A/B) for 4 min. Amino acid peaks were identified by comparing their retention times with that of the standard mixture. At the end of every set of samples, the column was washed with 20% acetonitrile–80% water for 30 min to remove any trace of salts, and then with 80% acetonitrile–20% water for 20 min and stored in solution.

Cell morphology

MiaPaCa-2, PANC1, and BxPC3 cells were plated onto 100-mm dishes in the complete growth medium at a density of 6×10^5, 6×10^5, and 1.2×10^6 per well, and they were treated with 350 μM FR054 after 24 h. At 48 h post-seeding, the cells were treated with 10 μM ERA. The images were collected with Olympus CX40 phase contrast microscope using a 20X objective using X_entry Alexasoft Imaging Software.

GSH and GSSG evaluation

To measure reduced glutathione (GSH) and oxidized glutathione (GSSG) content, MiaPaCa-2, PANC1, and BxPC3 cells were plated in six-well dishes at a density of 1×10^5, $1 \times$

10^5, and 2×10^5 per well, respectively. Intracellular GSH and GSSG levels were determined after 48 h of FR054 and erastin in single or combined treatment by VICTOR X3 multimode plate reader (PerkinElmer, Milan, Italy) using a Total GSH/GSSG colorimetric kit (CO-K097-M, Immunological Sciences, Rome, Italy) according to the manufacturer's instructions. The sample absorbance was measured at 412 nm. Relative GSH and GSSG content was normalized to the cell number.

BODIPY assay

To evaluate lipid peroxidation, the BODIPY 581/591 C11 dye (Life Technologies–Thermo Fisher Scientific, Waltham, MA, USA) staining was carried out. One day before treatment, MiaPaCa-2, PANC1 (5×10^3 cells) and BxPC3 (1×10^4 cells) were seeded onto a black 96-well plate in the complete growth medium. Then, cells were incubated in the complete medium with or without 350 μM FR054. After 24 h, cells were also treated with or without 10 μM ERA. All cell lines were also treated with 5 mM NAC or 5 mM BSO as controls for the presence of oxidative stress. Lipid peroxidation level was measured after 48 h of treatment. Cells were washed twice with PBS 1X and incubated in PBS 1X with 10 μM BODIPY C11 dye for 15 min at 37°C. Then, cells were washed again with PBS 1X, and the dye fluorescence was measured. Oxidation of BODIPY C11 resulted in a shift of the fluorescence emission peak from 590 nm to 510 nm proportional to lipid ROS generation and was analyzed using FLOUstar® Omega (BMG Labtech, Germany).

MDA assay

To evaluate the formation of the lipid peroxidation product, malondialdehyde (MDA), the cells were seeded at a density of 6×10^5 (MiaPaCa-2 and PANC1) or 1.2×10^6 (BxPC3) onto 100-mm dishes in the complete growth medium. The MDA levels in the cells were measured after 48 h of FR054 and ERA in single or combined treatment using MDA Colorimetric assay kit (CO-K028-M, Immunological Sciences, Rome, Italy) according to the manufacturer's instructions. The sample absorbance was measured at 532 nm by VICTOR X3 multimode plate reader (PerkinElmer, Milan, Italy) and the relative MDA concentration was normalized to the protein content.

Stable isotope labeling and GC/MS

All extraction experiments were performed within 3 weeks upon cell thawing. The cells were plated in six-well dishes at a density of 9×10^4 cells/well for MiaPaCa-2 and PANC1 cell lines or 1.1×10^5 cells/well for the BxPC3 cell line. After 24 h of seeding, the media were replaced with DMEM for mass spectrometry (Sigma-Aldrich, Merck Life Science, Milan, Italy) for MiaPaCa-2 and PANC1 cell lines, and with MS-Grade SILAC RPMI 1640 (Gibco, Thermo Fisher Scientific, Waltham, MA, USA) medium, without Phenol Red, L-Arginine, and L-Lysine, which were manually added at a concentration of 200 mg/ml and 40 mg/ml, respectively, for the BxPC3 cell line. In both media, 10% sterile-filtered dialyzed FBS was added (Gibco, Thermo Fisher Scientific, Waltham, MA, USA). For stable isotope labeling, in media, U13C Glucose and unlabeled Glutamine or U13C Glutamine and unlabeled Glucose (Sigma-Aldrich, Merck Life Science, Milan, Italy) were also added. After 48 h of FR054 and ERA in single or combined treatment, the medium of each condition was collected, and wells were washed with 0.9% NaCl solution to perform metabolite extraction following standard laboratory procedure as described in Ref (16).. Then, the polar phase (upper phase) was collected, dissolved in MeOH/IS water, and transferred to a GC/MS glass vial. The eluates were evaporated in a vacuum concentrator system (CentriVap; Labconco, Kansas City, MO, USA) and stored at −20°C until further analysis. Targeted analysis was carried out on an Agilent 7890B Gas Chromatograph equipped with a 30-m DB-35MS + 5-m Duraguard capillary column. Helium was used as carrier gas at a flow rate of 1 ml per minute. The system was connected to an Agilent 5975 Mass Spectrometer (Agilent Technologies, Santa Clara, CA, USA). Derivatization reagent N-tert-butyldimethylsilyl-N-methyltrifluoroacetamide, 1% tert-butyldimethylchlorosilane (MTBSTFA with 1% t-BDMCS; Restek Corporation, Bellefonte, PA, USA), and methoxylamine (MeOX), dissolved in pyridine at a concentration of 20 mg/ml, were added to protect metabolites. Mixing was carried out by an autosampler dissolving in MeOX/pyridine and shaking at 40°C for 90 min. Afterward, derivatization agents were injected into vials, shaken for 30 or 60 min at 40°C, and analyzed. The GC oven was set to 100°C for 2 min, increasing the temperature to 10°C per minute until it reached 300°C. Temperature was maintained for 3 min, raising it then by another 25°C. MS performed the electron ionization at 70 eV, the source had a constant temperature of 230°C, and quadrupoles had a constant temperature of 150°C. Analytes were detected in selected ion monitoring (SIM) mode. Raw GC/MS data were analyzed on MetaboliteDetector, an open-source software running on Linux-based operative systems developed by Karsten Hiller et al. (17). Chemical formulas for mass isotopomer distribution (MID) determination were taken from (18).

Gene expression analysis

Two biological replicates were used for gene expression analysis. In particular, MiaPaCa-2 and BxPC3 cell lines were seeded at a density of 5×10^6 cells in 100-mm dishes and, after 24 h, were treated with 350 μM FR054 and incubated for 48 h. Then, the cells, untreated and treated, were pelletized and the mRNA was extracted by using Qiagen RNeasy Kit (X) starting from 5×10^6 cells/sample. RNA-seq experiments, data extraction, and analysis were performed in outsourcing (GALSEQ, Milan, Italy). In particular, total RNA was quantified using a spectrophotometer and RNA integrity was evaluated using the Agilent 4200 TapeStation. RNA-stranded libraries were generated starting from 500 ng of total RNA, and mRNA was selected with poly-T oligo attached magnetic beads using an Illumina TruSeq® Stranded mRNA Library Prep kit (Catalog # 20020594). Libraries were quantified and quality checked

on an Agilent 4200 TapeStation system (High Sensitivity D1000), and then sequenced on an Illumina NovaSeq 6000 platform with paired-end reads 150 bp long, with a depth of 30 million clusters/sample. Fastq reads were quality checked using FastQC (https://www.bioinformatics.babraham.ac.uk/projects/fastqc/) for overall and per-base read quality and presence of adaptor sequences. Paired reads were subsequently aligned to the human reference genome (GRCh38/hg38) using the splice-aware aligner STAR v 2.5.0c and indexed with Samtools. Per-gene read counts were generated using the STAR quantMode geneCounts option. Raw per-gene read counts were then processed using the Bioconductor package DESeq2 package v. 1.30 (19) in order to perform the differential expression analysis. Genes with an adjusted *p*-value [Benjamini–Hochberg false discovery rate (FDR)] < 0.05 and log2FC <−2 or >2 were considered as differentially expressed. Sorted, indexed bam files were finally used for manual quality check of the alignment profiles. The RNA-seq data have been deposited at the NCB-GEO database, accession number GSE223303.

Statistical analysis

All statistical analyses were performed using GraphPad Prism v 8.0.2 (GraphPad Software Inc., La Jolla, CA) and data are presented as mean ± SD and as mean ± SEM from three or more independent experiments. For the inhibition of proliferation evaluated after treatment with different concentrations of FR054 and/or ERA/BPTES and for GSH, GSSG, and MDA determination, statistical significance (*$p < 0.05$, **$p < 0.01$, ***$p < 0.001$, ****$p < 0.0001$) was determined using one-way ANOVA with Tukey's multiple comparisons test. For GC/MS analysis performed with stable isotope labeling, statistical significance (*$p < 0.05$, **$p < 0.01$, ***$p < 0.001$) was determined with Student's *t*-test. Instead, for all other experiments, statistical significance (*$p < 0.05$, **$p < 0.01$, ***$p < 0.001$ ****$p < 0.0001$) was determined using two-way repeated measures ANOVA with Tukey's multiple comparisons test.

Results

Transcriptional analysis reveals upregulation of NRF2 and ferroptosis pathways following PDAC cells treatment with FR054

To gain insights into the transcriptional differences between the KRAS PDAC mutated cell line, MiaPaCa-2, and wild-type PDAC cell line, BxPC3, upon FR054 treatment, we compared FR054-regulated transcriptome to untreated samples in MiaPaCa-2 and BxPC3 cells by RNA-seq analyses. To find differentially expressed genes (DEGs), we used mRNAs showing twofold changes with *p*-values smaller than 0.05. The analysis of MiaPaCa-2 cells captured 1,648 DEGs, among which 910 were significantly upregulated and 738 were significantly downregulated in FR054-treated cells as compared to untreated cells (Figure 1A, Supplementary Table 1). In BxPC3 cells, the analysis identified 373 DEGs, among which 100 were significantly upregulated and 273 significantly downregulated in FR054-treated cells as compared to untreated cells (Figure 1B). We found that genes containing antioxidant response element (ARE) regulated by NRF2 protein, including *Heme Oxygenase 1 (HMOX1)*, *Glutamate-Cysteine Ligase Catalytic Subunit (GCLC)*, *Glutamate-Cysteine Ligase Modifier Subunit (GCLM)*, *Spermidine/Spermine N1-acetyltransferase 1* (*SAT1*), *Aldo-Keto Reductase Family 1 Member C1* (*AKR1C1*), *Oxidative Stress Induced Growth Inhibitor 1 (OSGIN1), Glutathione-Disulfide Reductase (GSR), SLC7A11, Thioredoxin Reductase 1 (TXNRD1) Ferritin Light Chain (FTL), Activating Transcription Factor 3 (ATF3), Aldehyde dehydrogenase 3A1 (ALDH3A1)*, and *Alpha/beta-hydrolase domain containing 4 (ABHD4)*, were the top enriched genes in treated cell lines compared with untreated cells. It should also be noted that the other top enriched genes were related to the anti-oxidant response regulated by NRF2 since *MAF BZIP Transcription Factor G* (*MafG*) heterodimerizes with NRF2 and *NmrA Like Redox Sensor 1* (*NMRAL1P1*), which encodes for an NADPH sensor protein, is tightly associated with the NRF2 pathway. In addition, as expected for the well-known capacity of FR054 to induce ER stress and UPR, some transcription factors (TFs), tightly linked to this response, including *DNA Damage Inducible Transcript 3/CHOP (DDIT3)*, *Early Growth Response 1 (EGR1)* and *Activating Transcription Factor 3 (ATF3)*, were more upregulated in MiaPaCa-2-treated cells. To computationally confirm the specific enrichment of some TFs as responsible for the observed changes in gene expression upon FR054 treatment, upregulated DEGs for both cell lines were used as a query to interrogate the ChEA3-ChIP-X Enrichment analysis libraries using the web-based software Enrichr (20). In particular, we used for MiaPaCa-2 cells 700 out of 910 upregulated DEGs with a $\log_2$FC ≥ 2 and the ReMap library (21). Conversely, since there are few upregulated DEGs for BxPC3 cells (specifically 100, but only 80 were recognized by the database), we decided to also accept for the TF enrichment analysis the upregulated DEGs with a $\log_2$FC ≥1.5 (upregulated genes used: 137) and the Top rank analysis that gives as readout the integrated results from all the ChEA3-ChIP-X libraries. As shown in Supplementary Tables 2, 3, in MiaPaCa-2 cells, we identified among the top 10 enriched TFs not only NRF2 (NFE2L2) but also other TFs related to NRF2 activity including CEBPB, ATF3, and MAFF. Equally in BxPC3 cells, we identified NRF2 and some other TFs related to NRF2 activity including MAFG, ATF3, and BACH1. In line with these results, gene set enrichment analysis (GSEA) of the RNA-seq transcriptional profiling showed in both cell lines an upregulation of NRF2, UPR, and ferroptotic pathways in treated cells compared with control cells (Figures 1C, D, Figures S1, S2). To further detail the activation of NRF2 and ferroptosis-related genes, we searched in our RNA-seq data mRNAs (*p*-values smaller than 0.05) related to NRF2-dependent activation mechanism as well as genes related to ferroptosis. In particular, we identified six different cellular processes linked to NRF2 activity and/or ferroptosis, namely gluthatione metabolism, iron metabolism, ROS metabolism, lipid metabolism, metabolism, and autophagy as well as TFs associated with NRF2. As shown in the dendrograms presented in Figure 2A, several mRNAs linked to these selected processes were significantly

10.3389/fonc.2023.1125855

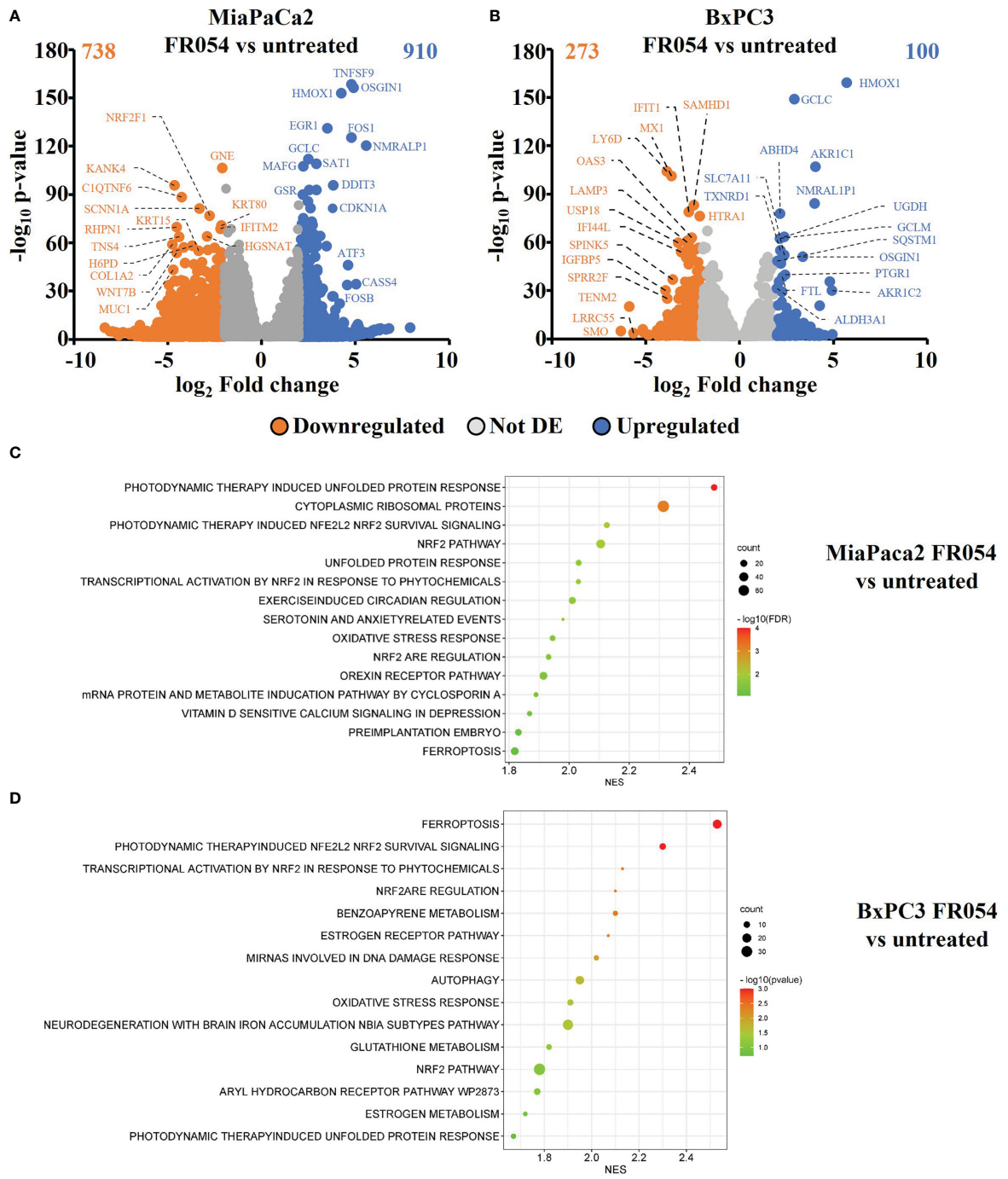

FIGURE 1
Identification and characterization of DEGs in PDAC cell lines upon FR054 treatment compared to control. **(A, B)** Volcano plot of DEGs identified in MiaPaCa-2- and BxPC3 FR054-treated cells versus untreated cells. Upregulated genes are indicated with cyan dots; downregulated genes are indicated with orange dots; not DEGs are indicated with gray dots. DEGs *p*-value <0.05. The top 15 DEGs are depicted. **(C, D)** Gene set enrichment analysis (GSEA) performed by using the DEGs shown in A and B of MiaPaCa-2- and BxPC3 FR054-treated cells versus untreated cells.

regulated upon FR054 treatment, especially in MiaPaCa-2 cells compared to BxPC3 cells. Indeed, FR054 treatment transcriptionally upregulated most of the genes involved in GSH metabolism [*cystine/glutamate antiporters SLC7A11* and *SLC3A2* and *Glutathione-Disulfide Reductase (GSR)*]; glutamine, cysteine, and glycine metabolism (*GLS1*, *GCLM*, *GCLC*, *GOT1*, *PHGDH*, and *PSAT1*); NADPH production (*G6PD*, *PGD*, and *ME1*); and genes involved in anti-ferroptosis mechanisms such as iron transport and storage (*FTH1* and *FTL*), Fe^{2+} sequestration (*NUPR1* and *LCN2*), membrane repair mechanisms (*AIFM2*, *NQO1*, and *AKR1Cs*), and autophagic genes associated with both NRF2 activation and ferroptosis (*GABARAPL1*, *MAP1LC3B2*, and *SQSTM1*). Conversely, genes associated with lipid metabolism, generally repressed by NRF2, such as *ACACA*, *SCD*, *LPCAT3*, *FADS2*, and

10.3389/fonc.2023.1125855

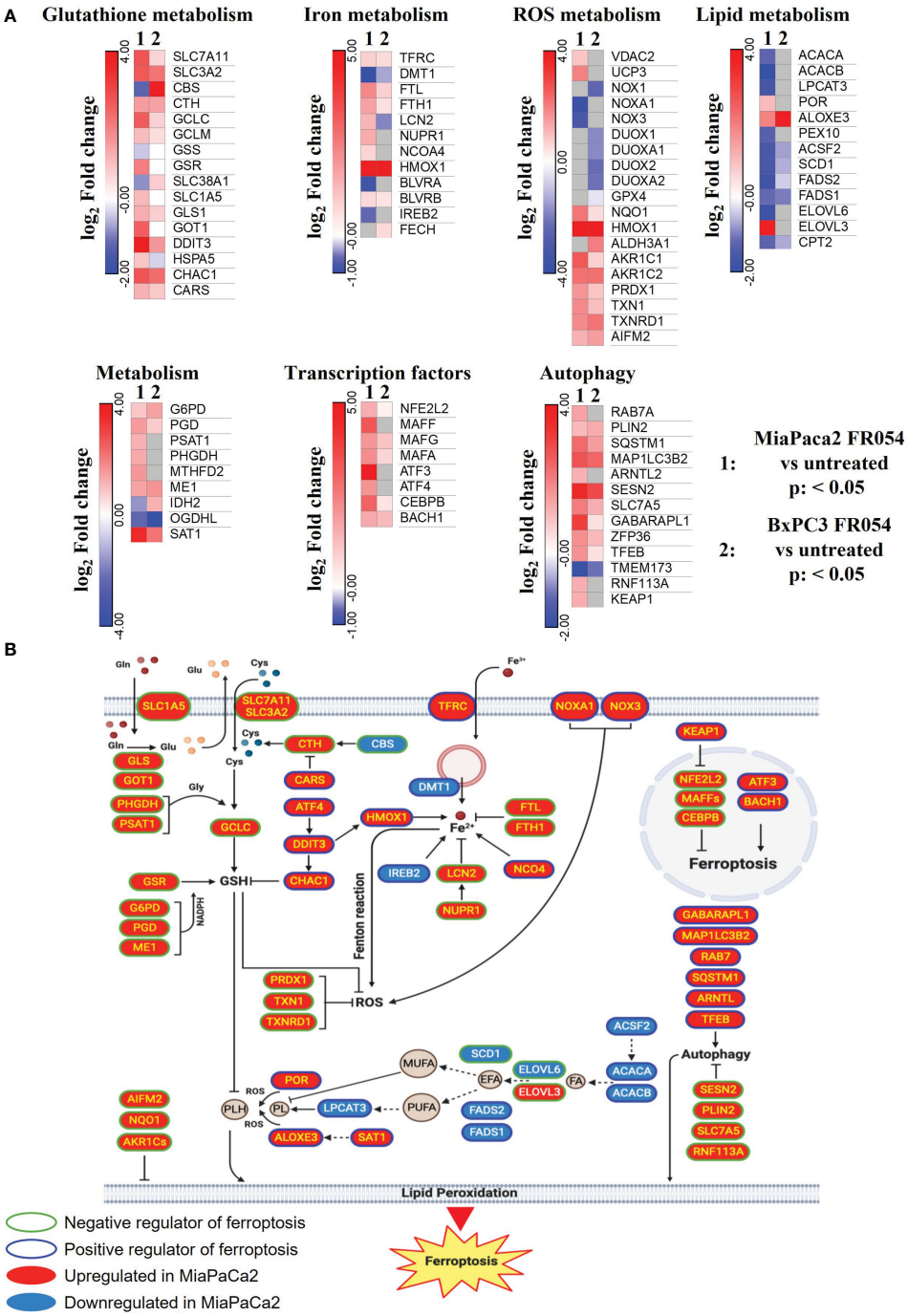

FIGURE 2
DEGs in MiaPaCa-2- and BxPC3 FR054-treated cells versus untreated cells are enriched of mRNAs involved in oxidative stress response and ferroptosis. **(A)** Dendrograms show genes belonging to the cellular processes described in the figure that are present in the list of the DEGs [*p*-value <0.05, Benjamini–Hochberg false discovery rate (FDR)]. In the heat map, color indicated $\log_2$ fold change; red represents upregulated genes, blue represents downregulated genes, white denotes no DEGs, and gray indicates missing values. **(B)** The cartoon shows the role of some of the genes identified in **(A)** in the ferroptosis process as described in the main text.

ELOVL6 were downregulated, further confirming an FR054-dependent activation of the NRF2 axis. The latter effect was also confirmed by the concomitant upregulation of different TFs related to the NRF2 pathway including *MAFA*, *MAFG*, *MAFF*, *CEBPB*, *ATF4*, and *NRF2* as well. Of note, FR054 also induced a few important ferroptosis genes including *CHAC1*, a γ-glutamyl cyclotransferase toward glutathione, a well-known ferroptosis marker, and HMOX1, the major intracellular source of iron Fe^{2+} (Figure 2B). Several of these genes were equally regulated in BxPC3 but to a lesser extent, suggesting a lower antioxidant response as compared to MiaPaCa-2 cells upon FR054 treatment. Altogether, transcriptional data demonstrate that, in both cell lines, FR054

treatment is associated with the induction of genes involved in a large NRF2-dependent antioxidant response and a significant alteration of genes associated with either inhibition or induction of ferroptosis (Figure 2B), therefore suggesting that drugs interfering with these mechanisms could be used in the experiment of synthetic lethality in combination with FR054.

Inhibition of glutamine/glutamate metabolism enhances the effect of FR054 by increasing PDAC cell death

NRF2 is a master regulator of antioxidative responses and plays critical roles in maintaining redox balancing; thus, NRF2 activators attenuate oxidative stress. Indeed, NRF2 is one of the key regulators of GSH metabolism. GSH synthesis enzyme glutamate-cysteine ligase, glutathione synthetase, and reductase are target genes of NRF2 (22). Glutaminase (GLS), which can catalyze glutamine into glutamate, is also promoted by NRF2 (23). Moreover, the expression of SLC7A11, the light chain subunit of the Xc- antiporter system (xCT), is activated by NRF2. xCT, a translocator of cystine and glutamate, imports and exports cystine and glutamate into and out of the cell, respectively. Since our transcriptional data clearly indicated an activation of the GSH metabolism upon FR054, we tested if inhibition of glutamine/glutamate utilization by PDAC cells could increase FR054 cytotoxicity, enlightening a cooperative lethal effect between HBP inhibition and GSH synthesis inhibition. To this end, MiaPaCa-2 cells were first treated for 24 h with FR054 (350 μM) and then treated for a further 24 h with two well-known inhibitors, ERA (10 μM), which blocks the activity of the antiporter SLC7A11, and Bis-2-(5-phenylacetamido-1,3,4-thiadiazol-2-yl)ethyl sulfide (BPTES) (10 μM), which blocks the activity of GLS1, either alone or in combination with FR054 (Figure S3A for the experimental scheme).

In MiaPaCa-2 cells, as result of vital cell count, ERA treatment reduced cell proliferation by around 30%, BPTES by approximately 43%, and FR054 by approximately 52% compared to untreated cells (Figure 3A), suggesting an important proliferative role of glutamine metabolism in this cell line. Remarkably, the FR054 anti-proliferative effect was significantly enhanced when combined with ERA and BPTES since the proliferation reduction reached the values of 69% and 61% in combined treatments, respectively.

Taking into consideration the greater outcome of the combination of FR054 and ERA, we decided to further detail this effect by increasing the amount and the time of the treatment with FR054. In particular, the cells were treated as described in the scheme of Figure S3B. Briefly, cells were treated for 24 h with two different amounts of FR054 (350 and 500 μM) and then treated for a further 48 h with ERA (10 μM) alone or in combination with FR054. The cell survival was analyzed by counting the cells at 72 h. As shown in Figure 3B, 48 h of ERA treatment caused almost a 30% reduction in cell proliferation. As previously published, a dose-dependent cell proliferation arrest was observed in MiaPaCa-2 cells treated for 72 h with FR054 (12). Indeed, FR054 treatment at 350 and 500 μM caused a cell number reduction of approximately 36% and 70%, respectively, as compared to control cells (Figure 3B). Remarkably, such an anti-proliferative effect was significantly enhanced by ERA since the proliferation reduction reached 92% and 95% at 72 h in combined treatments, suggesting that SLC7A11 antiporter activity is necessary for cancer survival under HBP inhibition.

To further evaluate the cooperative effect of ERA when combined with FR054, we tested the combination in MiaPaCa-2 and BxPC3 cells along a time course of 72 h, by using the lowest dose of FR054 (350 μM) and analyzing both proliferation and cell death by vital trypan blue staining. As shown in Figures 3C, D, ERA alone at 48 h, as previously published (24), had a lower effect in MiaPaCa-2 cells as compared to BxPC3. Nevertheless, at 72 h, both cell lines induced almost 60% of cell proliferation arrest. FR054 had a stronger effect as compared to ERA, at both time points and in both cell lines. Strikingly, the combined treatment at 72 h induced approximately 100% of cell proliferation reduction, confirming the significant effect of this combination. The cytotoxic analysis additionally confirmed the above results (Figures 3E, F). Twenty-four hours and 48 h of ERA treatment, in both cell lines, induced a slight effect on cell death. Conversely, FR054 treatment (48 h and 72 h of treatment) was significantly more cytotoxic since cell death values were significantly higher at both time points. Strikingly, combined treatment, significantly enhanced cell death in both cell lines at both time points, causing almost 100% cell death at 72 h (Figures 3E, F), strongly confirming the effective cooperative outcome between FR054 and ERA in PDAC cells. As ERA is known for its pro-ferroptosis activity (25) and FR054 was shown to be able to induce apoptosis (11, 12), next we analyzed the activation/cleavage of caspase-3 as an exclusive apoptotic marker. At 48 and 72 h in FR054-treated cells as well as in combined treatment, caspase-3 signals increased as compared to control. However, despite the significant increase in cell death observed at 72 h (Figures 3C, D), caspase-3 cleavage was less pronounced as compared to 48 h, also suggesting a non-apoptotic mechanism of cell death (Figures 3G, H, Figures S4, S5). Conversely, in ERA alone at both time points, despite the increased cell death observed in particular in BxPC3 cells (Figures 3C, D), caspase-3 signal was not or barely detectable, confirming that the ERA was inducing a non-apoptotic cell death (Figures 3G, H, Figures S4, S5). Furthermore, cell morphological study further confirmed that combined treatment induced different morphological alterations as compared to single treatments (Figures 3I, J). Altogether, these findings support the notion that the combined treatment induces both an apoptotic and a non-apoptotic cell death.

Cell death dependent on FR054 and ERA combination is associated with ER stress persistence and NRF2-dependent antioxidative response inactivation

Previously published data indicated that prolonged treatment with FR054 causes cell death by inducing ER stress and activation of UPR (11, 12). On the other hand, ERA treatment induces cysteine depletion and oxidative cell stress, causing both ER stress and then ferroptosis (26). Furthermore, transcriptional data shown in

10.3389/fonc.2023.1125855

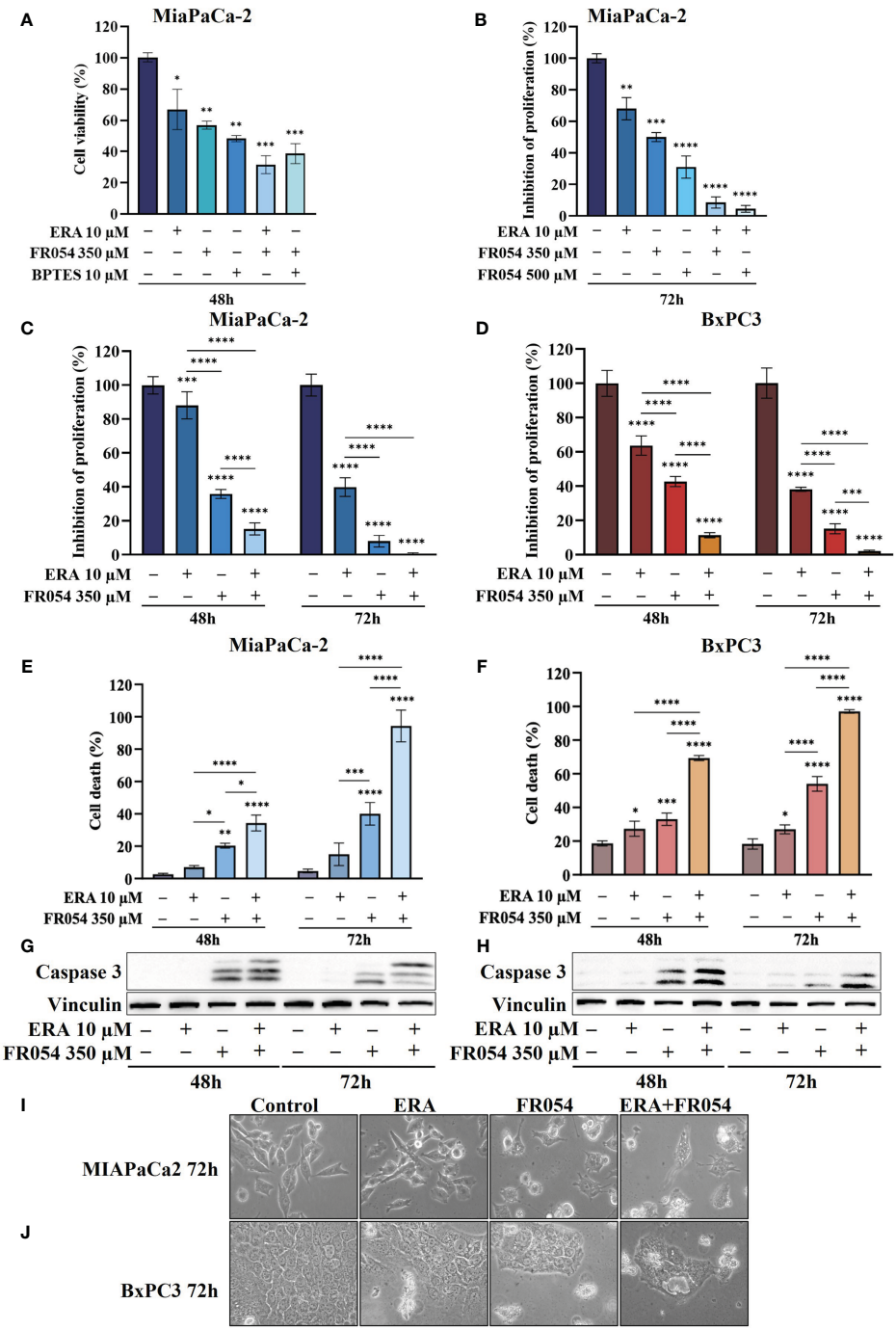

FIGURE 3
Combined treatment with FR054 and erastin enhances cell proliferation arrest and death of PDAC cell lines. **(A)** Trypan blue cell count after 48 h of treatment with FR054, erastin (ERA) 24 h, BPTES 24 h, or the combination of FR054 with ERA or BPTES added after 24 h of FR054 treatment. **(B)** Inhibition of proliferation expressed as percentage (trypan blue assay) after 72 h of treatment with two different doses of FR054 alone or in combination with ERA. **(C, D)** Inhibition of proliferation expressed as percentage (trypan blue assay) in MiaPaCa-2 and BxPC3 cells after 48 and 72 h of treatment with FR054 and ERA only or in combination. **(E, F)** Death cell percentage (trypan blue assay) in MiaPaCa-2 and BxPC3 cells after 48 and 72 h of treatment with FR054 and ERA only or in combination. **(G, H)** Western blot analysis of caspase 3 cleavage in cells treated as in **(C, D)**. Vinculine has been used as internal loading control. **(I, J)** Bright-field images of MiaPaCa-2 and BxPC3 cells treated as in **(C, D)** taken 48 h after the treatments. The data are presented as mean ± SD from three independent experiments. For **(A, B)**, statistical significance was determined using one-way ANOVA with Tukey's multiple comparisons test, while for all the others, statistical significance was determined using two-way ANOVA with Tukey's multiple comparisons test. *$p < 0.05$, **$p < 0.01$, ***$p < 0.001$ ****$p < 0.0001$.

Figure 2A further suggest activation of UPR and of antioxidant response, especially in MiaPaCa-2 cells. Therefore, we decided to evaluate UPR activation and cellular oxidative stress upon single and combined treatments by immunoblot analysis.

For UPR activation, we focused our analyses on eIF2α phosphorylation and protein expression of GRP78, linked to ER stress, ATF4, linked both to ER stress and cysteine depletion (27), and CHOP, a TF associated with cell cycle arrest (28) and induction of pro-apoptotic signals upon prolonged UPR activation (29). ERA treatment of MiaPaCa-2 cells, at both 48 and 72 h, resulted in an increased expression of GRP78, ATF4, and CHOP as compared to control cells (Figure 4A, Figure S4). No significant change in eIF2α phosphorylation was observed. FR054 treatment resulted in an increase of eIF2α phosphorylation, a slight increase of ATF4 at both 48 h and 72 h, and a more significant increase of CHOP as compared to control cells. No significant change in GRP78 expression was observed (Figure 4A, Figure S4). Of note in FR054-treated cells, ATF4 was induced at significantly lesser extent as compared to ERA treatment. Combined treatment resulted in higher levels of eIF2α phosphorylation, GRP78, and CHOP as compared to control and single drug-treated cells. ATF4 was induced at 48 h to significantly decrease at 72 h. Nevertheless, ATF4 level was significantly lower as compared to ERA-treated cells (Figure 4A, Figure S4). Next, we analyzed the behavior of the same proteins in BxPC3 cells, characterized by the expression of a wild-type K-Ras and known to be more sensitive to ferroptosis inducers. As shown in Figure 4B, Figure S5, in BxPC3 cells treated with ERA, the different UPR markers were generally upregulated but in no significant manner (eIF2α phosphorylation, ATF4, and CHOP) or downregulated in a significant manner (GRP78). FR054 treatment resulted in a time-dependent increase of eIF2α phosphorylation and CHOP, in a nonsignificant increase of ATF4 and a significant downregulation of GRP78 at 48 h (Figure 4A, Figure S4). Conversely, in cells treated with the combination, the three UPR markers, eIF2α phosphorylation, GRP78, and CHOP, increased significantly in a time-dependent manner, especially at 72 h, as compared to control and single-treated cells (Figure 4B, Figure S5). Of note in combined treatment, ATF4 expression, conversely to what was observed in MiaPaCa-2 cells, increased significantly only at 48 h to decrease at 72 h. Taken together, our findings, in line with previous reports showing the protective role of ATF4 (30, 31), could suggest that the ERA resistance of MiaPaCa-2 cells as compared to BxPC3 cells may be ascribed to a higher ATF4 level of expression as compared to BxPC3 cells and that such resistance is hindered by the ability of combined treatment to induce UPR, as highlighted by increased eIF2α phosphorylation as well as GRP78 and CHOP higher expression, in tight association with ATF4 decrease. Indeed, in the combination-treated cells, the sample in which we observed the highest level of cell death (Figure 3C), CHOP remained always higher as compared to ATF4. Such a protective role of ATF4 is further suggested by BxPC3 results, in which the highest values of cell death observed in combination-treated cells (Figure 3D, 72 h) were associated with low and high levels of ATF4 and CHOP, respectively. Previous transcriptional data indicated that FR054 treatment can transcriptionally induce an NFR2-dependent antioxidant response, proposing that FR054, as hitherto shown in breast cancer cells (11), induces cellular oxidative stress in PDAC cells. Since several data indicated that NRF2 and ATF4 interact and cooperatively upregulate a number of antioxidant and antiapoptotic genes involved in a protective response engaged during ER stress (32, 33), we decided to determine NRF2 expression under our experimental conditions. As expected, after 48 h, the protein level of NRF2 was upregulated in response to ERA and FR054 and such upregulation was stronger in combined treatment in both cell lines (Figures 4A, B, Figures S4, S5), indicating increased oxidative stress. Surprisingly, at 72 h, while NRF2 expression remained high (MiaPaCa-2 cells) or was further induced (BxPC3 cells) in ERA-treated cells, conversely in FR054-treated samples, especially upon combined treatment, it was significantly reduced. This behavior was observed especially in ERA-resistant MiaPaCa-2 cells, further suggesting that ATF4 and NRF2 levels may dictate ERA resistance (Figures 4A, B, Figures S4, S5). Oxidative stress as well as UPR, stabilizing and activating NRF2, regulates downstream gene transcription, including SLC7A11 and HMOX1 (34–36). The former amplifies glutamate secretion and cystine uptake, and facilitates GSH synthesis for reactive oxygen species (ROS) detoxification (37), while the latter helps keep the cellular redox balance by catalyzing the degradation of heme to carbon monoxide, iron, and biliverdin (38). Thus, to demonstrate NRF2 activation, we analyzed SLC7A11 and HMOX1 protein levels. As shown in Figure 4A, Figure S4, in MiaPaCa-2 cells, both SLC7A11 and HMOX-1 almost mirrored NRF2 expression at both time points. Conversely, in BxPC3 cells, both proteins were less modulated and only partially mirrored NRF2 expression, since both were only upregulated at 48 h and in particular SLC7A11 slightly increased only in ERA-treated cells and HMOX1 only in combined-treated cells. Nevertheless, both proteins significantly decreased at 72 h (Figure 4B, Figures S4, S5), further suggesting that the major sensitivity of BxPC3 cells to ERA and combined treatments may be ascribed to low ATF4 expression and NRF2 activation. To explore the oscillatory expression of NRF2 protein upon single and combined treatment, we then determined the expression level of *Kelch-like ECH-associated protein 1* (KEAP1), a well-known negative regulator of NRF2 protein stability (39). The expression of KEAP1 significantly increased only in FR054-treated cells and at 48 h since at a later timepoint the level decreased, especially in combined treatment (Figure 4A and Figures S4, S5), therefore justifying the reduced NRF2 expression in these cell samples. Altogether, these data suggest that increased cell death in combined treatment (Figures 3E, F) is tightly linked to a significantly higher expression of the pro-apoptotic protein CHOP and a greater antioxidative response at an early time point, as confirmed by the higher NRF2, SLC7A11, and HMOX1 levels, which, at a later time point, together with ATF4, abruptly decrease.

FR054 modulates SLC7A11 function without restraining the inhibitory effect of erastin

To better understand the relation between the observed level of SLC7A11 protein and its function as an exchanger of the anionic form of cystine and glutamate, we measured the amount of these

10.3389/fonc.2023.1125855

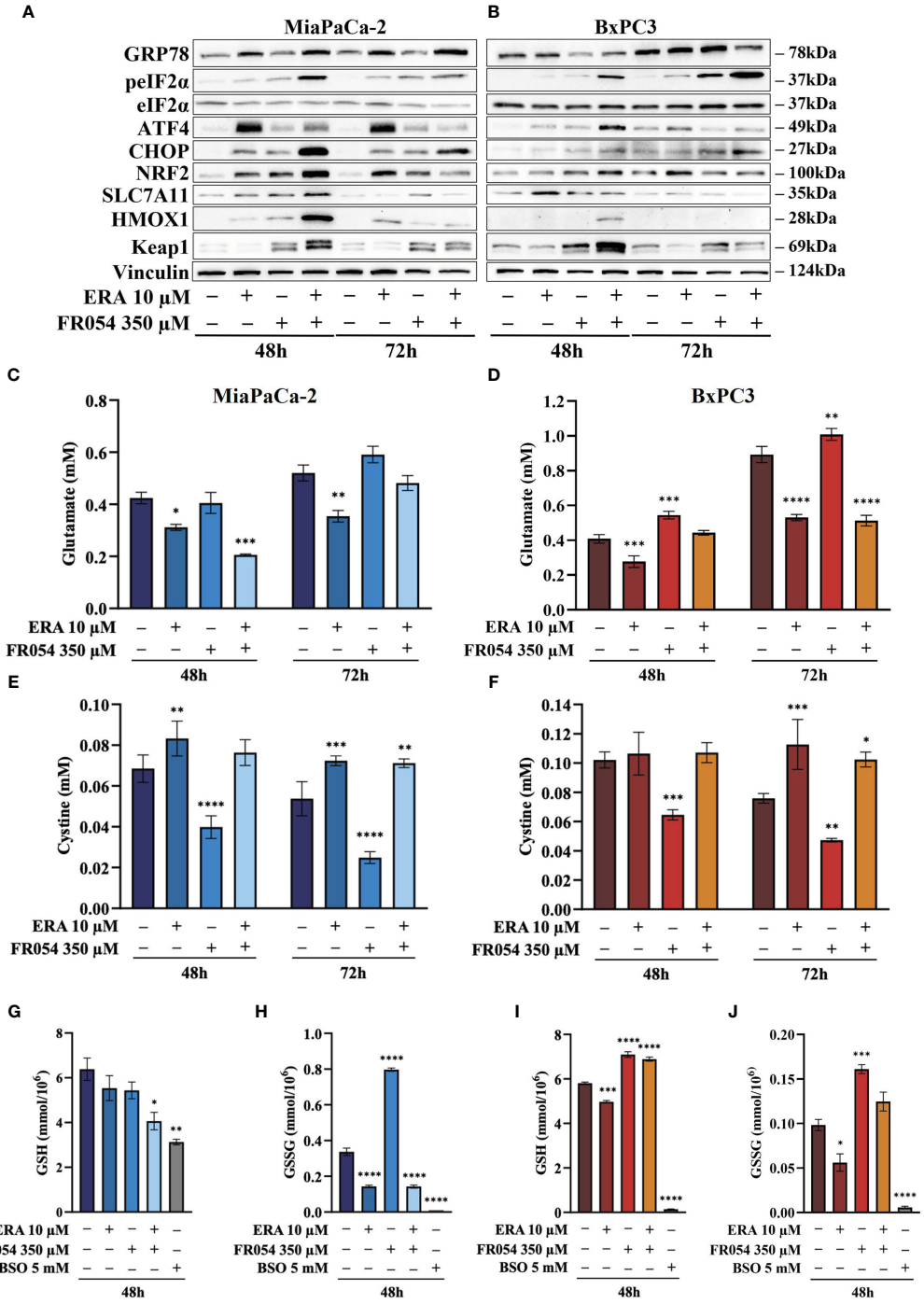

FIGURE 4
FR054 alone or in combination with erastin affects UPR and oxidative response protein expression, modifies SLC7A11 activity, and alters GSH and GSSG intracellular levels. **(A, B)** Immunoblot analysis showing the effects of the two compounds on different UPR and oxidative stress response proteins. **(C, D)** HPLC evaluation of the glutamate concentration in the growth medium of the MiaPaCa-2 and BxPC3 cells after the different treatments as indicated in the figure. **(E, F)** HPLC evaluation of the cystine concentration in the growth medium of the MiaPaCa-2 and BxPC3 cells after the different treatments as indicated in the figure. **(G, H)** Measurement of the intracellular concentration of GSH **(I)** and GSSG **(J)** in MiaPaCa-2 and BxPC3 cells after the different treatments as indicated in the figure. The data of GSH and GSSG concentration are presented as mean ± SEM from three independent experiments, while the other ones are presented as mean ± SD from three independent experiments. For **(C–E)**, and **(F)**, statistical significance was determined using two-way ANOVA with Tukey's multiple comparisons test, while for **(G–J)**, statistical significance was determined using one-way ANOVA with Tukey's multiple comparisons test. *$p < 0.05$, **$p < 0.01$ ***$p < 0.001$, ****$p < 0.0001$.

two amino acids into cultured media in both cell lines. While ERA, as expected, inhibited glutamate release in both cell lines and at both time points analyzed, FR054 alone, as predicted by the transcriptional data, albeit not statistically significant, caused a time-dependent increase in the amount of released glutamate (Figures 4C, D). Of note, despite the different temporal dynamics, ERA combined with FR054 still inhibited glutamate release in both cell lines counteracting the positive effect of FR054 treatment (Figures 4C, D). Since glutamate is secreted in exchange with cystine uptake, necessary for GSH synthesis, we analyzed extracellular levels of cystine. Both lines treated with ERA alone or in combination with FR054 showed a cystine uptake reduction as compared to control cells, mirroring the effect on glutamate efflux (Figures 4E, F). Conversely, in FR054-treated cells, a significant reduction of extracellular cystine was observed, confirming the ability of FR054 to increase the exchange between glutamate and cystine (Figures 4E, F). The latter result was also confirmed in BxPC3 cells treated with FR054 alone given that in this cell line, there was also a significant decrease of extracellular cystine (Figure 4F). Given that one molecule of cystine can then be converted into two molecules of cysteine, which is a committed step for GSH biosynthesis next, we evaluated at 48 h the intracellular level of GSH and GSSG. As technical control, we treated the cells for 24 h with 5 mM buthionine sulfoximine (BSO) alone, an inhibitor of GCLC activity. GSH in MiaPaCa-2 cells was statistically significantly reduced only in cells treated with the combination of the two drugs as compared to control cells. Indeed, in ERA- and FR054-treated cells, GSH still decreased but not in a statistically significant value (Figure 4G). Conversely, a significant variation of GSSG levels was observed in all treated cells as compared to the control (Figure 4H). In fact, in cells treated with ERA alone or in combination with FR054, in accordance with the significant reduction of cystine uptake, the GSSG levels were also drastically reduced (Figure 4H). A similar behavior was observed in BSO-treated cells, in which the prolonged inhibition of GCLC caused a significant decrease of both GSH and GSSG, as previously observed (40). Surprisingly, in FR054-treated cells, consequently to the significant cystine uptake, there was a significant accumulation of GSSG (Figure 4H). Analysis of GSH and GSSG levels in BxPC3 as compared with the control group showed that ERA induced a slight but significant reduction in both GSH and GSSG levels (Figures 4I, J). Conversely, in FR054-treated cells, either alone or in combination with ERA, both GSH and GSSG levels remained higher as compared to control cells (Figures 4I, J). Of note, BxPC3 cells were more sensitive to BSO treatment since 24 h treatment completely depleted both GSH and GSSG. Such a result in combined treatment was in part unexpected because following this treatment a significant reduction in extracellular glutamate as well as in cystine uptake was observed. However, based on our transcriptional data (Figure 2A), we cannot exclude the role of the trans-sulfuration pathway in intracellular synthesis of cysteine given that the *Cystathionine Beta-Synthase* (*CBS*) mRNA was significantly upregulated only in this cell line upon FR054 treatment. Altogether, these findings suggest that FR054 alone increases in both cell lines SLC7A11 glutamate/cystine exchange and intracellular GSSG level. Conversely, when combined with ERA, MiaPaCa-2 cells might promote cell death by reducing glutamate/cystine exchange and GSH synthesis, while in BxPC3, its proapoptotic effect, despite being linked to a significant reduction of glutamate/cystine exchange, does not appear to be related to GSH level reduction.

The combined effect between FR054 and erastin on cell survival is associated with oxidative imbalance, causing lipid peroxidation

To evaluate the effect of intracellular GSH modulation and oxidative stress on PDAC cell survival under single and combined treatments with ERA and/or FR054, we used, as schematized in Figure S3C, two different approaches: 24 h of cotreatment with *N*-acetyl-L-cysteine (NAC, 5 mM), a cysteine prodrug, able to replenish intracellular GSH levels, or 24 h of cotreatment with BSO (5 mM) to block *de novo* synthesis of GSH. NAC cotreatment, as measured by trypan blue vital assay, led to decreased cell death in both cell lines and in all the conditions analyzed as compared to control cells (Figures 5A, B). Conversely, cotreatment with BSO led to increased cell death in cells treated with ERA alone or in combination with FR054 (Figures 5A, B). Of note, in FR054-treated samples, in which previous data indicated a significant enhancement of SLC7A11 activity tightly associated with a great accumulation of GSSG, suggesting a more functionally GSH biosynthetic pathway (Figures 2 and 4), the effect of BSO was negligible.

Based on our transcriptional data, revealing a role of ferroptosis in PDAC cells after FR054 treatment, given the significant effect of FR054 on NRF2 pathway activation as well as the noteworthy impact of BSO on PDAC cell survival when combined with ERA alone or in combination with FR054, we next sought to measure lipid peroxidation (lipid ROS) at 48 h as a hallmark of cystine depletion as well as ferroptosis by using the fluorescent probe C11-BODIPY. As expected from previous results, treatment with ERA or FR054 alone increased fluorescence, especially in ERA-sensitive BxPC3 and slightly in FR054-treated MiaPaCa-2 cells. Conversely, combined treatment induced a significant increase in fluorescence in both cell lines (Figures 5C, D). As expected by cell survival data, NAC and BSO treatments reduced and increased lipid ROS, respectively, especially in cells treated with the drug combination, suggesting that these cells are more sensitive to intracellular redox state. To further demonstrate lipid peroxidation, we measured the MDA, an end product of lipid peroxides, generated during ferroptosis and other oxidative stress context. As shown in Figures 5E, F, in both cell lines, MDA levels almost resembled C11-BODIPY staining, given the increase upon all treatments, especially in combined treated samples. Thus, these findings indicate that FR054, increasing cell dependence for the SLC7A11–GSH axis, causes a significant increase in Lipid-ROS when combined with ERA, and this effect occurs in both cell lines.

10.3389/fonc.2023.1125855

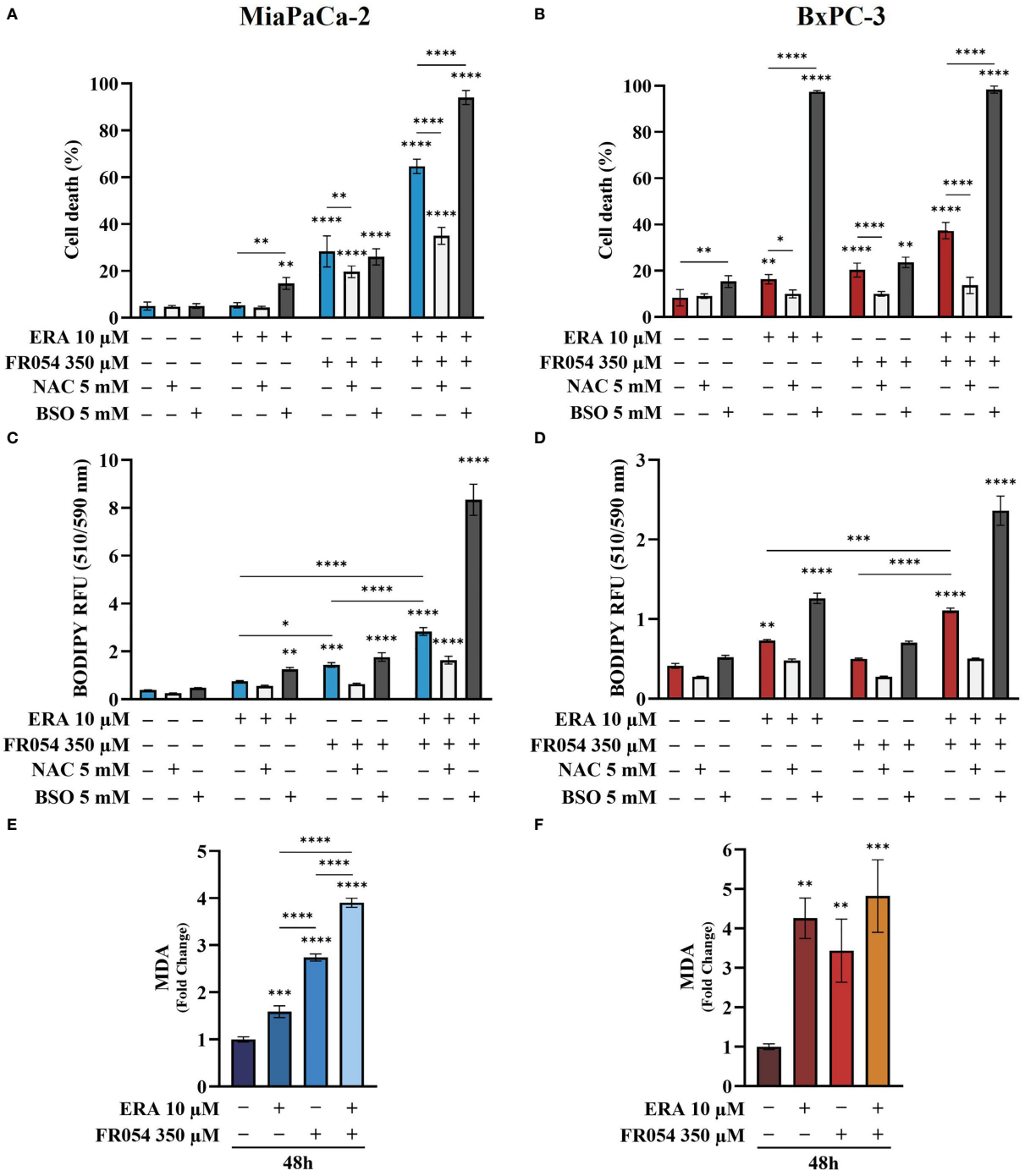

FIGURE 5
Variation of intracellular level of GSH by using NAC or BSO preserves or impairs, respectively, PDAC cell vitality by decreasing or increasing lipid peroxidation in PDAC cells. **(A, B)** Death cell percentage data (trypan blue assay) of MiaPaCa-2 and BxPC3 cells after the indicated treatments. **(C, D)** Intracellular lipid-ROS levels in MiaPaCa-2 and BxPC3 cells after the indicated treatments. **(E, F)** Malondialdehyde (MDA) assay to evaluate the lipid peroxidation in MiaPaCa-2 and BxPC3 cells after the indicated treatments. The death cell percentage data and MDA assay data are presented as mean ± SD from three independent experiments, while intracellular lipid-ROS data are presented as mean ± SEM from three independent experiments. For **(A–D)**, statistical significance was determined using two-way ANOVA with Tukey's multiple comparisons test, while for **(E, F)**, statistical significance was determined using one-way ANOVA with Tukey's multiple comparisons test. *$p < 0.05$, **$p < 0.01$ ***$p < 0.001$, ****$p < 0.0001$.

Stable-isotope-assisted metabolomics analysis of central carbon metabolism indicates that the FR054 enhancing effect on ferroptosis is associated with a reduction of glucose entry into the TCA cycle and an increased glutaminolysis

To further investigate the underlying basis for the role of FR054 in increasing ERA sensitivity, we conducted a stable-isotope-assisted metabolomics analysis comparing all cell lines after the different treatments as described in Figure S3D. Metabolic analysis was performed by labeling the different cell lines with either [U-$^{13}C_6$]-glucose or [U-$^{13}C_5$]-glutamine and quantified isotopic enrichment in the form of MIDs. To analyze glycolysis, TCA cycle, and glutaminolysis, we analyzed the glucose or glutamine carbon contribution to the generation of pyruvate, citrate, α-ketoglutarate, and glutamate. In both cell lines, we observed a significant reduction of M4 and M5 citrate when cells were treated with FR054 alone (MiaPaCa-2, M4: −28%, M5: −33%; BxPC3, M4: −22%, M5: −29%) or in combination with ERA (MiaPaCa-2, M4: −34%, M5: −49%; BxPC3, M4: −22%, M5: −22%), suggesting a reduced activity of both pyruvate dehydrogenase (PDH) and pyruvate carboxylase (PC) (Figures 6A, 7A, Figure S6A, Supplementary Table 4). We also observed this reduction in the M2 of α-ketoglutarate when cells were treated with FR054 alone (MiaPaCa-2, M2: −24%; BxPC3, M2: −8%) or in combination with ERA (MiaPaCa-2, M2: −41%; BxPC3, M2: −15%) (Figures 6A, 7A, Supplementary Table 4), a key TCA cycle intermediate, pointing towards an overall reduction of glucose entry into the TCA cycle. Indeed, in both cell lines, we observed a significant decrease in the glucose carbon contribution for their synthesis (Figures 6C, 7C). The effect of FR054, however, was much stronger in MiaPaCa-2 cells compared to BxPC3. Decreased glucose contribution suggests that cells were more dependent on glutamine for TCA cycle anaplerosis. In fact, analysis of the same metabolites in cells labeled with [U-$^{13}C_5$]-glutamine indicated significantly higher enrichment of M5 glutamate (MiaPaCa-2, ERA: 10%, FR054: 13%; ERA+FR054: 30%; BxPC3, ERA: 2%, FR054: 5%; ERA+FR054: 5%), M5 α-ketoglutarate (MiaPaCa-2, ERA: 8%, FR054: 9%; ERA+FR054: 21%; BxPC3, ERA: 1%, FR054: 4%; ERA+FR054: 4%), and M4 citrate (MiaPaCa-2, ERA: 14%, FR054: 12%; ERA +FR054: 20%; BxPC3, ERA: 0%, FR054: 4%; ERA+FR054: 4%) upon all treatments and especially in the combined treatment (Figures 6B, 7B, Figure S6B, Supplementary Table 4), suggesting that FR054 enhances glutaminolysis, as confirmed by the significant increase of relative glutamine carbon contributions for their synthesis (Figures 6C, 7C). Similar to the [U-$^{13}C_6$]-glucose results, the effect was much stronger in MiaPaCa-2 cells compared to BxPC3. An increase in labeled M3 pyruvate was observed only in ERA-treated samples in MiaPaCa-2 cells, suggesting only a slight alteration of malic enzyme activity in ERA-treated cells (Figure 6B). Nonetheless, analysis of the glutamine carbon contribution confirmed that in FR054-treated BxPC3 cells, glutamine becomes more relevant but to a lesser extent as compared to K-Ras mutated MiaPaCa-2 cells (Figure 7C). Altogether, metabolomics analysis suggests that in both cell lines, treatment with FR054 alone or in combination, with a different magnitude, reduces glucose utilization through the TCA cycle. Here, we report that especially in MiaPaCa-2 cells, FR054 treatment significantly enhances cell dependence on glutamine and glutaminolysis, in line with previous findings describing glutaminolysis as a mechanism to increase ferroptosis cell death (41).

Combined treatment between ERA and FR054 induces enhancement of ferroptosis in PDAC cell lines independent on K-Ras mutation

To further reinforce the notion that ERA and FR054 treatment could cooperate in inducing ferroptosis in PDAC cell models, we treated human pancreatic cancer PANC1 cells, characterized by K-Ras mutation and a great sensitivity to cysteine depletion, with ERA and FR054 alone or in combination along a time course of 72 h. We observed a significant effect of all treatments on proliferation (Figure 8A) and a time-dependent effect on cell death (Figure 8B). In both types of analysis, the combinatorial treatment induced the stronger outcome as confirmed also by morphological cell analysis, in which cell swelling before cell disruption was observed (Figure 8C). Next, we analyzed glutamate and cystine levels, confirming that ERA alone or in combination significantly inhibited SLC7A11 function (Figures 8D, E) and FR054 alone induced a significant increase in SLC7A11 function. To evaluate the downstream effects of SLC7A11 modulation by the different treatments, we measured GSH and GSSG levels. The effect of all treatments significantly reduced GSH levels, and such reduction was much stronger compared to MiaPaCa-2 and BxPC3 cells (Figure 8F). Of note, GSSG levels were significantly modulated by all treatments and to the same extent as in MiaPaCa-2 cells, further confirming the ability of ERA and FR054 to decrease or increase GSSG level, respectively (Figure 8G). Then, we examined whether, upon all treatments and adding NAC or BSO, PANC1 cells promoted lipid ROS and MDA generation. Single and combined treatments significantly increased C11-BODIPY fluorescence and intracellular MDA (Figures 8H, I). NAC and BSO treatment, as previously observed for the other two PDAC cell lines, significantly reduced or increased C11-BODIPY fluorescence, suggesting that, also in PANC1 cells, the combined treatment enhanced ferroptosis. Remarkably, our findings confirmed the great sensitivity of PANC1 cells to ERA treatment, as previously described, a sensitivity that was further enhanced by FR054. Thus, the enhancer role of FR054 in ferroptosis could be attributed to the boosting of lipid peroxidation.

To further dissect the mechanism by which FR054 increased ERA sensitivity in PANC1 cells as compared to two other PDAC cell lines, we also conducted in PANC1 a stable-isotope-assisted metabolomics analysis as previously described. In PANC1 cells, we observed a significant reduction of M4 (ERA: −11%, FR054: −8%; ERA+FR054: −23%) and M5 citrate (ERA: −26%, FR054: −17%; ERA+FR054: −54%) when cells were treated with ERA and FR054

10.3389/fonc.2023.1125855

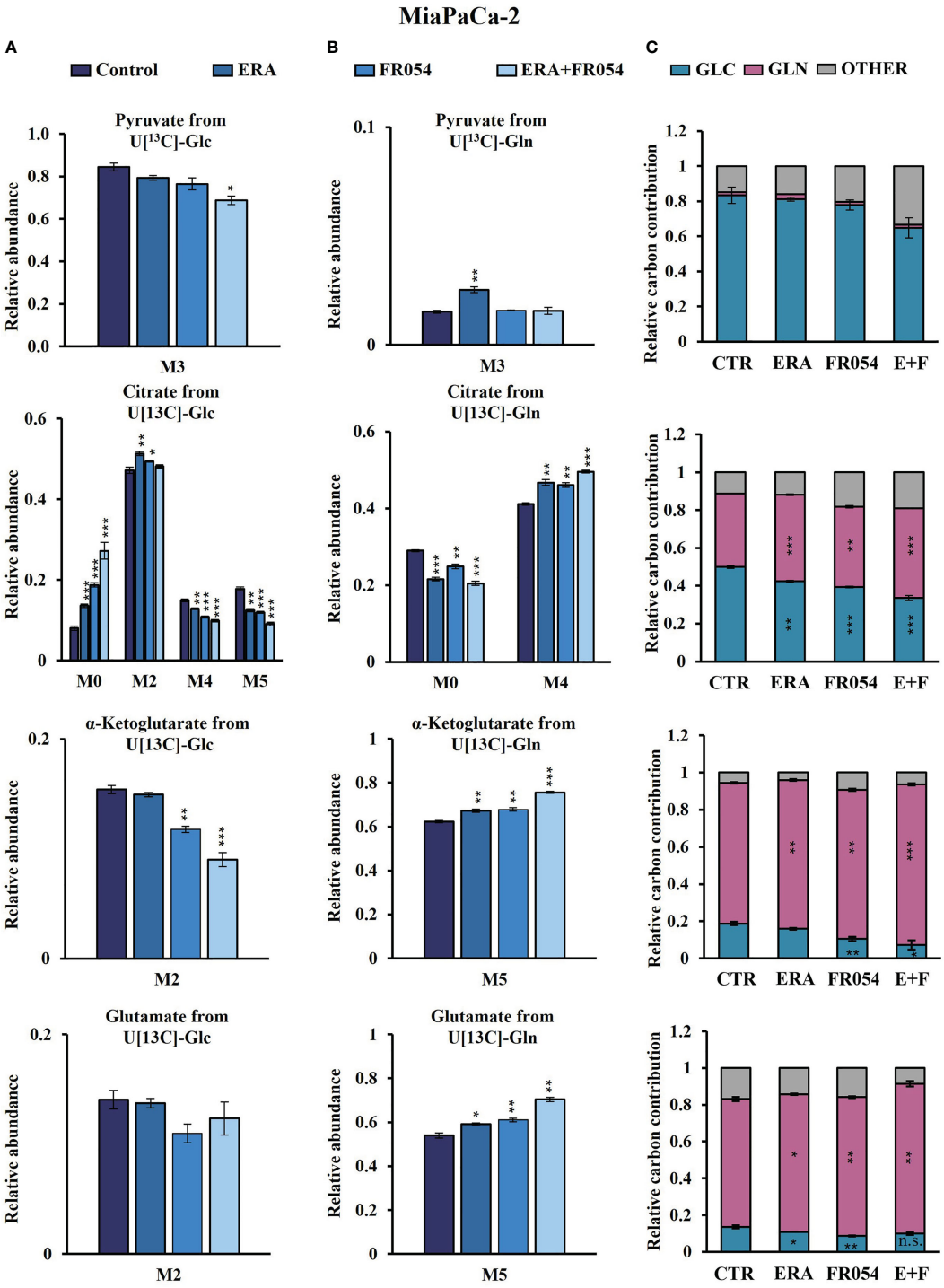

FIGURE 6
Combined treatment in MiaPaCa-2 cells favors glutaminolysis over glycolysis. **(A, B)** 13C labeling of pyruvate, citrate, a-ketoglutarate, and glutamate from MiaPaCa-2 cells incubated in [U-$^{13}C_6$]-glucose or [U-$^{13}C_5$]-glutamine medium for 48 h. **(C)** Relative carbon fractional contribution of glucose and glutamine to pyruvate, citrate, a-ketoglutarate, and glutamate formation. The data are presented as mean ± SEM from three independent experiments. The statistical significance was performed with Student's *t*-test. *$p < 0.05$, **$p < 0.01$, ***$p < 0.001$.

alone or in combination, suggesting a reduced activity of both PDH and PC (Figure S7A, Supplementary Table 4). We also observed this reduction in the M2 of α-ketoglutarate (ERA: −7%, FR054: −3%; ERA+FR054: −23%) and glutamate (ERA: −7%, FR054: −4%; ERA+FR054: −25%) (Figure S7A), further suggesting an overall reduction of glucose entry into the TCA cycle as demonstrated also by the significant decrease in the glucose carbon contribution for their synthesis (Figure S7C). Next, we analysed the same metabolites in PANC1 cells labeled with [U-$^{13}C_5$]-glutamine. A significant higher enrichment of M5

10.3389/fonc.2023.1125855

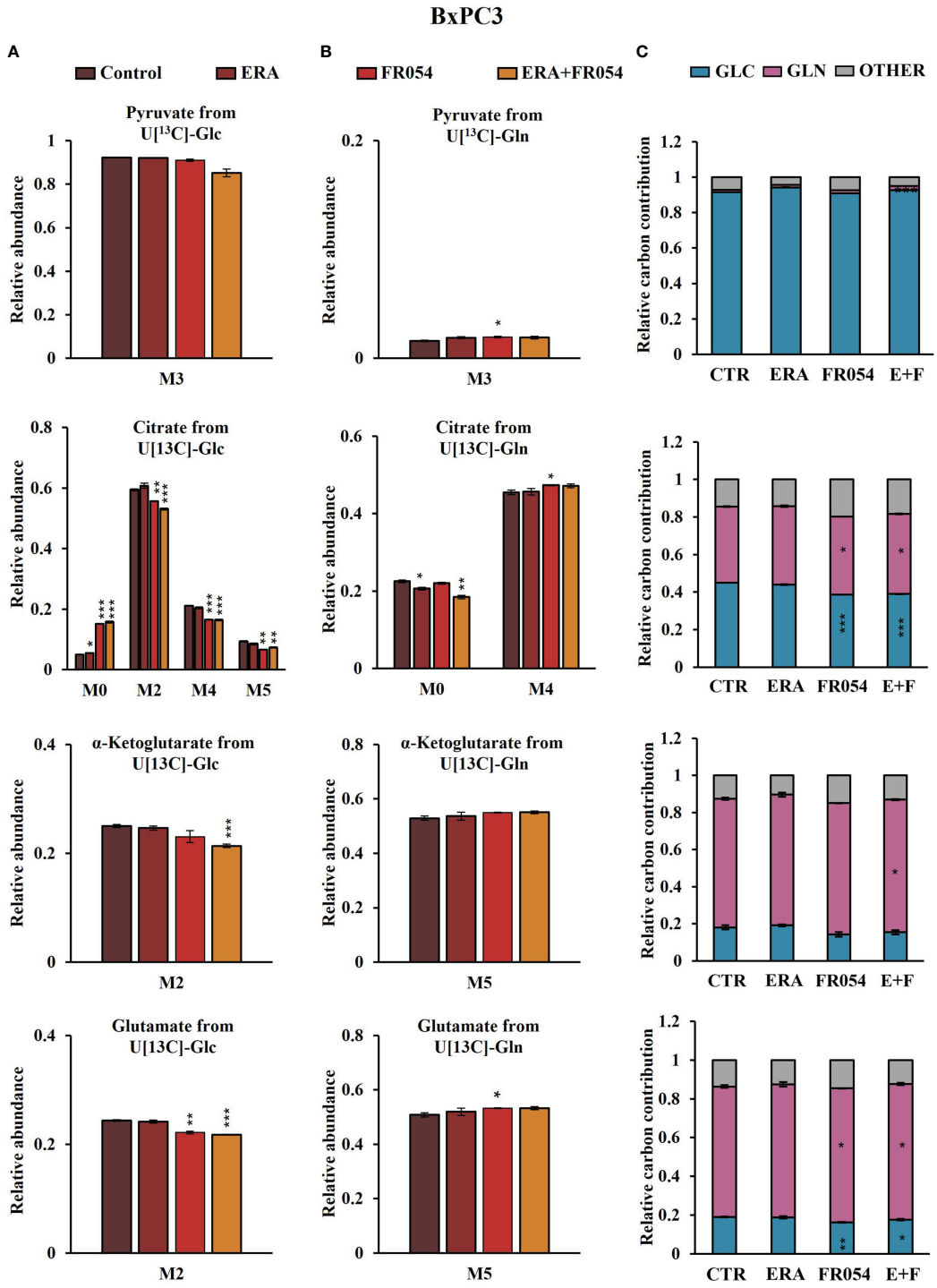

FIGURE 7
Combined treatment in BxPC3 cells reduces glucose utilization through the TCA cycle and slightly increases glutaminolysis. **(A, B)** ^{13}C labeling of pyruvate, citrate, a-ketoglutarate, and glutamate from BxPC3 cells incubated in [U-$^{13}C_6$]-glucose or [U-$^{13}C_5$]-glutamine medium for 48 h. **(C)** Relative carbon fractional contribution of glucose and glutamine to pyruvate, citrate, a-ketoglutarate, and glutamate formation. The data are presented as mean ± SEM from three independent experiments. The statistical significance was performed with Student's *t*-test. *$p < 0.05$, **$p < 0.01$, ***$p < 0.001$.

glutamate (ERA: 39%, FR054: 13%; ERA+FR054: 68%), M5 α-ketoglutarate (ERA: 36%, FR054: 12%; ERA+FR054: 62%), and M4 citrate (ERA: 35%, FR054: 10%; ERA+FR054: 54%) upon all treatments and especially in combined treatment was observed (Figure S7B, Supplementary Table 4), suggesting that the combined treatment enhances glutaminolysis, as confirmed by the significant increase of relative glutamine carbon contributions for their synthesis (Figure S7C). Altogether, metabolomics analysis

10.3389/fonc.2023.1125855

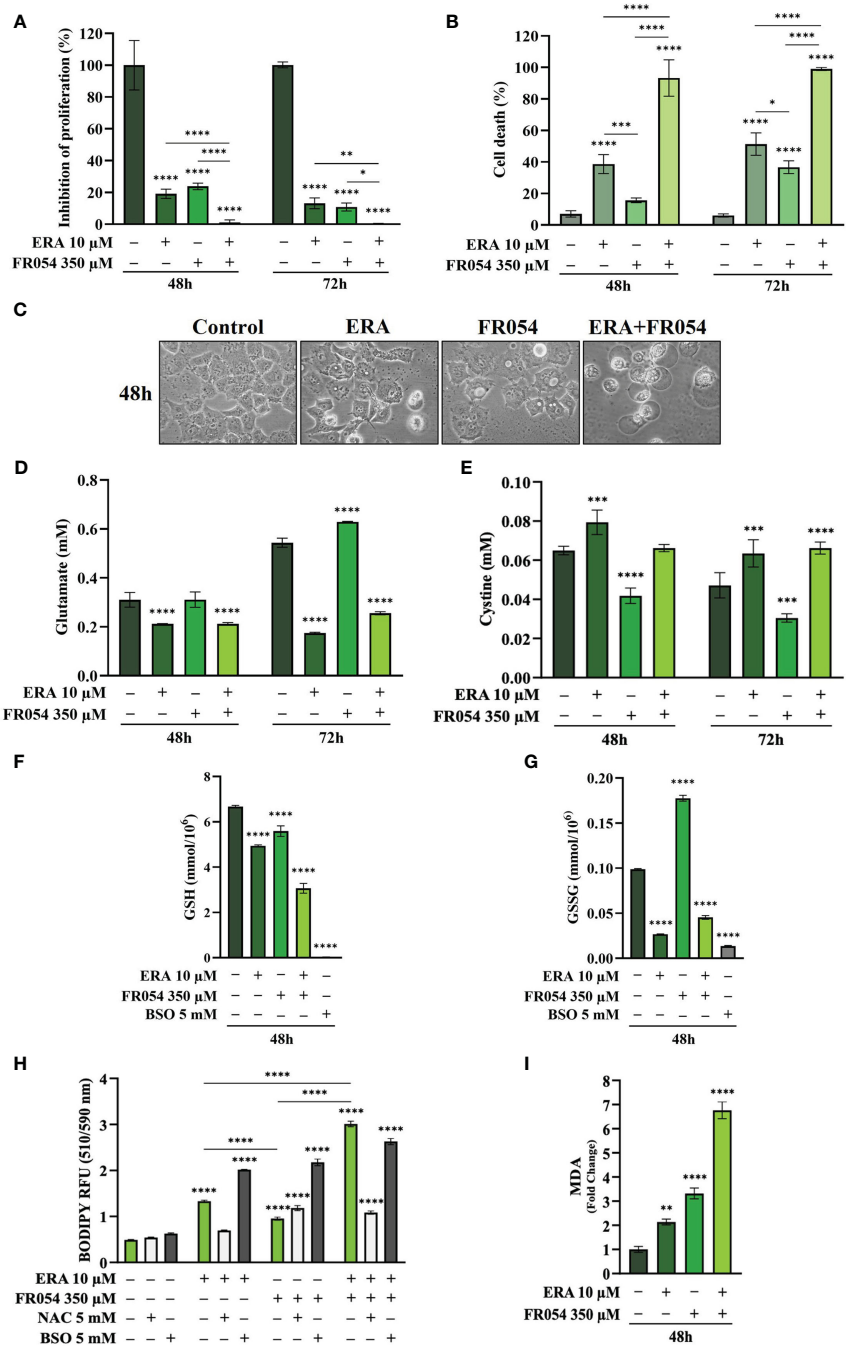

FIGURE 8
Combined treatment with FR054 and erastin enhances cell proliferation arrest and death of PANC1 cells by interfering with SLC7A11 activity and GSH metabolism and causing lipid peroxidation. **(A)** Trypan blue cell count in percentage after 48 h and 72 h of treatment with FR054, erastin (ERA) 24 h or 48 h, or their combination. **(B)** Cell death expressed as percentage (trypan blue assay) after 48 and 72 h of treatment with FR054 alone or in combination with ERA. **(C)** Bright-field images of PANC1 cells treated as **(A)** taken 48 h after the treatment. **(D, E)** HPLC evaluation of glutamate and cystine growth medium concentration, respectively, after the different treatments as indicated in the figure. **(F)** GSH and **(G)** GSSG intracellular analysis upon the different treatments as indicated in the figure. **(H)** Intracellular lipid-ROS levels in PANC1 cells after the indicated treatments. **(I)** Malondialdehyde (MDA) assay to evaluate the lipid peroxidation in PANC1 cells after the indicated treatments. The data are presented as mean ± SD from three independent experiments. Only the data of GSH and GSSG concentration, and the data of lipid-ROS levels are presented as mean ± SEM from three independent experiments. For **(A–E)**, and **(H)**, statistical significance was determined using two-way ANOVA with Tukey's multiple comparisons test, while for **(F)**, **(G)**, and **(I)**, statistical significance was determined using one-way ANOVA with Tukey's multiple comparisons test. *$p < 0.05$, **$p < 0.01$, ***$p < 0.001$ ****$p < 0.0001$.

indicated also that in PANC1 cells, as observed in MiaPaCa-2 cells, the combined treatment reduces glucose utilization through the TCA cycle and significantly enhances cell dependence on glutamine and glutaminolysis, suggesting a role of glutaminolysis in ferroptosis induced by the combined treatment.

Discussion

Previous studies suggested that PDAC exhibits extensive metabolic reprogramming necessary to support survival and growth and that such metabolic changes could represent new possible therapeutic targets (42). On the other hand, it has been recently shown that cysteine depletion induces PDAC cell death through a process named ferroptosis, a novel mechanism of non-apoptotic cell death, recently identified as another promising tumor therapeutic strategy (24). In this study, we investigated the anticancer effect of FR054, an inhibitor of the metabolic route named HBP, found altered in PDAC (6, 12, 13, 43), in combination with ERA, a specific inhibitor of the antiporter SLC7A11, able to reduce cysteine uptake, and hence to stimulate ferroptosis. We show that such a combination, tested for the first time to the best of our knowledge, induces a significant enhancement of the ERA effect causing massive cell death, the latter characterized by both apoptosis and ferroptosis. Of note, we show that the combination stimulates, as compared to single treatments, an ER stress-dependent mechanism of cell protection, namely, the ATF4–NRF2–SLC7A11–GSH axis, which causes an increased dependence on SLC7A11 activity, whose inhibition with ERA leads to massive cell death. Of note, although recent reports indicate both positive and negative association between ER stress and ferroptosis (44, 45), the mechanism supporting a contribution of ER stress in ferroptosis remains to be further clarified.

Here, by using RNA-seq data and GSEA, we identified that UPR activation, due to HBP inhibition, stimulates a wide transcriptional response involving several key regulators of cellular antioxidative response including the TFs NRF2, which lies at the center of a complex regulatory network governing cellular oxidative stress. Indeed, we identified several mRNAs involved in GSH synthesis, ROS detoxification, iron metabolism, and metabolic enzymes all upregulated especially in oncogenic K-Ras expressing MiaPaCa-2 cells as compared to wild-type expressing K-Ras BxPC3 cells. Such antioxidant response activated by UPR has been already described; indeed, accumulation of unfolded proteins causes an internal ER oxidative stress at which ER reacts by the activation of a complex response among which is the induction of NRF2 (46). Importantly, cellular oxidative stress is able to activate ER stress as well (47). In addition, UPR modulates autophagy and ROS metabolism. More recent findings indicate that it may have an important impact also on cellular iron homeostasis, i.e., by modulating the gene expression of ferroportin and ferritin (48). Therefore, in line with our previous findings (11, 12), we can assume that FR054, interfering with protein folding, is a potent UPR inducer, as confirmed by our transcriptional data in which we observed upregulation of some UPR targets in both cell lines such as DDIT3 (CHOP), ATF4, ATF3, and CHAC1 (Figure 2). Intriguingly our transcriptional analysis showed that FR054 treatment caused a rather contrasting effect since we observed a significant upregulation of several mRNAs encoding for proteins involved in GSH metabolism such as SLC7A11 and HMOX1, the latter being an ER-resident protein, whose expression has been related to the induction of ferroptosis (49, 50).

Based on these findings and considering that ferroptosis can be exploited and then applied in clinical treatment strategies, we reasoned that a ferroptosis inducer, ERA, could significantly enhance the effect of FR054 in stimulating cell death. Indeed, in all the PDAC cell lines described in the manuscript, independently of their mutation status in K-Ras protein, the combined treatment as compared to single treatment caused an earlier cell proliferation arrest and then almost 100% cell death. Of interest, analysis of the pro-apoptotic protein CHOP confirmed its expression in both ERA- and FR054-treated cell samples, therefore substantiating a possible apoptotic mechanism activated by the single and combined treatments. On the other hand, another key factor involved in UPR response is ATF4. Previous studies have demonstrated that ATF4 has a protective role against ferroptosis or amino acid deprivation in cancer cells (26, 30, 51). However, other studies also indicated that ATF4 may contribute to cell death under the same types of stress (51–53). Therefore, ATF4 has a dual role in cell death, and consequently, its final effect as a regulator of ferroptosis appears to be cell context-dependent.

Here, we demonstrated that in ERA resistant-MiaPaCa-2 cells, ERA treatment was able to induce the UPR, as confirmed by increased GRP78 and CHOP expression, a pro-survival anti-oxidative response, as confirmed by NRF2 enhanced expression and above all a high level of ATF4, imputable to cystine deprivation. Conversely, FR054 in the same cells also induced UPR and the anti-oxidative response but not a comparable level of ATF4, since no cystine depletion was observed upon this treatment. Strikingly, MiaPaCa-2 cells treated with the combination showed at an early time point (48 h) a significant stronger activation of UPR and of the anti-oxidative response but a lower level of ATF4 as compared to ERA. However, at a later time point (72 h), only the UPR remained significantly active as the anti-oxidative response as well as ATF4 significantly declined. On the other hand, the regulation of the same proteins in BxPC3 cells indicated their different behavior following the different treatments. Indeed, in ERA- and FR054-treated cells, the UPR, ATF4, and anti-oxidative responses were slowly activated and in a minor measure as compared to MiaPaCa-2 cells. Nonetheless, also in this cell line, the combined treatment induced a persistent UPR and a significant decrease of the anti-oxidative response as well as of ATF4, suggesting a minor cysteine depletion, as we observed, and slower intracellular oxidative stress. From these data, we can argue that the lower sensibility to ERA of MiaPaCa-2 cells as compared to BxPC3 cells, as previously described (24), must be probably ascribed to their ability to induce an ATF4-dependent response that together with NRF2 activation is able to avoid the cytotoxic effect of ERA. Instead, in BxPC3 cells, despite the fact that we observed only a significant reduction of extracellular glutamate and almost any change in extracellular cystine accumulation, ERA treatment induced almost 30% of cell death and a significantly reduced ATF4 accumulation,

probably justifying their greater sensitivity. The ATF4 behavior in cells treated with the drug combination is quite interesting. Indeed, since ATF4 expression may be associated with cancer cell resistance to ERA, particularly in MiaPaCa-2 cells, its decreased expression at a later time point fits well with the highest levels of cell death observed (Figure 3E). Its reduction may be ascribed to the prolonged UPR activation, due to FR054 treatment under stressing conditions. Indeed, CHOP-dependent apoptosis is characterized by a specific restoration of protein translation, in order to transcribe pro-apoptotic genes (54, 55). In such a condition, ATF4 becomes less active, due to either the expression of the inactive kinase *Tribbles Pseudokinase 3* (*TRIB3*), which acts as a negative feedback regulator of the ATF4-dependent transcription during the UPR (56), or its degradation by a ubiquitination-dependent mechanism (57, 58). In this regard, we would underline that FR054, as shown by the results from our RNA-seq data, is able to transcriptionally induce *TRIB3* (log_2FoldChange: 9.53 and 1.71 in MiaPaCa-2 and BxPC3 cells, respectively), suggesting a possible *TRIB3*-dependent mechanism of ATF4's function. Furthermore, it has been recently shown that Glycogen Synthase Kinase 3 Beta (GS3K) can target ATF4 for degradation. Such mechanism is controlled by the state of activation of AKT Serine/Threonine Kinase (AKT). Indeed, attenuation of the AKT pathway, leading to GSK3 activity, causes ATF4 degradation (59). Notably, our previous findings demonstrated that FR054 can significantly reduce AKT activation in PDAC cells (12), therefore corroborating this mechanism as a possible way to induce degradation of ATF4 and to avoid its protective role. Our findings also indicated that FR054 also reduces NRF2 expression (Figures 4A, B). Interestingly, GSK3 activity also controls NRF2 ubiquitination and degradation, suggesting a common mechanism of action on both NRF2 and ATF4 (60, 61). Furthermore, analysis of KEAP1 expression, a key protein in NRF2 degradation, indicated that KEAP1, in both cell lines, is significantly induced in an FR054-dependent fashion, as shown in Figure 4A (compare lanes 3, 4, 7, and 8 with lanes 1, 2, 5, and 6) and Figure 4B (compare lanes 3, 4, 7, and 8 with lanes 1, 2, 5, and 6). The parallel increase of both NRF2 and KEAP1 suggests, as previously observed, a post-induction of KEAP1 in order to turn off the NRF2 signaling (62) that ultimately fits well with the increased cell death observed in FR054-treated samples at 72 h. Regarding the observed parallel increase of NRF2 and KEAP1, it is noteworthy to observe that some authors demonstrated that persistent accumulation of NRF2 is harmful (63, 64). In this regard, some reports indicated that NRF2 is able to activate an auto-regulatory loop by inducing the expression of KEAP1 (65, 66). Intriguingly, O-linked N-acetylglucosamine (GlcNAc) transferase (OGT) activation, the only enzyme deputy to protein O-glycosylation, has been associated with NRF2-dependent stress response, since OGT inhibition may facilitate NRF2 activation (67, 68). The mechanism described for such an OGT-dependent NRF2 regulation is the O-GlcNAcylation status of KEAP1 (69). Indeed, O-GlcNAcylation of KEAP1 is required for the efficient ubiquitination and degradation of NRF2 (69). Of interest, NRF2 degradation and ferroptosis have also been recently linked through protein O-GlcNAcylation. In particular, protein O-GlcNAcylation regulates ferritinophagy and mitochondria behaviors to dictate ferroptosis; in particular, it has been shown that inhibition of O-GlcNAcylation promotes ferroptosis (70). In this scenario, we may hypothesize that ERA and FR054 cotreatment causes an overactivation of NRF2, following UPR and oxidative stress increase, as well as protein de-glycosylation (11, 12), that will eventually activate a KEAP1-dependent regulatory negative loop that causes NRF2 degradation and cellular oxidative stress. This hypothesis is supported by our observation of a robust activation of NRF2 and KEAP1 in combined treatment in both cell lines (Figures 4A, B, Figures S6, S7), an increased lipid peroxidation (Figures 5C–F), and cell death (Figures 5A, B). Despite the fact that we have yet to test protein expression in PANC1 cells, our hypothesis is also strongly supported in this cell line as shown in Figure 8 in which the combined treatment induces a significant increase in cell death, inhibits SLC7A11 activity, and increases ferroptosis markers.

In cancer cells, inhibition of system SLC7A11-mediated cystine uptake by ERA may be sufficient to initiate ferroptosis by interfering with GSH and GSSG intracellular levels. Our results in the three PDAC cell lines indicated that ERA was able to induce a small but significant decrease in GSH level only in PANC1 and BxPC3 cells (Figures 4I, J, 8F and G), given that, in MiaPaCa-2 cells, the decrease was unimportant. However, these findings agree with previous research, showing that PANC1 and BxPC3 cells are more sensitive to imidazole ketone erastin (IKE), an erastin analogue, as compared to MiaPaCa-2 cells, suggesting that the cell ability to avoid ERA effect is associated with GSH intracellular levels (24). Accordingly, combined treatment, able to significantly increase a ferroptosis mechanism of cell death (Figures 5C–F, 8H, J), significantly reduced GSH levels in MiaPaCa-2 and PANC1 cells. Regarding the GSH level in BxPC3, it must be underlined that although we observed a significant reduction and accumulation of extracellular glutamate and cystine, respectively, in the combined treatment, we did not observe a GSH reduction, suggesting a more complex mechanism causing ferroptosis in this cell line. Of note, in all three cell lines, upon ERA and combined treatments, we observed a consistent and significant decrease of GSSG. This result is both in agreement (24, 52, 71, 72) and in disagreement with other published observations because other researchers have shown that GSH depletion is accompanied by high GSSG levels. While we do not have an explanation about our different results, we would underline that in our experimental conditions, BSO treatment also caused a significant reduction of both GSH and GSSG as compared to control cells, suggesting that the decline of total GSH may have a role in ferroptosis onset (24, 72). Whether the GSSG level plays a role in the execution of ferroptosis remains unclear. An almost completely opposite behavior was observed in FR054-treated cells. Indeed, in line with the transcriptional data and the glutamate/cystine measurements, the effect of FR054 on GSH level as compared to control cells varied among cell lines (no change in MiaPaCa-2 cells, slightly high in BxPC3 cells, and slightly low in PANC1 cells). Nevertheless, in all three cell lines upon FR054 treatment, the GSSG levels significantly increased, suggesting that these cells were actively using GSH for cellular detoxification maybe to restore protein folding and cope with UPR stress (73). In this regard, a recent manuscript has proposed an important role for

GSSG in controlling endoplasmic reticulum (ER) function. Indeed, it has been shown that increased GSSG level may, directly or indirectly, alter ER oxidative protein maturation and protect ER homeostasis (74). How the level of GSSG may control ER homeostasis and ferroptosis is not the topic of this manuscript, but since few authors addressed this role, it could be the topic of a future investigation.

Nevertheless, the cell death mechanism observed in all the PDAC cell lines and particularly in the combined treatment is clearly dependent on GSH levels, since we observed that cell survival was almost completely restored or significantly reduced by adding NAC or BSO, respectively (Figures 5A, B). Moreover, analysis of lipid peroxidation and MDA confirmed the induction of a ferroptosis mechanism of cell death especially in the combined treatment (Figures 5C–F, 8H, I). Notably, lipid peroxidation was also observed in FR054-treated cells, which was consistent with previous findings showing a crosstalk between the two processes, ER stress and ferroptosis, in controlling cell death through the activation of the PERK–eIF2α–ATF4–CHOP axis (75) or the PERK–Nrf2–HMOX1 axis (44). It was intriguing that HMOX1 was identified as one of the most regulated mRNA in both cell lines upon FR054 treatment (Figures 1, 2), inferring that accumulation of ferrous iron (Fe^{2+}), generated by HMOX1 activity could cause further lipid peroxidation in the combined treatment. Indeed, Western blot analysis indicated that both MiaPaCa-2 and BxPC3 cells were also induced at the protein level (Figure 4A). Of note, we have to highlight that although it was significantly induced at the mRNA level upon FR054 treatment in both cell lines, it was detected only in MiaPaCa-2 cells at the protein level. We do not have an explanation for this discrepancy, but we would emphasize that all the other mRNAs tested by Western blot, specifically ATF4, DDIT3/CHOP, NRF2, and SLC7A11, were modulated similarly at both the mRNA and protein levels.

The role of cellular metabolism in ferroptosis execution has been addressed in several studies as reviewed in (76), and in fact, an increasing number of metabolic pathways appear to converge on ferroptosis. Intriguingly, we show that in all the PDAC cell lines, and especially in K-Ras mutated cell lines, the combined treatment causes a metabolic rewiring leading to a reduction of glucose entry into the TCA cycle. This effect, but to a lesser extent, was observed also following the single treatments (Figures 6A, 7A and Figure S7A). The effect correlates well with our transcriptional data in which we observed that FR054 treatment upregulates several genes of the glycolytic branches able to generate NADPH, such as *Glucose-6-Phosphate Dehydrogenase* (*G6PD*) and *6-Phosphogluconate Dehydrogenase* (*PGD*) or *Phosphoserine Aminotransferase 1 (PSAT1)* and *Phosphoglycerate Dehydrogenase (PHGDH)*, necessary for the recycling of the oxidized GSH through GSR activity in order to maintain the cellular redox homeostasis (77). Furthermore, we show that such glycolytic rewiring is associated with a concurrent increase in glutamine dependence of PDAC cells especially in K-Ras mutated MiaPaCa-2 and PANC1. The role of glutamine in ferroptosis is quite complex; however, some authors showed that glutamine drives ferroptosis in combination with cystine deprivation through glutaminolysis. Indeed, it has been proposed that the inhibition of SLC7A11 activity, which increases glutaminolysis, causes a greater glutamate conversion into α-KG that boosts the TCA cycle, the mitochondria activity, the fatty acid synthesis, and the generation of ROS that eventually altogether concur with ferroptosis (78, 79). Importantly, glutaminolysis alone is not able to trigger ferroptosis, pointing out that ferroptosis may happen only when glutaminolysis is activated in a cysteine depletion condition (79–81). In contrast, it has also been shown that ferroptosis is further accelerated by inhibition of ETC complexes and OXPHOS (71, 82). The discrepancy between previous studies and ours can be explained by the differences in cell type, ferroptosis inducers, and exposure time. In particular, activation of ferroptotic signaling in response to ferroptosis inducers (RSL3, erastin, and cysteine deprivation) might be mediated through different mechanistic pathways in mitochondria. On the other hand, other authors have shown that ferroptosis sensitivity is also associated with metabolic compartmentalization. Indeed, genetic silencing and pharmacological inhibition of glutaminolysis through GLS2, but not GLS1, or GOT1 have been shown to inhibit erastin-induced ferroptosis (79, 83, 84). Furthermore, also in our study, while the combined treatment was able to increase ferroptosis in all PDAC cells, we observed some differences between K-Ras mutated cell lines and K-Ras wild-type cells, especially regarding glutaminolysis activation (compare Figures 6, 7, Figure S7, and Supplementary Table 4). A role of oncogenic K-Ras in favoring glutamine utilization has been widely described (85, 86). However, if the oncogenic K-Ras-dependent enhancement of glutamine utilization is an important cause of the increased sensitivity of MiaPaCa-2 and PANC1 cells to the combined treatment-induced ferroptosis, it needs further experiments. Indeed, as recently described, genes involved in ferroptosis also exert other functions in different cell contexts, and therefore, the role of glutamine in ferroptosis may also be dependent and not dependent on K-Ras status (87). Therefore, the differences emerging from our study and from other studies possibly reflect the incomplete understanding of how various factors dictate sensitivity to ferroptosis.

In conclusion, our findings indicate that FR054 alone or in combination with ERA is able to modulate oxidative stress response and central carbon metabolism, favoring glutaminolysis over glycolysis, which, under conditions of SLC7A11 inhibition following ERA treatment, causes imbalance in cellular redox state, GSH depletion, lipid-ROS accumulation, and finally ferroptosis. Based on our *in vitro* data, we propose that FR054, together with a drug capable of modulating the intracellular level of cysteine, such as ERA, may become a novel candidate for *in vivo* ferroptosis induction for the targeted killing of PDAC cells.

Limitations

The aim of our study was to identify possible pathways or proteins whose inhibition/activation could synergize with FR054, a

novel HBP inhibitor, in inducing PDAC cell death. However, our study contains certain limitations. First, a Q-PCR validation of some DEGs was not conducted in order to determine if some specific pathways were more activated by FR054 treatment. Second, we did not test the effect of a specific ferroptosis inhibitor such as Ferrostatin-1 to confirm the ability of the combined treatment in inducing ferroptosis. Third, we did not test our combination in immortalized pancreatic cells such as human pancreatic duct epithelial cells to support the use of the combination in preclinical *in vivo* models. Fourth, to dissect the role of glutaminolysis in the three PDAC cell lines characterized by a different K-Ras mutational status, we could test the effect of the mutated K-Ras activity reduction by using some of the available mutation-specific inhibitors (88). Finally, we did not directly assess the mitochondrial activity and the role of metabolism compartmentalization, as we have done previously (89), in our cell models with the different treatments, causing ferroptosis.

Data availability statement

The datasets presented in this study can be found in online repositories. The names of the repository/repositories and accession number(s) can be found below: GEO database, accession number GSE223303.

Author contributions

Conception and design: AW and FC. Development of methodology: BZ, MG, TL, AP, LB, AW, and FC. Performing research: BZ, MB, TL, VB, and AP. Analysis and interpretation of data: BZ, MG, TL, AP, LB, AW, and FC. Writing the draft of the manuscript: FC. Review of the manuscript: BZ, VB, AW, and FC. Revision of the manuscript: all authors. All authors contributed to the article and approved the submitted version.

Funding

Work in FC's laboratory was supported by grants from MAECI (Executive Programme of Scientific and Technological Cooperation Italy-China 2019–2021, #CN19GR03), Research facilitation fund (Fondo per le Agevolazioni alla Ricerca—FAR), and Fondo di Ateneo-Quota Competitiva (Bicocca, Italy, #ATEQC-0006). BZ doctoral contract is supported by the Italian Minister of University and Research (MUR). Work in AW's laboratory was supported by the MWK of Lower Saxony (SMART BIOTECS alliance between the Technische Universität Braunschweig and the Leibniz Universität Hannover) and BMBF (PeriNAA - 01ZX1916B).

Conflict of interest

The authors declare that the research was conducted in the absence of any commercial or financial relationships that could be construed as a potential conflict of interest.

Publisher's note

Supplementary material

The Supplementary Material for this article can be found online at: https://www.frontiersin.org/articles/10.3389/fonc.2023.1125855/full#supplementary-material

References

1. Siegel RL, Miller KD, Jemal A. Cancer statistics, 2019. *CA Cancer J Clin* (2019) 69 (1):734. doi: 10.3322/caac.21551

2. Ducreux M, Seufferlein T, van Laethem J-L, Laurent-Puig P, Smolenschi C, Malka D, et al. Systemic treatment of pancreatic cancer revisited. *Semin Oncol* (2019) 46 (1):2838. doi: 10.1053/j.seminoncol.2018.12.003

3. Vaziri-Gohar A, Zarei M, Brody JR, Winter JM. Metabolic dependencies in pancreatic cancer. *Front Oncol* (2018) 8:617. doi: 10.3389/fonc.2018.00617

4. Shukla SK, Purohit V, Mehla K, Gunda V, Chaika N v., Vernucci E, et al. MUC1 and HIF-1alpha signaling crosstalk induces anabolic glucose metabolism to impart gemcitabine resistance to pancreatic cancer. *Cancer Cell* (2017) 32(1):71–87.e7. doi: 10.1016/j.ccell.2017.06.004

5. Tadros S, Shukla SK, King RJ, Gunda V, Vernucci E, Abrego J, et al. *De novo* lipid synthesis facilitates gemcitabine resistance through endoplasmic reticulum stress in pancreatic cancer. *Cancer Res* (2017) 77(20):550317. doi: 10.1158/0008-5472.CAN-16-3062

6. Guillaumond F, Leca J, Olivares O, Lavaut M-N, Vidal N, Berthezène P, et al. Strengthened glycolysis under hypoxia supports tumor symbiosis and hexosamine biosynthesis in pancreatic adenocarcinoma. *Proc Natl Acad Sci* (2013) 110(10):391924. doi: 10.1073/pnas.1219555110

7. Ying H, Kimmelman AC, Lyssiotis CA, Hua S, Chu GC, Fletcher-Sananikone E, et al. Oncogenic kras maintains pancreatic tumors through regulation of anabolic glucose metabolism. *Cell* (2012) 149(3):65670. doi: 10.1016/j.cell.2012.01.058

8. Akella NM, Ciraku L, Reginato MJ. Fueling the fire: emerging role of the hexosamine biosynthetic pathway in cancer. *BMC Biol* (2019) 17(1):52. doi: 10.1186/s12915-019-0671-3

9. Chiaradonna F, Ricciardiello F, Palorini R. The nutrient-sensing hexosamine biosynthetic pathway as the hub of cancer metabolic rewiring. *Cells* (2018) 7(6):53. doi: 10.3390/cells7060053

10. Paiotta A, D'Orazio G, Palorini R, Ricciardiello F, Zoia L, Votta G, et al. Design, synthesis, and preliminary biological evaluation of GlcNAc-6P analogues for the modulation of phosphoacetylglucosamine mutase 1 (AGM1/PGM3). *Eur J Org Chem* (2018) 2018(17):194652. doi: 10.1002/ejoc.201800183

11. Ricciardiello F, Votta G, Palorini R, Raccagni I, Brunelli L, Paiotta A, et al. Inhibition of the hexosamine biosynthetic pathway by targeting PGM3 causes breast cancer growth arrest and apoptosis. *Cell Death Dis* (2018) 9(3):377. doi: 10.1038/s41419-018-0405-4

12. Ricciardiello F, Gang Y, Palorini R, Li Q, Giampà M, Zhao F, et al. Hexosamine pathway inhibition overcomes pancreatic cancer resistance to gemcitabine through

unfolded protein response and EGFR-akt pathway modulation. *Oncogene* (2020) 39 (20):410317. doi: 10.1038/s41388-020-1260-1

13. Ricciardiello F, Bergamaschi L, de Vitto H, Gang Y, Zhang T, Palorini R, et al. Suppression of the HBP function increases pancreatic cancer cell sensitivity to a pan-RAS inhibitor. *Cells* (2021) 10(2):431. doi: 10.3390/cells10020431

14. Robinson CM, Talty A, Logue SE, Mnich K, Gorman AM, Samali A. An emerging role for the unfolded protein response in pancreatic cancer. *Cancers (Basel)* (2021) 13(2):261. doi: 10.3390/cancers13020261

15. Borrello MT, Martin MB, Pin CL. The unfolded protein response: an emerging therapeutic target for pancreatitis and pancreatic ductal adenocarcinoma. *Pancreatology* (2022) 22(1):14859. doi: 10.1016/j.pan.2021.10.007

16. Sapcariu SC, Kanashova T, Weindl D, Ghelfi J, Dittmar G, Hiller K. Simultaneous extraction of proteins and metabolites from cells in culture. *MethodsX* (2014) 1:7480. doi: 10.1016/j.mex.2014.07.002

17. Hiller K, Hangebrauk J, Jäger C, Spura J, Schreiber K, Schomburg D. MetaboliteDetector: comprehensive analysis tool for targeted and nontargeted GC/MS based metabolome analysis. *Anal Chem* (2009) 81(9):342939. doi: 10.1021/ac802689c

18. Wegner A, Weindl D, Jäger C, Sapcariu SC, Dong X, Stephanopoulos G, et al. Fragment formula calculator (FFC): determination of chemical formulas for fragment ions in mass spectrometric data. *Anal Chem* (2014) 86(4):22218. doi: 10.1021/ac403879d

19. Paez J, Wendt M, Lanman N. scTree: an r package to generate antibody-compatible classifiers from single-cell sequencing data. *J Open Source Softw* (2020) 5 (48):2061. doi: 10.21105/joss.02061

20. Keenan AB, Torre D, Lachmann A, Leong AK, Wojciechowicz ML, Utti V, et al. ChEA3: transcription factor enrichment analysis by orthogonal omics integration. *Nucleic Acids Res* (2019) 47(W1):W21224. doi: 10.1093/nar/gkz446

21. Hammal F, de Langen P, Bergon A, Lopez F, Ballester B. ReMap 2022: a database of human, mouse, drosophila and arabidopsis regulatory regions from an integrative analysis of DNA-binding sequencing experiments. *Nucleic Acids Res* (2022) 50(D1): D31625. doi: 10.1093/nar/gkab996

22. Taguchi K, Yamamoto M. The KEAP1–NRF2 system in cancer. *Front Oncol* (2017) 7:85. doi: 10.3389/fonc.2017.00085

23. DeBlasi JM, DeNicola GM. Dissecting the crosstalk between NRF2 signaling and metabolic processes in cancer. *Cancers (Basel)* (2020) 12(10):3023. doi: 10.3390/cancers12103023

24. Badgley MA, Kremer DM, Maurer HC, DelGiorno KE, Lee H-J, Purohit V, et al. Cysteine depletion induces pancreatic tumor ferroptosis in mice. *Sci (1979)* (2020) 368 (6486):859. doi: 10.1126/science.aaw9872

25. Dolma S, Lessnick SL, Hahn WC, Stockwell BR. Identification of genotype-selective antitumor agents using synthetic lethal chemical screening in engineered human tumor cells. *Cancer Cell* (2003) 3(3):28596. doi: 10.1016/S1535-6108(03)00050-3

26. Dixon SJ, Patel DN, Welsch M, Skouta R, Lee ED, Hayano M, et al. Pharmacological inhibition of cystine–glutamate exchange induces endoplasmic reticulum stress and ferroptosis. *Elife* (2014) 3:e02523. doi: 10.7554/eLife.02523

27. Daher B, Vučetić M, Pouysségur J. Cysteine depletion, a key action to challenge cancer cells to ferroptotic cell death. *Front Oncol* (2020) 10:723. doi: 10.3389/fonc.2020.00723

28. Sano R, Reed JC. ER stress-induced cell death mechanisms. *Biochim Biophys Acta (BBA) - Mol Cell Res* (2013) 1833(12):346070. doi: 10.1016/j.bbamcr.2013.06.028

29. Oyadomari S, Mori M. Roles of CHOP/GADD153 in endoplasmic reticulum stress. *Cell Death Differ* (2004) 11(4):3819. doi: 10.1038/sj.cdd.4401373

30. Gao R, Kalathur RKR, Coto-Llerena M, Ercan C, Buechel D, Shuang S, et al. YAP/TAZ and ATF4 drive resistance to sorafenib in hepatocellular carcinoma by preventing ferroptosis. *EMBO Mol Med* (2021) 13(12):e14351. doi: 10.15252/emmm.202114351

31. Sbodio JI, Snyder SH, Paul BD. Golgi stress response reprograms cysteine metabolism to confer cytoprotection in huntington's disease. *Proc Natl Acad Sci* (2018) 115(4):7805. doi: 10.1073/pnas.1717877115

32. Mimura J, Inose-Maruyama A, Taniuchi S, Kosaka K, Yoshida H, Yamazaki H, et al. Concomitant Nrf2- and ATF4-activation by carnosic acid cooperatively induces expression of cytoprotective genes. *Int J Mol Sci* (2019) 20(7):1706. doi: 10.3390/ijms20071706

33. Komatsu M, Kurokawa H, Waguri S, Taguchi K, Kobayashi A, Ichimura Y, et al. The selective autophagy substrate p62 activates the stress responsive transcription factor Nrf2 through inactivation of Keap1. *Nat Cell Biol* (2010) 12(3):21323. doi: 10.1038/ncb2021

34. He F, Ru X, Wen T. NRF2, a transcription factor for stress response and beyond. *Int J Mol Sci* (2020) 21(13):4777. doi: 10.3390/ijms21134777

35. Lewerenz J, Hewett SJ, Huang Y, Lambros M, Gout PW, Kalivas PW, et al. The Cystine/Glutamate antiporter system x_c^- in health and disease: from molecular mechanisms to novel therapeutic opportunities. *Antioxid Redox Signal* (2013) 18 (5):52255. doi: 10.1089/ars.2011.4391

36. Han J, Kaufman RJ. Physiological/pathological ramifications of transcription factors in the unfolded protein response. *Genes Dev* (2017) 31(14):141738. doi: 10.1101/gad.297374.117

37. Koppula P, Zhang Y, Zhuang L, Gan B. Amino acid transporter SLC7A11/xCT at the crossroads of regulating redox homeostasis and nutrient dependency of cancer. *Cancer Commun* (2018) 38(1):12. doi: 10.1186/s40880-018-0288-x

38. Gozzelino R, Jeney V, Soares MP. Mechanisms of cell protection by heme oxygenase-1. *Annu Rev Pharmacol Toxicol* (2010) 50(1):32354. doi: 10.1146/annurev.pharmtox.010909.105600

39. McMahon M, Itoh K, Yamamoto M, Hayes JD. Keap1-dependent proteasomal degradation of transcription factor Nrf2 contributes to the negative regulation of antioxidant response element-driven gene expression. *J Biol Chem* (2003) 278 (24):21592600. doi: 10.1074/jbc.M300931200

40. Andringa KK, Coleman MC, Aykin-Burns N, Hitchler MJ, Walsh SA, Domann FE, et al. Inhibition of glutamate cysteine ligase activity sensitizes human breast cancer cells to the toxicity of 2-Deoxy-D-Glucose. *Cancer Res* (2006) 66(3):160510. doi: 10.1158/0008-5472.CAN-05-3462

41. Luo M, Wu L, Zhang K, Wang H, Zhang T, Gutierrez L, et al. miR-137 regulates ferroptosis by targeting glutamine transporter SLC1A5 in melanoma. *Cell Death Differ* (2018) 25(8):145772. doi: 10.1038/s41418-017-0053-8

42. Mukhopadhyay S, vander Heiden MG, McCormick F. The metabolic landscape of RAS-driven cancers from biology to therapy. *Nat Cancer* (2021) 2(3):27183. doi: 10.1038/s43018-021-00184-x

43. Kim PK, Halbrook CJ, Kerk SA, Radyk M, Wisner S, Kremer DM, et al. Hyaluronic acid fuels pancreatic cancer cell growth. *Elife* (2021) 10:e62645. doi: 10.7554/eLife.62645

44. Wei R, Zhao Y, Wang J, Yang X, Li S, Wang Y, et al. Tagitinin c induces ferroptosis through PERK-Nrf2-HO-1 signaling pathway in colorectal cancer cells. *Int J Biol Sci* (2021) 17(11):270317. doi: 10.7150/ijbs.59404

45. Chen Y, Mi Y, Zhang X, Ma Q, Song Y, Zhang L, et al. Dihydroartemisinin-induced unfolded protein response feedback attenuates ferroptosis *via* PERK/ATF4/HSPA5 pathway in glioma cells. *J Exp Clin Cancer Res* (2019) 38(1):402. doi: 10.1186/s13046-019-1413-7

46. Bravo R, Parra V, Gatica D, Rodriguez AE, Torrealba N, Paredes F, et al. Endoplasmic reticulum and the unfolded protein response. *Dans* (2013) 301:215–290. doi: 10.1016/B978-0-12-407704-1.00005-1

47. Bhandary B, Marahatta A, Kim H-R, Chae H-J. An involvement of oxidative stress in endoplasmic reticulum stress and its associated diseases. *Int J Mol Sci* (2012) 14 (1):43456. doi: 10.3390/ijms14010434

48. Oliveira SJ, Pinto JP, Picarote G, Costa VM, Carvalho F, Rangel M, et al. ER stress-inducible factor CHOP affects the expression of hepcidin by modulating C/EBPalpha activity. *PloS One* (2009) 4(8):e6618. doi: 10.1371/journal.pone.0006618

49. Chang L-C, Chiang S-K, Chen S-E, Yu Y-L, Chou R-H, Chang W-C. Heme oxygenase-1 mediates BAY 11–7085 induced ferroptosis. *Cancer Lett* (2018) 416:12437. doi: 10.1016/j.canlet.2017.12.025

50. Kwon M-Y, Park E, Lee S-J, Chung SW. Heme oxygenase-1 accelerates erastin-induced ferroptotic cell death. *Oncotarget* (2015) 6(27):24393403. doi: 10.18632/oncotarget.5162

51. Ye J, Kumanova M, Hart LS, Sloane K, Zhang H, de Panis DN, et al. The GCN2-ATF4 pathway is critical for tumour cell survival and proliferation in response to nutrient deprivation. *EMBO J* (2010) 29(12):208296. doi: 10.1038/emboj.2010.81

52. Daher B, Parks SK, Durivault J, Cormerais Y, Baidarjad H, Tambutte E, et al. Genetic ablation of the cystine transporter xCT in PDAC cells inhibits mTORC1, growth, survival, and tumor formation via nutrient and oxidative stresses. *Cancer Res* (2019) 79(15):387790. doi: 10.1158/0008-5472.CAN-18-3855

53. Xu Y, Zhang N, Chen C, Xu X, Luo A, Yan Y, et al. Sevoflurane induces ferroptosis of glioma cells through activating the ATF4-CHAC1 pathway. *Front Oncol* (2022) 12:859621. doi: 10.3389/fonc.2022.859621

54. Han J, Back SH, Hur J, Lin Y-H, Gildersleeve R, Shan J, et al. ER-stress-induced transcriptional regulation increases protein synthesis leading to cell death. *Nat Cell Biol* (2013) 15(5):48190. doi: 10.1038/ncb2738

55. Ma Y, Hendershot LM. Delineation of a negative feedback regulatory loop that controls protein translation during endoplasmic reticulum stress. *J Biol Chem* (2003) 278(37):3486473. doi: 10.1074/jbc.M301107200

56. Jousse C, Deval C, Maurin A-C, Parry L, Chérasse Y, Chaveroux C, et al. TRB3 inhibits the transcriptional activation of stress-regulated genes by a negative feedback on the ATF4 pathway. *J Biol Chem* (2007) 282(21):1585161. doi: 10.1074/jbc.M611723200

57. Wortel IMN, van der Meer LT, Kilberg MS, van Leeuwen FN. Surviving stress: modulation of ATF4-mediated stress responses in normal and malignant cells. *Trends Endocrinol Metab* (2017) 28(11):794806. doi: 10.1016/j.tem.2017.07.003

58. Lassot I, Berlioz-Torrent C, Durand H, Groussin L, Hai T, Benarous R, et al. ATF4 degradation relies on a phosphorylation-dependent interaction with the SCF (βTrCP) ubiquitin ligase. *Mol Cell Biol* (2001) 21(6):2192202. doi: 10.1128/MCB.21.6.2192-2202.2001

59. Nagao Y, Amo-Shiinoki K, Nakabayashi H, Hatanaka M, Kondo M, Matsunaga K, et al. Gsk-3-Mediated proteasomal degradation of ATF4 is a proapoptotic mechanism in mouse pancreatic β-cells. *Int J Mol Sci* (2022) 23(21):13586. doi: 10.3390/ijms232113586

60. Rada P, Rojo AI, Chowdhry S, McMahon M, Hayes JD, Cuadrado A. SCF/β-TrCP promotes glycogen synthase kinase 3-dependent degradation of the Nrf2

transcription factor in a Keap1-independent manner. *Mol Cell Biol* (2011) 31 (6):112133. doi: 10.1128/MCB.01204-10

61. Rada P, Rojo AI, Evrard-Todeschi N, Innamorato NG, Cotte A, Jaworski T, et al. Structural and functional characterization of Nrf2 degradation by the glycogen synthase kinase 3/β-TrCP axis. *Mol Cell Biol* (2012) 32(17):348699. doi: 10.1128/MCB.00180-12

62. Sun Z, Zhang S, Chan JY, Zhang DD. Keap1 controls postinduction repression of the Nrf2-mediated antioxidant response by escorting nuclear export of Nrf2. *Mol Cell Biol* (2007) 27(18):633449. doi: 10.1128/MCB.00630-07

63. Fan R-F, Tang K-K, Wang Z-Y, Wang L. Persistent activation of Nrf2 promotes a vicious cycle of oxidative stress and autophagy inhibition in cadmium-induced kidney injury. *Toxicology* (2021) 464:152999. doi: 10.1016/j.tox.2021.152999

64. Tsakiri EN, Gumeni S, Iliaki KK, Benaki D, Vougas K, Sykiotis GP, et al. Hyperactivation of Nrf2 increases stress tolerance at the cost of aging acceleration due to metabolic deregulation. *Aging Cell* (2019) 18(1):e12845. doi: 10.1111/acel.12845

65. Lee O-H, Jain AK, Papusha V, Jaiswal AK. An auto-regulatory loop between stress sensors INrf2 and Nrf2 controls their cellular abundance. *J Biol Chem* (2007) 282 (50):3641220. doi: 10.1074/jbc.M706517200

66. Kaspar JW, Jaiswal AK. An autoregulatory loop between Nrf2 and Cul3-Rbx1 controls their cellular abundance. *J Biol Chem* (2010) 285(28):2134958. doi: 10.1074/jbc.M110.121863

67. Tan EP, McGreal SR, Graw S, Tessman R, Koppel SJ, Dhakal P, et al. Sustained O-GlcNAcylation reprograms mitochondrial function to regulate energy metabolism. *J Biol Chem* (2017) 292(36):1494062. doi: 10.1074/jbc.M117.797944

68. Xu T-H, Du Y, Sheng Z, Li Y, Qiu X, Tian B, et al. OGT-mediated KEAP1 glycosylation accelerates NRF2 degradation leading to high phosphate-induced vascular calcification in chronic kidney disease. *Front Physiol* (2020) 11:1092. doi: 10.3389/fphys.2020.01092

69. Chen P, Smith TJ, Wu J, Siesser PF, Bisnett BJ, Khan F, et al. Glycosylation of KEAP1 links nutrient sensing to redox stress signaling. *EMBO J* (2017) 36(15):223350. doi: 10.15252/embj.201696113

70. Yu F, Zhang Q, Liu H, Liu J, Yang S, Luo X, et al. Dynamic O-GlcNAcylation coordinates ferritinophagy and mitophagy to activate ferroptosis. *Cell Discovery* (2022) 8(1):40. doi: 10.1038/s41421-022-00390-6

71. Kremer DM, Nelson BS, Lin L, Yarosz EL, Halbrook CJ, Kerk SA, et al. GOT1 inhibition promotes pancreatic cancer cell death by ferroptosis. *Nat Commun* (2021) 12 (1):4860. doi: 10.1038/s41467-021-24859-2

72. Banjac A, Perisic T, Sato H, Seiler A, Bannai S, Weiss N, et al. The cystine/cysteine cycle: a redox cycle regulating susceptibility versus resistance to cell death. *Oncogene* (2008) 27(11):161828. doi: 10.1038/sj.onc.1210796

73. Cao SS, Kaufman RJ. Endoplasmic reticulum stress and oxidative stress in cell fate decision and human disease. *Antioxid Redox Signal* (2014) 21(3):396413. doi: 10.1089/ars.2014.5851

74. Gansemer ER, McCommis KS, Martino M, King-McAlpin AQ, Potthoff MJ, Finck BN, et al. NADPH and glutathione redox link TCA cycle activity to endoplasmic reticulum homeostasis. *iScience* (2020) 23(5):101116. doi: 10.1016/j.isci.2020.101116

75. Lee Y-S, Lee D-H, Choudry HA, Bartlett DL, Lee YJ. Ferroptosis-induced endoplasmic reticulum stress: cross-talk between ferroptosis and apoptosis. *Mol Cancer Res* (2018) 16(7):10736. doi: 10.1158/1541-7786.MCR-18-0055

76. Zheng J, Conrad M. The metabolic underpinnings of ferroptosis. *Cell Metab* (2020) 32(6):92037. doi: 10.1016/j.cmet.2020.10.011

77. Sies H, Berndt C, Jones DP. Oxidative stress. *Annu Rev Biochem* (2017) 86 (1):71548. doi: 10.1146/annurev-biochem-061516-045037

78. Gao M, Yi J, Zhu J, Minikes AM, Monian P, Thompson CB, et al. Role of mitochondria in ferroptosis. *Mol Cell* (2019) 73(2):354–363.e3. doi: 10.1016/j.molcel.2018.10.042

79. Gao M, Monian P, Quadri N, Ramasamy R, Jiang X. Glutaminolysis and transferrin regulate ferroptosis. *Mol Cell* (2015) 59(2):298308. doi: 10.1016/j.molcel.2015.06.011

80. Shin D, Lee J, You JH, Kim D, Roh J-L. Dihydrolipoamide dehydrogenase regulates cystine deprivation-induced ferroptosis in head and neck cancer. *Redox Biol* (2020) 30:101418. doi: 10.1016/j.redox.2019.101418

81. Li Y, Wang X, Huang Z, Zhou Y, Xia J, Hu W, et al. CISD3 inhibition drives cystine-deprivation induced ferroptosis. *Cell Death Dis* (2021) 12(9):839. doi: 10.1038/s41419-021-04128-2

82. Alvarez SW, Sviderskiy VO, Terzi EM, Papagiannakopoulos T, Moreira AL, Adams S, et al. NFS1 undergoes positive selection in lung tumours and protects cells from ferroptosis. *Nature* (2017) 551(7682):63943. doi: 10.1038/nature24637

83. Suzuki S, Venkatesh D, Kanda H, Nakayama A, Hosokawa H, Lee E, et al. GLS2 is a tumor suppressor and a regulator of ferroptosis in hepatocellular carcinoma. *Cancer Res* (2022) 82(18):320922. doi: 10.1158/0008-5472.CAN-21-3914

84. Zhang K, Wu L, Zhang P, Luo M, Du J, Gao T, et al. miR-9 regulates ferroptosis by targeting glutamic-oxaloacetic transaminase GOT1 in melanoma. *Mol Carcinog* (2018) 57(11):156676. doi: 10.1002/mc.22878

85. Gaglio D, Metallo CM, Gameiro PA, Hiller K, Danna LS, Balestrieri C, et al. Oncogenic K-ras decouples glucose and glutamine metabolism to support cancer cell growth. *Mol Syst Biol* (2011) 7(1):523. doi: 10.1038/msb.2011.56

86. Bryant KL, Mancias JD, Kimmelman AC, Der CJ. KRAS: feeding pancreatic cancer proliferation. *Trends Biochem Sci* (2014) 39(2):91100. doi: 10.1016/j.tibs.2013.12.004

87. Andreani C, Bartolacci C, Scaglioni PP. Ferroptosis: a specific vulnerability of RAS-driven cancers? *Front Oncol* (2022) 12:923915. doi: 10.3389/fonc.2022.923915

88. Sattler M, Mohanty A, Kulkarni P, Salgia R. Precision oncology provides opportunities for targeting KRAS-inhibitor resistance. *Trends Cancer* (2023) 9 (1):4254. doi: 10.1016/j.trecan.2022.10.001

89. Nonnenmacher Y, Palorini R, d'Herouël AF, Krämer L, Neumann-Schaal M, Chiaradonna F, et al. Analysis of mitochondrial metabolism in situ: combining stable isotope labeling with selective permeabilization. *Metab Eng* (2017) 43:14755. doi: 10.1016/j.ymben.2016.12.005

Frontiers in Oncology

Advances knowledge of carcinogenesis and tumor progression for better treatment and management

The third most-cited oncology journal, which highlights research in carcinogenesis and tumor progression, bridging the gap between basic research and applications to imrpove diagnosis, therapeutics and management strategies.

Discover the latest Research Topics

See more →

Frontiers

Avenue du Tribunal-Fédéral 34
1005 Lausanne, Switzerland
frontiersin.org

Contact us

+41 (0)21 510 17 00
frontiersin.org/about/contact